UNIVERSITY OF OKLAHOMA

GRADUATE COLLEGE

INVESTIGATION OF MATRIX INTERFERENCES IN QUANTITATIVE LIQUID

CHROMATOGRAPHY-ELECTROSPRAY IONIZATION MASS SPECTROMETRY

ANALYSIS OF BIOLOGICAL SAMPLES

A DISSERTATION

SUBMITTED TO THE GRADUATE FACULTY

in partial fulfillment of the requirements for the

degree of

DOCTOR OF PHILOSOPHY

By

LIHONG DU

Norman, Oklahoma

2007

UMI Number: 3261093

UMI®

INVESTIGATION OF MATRIX INTERFERENCES IN QUANTITATIVE LIQUID
CHROMATOGRAPHY-ELECTROSPRAY IONIZATION MASS SPECTROMETRY
ANALYSIS OF BIOLOGICAL SAMPLES

A DISSERTATION APPROVED FOR THE
DEPARTMENT OF CHEMISTRY AND BIOCHEMISTRY

BY

_____
Robert L. White (Chair)

_____
C. LeRoy Blank

_____
Charles V. Rice

_____
Wai T. Yip

_____
Lance L. Lobban

ACKNOWLEDGMENTS

I would like to acknowledge the support of my family and thank my advisors at Merck Research Laboratories and the University of Oklahoma for their invaluable contribution to this accomplishment.

I would like to express my thanks to my husband, Fenglei, who has taken all of the housework and child care so that I can complete the dissertation wholeheartedly. My appreciations go to my supervisors at Merck: Dr. Amy Q. Wang, Dr. Donald G. Musson, Mr. Michael S. Schwartz and Dr. Eric J. Woolf. They have recognized my working ability and provided me the opportunity for continue education.

I sincerely thank Dr. Robert L. White, my mentor, and for his thoughtful guidance and advice throughout my entire graduate study at Oklahoma University. I also thank the other members of my graduate committee: Dr. LeRoy L. Blank, Dr. Richard W. Taylor, Dr. Charles V. Rice, Dr. Wai T. Yip and Dr. Lance L. Lobban for their interest for my research and valuable inputs.

I must express my gratitude my friends: Dr. Nathan D. Hesse and Dr. Rong Lin, the past students in Dr. White's research group, for their useful information and supportive discussions.

TABLE OF CONTENTS

INVESTIGATION OF MATRIX INTERFERENCES IN QUANTITATIVE LIQUID

CHROMATOGRAPHY-ELECTROSPARY IONIZATION MASS SPECTROMETRY

ANALYSIS OF BIOLOGICAL SAMPLES

ABSTRACT

Matrix interferences can severely affect the quantitative analysis of biological samples when electrospray ionization (ESI) is employed with liquid chromatography-tandem mass spectrometry (LC-MS/MS). Before these effects can be eliminated or minimized, it is necessary to identify their sources. The role of glycerophosphocholine (GPCho) lipids in matrix interferences caused by the endogenous components in human plasma was investigated for assays involving representative pharmaceutical compounds. Conventional liquid-liquid extraction (LLE) was compared to high turbulent flow liquid chromatography (HTLC) online extraction and to ultra performance liquid chromatography (UPLC) as far as their abilities to reduce matrix interferences. GPCho lipids were found to be a primary source of matrix interferences for assays involving human plasma samples. Extraction solvents were unable to completely remove GPCho lipids. The efficiency for reducing the lipids by using online HTLC extraction was found to be dependent on the organic content of the transfer solvent employed. Turbulent flow had no significant effect on removing them. UPLC analysis eliminated lipid interferences by means of high resolution chromatographic separation. For the examined analytes, UPLC was more effective at removing lipid derived interferences than HTLC online extraction, which was more effective than conventional LLE.

The mechanisms by which endogenous GPCho lipids interfere with analyte electrospray ionization were investigated with the aid of a partition equilibrium mathematical model. A linear equation, which was derived by modifying previously published models, was used to quantitatively predict analyte MS responses. The correlation between analyte MS response and solution concentration was examined for four situations: analyte in solvent, analyte in solvent containing an HPLC compatible buffer, analyte in solvent containing a co-analyte, and analyte in solvent containing GPCho lipids and buffer. It was found that the experimental results could be explained by the linear equation of the new model over a wide concentrations range. The analyte behaviors in a salt solution, which could not be explained by the previous model, could be elucidated here. Moreover, the new model is easier to use for modeling solutions containing multiple species. It was concluded that analyte MS response was determined by a competition mechanism that was driven by equilibrium considerations and involved analyte and background electrolytes.

CHAPTER 1

INTRODUCTION

1.1 Overview of Biological Sample Matrix Interferences

Development of atmospheric pressure ionization techniques (API) has enabled the coupling of high performance liquid chromatography with mass spectrometry (HPLC-MS) [1,2]. The combination of liquid chromatography and tandem mass spectrometry (LC-MS/MS) via electrospray ionization (ESI) or atmospheric pressure chemical ionization (APCI) is currently considered to be the primary analytical technology for the determination of non-volatile trace drug candidates in biological samples [3-8]. Compared to conventional spectroscopic and electrochemical detection techniques, LC-MS/MS analysis provides many advantages, particularly in specificity and sensitivity. Due to the inherent mass selectivity of the mass spectrometer, interferences can be removed by mass filtration, which has led to the development of high throughput analysis methods. Unfortunately, the benefits of MS detection often cause researchers to overlook the importance of chromatographic separation and sample preparation. Direct injections of unprocessed samples onto LC-MS/MS systems are infrequently reported. Instead, many articles focus on assay procedure development and optimization of parameters such as: recovery, linearity, precision and limit of quantification [9]. An important issue associated with LC-MS/MS applications is related to matrix interferences. It is a phenomenon that analyte MS responses are suppressed or enhanced by the presence of other compounds, and this generally happens when complicated matrices are analyzed [10-16]. This adverse effect normally is not reproducible between various sample batches

or even for a single sample source collected at different times. Even though these interferences may not be directly observed in the spectrum, their presence can dramatically influence the accuracy and precision of analyte quantification. It is generally accepted that matrix interferences are associated with the analyte ionization process. ESI is more prone to these interferences than APCI [17-20]. However, most applications utilize ESI rather than APCI because ESI is sensitive, consumes less solvent, is suitable for a wider polarity range of materials, and can be used for thermally labile compounds. At present, the reasons for matrix interferences in ESI mass spectrometry are not well understood. Interferences are usually attributed to a change in analyte ionization efficiency by the presence of co-eluting substances, such as endogenous materials from the matrix, mobile phase additives, and other exogenous compounds. Depending on the ionization environment, the signal of a target analyte may decrease (majority of the cases) or increase. The importance of matrix interferences on the reliability of a quantitative assay has been clearly defined in the recently issued "U.S. FDA Guidance for Industry on Bioanalytical Method Validation". It states that "In the case of LC-MS and LC-MS/MS based procedures, matrix effects should be investigated to ensure that precision, selectivity, and sensitivity will not be compromised" [21]. With regard to small molecule analysis in biological fluids, previous research has focused on the origin and nature of matrix interferences, methodologies for assessing and minimizing these effects, and elucidating mechanisms for these phenomena.

1.2 Origins and Consequences of Matrix Interferences in Bioanalysis

The analysis of drugs and metabolites in: plasma, urine, bile, feces, and tissue homogenates for the determination of pharmacokinetic parameters and metabolic

2

pathways is a crucial step in the drug development process. When tandem mass spectrometry is used for quantification, in most cases, only the desired analyte is observed in the MS spectrum when the specificity of selective reaction monitoring is employed. Nevertheless, substances that are not detected, but that co-elute with the analyte, may adversely affect the analyte ionization process and result in MS signal variation. Matrix interferences are typically caused by the presence of endogenous components in the sample matrix. Sample pretreatment can effectively remove large amounts of matrix components. However, due to the high concentrations of endogenous materials such as: salts, amines, fatty acids and triglycerides, the amounts of these species in sample extracts may still be sufficient to affect the analysis of drug candidates. Because these matrix components typically cause analyte signal suppression and the suppression degree depends on the nature of the matrix compounds present and the relative concentrations of analyte and matrix components, the consequences of matrix effects on quantitative measurements can be reflected in various aspects of the analysis method, including: reduced sensitivity, decreased reproducibility, and calibration curve deviation from linearity. These problems normally lead to unacceptable precision and accuracy for the analysis method.

An investigation into the causes of MS signal variations during quantitative analysis of a platelet-activating factor receptor antagonist in human plasma was the incentive for initiating research into the nature of interferences caused by matrix components [22]. Inconsistent analyte ion intensities were obtained for control plasma extracts obtained by hexane liquid-liquid extraction (LLE), ethyl acetate back-extraction, and mix mode solid phase extraction (SPE), and the analyte signal was found to be

inversely related to the intensities of detected matrix peaks found in the full scan mass spectra. The effect of endogenous components on analyte analyses has also been illustrated by another persuasive case. When human plasma samples were extracted by using a generic non-selective or a pH adjusted selective LLE method, and then analyzed by using a 90% acetonitrile mobile phase or by using 50% acetonitrile, the peak areas, precisions, and accuracies of results were found to be significantly affected. Selective extraction combined with chromatographic separation can considerably improve the quantitative results [23]. The analyte ionization suppression effects have also been observed for human blood [24] and serum [25] analyses. Even though the composition of human urine is quite different, its endogenous components have been found to cause an ionization suppression effect too. A peak area reduction of about 50% was observed for an analyte diluted with urine when compared to mobile phase dilution. Low reproducibility was associated with this signal suppression as was indicated by large variations among five urine batches. Assay performance was significantly improved when LLE was employed [26]. A comparison of matrix interferences in three biofluids: human urine, oral fluids, and plasma, processed by direct injection, dilution, protein precipitation (PP) and SPE, has additionally confirmed that the presence of these adverse matrix effects are not only associated with sample preparation techniques, but also depend on the analyzed biofluids [27]. Generally, PP provides the worst analyte ionization suppression effects due to its non-selective nature, and SPE and LLE do not always guarantee satisfactory performance. Although each biofluid possesses characteristic matrix components that may interfere at different points in an assay and to varying extents, plasma usually contains more interferences than other biological fluids.

In addition to the influence of matrix components, the ESI signal is also affected by several factors: such as mobile phase composition, exogenous materials, and ion source configuration. Volatile mobile phase additives and ion-pairing reagents have been studied for their ion suppression or enhancement effects. The typical reason for using a mobile phase modifier in LC-MS/MS is to increase the buffer capacity in order to achieve reproducible retention times or to improve the chromatographic separation of basic compounds by forming pseudo-neutral ion pairs. Typical mobile phase additives such as: formic acid, ammonium hydroxide and ammonium formate, as well as the fraction of organic solvent (methanol or acetonitrile) in the mobile phase, have been evaluated for their effects on analyte MS response in both positive and negative ionization modes [28-31]. Although a wide disparity has been observed among the analytes studied, all MS responses decrease when additive concentrations are increased to mM levels regardless of the additive type. It was concluded that analyte ESI MS response was compound dependent, and that mobile phase composition affects the formation of ionic species. An optimal LC-MS assay must have a balance between LC performance and ESI efficiency. Ion-pair reagents are widely used as mobile phase modifiers in HPLC/UV assays to improve peak shapes and chromatographic resolution. However, when used for LC-MS analysis, ionization suppression effects are observed. Case studies include trifluoroacetic acid (TFA) and tetra-alkylammonium salts [31-34]. The strong ionization suppression effect of TFA was attributed to the formation of "neutral" ion pairs between the TFA anion and the protonated analyte cation, which prevents ion ejection from the electrospray droplet. One solution to this problem is to use weaker acids instead of TFA or to use post-column addition of mobile phase modifiers such as isopropanol and

propionic acid to decrease surface tension [32,33]. The effects of di- and trialkylammonium acetates on separation efficiency and ion signal intensity have been compared to tetra-ammonium salts and ammonium acetate [34]. A similar strategy that utilizes mono- di- or trialkylammonium acetates to replace tetra-ammonium ions while retaining chromatographic performance was proposed to overcome the significant ion suppression effects of tetra-alkylammonium salts.

Exogenous materials employed during the course of sample collection, storage, and processing may also cause ionization suppression. In a typical pharmacokinetic study, serial blood samples are collected for drug ADME (absorption, distribution, metabolism and excretion) profile determination. Anticoagulant tubes containing Na-, K- and Li-heparin, and EDTA are used to prevent blood from coagulating during plasma sample processing. When the collected samples are stored and analyzed, different plastic wares such as pipette tips, tubes, and 96-well plates are used. In addition, during the early stages of drug discovery, potential drug candidates are dosed as a solution consisting of water and excipients such as: ethanol, polyethylene glycol 400 (PEG 400), propylene glycol, hydroxypropyl β-cyclodextrin, and polysorbate 80 (Tween 80) [35]. The potential for the anticoagulants, polymeric materials in plastic wares [36-38], and dosing vehicle excipients [39,40] to produce matrix effects has been examined. It was demonstrated that analytes containing different types of anticoagulant or prepared by using different brands of plastic ware generated variable responses [36]. Interferences derived from excipients, particularly the polymeric vehicles PEG 400 and Tween 80, significantly suppressed signal intensities [39], which resulted in a 2-5 fold increase in plasma clearance values [40]. To minimize exogenous matrix effects, a single brand of plastic ware should be

used throughout the assay. Enhanced sample purification and chromatographic separation were suggested to reduce the effects derived from anticoagulants and excipients.

Ion source geometry is another important factor that can affect ionization. The general dependence for the degree of ionization suppression on instrumental configuration is: Z-spray < orthogonal spray < linear spray [34,41]. Depending on the compound, using a mass spectrometer designed by a different vendor may reduce matrix interferences [36].

1.3 Matrix Interference Characterization

The importance of matrix effects in LC-MS applications has been widely discussed and it has been concluded that these effects should be evaluated for each newly developed LC-MS assay [42,43]. However, there are no standardized experiments or evaluation criteria for verifying that matrix effects have been effectively eliminated from an assay method. Several approaches, including: blank extract addition, post-column infusion, and multiple-batch precision have been proposed as methods to study ionization suppression. In the blank extract addition approach, target analyte is spiked with neat solvent and with control biofluid extract, which is a blank fluid processed by using the sample extraction procedure. The prepared solutions are measured simultaneously by either flow injection analysis [44,45] or chromatographic separation [22,23,46,47]. The MS signal for the neat standard is employed as a benchmark and the magnitude of the matrix effect is determined by the response ratio of analyte in neat solvent to analyte in the control extract. Because the prepared solutions are injected without an HPLC column in flow injection analysis, results reflect the total effects of extracted matrix components on the analyte signal. This approach can be used to compare the effectiveness of different

sample extraction techniques for reducing matrix effects. Chromatographic separation can be used instead of an extraction to minimize ionization suppression effects.

Whereas the blank extract addition method provides quantitative information about matrix effects, semi-quantitative post-column infusion offers a dynamic overview of this effect [44,45,48,49]. This method uses an infusion pump to deliver a constant flow of target analyte into HPLC eluent via a mixing tee located before the mass spectrometer ion source. Because the rate of analyte introduction is constant, a steady MS response should be observed in the absence of interferences. A variation in the analyte signal indicates the existence of matrix interferences. The effect of background material on analyte MS response is measured throughout the entire chromatographic run and the regions where matrix effects are significant can be detected.

Although the blank extract addition and post-column infusion methods are able to confirm the presence or absence of matrix effects, they do not provide enough detailed information to be useful for examining the mechanisms responsible for the matrix effects. In clinical trials, biofluid samples are collected from a large number of patients and healthy people, and the matrix composition is highly variable among subjects. Therefore, the single batch addition or infusion methods cannot elucidate the matrix issues for all of the studied subjects. To address matrix variability, the approach of multiple-batch precision is proposed [50,51]. Target analyte is prepared in 5 different batches of control extract at concentrations spanning the assay range. A precision (n=5) of less than 10% (relative standard variation) and accuracy within 15% for all analyte samples indicates acceptable minimization of matrix effects.

1.4 Solutions to the Matrix Interference Problem

Because the matrix effect is caused by co-eluting interfering components, the straight forward strategy to minimize this effect is to reduce the amount of interfering materials introduced to the mass spectometer ion source or to separate them from analytes before MS analysis. Efficient chromatographic separation, selective sample preparation, and combinations of these two approaches have been attempted. The classic biological sample preparation techniques are PP, LLE, and SPE [52-54]. Two-dimensional chromatography (2D-LC) utilizing column switching to isolate and analyze samples online is another sample processing method. Because of the advantage of being able to automate sample analysis procedures, online extraction is becoming an attractive choice for sample processing [4,5]. Although the "dilute and shoot" PP procedure is considered to be a relatively dirty method compared to LLE and SPE, this simple and fast sample pretreatment technique is still the primary choice for drug discovery due to high sample throughputs.

The use of ultra-fast gradient (mobile phase changing from 95% aqueous to 95% organic solvent in less than 2 min) HPLC has been compared to typical fast isocratic LC (more than 70% organic solvent at flow rate of 1 mL/min) for minimizing matrix effects after PP sample preparation [55,56]. The use of a rapid gradient is superior to fast isocratic LC. Although the best method for reducing matrix effects is by specific extraction, this costs more sample handling time and may not always be an acceptable option. The advantages of using gradient elution are: first, allowing at least partial separation of target analyte from endogenous components, especially non-retained inorganic salts or other hydrophilic components; second, preventing run-to-run interferences resulting from late eluting compounds by washing the column with a strong

solvent at the end of each injection. Utilizing a more selective chromatographic separation to reduce the chances for the analyte to co-elute with interferences has been used by many researchers. It generally involves decreasing the percentage of strong solvent in isocratic LC or reducing the initial content of organic solvent in gradient LC in order to enhance the HPLC column resolution. A progressive increase in analyte signals for both muscle tissues and organ samples has been detected when mobile phase gradient strength is gradually decreased. These results suggest that undesired ionization suppression effects were satisfactorily eliminated by chromatographic separation [57,58]. Similarly, a crossover comparison has been conducted for 27 pharmaceutical compounds derived from microsomal incubation. These analytes were treated with generic PP or SPE and subsequently analyzed by flow injection analysis or fast gradient LC. When SPE was used, the average matrix effect for these analytes was greatly reduced. Comparable results were obtained by using the fast gradient separation, but no further improvement was achieved for the combination of SPE and fast gradient LC separation [59].

The improvement of assay performance associated with extraction selectivity has demonstrated the importance of specific sample preparation methods for matrix effect reduction. When a LLE was conducted prior to SPE to achieve a more selective extraction, and a pH adjusted eluting solvent was employed, both the signal to noise ratio and assay reproducibility were significantly increased. An additional column wash step to remove late eluting interferences has also been found to contribute to a reduction of matrix effects [60]. In another case, after serum samples were treated with generic sample preparations methods: LLE, mixed mode SPE, PP, and a combination of PP with mixed mode SPE, samples prepared by the mixed mode SPE were found to exhibit less

ionization suppression for the two compounds tested [61]. It should be noted that the choice of SPE sorbents is an important factor that can affect the suppression effect. Different plasma suppression effects were detected for analyses with a mixed mode cation exchange, anion exchange SPE, and an Oasis HLB (Hydrophilic-Lipophilic-Balanced copolymer) with different washes [31]. Likewise, polydivinylbenzene (PDVB) cartridges demonstrated less ionization suppression than C_{18} for assay of an illegal growth promoter in urine samples. Due to greater hydrophobic character and additional π-π interaction possibilities, PDVB permits a more effective cleanup of interfering materials and ionization suppression is significantly decreased [62].

2D-LC utilizes the separation power of two columns for sample measurements. Most online 2D-LC operations involve an extraction column for sample cleanup and an analytical column for chromatographic separation. Samples are loaded onto the extraction column to remove matrix components; afterwards, the retained analytes are transferred to the analytical column for chromatographic separation via back flushing. The extraction column can be either a regular small particle packed reversed phase column operated at laminar flow or a large particle filled turbulent flow column used under ultra fast flow. Online 2D-LC equipped with various lengths of C_{18} and RAM (restricted access media) extraction columns have been used for analyzing water diluted and PP plasma samples. For three analytes, application of online 2D-LC sample cleanup significantly reduced the signal suppression effect compared to direct injection analysis using a single column [63]. A similar reduction in matrix effects has been observed in post-column infusion mass spectrometry when an optimized 2D-LC method using a reversed phase extraction column was employed for tissue sample analyses [64,65]. Few reports have been

published regarding the use of turbulent flow extraction. One article described the use of a RAM column, two large particle packed columns, and a monolithic column to extract water diluted and PP plasma at fast flow rates. Due to the relatively large column ID, the loading rate used may not have been sufficient to achieve turbulent flow or eddy formation. Post-column infusion mass spectra indicated that PP processed plasma exhibited a substantial decrease in matrix effects relative to water diluted plasma samples [66]. However, the characteristics of each extraction column and the optimized extraction parameters for the procedure were not given.

In addition to enhancing the specificity and selectivity of sample analysis, other options for eliminating matrix interferences are: internal standard (ISTD) compensation, ion source alteration, and nano-spray utilization. In LC-MS/MS quantification, the most common method is using an ISTD to account for matrix interferences [67-72]. If the matrix affects the analyte and ISTD equally, the response ratio (analyte/ISTD) would be expected to be unaffected even when their absolute responses are greatly impacted. A major drawback to using this approach is the requirement that the ISTD must be very similar to the analyte. An ideal ISTD should be able to exactly match the ionization properties of the analyte under various matrix compositions. A stable isotope labeled ISTD normally works better than a structural analogue. However, if the analyte and ISTD do not co-elute, the two compounds may be subjected to different ionization environments, which mostly likely would result in different ionization suppression effects [73,74]. The reported observation of unacceptable matrix effects during analysis of human urine samples by using a hepta-deuterated ISTD demonstrates that the stable isotope ISTD method may not always guarantee a constant analyte/ISTD response ratio

[45]. In addition to difficulties in obtaining isotopic ISTDs, especially during the early stages of drug development, an ISTD must have high purity and integrity [75]. Unlabeled impurities and incompletely converted materials contribute to analyte concentration and significant deviations can be observed, particularly at low analyte concentrations. The use of an ISTD, while highly desirable, is not necessarily the best route for minimizing the ionization suppression effect. If ionization suppression significantly reduces the analyte signal, assay sensitivity may be compromised and consequently the accuracy and precision of the method will be affected [76]. Therefore, ionization suppression effects should be investigated even if an ISTD is employed in the assay. As stated previously, a suitable ISTD should possess chromatographic and ionizing properties that are comparable to the analyte. Thus, when multiple analytes with varying degrees of polarity are measured, appropriate ISTDs should be used for each analyte. During routine sample analysis, the absolute ISTD responses in unknown samples can be monitored to detect matrix effect variability.

Another practical approach for removing matrix effects is by changing the ionization source. Although matrix effects have potential deleterious impacts on both ESI and APCI, the effect appears to be more pronounced with ESI than with APCI [17-20]. Information regarding APCI ionization suppression mechanisms is very limited. APCI ionization occurs through gas phase proton transfer (positive ion mode) [77,78], during which analyte molecules collide with reagent ions, which are created by corona discharge initiated sequential ion/molecule reactions of vaporized solvents. The mass spectrometer signal intensity is determined by the analyte structure and the solvents employed [79]. However, it should not be assumed that using APCI removes matrix effects. There are

reports of an ionization suppression effect when APCI was employed [80-82]. These were attributed to the effects of matrix components on proton transfer efficiencies in either liquid or gas phases. Due to the APCI limitation that the analyte must be thermally stable and readily ionized, APCI is usually employed only after confirming that ESI results in unacceptable matrix interferences [83,84].

Nanoelectrospray ionization (nano-ESI), which employs a sprayer with a micrometer size tip and is characterized by a flow rate ranging from tens to hundreds of nL/min has been shown to increase assay sensitivity and reduce ionization suppression [85,86]. The advantages of nano-ESI are attributed to the reduction of the initial droplet size during the spraying process [87,88]. The smaller droplets need fewer solvent evaporation shrinkage steps and Coulomb fissions before gas phase ions are formed. Along with the droplet size, other parameters including: surface to volume ratio, ion current, and excess surface charge are also substantially different. Consequently, ionization efficiency is increased and the analyte ionization suppression effect is reduced. Nano-ESI has been applied to biological sample quantitative analysis. An LC-MS/MS method for dialysis samples has been downscaled to nano-dimensions by using a nano-column (ID: 75 μm) coupled with a nanosprayer ion source. Compared with capillary chromatography analysis and microbore column switching methods, the nano-LC-MS/MS assay was superior in terms of sensitivity, matrix effects, and accuracy and precision [89]. Nano-ESI has also been used for direct infusion analysis. In the absence of chromatographic separation, sample extracts were directly infused into the mass spectrometer via a chip based nano-ESI emitter, which is an array of nozzles with diameters in the micrometer range fabricated on a silicon chip [90,91]. Although the

14

analyte was not resolved from matrix components, removal of the ionization suppression effect was demonstrated by the fact that reasonable assay variations were obtained. The inherent benefit of nano-ESI on MS response and reduction of ionization suppression effects has also been demonstrated by reducing the flow rate from 200 to 0.1 µL/min by using a post-column nanoflow splitting device [92]. Both the absolute signal and signal variation were improved when the nano-splitter was employed. The major barriers to the widespread use of nano-ESI are feasibility and reproducibility. Practical difficulties with leakage and blockage and difficulties during installation and troubleshooting have emerged due to miniaturization. Because the shape and aperture size of the spray tip dramatically affect the size of primary droplets, which determines the analyte signal intensity and the relative ionization efficiency of droplet components, the main challenge for using nano-ESI to conduct quantitative measurements is the requirement for high sprayer reproducibility.

1.5 Understanding the Nature of Matrix Interferences

In order to propose an effective solution to matrix effect problems, it is essential to understand the nature of ionization suppression in ESI. Because of the complexity of transferring molecules from solution to the gas phase, a complete understanding of the mechanisms involved in ESI gas phase ion production is not available. Although much research has been conducted to investigate ESI processes, it is difficult to obtain a fundamental model to use for predicting the mutual influence of solvent and undetected components on analyte ionization. The first quantitative explanation of the dependence of analyte ion intensity on its solution phase concentration and the presence of other electrolytes was proposed by Tang and Kebarle. It was based on competitive processes

during gas phase ion formation [93,94]. It was observed that the analyte ion signal decreased as the concentration of other electrolytes increased and the extent of this decrease depended on the nature of the electrolyte, which was represented by coefficient k. By choosing a buffer with a low coefficient, the adverse effects of the buffer on analyte detection could be minimized. A general ion competition process was described in more detail in the ion partitioning model [95]. In this model, droplet components compete for a fixed amount of surface charge. It was postulated that equilibrium exists between the charged surface and the neutral interior phase of the ESI droplets. The equilibrium constant for an analyte, which is determined by several parameters, including: solvent energy, charge density, and hydrophobicity, determines the surface affinity of a given ion. The analyte MS response is proportional to its surface concentration. To verify the validity of this model, the following studies were conducted: the effect of salt concentration on analyte MS response was measured and compared to the predicted effect based on the equilibrium partitioning model [96]; the relationship between the analyte surface affinity and its non-polar character, which was measured according to chromatographic retention times, was investigated by using small peptides [97,98]; and the equilibrium partitioning concept was expanded to include the uneven fission of offspring droplets from the initial droplet [99]. A simple method for determining the relative equilibrium constant for analyte and electrolyte ions was proposed for this model [100], and the effects of electrophoretic mobility, viscosity, ion pairing and ionic strength on analyte surface affinity and subsequent ESI response have been examined [101,102]. The correlation between measured ESI linear dynamic range and theoretical predictions based on the excess charge capacity illustrates the importance of charge competition

16

processes in quantitative assays [103]. Although many analyte MS response properties, which were studied in the presence of various electrolytes and co-analytes, have been explained, confirming this ESI model will be a challenge because of factors such as: stability of the spray current, analyte multiplicities, the formation of cluster ions and fragmentation ions, as well as the interdependencies of these parameters.

Because abundant protonated ions are produced from basic solutions [104] and deprotonated ion are produced from acidic solutions [105], the effects of gas phase proton transfer reactions on analyte ESI response has been investigated as another potential cause of ionization suppression. It was observed that the introduction of solvent vapor with a higher gas phase proton affinity caused more signal suppression than for a solvent with a relatively lower proton affinity, and the dominate signal from a mixed solvent was derived from the protonated solvent with the higher proton affinity [106]. When weak acids were added to solutions, the analyte negative ESI response increased. This phenomenon was attributed to the higher gas phase proton affinity for the acid's anions [107]. The studies of the ionization dependence of a weak base on electrospray voltage also revealed the importance of gas phase chemical ionization on ESI response [108]. However, contradictory results were reported by other researchers. Experiments designed to investigate ESI droplet ionization pathways by using biological extracts have shown that the reactions that occur after gas phase ion formation do not significantly affect analyte MS response. The presence of nonvolatile or less volatile solutes, which changes the properties of the sprayed droplets, was cited as the most likely cause of ionization suppression [109]. Whether the matrix effect is caused by the competition in solution phase for excess charge at the droplet surface or by proton transfer in the gas phase, the

chemical nature of the analyte has a significant effect on the magnitude of the matrix interferences.

1.6 Research Objectives

Matrix interferences are not directly observed in the analyte chromatograms, but they have a deleterious impact on the accuracy and precision of sample analysis, which might result in incorrect results. Compared to mobile phase additives and exogenous materials added during the sample handling process, the effects from the endogenous components are more significant because of the highly heterogeneous nature of the samples typically studied for drug analysis. Unfortunately, the current understanding of ionization suppression effects caused by endogenous materials and strategies for eliminating these effects are inadequate. Human plasma is the most common matrix utilized for clinical pharmacokinetic studies and almost all published articles dealing with quantitative LC-ESI-MS/MS plasma analysis attribute matrix interferences to endogenous components such as salts, amines, and fatty acids in general. Further investigation to determine the specific identities of the interfering compounds and to elucidate the interfering mechanism for each of these compounds is needed. It is not practical to propose a method for reducing matrix interferences without first knowing the identities of the interfering materials. Because selective extraction methods are designed based on target analyte property considerations, they may not suitable for eliminating matrix components. Likewise, mobile phase modifications designed to improve chromatographic separation generally require longer analysis times and may not always solve the problem. Although the post-column infusion approach provides an opportunity to shift the analyte elution time in order to minimize overlap with co-eluting background

compounds, adjusting LC conditions involves the same dilemma encountered with selective extraction. Modified chromatographic conditions may alter the interfering component retention and result in a time shift similar to that for analytes. Because post-column infusion optimization must be repeated every time the chromatographic conditions are modified, it is very tedious and labor intensive. In addition, MS responses vary with the changing mobile phase composition, resulting in matrix effect masking. The use of ISTDs may compensate for matrix interferences, but assay sensitivity will still be affected due to analyte signal suppression.

To eliminate or minimize the matrix effect, the source of the interfering components must be considered regardless of whether the interfering species are from the current sample matrix or from late eluting substances from previously injected samples. Because phospholipids are abundant in plasma and vary considerably between individuals, there is interest in testing these substances to see if they are responsible for matrix interferences. Soon after a report that phosphatidylcholine lipids can affect analyte ionization [110,111], approaches to minimize this effect by sample pretreatment and to monitor the behavior of these materials during assay development were described [112,113]. It was found that cation exchange SPE was significantly better than mixed mode SPE for phospholipid removal although the reason for choosing the *m/z* of 522 → 184 transition to represent phospholipids in plasma was not specified [112]. An in-source MRM (multiple reaction monitoring) method has been suggested as a means of detecting the elution of phosphatidylcholine lipids by generating a common fragment ion (*m/z* 184) in the mass spectrometer ion source and monitoring the 184 → 184 MRM transition [113]. It is very likely that phospholipids are a major source of matrix interferences

encountered in plasma analysis because of their abundance, polarity, and sample-to-sample concentration variability. Inorganic salts are well known to suppress the intensities of analyte ions, but they are not retained on reversed phase HPLC columns and should be separated from the analytes. Macromolecules such as proteins have a tendency to accumulate on the stationary phase and result in column deterioration. If they were the main source of matrix effects, distorted chromatographic peaks and increased column back pressure would be associated with the ionization suppression. However, when matix effects are detected, no abnormal analysis conditions are observed. Phospholipids with a polar head and non-polar fatty acids are difficult to remove by sample treatment or chromatographic separation because they can partition between polar and non-polar phases like the analyte and their polarity varies with their fatty acid chain length. In addition, they are typically present at concentrations that are much higher than those of target analytes. Thus, even the amounts remaining after extraction procedures might be sufficient to cause matrix interferences.

The aim of this research is to provide insight into the origin, removal, and mechanism of matrix interferences in clinical laboratory biofluid assays and to propose approaches for overcoming matrix effect problems in quantitative LC-ESI-MS/MS methodologies. Human plasma was selected as the biological fluid for this research because it is widely used in clinical studies. The role of phospholipids in ionization suppression will be examined and the primary interfering lipids will be identified. Novel sample handling techniques including high turbulent flow liquid chromatography (HTLC) and online extraction coupled with ultra high performance liquid chromatography (UPLC) will be compared to conventional LLE in terms of their abilities

to reduce observed matrix effects. SPE was not examined because this approach is normally used as a replacement for LLE. Characterized by high separation efficiency at fast flow rates, turbulent flow LC possesses a performance profile beyond the description of the van Deemter plot, where the reduced plate height decreases with increasing flow rate. The HTLC technique was recently employed for extracting biological samples by utilizing its unique mass transfer features to rapidly separate macromolecules from desired analytes. UPLC employs small particle packed columns to shorten the diffusion path lengths of molecules in order to achieve improved resolution. After many years of pioneering work, a commercial instrument (Waters) is now available which can tolerate a back pressure up to 15000 psi with a column filled with 1.7 μm particles. Because both of the selected techniques have the capability to reduce sample handling time and to increase assay throughput, they both will likely become valuable tools for quantitative analysis. In this research, the capabilities of these two techniques for reducing bioassay matrix effects derived from endogenous materials will be explored in detail. In addition, the influence of mobile phase additives, co-analytes, and the identified endogenous components responsible for interferences on analyte ionization during ESI will be investigated. Results obtained by these experiments will help elucidate matrix interference mechanisms. This information may also be helpful for modifying the existing ESI ionization models, which are currently not able to explain the MS responses obtained from complicated clinical samples. The practical goals of this research are to learn how matrix interferences occur in clinical assays and to develop improved LC-ESI-MS/MS assay methods for biological sample analysis.

1.7 References

[1] Doles, M.; Mack, L. L.; Hines, R. L.; Mobley, R. C.; Ferguson, L. D.; Alice, M. B. *J. Chem. Phys.* **1968**, 49, 2240

[2] Yamashita, M.; Fenn, J. B. *J. Chem. Phys.* **1984**, 88, 4451

[3] Ackermann, B. L.; Berna, M. J.; Murphy, A. T. *Curr. Topics Med. Chem.* **2002**, 2, 53

[4] Hopfgartner, G.; Bourgogne, E. *Mass Spectrom. Rev.* **2003**, 22, 195

[5] Mohammed, J.; Xia, Y. *Curr. Drug Met.* **2006**, 7, 491

[6] Lagerwerf, F. M.; van Dongen, W. D.; Steenvoorden, R. J. J. M; Honing, M.; Jonkman, J. H. G. *Trends Anal. Chem.* **2000**, 19, 418

[7] Brewer, E.; Henion, J. *J. Pharm. Sci.* **1998**, 87, 395

[8] Dooley, C. K. *Biochem.* **2003**, 36, 471

[9] Taverniers, I.; De Loose, M.; Van Bockstaele, E. *Trends Anal. Chem.* **2004**, 23, 535

[10] Taylor, P. J. *Clin. Biochem.* **2005**, 38, 328

[11] Jessome, L. L.; Dietrich, A. V. *LC • GC Nor. Am.* **2006,** 24, 498

[12] Antignac, J.; de Wasch, K.; Monteau, F.; De Brabander, H.; Andre, F.; Le Bizec, B. *Anal. Chim. Acta* **2005**, 529, 129

[13] Tiller, P. R.; Romanyshyn, L. A. *Rapid Commun. Mass. Spectrom.* **2002**, 16, 92

[14] Basilicata, P.; Miraglia, N.; Pieri, M.; Acampora, A.; Soleo, L.; Sannolo, N. *J. Chromatogr. B* **2005**, 818, 293

[15] Zrostlíková, J.; Hajlová, J.; Poustka, J.; Begany, P. *J. Chromatogr. A* **2002**, 973, 13

[16] Kloepfer, A.; Quintana, J. B.; Reemtsma, T. *J. Chromatogr. A* **2005**, 1067, 153

[17] Schuhmacher, J.; Zimmer, D.; Tesche, F.; Pickard, V. *Rapid Commun. Mass Spectrom.* **2003**, 17, 1950

[18] Souverain, S.; Rudaz, S.; Veuthey, J. *J. Chromatogr. A* **2004**, 1058, 61

[19] Smeraglia, J.; Baldrey, S. F.; Waston, D. *Chromatographia* **2002**, 55, S95

[20] Hsieh, Y.; Chintala, M.; Mei, H.; Agans, J.; Brisson, J.; Ng, K.; Korfmacher, W. A. *Rapid Commun. Mass Spectrom.* **2001**, 15, 2481

[21] Department of Health and Human Services, Food and Drug Administration, *Guidance for Industry on Bioanalytical Method Validatioon. Fed. Regist.* 2001, 66 (100), 28526

[22] Buhrman, D. L.; Price, P. I.; Rudewicz, P. J. *J. Am. Soc. Mass Spectrom.* **1996**, 7, 1099

[23] Matuszewski, B. K.; Constanzer, M. L.; Chavez-Eng, C. M. *Anal. Chem.* **1998,** 70, 882

[24] Qin, C. J.; Reimer, M. T.; El-Shourbagy, T. A. *J. Chromatogr. B* **2004**, 805, 67

[25] Qi, L.; Danielson, N. D. *J. Pharm. Biomed. Anal.* **2005**, 37, 225

[26] Fu, I.; Woolf, E. J.; Matuszewski, B. K. *J. Pharm. Biomed. Anal.* **1998**, 18, 347

[27] Dams, R.; Huestis, M. A.; Lambert, W. E.; Murphy, C. M. *J. Am. Soc. Mass Spectrom.* **2003**, 14, 1290

[28] Temesi, D.; Law, B. *LC • GC Nor. Am.* **1999,** 17, 626

[29] Zhou, S.; Hamburger, M. *Rapid Commun. Mass Spectrom.* **1995,** 9, 1516

[30] Kamel, A.; Brown, P. R.; Munson, B. *Anal. Chem.* **1999**, 71, 5481

[31] Mallet, C. R.; Lu, Z.; Mazzeo, J. R. *Rapid Commun. Mass Spectrom.* **2004**, 18**,** 49

[32] Kuhlmann, F. E.; Apffel, A.; Fischer, S. M.; Goldberg, G.; Goodley, P. C. *J. Am. Soc. Mass Spectrom.* **1995**, 6, 1221

[33] Apffel, A.; Fischer, S. M.; Goldberg, G.; Goodley, P. C. ; Kuhlmann, F. E. *J. Chromatogr. A* **1995**, 712, 177

[34] Holčapek, M.; Volná, K.; Jandera, P.; Kolářová, L.; Lemr, K.; Exner, M.; Cǐrkva, A. *J. Mass Spectrom.* **2004**, 39, 43

[35] Fort, F. L.; Heyman, I. A.; Kesterson, J. W. *J. Parenter. Sci. Technol.* **1984**, 38, 82

[36] Mei, H.; Hsieh, Y.; Nardo, C.; Xu, X.; Wang, S.; Ng, K.; Korfmacher, W. *Rapid Commun. Mass Spectrom.* **2003**, 17, 97

[37] Xia, Y.; Patel, S.; Bakhtiar, R.; Franklin, R. B.; Doss, D. A. *J. Am. Soc. Mass Spectrom.* **2005**, 16, 417

[38] Chin, C.; Zhang, Z. P.; Karnes, H. T. *J. Pharm. Biomed. Anal.* **2004**, 35, 1149

[39] Shou, W. Z.; Weng, N. *Rapid Commun. Mass Spectrom.* **2003**, 17, 589

[40] Tong, X.; Wang, J.; Zheng, S.; Pivnichny, J. V.; Griffin, P. R.; Shen, X.; Donnelly, M.; Vakerich, K.; Nunes, C.; Fenyk-Melody, J. *Anal. Chem.* **2002**, 74, 6305

[41] Marvin, L. F.; Delatour, T.; Tavazzi, I.; Fay, L. B.; Cupp, C.; Guy, P. A. *Anal. Chem.* **2003**, 75, 261

[42] Rogatsky, E.; Stein, D. *J. Am. Soc. Mass Spectrom.* **2005**, 16, 1757

[43] Shah, V. P.; Midha, K. K.; Findlay, J. W. A.; Hill, H. M.; Hulse, J. D.; McGilveray, I. J.; McKay, G.; Miller, K. J.; Patnaik, R. N.; Powell, M. L.; Tonelli, A.; Viswanathan, C. T.; Yacobi, A. *Pharm. Res.* **2000**, 17, 1551

[44] Bonfiglio, R.; King, R. C.; Olah, T. V.; Merkle, K. *Rapid Commun. Mass Spectrom.* **1999**, 13 1175

[45] Miller-stein, C.; Bonfiglio, R.; Olah, T. V.; King, R. C. *Am. Pharm. Rev.* **2000**, 54,

[46] Polson, C.; Sarkar, P.; Incledon, B.; Raguvaran, V.; Grant, R. *J. Chromatogr. B* **2003**, 785, 263

[47] Mohammed, J.; Schuster, A.; Whigan, D. B. *Rapid Commun. Mass Spectrom.* **2003**, 17, 1723

[48] Souverain, S.; Rudaz, S.; Veuthey, J. *J. Pharm. Biomed. Anal.* **2004**, 35, 913

[49] Hsieh, Y.; Wang, G.; Wang, Y.; Chackalamanni, S.; Brisson, J.; Korfmacher, W. A. *Rapid Commun. Mass Spectrom.* **2002**, 16, 944

[50] Avery, M. J. *Rapid Commun. Mass Spectrom.* **2003**, 17, 197

[51] Matuszewski, B. K.; Constanzer, M. L.; Chavez-Eng, C. M. *Anal. Chem.* **2003**, 75, 3019

[52] Thurman, E. M.; Mills, M. S. *Solid-Phase Extraction: Principles and Practice*, Wiley, New York, 1998

[53] Wells, D. A. *High Throughput Bioanalytical Sample Preparation: Methods and Automation Strategies,* Elsevier Science, 2003

[54] Henion, J.; Brewer, E.; Rule, G. *Anal. Chem.* **1998**, 70, 650A

[55] Tiller, P. R.; Romanyshyn, L. A. *Rapid Commun. Mass Spectrom.* **2002**, 16, 92

[56] Romanyshyn, L. A.; Tiller, P. R.; Alvaro, R.; Pereira, A.; Hop, C. *Rapid Commun. Mass Spectrom.* **2001**, 15, 313

[57] Bogialli, S.; Curini, R.; Corcia, A. D.; Nazzari, M.; Samperi, R. *Anal. Chem.* **2003**, 75, 1798

[58] Bogialli, S.; Curini, R.; Corcia, A. D.; Nazzari, M.; Sergi, M. *Rapid Commun. Mass Spectrom.* **2003**, 17, 1146

[59] Zheng, J. J.; Lynch, E. D.; Unger, S. E. *J. Pharm. Biomed. Anal.* **2002**, 28, 279

[60] Smeraglia, J.; Baldery, S. F.; Waston, D. *Chromatographia* **2002**, 55, Suppl., S95

[61] Müller, C.; Schäfer, P.; Störtzel, M.; Vogt, S.; Weinmann, W. *J. Chromatogr. B* **2002**, 773, 47

[62] van Hout, M. W. J.; Hofland, C. M.; Niederländer, H. A. G.; de Jong, G. J. *Rapid Commun. Mass Spectrom.* **2000**, 14, 2103

[63] Pascoe, R.; Foley, J. P.; Gusev, A. I. *Anal. Chem.* **2001**, 73, 6014

[64] Heinig, K.; Bucheli, F. *J. Chromatogr. B* **2002**, 769, 9

[65] Choi, B. K.; Hercules, D. M.; Gusev, A. I. *J. Chromatogr. A* **2001**, 907, 337

[66] Marchi, I.; Rudaz, S.; Selman, M.; Veuthey, J. *J. Chromatogr. B* **2007**, 845, 244

[67] Jacob, P. III; Wilson, M.; Yu, L.; Mendelson, J.; Jones, R. T. *Anal. Chem.* **2002**, 74, 5290

[68] Tai, S. S.-C.; Welch, M. J. *Anal. Chem.* **2005**, 77, 6359

[69] Bicker, W.; Lammerhofer, M.; Keller, T.; Schuhmacher, R.; Krska, R.; Lindner, W. *Anal. Chem.* **2006**, 78, 5884

[70] Sin, D. W.; Wong , Y.; Ip, A. C. *J. Pharm. Biomed. Anal.* **2004**, 34, 651

[71] Zhang, J. Y.; Fast, D. M.; Breau, A. P. *J. Chromatogr. B* **2003**, 785, 123

[72] Chi, C.; Liang, L.; Padovani, P.; Unger, S. *J. Chromatogr. B* **2003**, 785, 163

[73] Kitamura, R.; Matsuoka, K.; Matsushima, E.; Kawaguchi, Y. *J. Chromatogr. B* **2001**, 754, 113

[74] Wang, S.; Cyronak, M.; Yang, E. *J. Pharm. Biomed. Anal.* **2007**, 43, 701

[75] Chavez-Eng, C. M.; Constanzer, M. L.; Matuszewski, B. K. *J. Chromatogr. B* **2002**, 767, 117

[76] Sojo, L. E.; Lum, G.; Chee, P. *Analyst* **2003**, 128, 51

[77] Thomson, B. A. *J. Am. Soc. Mass Spectrom.* **1998**, 9, 187

[78] Sunner, J.; Nicol, G.; Kebarle, P. *Anal. Chem.* **1988**, 60, 1300

[79] Kolakowski, B. M.; Grossert, J. S.; Ramaley, L. *J. Am. Soc. Mass Spectrom.* **2004**, 15, 311

[80] Liang, H.; Foltz, R. L.; Meng, M.; Bennett, P. *Rapid Commun. Mass Spectrom.* **2003**, 17, 2815

[81] van Hout, M. W. J.; Niederländer, H. A. G.; de Zeeuw, R. A.; de Jong, G. J. *Rapid Commun. Mass Spectrom.* **2003**, 17, 245

[82] Sangster, T.; Spence, M.; Sinclair, P.; Payne, R.; Smith, C. *Rapid Commun. Mass Spectrom.* **2004**, 18, 1361

[83] Liang, H.; Takagaki, T.; Foltz, R. L.; Bennett, P. *J. Chromatogr. B* **2005**, 824, 36

[84] Keski-Hynnilä, H.; Luukkanen, L.; Taskinen, J.; Kostiainen, R. *J. Am. Soc. Mass Spectrom.* **1999**, 10, 537

[85] Wilm, M. S.; Mann, M. *Anal. Chem.* **1996**, 68, 1

[86] Juraschek, R.; Dűlcks, T.; Karas, M. *J. Am. Soc. Mass Spectrom.* **1999**, 10, 300

[87] Wilm, M. S.; Mann, M. *Int. J. Mass Spectrom. Ion Processes* **1994**, 136, 167

[88] Schmidt, A.; Karas, M.; Dűlcks, T. *J. Am. Soc. Mass Spectrom.* **2003**, 14, 492

[89] Lanckmans, K.; Eeckhaut, A. V.; Sarre, S.; Smolders, I.; Michotte, Y. *J. Chromatogr. A* **2006**, 1131, 166

[90] Dethy, J.; Ackermann, B. L.; Delatour, C.; Henion, J. D.; Schultz, G. A. *Anal. Chem.* **2003**, 75, 805

[91] Chen, J.; Yang, L.; Kapron, J. T.; Ma, L.; Pace, E.; Van Pelt, C. K.; Rudewicz, P. J. *J. Chromatogr. B* **2004**, 809, 205

[92] Gangl, E. T.; Annan, M.; Spooner, N.; Vouros, P. *Anal. Chem.* **2001**, 73, 5635

[93] Tang, L.; Kebarle, P. *Anal. Chem.* **1993**, 65, 3654

[94] Kebarle, P.; Tang, L. *Anal. Chem.* **1993**, 65, 972A

[95] Enke, C. G. Anal. Chem. **1997**, 69, 4885

[96] Constantopoulos, T. L.; Jackson, G. S.; Enke, C. G. *J. Am. Soc. Mass Spectrom.* **1999**, 10, 625

[97] Cech, N. B.; Enke, C. G. *Anal. Chem.* **2000**, 72, 2717

[98] Cech, N. B.; Krone, J. R.; Enke, C. G. *Anal. Chem.* **2001**, 73, 208

[99] Cech, N. B.; Enke, C. G. *Anal. Chem.* **2001**, 73, 4632

[100] Sjöberg, P. J. R.; Bökman, C. F.; Bylund, D.; Markides, K. E. *Anal. Chem.* **2001**, 73, 23

[101] Bökman, C. F.; Bylund, D.; Sjöberg, P. J. R.; Markides, K. E. *J. Am. Soc. Mass Spectrom.* **2006**, 17, 318

[102] Zhou, S.; Cook, K. D. *J. Am. Soc. Mass Spectrom.* **2001**, 12, 206

[103] Tang, K.; Page, J. S.; Smith, R. D. *J. Am. Soc. Mass Spectrom.* **2004**, 15, 1416

[104] Loo, J. A.; Udseth, H. R.; Smith, R. D. *Rapid Commun. Mass Spectrom.* **1988,** 2, 207

[105] Ferrer, I.; Thurman, E. M.; Barceló, D. *Anal. Chem.* **1997**, 69, 4547

[106] Amad, M. H.; Cech, N. B.; Jackson, G. S.; Enke, C. G. *J. Mass Spectrom.* **2000**, 35, 784

[107] Wu, Z.; Gao, W.; Phelps, M. A.; Wu, D.; Miller, D. D.; Dalton, J. T. *Anal. Chem.* **2004**, 76, 839

[108] Zhou, S.; Cook, K. D. *J. Am. Soc. Mass Spectrom.* **2000**, 11, 961

[109] King, R. C.; Bonfiglio, R.; Fernandez-Metzler, C.; Miller-Stein C.; Olah, T. *J. Am. Soc. Mass Spectrom.* **2000**, 11, 942

[110] Bennett, P. *American Association of Pharmaceutical Scientists (AAPS) Conference,* Salt Lake City, UT, Oct. 2003

[111] Ahnoff, M.; Hagelin, H. *American Society for Mass Spectrometry (ASMS) Conference,* Nashville, TN, May 2004

[112] Shen J. X.; Motyka, R. J.; Roach, J. P.; Hayes, R. N. *J. Pharm. Biomed. Anal.* **2005**, 37, 359

[113] Little, J. L.; Wempe, M. F.; Buchanan, C. M. *J. Chromatogr. B* **2006**, 833, 219

CHAPTER 2

EXPERIMENTAL

2.1 Chemicals and Reagents

Trimethoprim (free base, > 99 % purity), propanolol (HCl salt, > 99 % purity), Terfenadine (free base, > 99% purity), and niflumic acid (> 98% purity) were purchased from Sigma-Aldrich (St. Louis, MO, USA). n-Phenyl-succinamic acid (> 98% purity) was obtained from TimTec Corporation (Newark, DE, USA). All glycerophosphocholines (GPCho) (> 99 % purity), including: 1-palmitoyl-2-hydroxy-sn-glycero-3-phosphocholine, 1- stearoyl-2-hydroxy-sn-glycero-3-phosphocholine, 1-oleoyl-2-hydroxy-sn-glycero-3-phosphocholine, and 1-palmitoyl-2-linoleoyl-sn-glycero-3-phos-phocholine, were purchased from Avanti Polar Lipids, Inc. (Alabaster, AL, USA). The chemical structures, properties and abbreviations for these substances are shown in Tables 2-1 and 2-2. Human control sodium heparin plasma was obtained from the Biological Specialty Corporation (Colmar, PA, USA). All other chemicals, such as HPLC grade acetonitrile, methanol, tetrahydrofuran, acetone, methyl t-butyl ether, hexene, and ethyl acetate, as well as Certified A.C.S. Plus grade acetic acid, formic acid, ammonium hydroxide, ammonium acetate and sodium carbonate were obtained from Fisher Scientific (Pittsburgh, PA, USA). The water used was deionized water purified with a Milli-Q water purifying system (Millipore Corporation, Bedford, MA, USA).

Substances listed in Table 2-1 were stored in a 5°C refrigerator with desiccants; human control plasma and GPCho lipids (Table 2-2) were stored at -20°C in a freezer. The organic solvents, acids, and bases were separately stored in ambient fume cabinets.

Table 2-1. Chemical structures and physical properties of compounds used in this study
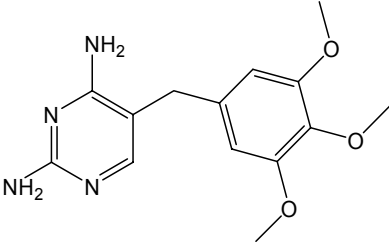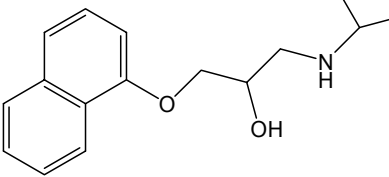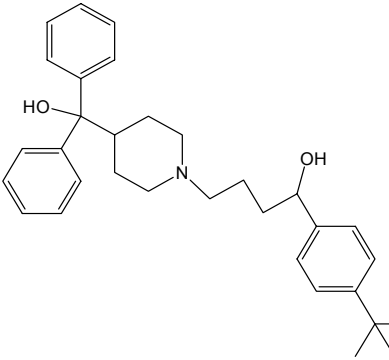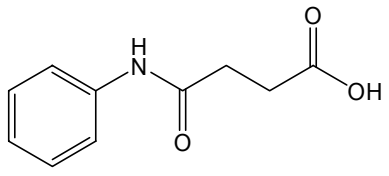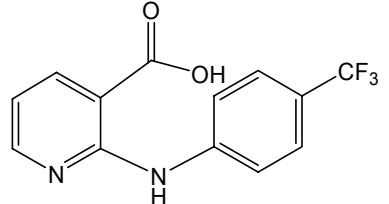
	Name	Structure	Property
B1	Trimethoprim 5-(3,4,5-trimethoxybenzyl) pyrimidine-2,4-diamine		Formula: $C_{14}H_{18}N_4O_3$ M.W.: 290.32 Exact Mass: 290.138 Log P: 1.43
B2	Propanolol 1-(isopropylamino)-3-(1-naphthyloxy)propan-2-ol		Formula: $C_{16}H_{21}NO_2$ M.W.: 259.35 Exact Mass: 259.157 Log P: 3.35
B3	Terfenadine 1-(4-tert-butylphenyl)-4-{4-[hydroxyl (diphenyl)methyl] piperidin-1-yl}butan-1 ol		Formula: $C_{32}H_{41}NO_2$ M.W.: 471.68 Exact Mass: 471.314 Log P: 6.96
A1	n-Phenyl-succinamic acid 4-anilino-4-oxobutanoic acid		Formula: $C_{10}H_{11}NO_3$ M.W.: 193.20 Exact Mass: 193.074 Log P: 0.61
A2	Niflumic acid 2-{[4-(trifluoromethyl) phenyl]amino}nicotinic acid		Formula: $C_{13}H_9N_2O_2F_3$ M.W.: 282.22 Exact Mass: 282.062 Log P: 3.36

Table 2-2. Chemical structures and physical properties of GPCho lipids

	Name, Properties and Structure
16:0 LPC	1-palmitoyl-2-hydroxy-*sn*-glycero-3-phosphocholine Formula: $C_{24}H_{50}NO_7P$ M.W.: 495.64 Exact Mass: 495.332
18:0 LPC	1-stearoyl-2-hydroxy-*sn*-glycero-3-phosphocholine Formula: $C_{26}H_{54}NO_7P$ M.W.: 523.69 Exact Mass: 523.364
18:1 LPC	1-oleoyl-2-hydroxy-*sn*-glycero-3-phosphocholine Formula: $C_{26}H_{52}NO_7P$ M.W.: 521.68 Exact Mass: 521.348
16:0-18:2 PC	1-palmitoyl-2-linoleoyl-*sn*-glycero-3-phosphocholine Formula: $C_{42}H_{80}NO_8P$ M.W.: 758.07 Exact Mass: 757.562

2.2 Equipment

2.2.1 Analytical Balance

A Sartorius MC 5 Microbalance (Data Weighing Systems, Inc., Elk Grove, IL, USA) was utilized to weigh all of the compounds for solution preparation. With a fully automatic calibration function, the microbalance was able to accurately weigh small amounts of samples (1 – 10 mg) with a precision of 3 significant figures.

2.2.2 Automatic Pipette

Liquid transfer was achieved by using an Eppendorf ® EDOS 5222 Electronic Dispensing System (Eppendorf North America Inc., New York, NY, USA). By changing the pipette adapter and Combi tip, the pipette was used for single dispensing and multiple dispensing with various aspirating and dispensing speeds. Volumes from 10 µL to 1000 µL for single liquids and up to 1/125 of the volume of Combi tip for multiple liquids could be dispensed by this apparatus.

2.2.3 Syringe Infusion Pump

An "11" Plus mode single syringe pump (Harvard Apparatus Inc., Holliston, MA, USA) with a 1 mL or 10 mL Hamilton Microliter syringe was employed to introduce sample solutions to the mass spectrometer. The flow rate, which depended on the inner diameter of the syringe, could be manually changed from the keyboard. Fluid with a constant flow rate could be accurately delivered from the syringe.

2.2.4 AB Sciex API 4000 Mass Spectrometer

A mass spectrometer is an instrument that measures the mass to charge (m/z) ratio of electrically charged gas phase ions. Mass spectrometry (MS) is an analytical technique that can be used for identification of unknown compounds, quantification of known

compounds, and elucidation of molecular structure features. LC-MS/MS is a combined

analytical technique consisting of liquid chromatography separation and triple quadrupole

mass spectrometric determination. The Applied Biosystems MDS SCIEX API 4000

(Ontario, Canada) mass spectrometer with Analyst 1.4 software was used for the research

described here (Fig. 2-1) [1].

Figure 2-1. Schematic of the API 4000 mass spectrometer
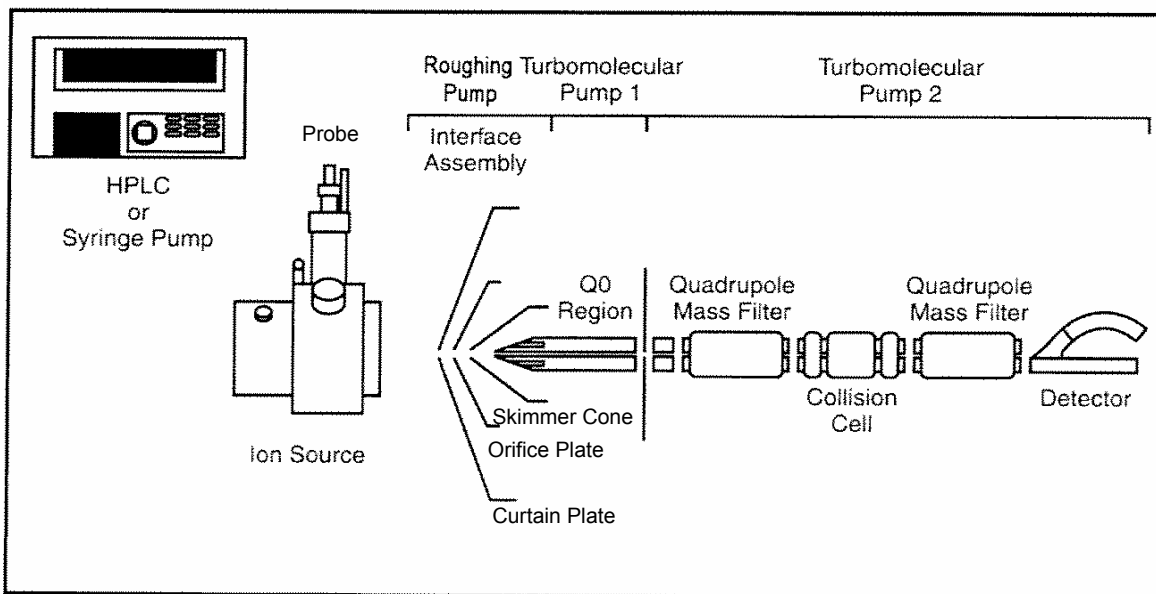
(Reprinted from the API 4000 hardware manual)

The ion source of the mass spectrometer is where gas phase ions are produced; the

ions formed there are then subjected to mass analysis. The ion source of the API 4000

employs a Turbo V source housing and a removable probe which is inserted into the top

of the source housing. Liquid samples are introduced to the ion source from either the

TurboIonSpray (TIS) or the atmospheric pressure chemical ionization (APCI) probe by

using an external LC pump or a syringe pump. The TIS probe is located between two

turbo heaters that are placed at 45° angles relative to each side. The probe jet output and

the heated dry gas from the turbo heaters are perpendicular to the direction of the orifice

plate. This orthogonal arrangement increases the rate of droplet evaporation and minimizes contamination. A high ion spray voltage is applied to the probe to produce the charged droplets. The probe temperature (TEM) is monitored and is maintained to within $5^{o}C$ of the turbo heater temperature. Gas, high voltage, and electrical connections to the probe enter through the front plate of the interface and connect internally through the source housing. The probe can be positioned vertically or horizontally for optimal performance.

The vacuum system consists of the vacuum interface, vacuum control system and the vacuum chamber. The vacuum interface includes a curtain plate, orifice plate, and skimmer cone. The atmospheric pressure inside the ion source is separated from the low pressure vacuum chamber by the orifice plate. The function of the vacuum interface is to allow the transfer of gas phase ions from the ion source to the vacuum chamber while restricting the transfer of liquid phase droplets and ambient air. A pure, inert curtain gas is flushed between the curtain plate and the orifice plate, and solvated ions collide with gas molecules to assist in breaking up ion clusters. Ions are drawn from the curtain gas interface into a roughing pump maintained low pressure region by the pressure differential and transferred to the vacuum chamber by the voltage difference between the orifice plate and the skimmer cone.

The vacuum control system maintains and monitors the system pressure and gas flow. The roughing pumps maintain a pressure (< 2 torr) low enough to facilitate the operation of the high vacuum turbo pumps. The two turbo pumps maintain low pressures for the Q0 region (10^{-3} torr) and for the mass analyzer region (10^{-5} torr), respectively. The system pressure is monitored by a triode vacuum gauge. The gas system of the instrument

includes the TIS nebulizer gas (Gas 1), TIS heater gas (Gas 2), sheath gas, curtain gas, and collision activated dissociation (CAD) gas. Compressed air was used for Gas 1, Gas 2, and the sheath gas; the curtain gas and CAD gas were 99.999 % pure nitrogen. Gas 1 and Gas 2 flow co-axially with the probe inlet to accelerate solvent evaporation and therefore assist in the conversion of liquid samples into small droplets. The sheath gas was used to cool the nebulizer assembly and the curtain gas was used to prevent neutral molecules from entering the vacuum chamber. Ions are fragmented by colliding with the CAD gas in the collision cell located in the Q2 region.

The vacuum chamber includes quadrupole rod sets, ion optics, the collision cell, and a channel electron multiplier (CEM) detector. A mass analyzer quadrupole, which defines the ion path, consists of four cylindrical rods mounted in a ceramic collar. Changing the radio frequency (RF) and direct current (DC) voltages applied to the quadrupole rods allows ions with a particular mass to charge ratio to be selected [2, 3]. Ions with a certain *m/z* ratio pass through the quadrupole while all other ions collide with the quadrupole rods and are removed from the ion stream. An RF-only quadrupole, which transmits ions without mass filtering is similar in construction to a mass analyzer quadrupole, but is only operated with an RF voltage. In a triple quadrupole mass spectrometer, Q1 and Q3 are identical mass analyzer quadrupoles and Q0 and Q2 are RF-only quadrupoles. Q0, located in front of the mass filter, focuses and transfers ions from the vacuum interface to the high vacuum mass analyzer region. Q1 and Q3 are separated by the ceramic collision cell, where Q2 is located. Ions passing through Q1 are fragmented by collisions with neutral gas molecules in the collision cell, a process referred to as CAD. All of the ions in the collision cell are then transferred to Q3. Ions

selected by Q1 are called precursor ions and the collision products are called fragment or product ions. The product ions are selectively filtered by Q3 before they are collected by the detector. The ion optics are designed to help guide and focus the ions in the mass filters and deliver the selected ions to the CEM. The CEM is a continuous dynode device. When struck by an ion, it emits an electron pulse. The electron pulses are collected and converted to a digital signal, called ion intensity, which is measured as a function of mass to charge ratio. In this research, the API 4000 mass spectrometer was operated as both a single quadrupole (MS) and a triple quadrupole (MS/MS) in four scan modes.

Q1 scan (MS): In single quadrupole operation, Q1 is used. All of the ions formed in the source are separated and counted according to their mass to charge ratios. A full scan mass spectrum shows the intensities of all the detected ions acquired over a certain scan range. Multichannel accumulation (MCA) is normally applied to sum successive scans to produce better signal-to-noise ratio.

Product ion scan (MS/MS): In this mode, the first mass analyzer, Q1, separates ions according to their *m/z* ratios and allows only the desired ion (precursor ion M^+) to enter the collision cell (Q2). That ion then collides with neutral N_2 molecules and fragments through CAD, and the generated fragment ions (product ions) are passed into Q3 for mass analysis. Scanning Q3 over a specified mass range produces a product ion spectrum of M^+.

Precursor ion scan (MS/MS): In this mode, a specified product ion (T^+) is selected by the second mass analyzer, Q3, and Q1 is scanned over a range. All of the precursor ions that produce T^+ are displayed in the resulting spectrum.

Multiple reaction monitoring (MRM) (MS/MS): In this mode, Q1 is used to select the

desired precursor ion (M+); it is dissociated in Q2; and then Q3 is used to detect a specific product ion (F^+). This operation, which allows a particular fragment reaction ($M^+ \rightarrow F^+ + N$) to be monitored, is called selected reaction monitoring (SRM). When a set of SRM fragmentation reactions are monitored, it is called MRM. This mode of operation is extensively used in quantitative analysis due to its increased sensitivity and selectivity compared to other modes.

2.2.5 Aria^{TM} High Turbulence Liquid Chromatography System

The Cohesive Technologies (Franklin, MA, USA) High Turbulence Liquid Chromatography (HTLC) system is designed for online biological sample extraction and analysis. The system consists of the following components: a loading pump, an eluting pump, a CTC Analytics PAL autosampler, and a valve interface module. The loading pump, which delivers mobile phases to the extraction column via the autosampler, is connected with the eluting pump through the valve interface module. The interface includes two automatic six-port valves controlled by the Aria^{TM} 1.4 operating software. Data acquisition and processing are conducted by using the software (Analyst 1.4) for the mass spectrometer. The communication between the Aria^{TM} and the Analyst is established by AriaLink^{TM}.

The loading and eluting pumps were Shimadzu LC-10AD*VP* Micro-volume double plunger pumps. The low pressure gradient loading pump [6] was able to deliver four solvents, and these degassed multiple solvents were mixed before transferring them to the autosampler. The binary eluting pump provided a high pressure gradient [6] which delivered a stable flow with small void volume. These pumps could be operated with a flow rate ranging from 0.1 to 9.9 mL/min and with a 0.1% solvent mixing ratio.

The CTC Analytics PAL autosampler was used for sample storage and injection. It could hold up to six sample plates and the storage temperature could be varied from 5 to 45°C. Individual samples in 96-well or 54-well format were randomly accessed according to the programmed injection sequence. Samples were aspirated with a conventional glass syringe and injected directly into a sample loop without the need for transfer lines. The injector and syringe were coordinated by adjusting the x, y, z position of the syringe., The sample was delivered to the column by using a six-port injection valve. After each injection, the syringe was rinsed both inside and outside by a wash station containing two different cleaning solvents to minimize carryover (Fig. 2-2).

Figure 2-2. Operation of the CTC autosampler

Fill Sample Loop   Loading Sample onto Column
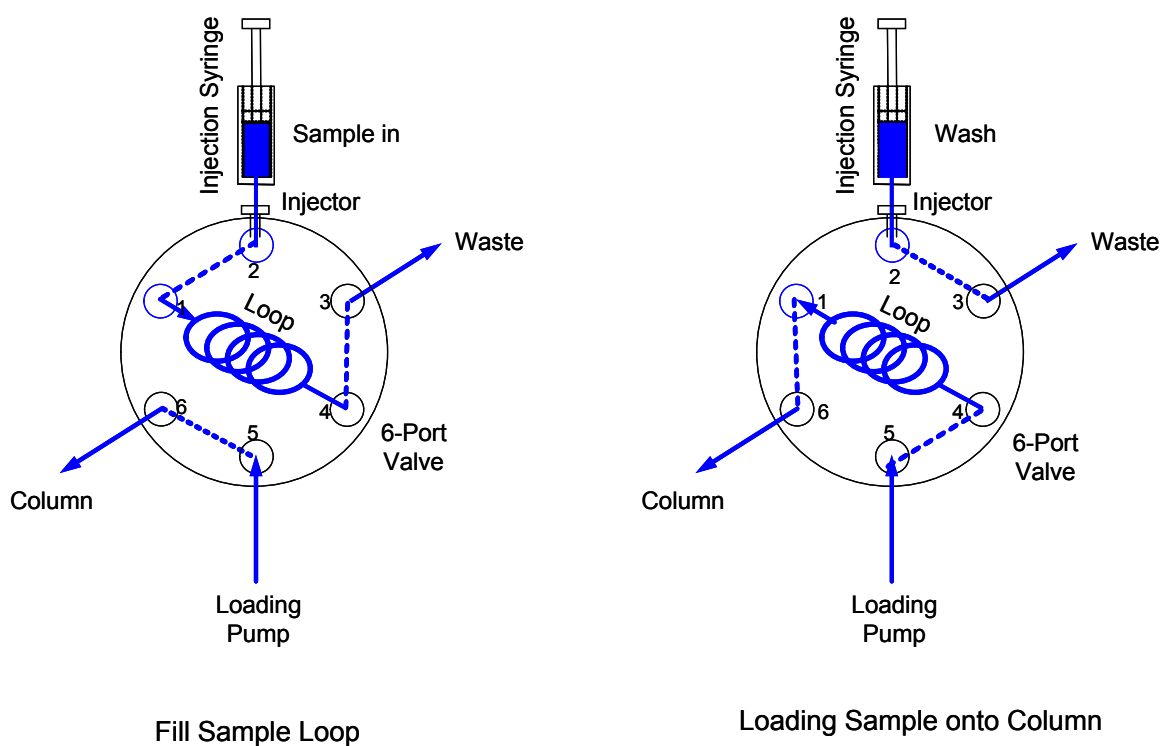
The valve interface manages the source and destination of the multiple solvents delivered by the loading and eluting pumps. The two valves, where solvents reservoirs

and columns were connected, could be selectively switched according to the LC method. The mobile phase and flow direction on the column could thus be changed during sample analysis. Sample extraction was conducted on the HTLC extraction column by using turbulent flow chromatography. The narrow-bore (ID: 0.5 mm) extraction column packed with 50 or 60 µm particles generated a moderate backpressure at high flow rates. Depending on the analytes, various extraction columns such as: Cylcone, C_{18}, and Polar plus were employed. Sample analysis, which was conducted immediately after sample extraction, was performed by regular HPLC.

2.2.6 ACQUITY Ultra Performance LC™

The ACQUITY Ultra Performance LC™ (UPLC) system from Waters Corporation (Milford, MA, USA) was employed to achieve high resolution separations [5,7]. This system included a binary solvent manager, a sample manager, a column manager, a detector, and sub-2µm columns.

The binary solvent manager was a high pressure pump [6] that delivered mobile phases for the system. It included two independent pumps: A and B, and each pump contained two linear-drive actuators which separately delivered a precise flow of a single solvent. The two solvents transferred by the pumps were combined at a filter/tee mixer, and then the mixed solvent flowed to the sample manager. The mixing ratio of the two solvents was controlled by varying the flow rate of pump A relative to that of pump B. A steady (pulse free) solvent flow of up to 1 mL/min with maximum pressure of 1034 bar (15000 psi) was provided.

The sample manager injected samples from 96-well plates or 1.5 mL HPLC vials into the solvent flow stream. When an injection was requested, the injection needle

moved diagonally to the specified well location. A stainless steel puncture needle pierced the well cover and the sampling needle, which resides inside the puncture needle, extended into the sample. After drawing the sample, the needle assembly was cleaned in a wash block to remove any sample trapped between the two needles, and then the sample was injected into a sample loop by using a metering syringe (Fig. 2-3). The sample plates were placed in the sample manager via the front door, or the sample organizer. Sample plates were stored at temperatures between 4 and 40º C.

Figure 2-3. The UPLC sample manager

Column

Column

Pump

1 2 3

Loop

6 5 4

6-Port Valve

Metering Syringe

Sample

Fill Sample Loop

Column

Pump

1 2 3

Loop

6 5 4

6-Port Valve

Metering Syringe

Wash

Loading Sample onto Column
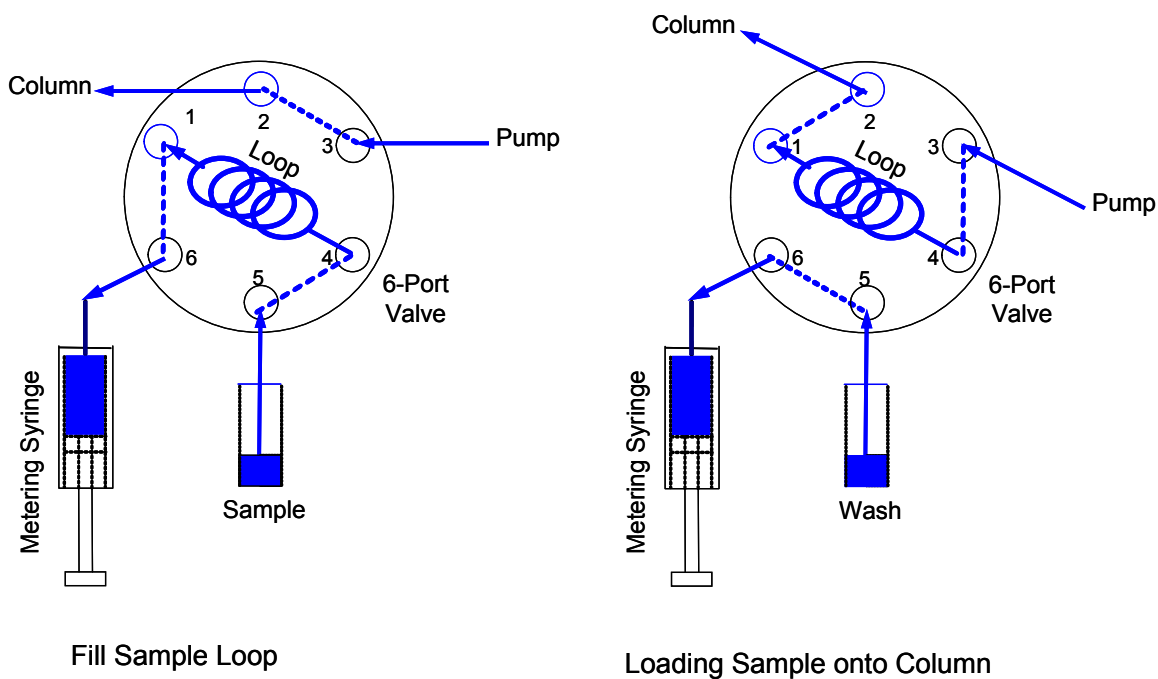
The column manager, which is a U-shaped tray that swivels outward, accommodates columns up to 4.6 mm ID and 150 mm long. The column compartment temperature can be varied from 5 to 65º C to facilitate chromatographic separation needs. A passive column stabilizer is placed in front of the column to minimize temperature fluctuations. The column tray swings outward from 0 to 180° to minimize the length of

tubing needed between instruments, which reduces dead volume and associated band spreading.

The UPLC system contained a built-in photodiode array (PDA) optical detector. The system, including the PDA detector, was managed by MassLynx software, which executed the commands in a batch sequence. When the instrument was connected to the mass spectrometer, data acquisition and processing were performed by the Analyst software.

ACQUITY UPLC columns were packed with 1.7 μm, bridged, ethane-silicon, hybrid particles. The column hardware and matched outlet tubing could tolerate a high pressure of up to 1034 bar (15000 psi). A 2.1 mm column ID allowed mass spectrometer compatible flow rates. Each column also included an information chip, called an eCord, which tracked the column usage history.

Tetraethoxysilane   Bis(triethoxysilyl)ethane   Polyethoxysilane
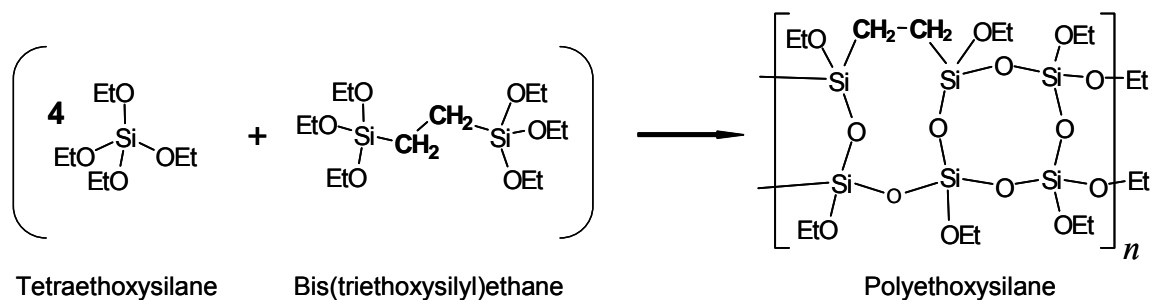
2.3 Sample Preparation for Chapter 4: Procedures for Reducing Matrix Effects and Investigation of the Role of Glycerophosphocholine Lipid Endogenous Interferences

2.3.1 Primary Standard Stock Solutions

About 5.0 mg of the compounds listed in Table 2-1 were individually weighed and transferred to 10 mL volumetric flasks. Actual weights were recorded. Compounds were dissolved in 5 mL of acetonitrile (ACN) and then diluted to the mark with water.

Solutions were mixed well with a vortex.

About 5.0 mg of the lipids listed in Table 2-2 were individually weighed and transferred to 5 mL volumetric flasks. Actual weights were recorded. Lipids were dissolved in 3 mL of tetrahydrofuran (THF) and then diluted to the mark with water. Solutions were mixed well with a vortex.

2.3.2 Secondary Standard Stock Solutions

Molar concentrations of the primary stock standards were calculated, taking into account the purity and salt content of the starting materials. Depending on the calculated concentrations, appropriate volumes of the primary standards were pipetted into 10 mL volumetric flasks to prepare 100.0 µM secondary stock standards for each compound. Standards for the compounds listed in Table 2-1 were diluted with 50:50 ACN:H_2O and standards for the lipids listed in Table 2-2 were diluted with 50:50 MeOH:H_2O. Solutions were well mixed with a vortex.

The stock standards (2.3.1 and 2.3.2) were stored in 13 mL polypropylene tubes with screw caps (Sarstedt AG & Co., Newton, NC, USA) at -20°C in a freezer. Frozen standards were thawed, sonicated and vortexed thoroughly before further dilution.

2.3.3 Buffer Solutions

Sodium carbonate (2.6 g) was weighed and dissolved in 25 mL of water to obtain a 1.0 M solution. About 0.77 g of ammonium acetate was weighed and dissolved in 10 mL of water to obtain a 1.0 M solution. Formic acid (FA, 0.43 mL) and 1.36 mL of ammonium hydroxide were separately diluted to 10 mL with water to prepare 1 M solutions. All solutions were mixed well.

2.3.4 Infusion Solutions

2.3.4-A Plasma supernatant

Human control plasma from five lots were pooled. To a 13 mL polypropylene tube, a 2 mL aliquot of plasma was placed. Then, 6 mL of ACN was added to precipitate proteins. The solution was then vortexed and centrifuged. The supernatant was removed and diluted with water in 1 to 1 ratio.

2.3.4-B Analyte tuning solutions

For acidic compounds, 100 µL of the secondary stock standard (2.3.2) for A1 and A2 analytes were mixed in a 10 mL volumetric flask and then diluted to the mark with 50:50 ACN:H_2O. For basic compounds, 100 µL of the secondary stock standard for B1, B2 and B3 analytes were mixed in a 10 mL volumetric flask and diluted to the mark with 50:50 ACN:H_2O.

2.3.4-C Post-column infusion solutions

A solution that was 5 µM in the five analytes was prepared by pipetting 500 µL of the secondary stock standards (2.3.2) for the compounds listed in Table 2-1 into a 10 mL volumetric flask, and then diluting with 50:50 ACN:H_2O.

Based on the calculated concentrations of the GPCho lipid primary standards (2.3.1), a 50 µM solution containing the four lipids in Table 2-2 was prepared by pipetting an appropriate volume of each primary standard into a 10 mL volumetric flask and then diluting with 50:50 MeOH:H_2O. These solutions were stored in 13 mL polypropylene tubes at -20°C in a freezer.

2.3.5 Working Standards

Standards with concentrations of 100.0 µM for the acidic compounds (A1 and A2) and the basic compounds (B1, B2 and B3) were prepared by transferring the

appropriate volumes of the corresponding primary standards (2.3.1) to 10 mL volumetric flasks and diluting with 15:85 ACN:H_2O. The 100.0 μM standards were further diluted according to Table 2-3 with 15:85 ACN:H_2O to obtain the working standards. The working standards were stored in 13 mL polypropylene tubes at 5°C in a refrigerator.

Table 2-3. Working standards

	Working Std. Conc. (μM)	Vol. of Transf. Std. (μL)	Conc. of Transf. Std. (μM)	Dil. Vol. (mL)
I-1 a	10.0	1000	100.0	10
I-1 b	8.0	800	100.0	10
I-1 c	2.0	200	100.0	10
I-1 d	0.50	50	100.0	10
I-1 e	0.20	200	10.0	10
I-1 f	0.040	40	10.0	10
I-1 g	0.020	20	10.0	10

2.3.6 Liquid-liquid Extraction Solutions

2.3.6-A Recovery solutions

Extraction solvents including: methyl t-butyl ether (MtBE), hexene (Hex) and ethyl acetate (EA) as well as the combinations: 50:50 MtBE:Hex, 70:30 MtBE:EA and 70:30 Hex:EA were examined at three pHs: 4, 7 and 10. Ten μL aliquots of 12.5% FA, H_2O, and 1 M Na_2CO_3 were added to 5 mL glass centrifuge tubes, respectively, which contained 250 μL of 50 μM GPCho lipids (2.3.4-C). After pH adjustment, 1mL of the extraction solvent was added. Then, the solutions were vortexed for 30 sec, and centrifuged at 3000 rpm for 2 min. The upper layer (800 μL) was transferred to a 96-well plate. The plate was dried under flowing N_2 at 35°C and the residue was reconstituted in 200 μL of 50:50 MeOH:H_2O. The analytes were extracted with the same procedure by using the 200 nM solutions (2.3.5). For acidic compounds, the pH was adjusted to 4 and

7; for basic compounds, the pH was adjusted to 7 and 10. The analytes were reconstituted in 15:85 ACN:H_2O. All of the recovery solutions were prepared in triplicate.

2.3.6-B Matrix effect solutions

For each of the five different human control plasma lots, 225 μL was dispensed into a 5 mL glass centrifuge tube containing 25 μL of 15:85 ACN:H_2O. Then, 10 μL of 12.5% FA and 1 M Na_2CO_3 were added to adjust the pH to 4 and 10, respectively. After adding 1 mL of MtBE, the solutions were vortexed for 30 sec, and centrifuged at 3000 rpm for 2 min. The upper 800 μL of each solution was transferred to a 96-well plate and the plate was dried under flowing N_2 at 35°C. Separately, 25 μL of the acidic and basic compound working standards at concentrations of 0.04, 0.5 and 8.0 μM (2.3.5) were pipetted into the corresponding wells containing acidified plasma residue and basified plasma residue. The standards were diluted with 225 μL of 15:85 ACN:H_2O. A neat standard set was prepared in clean wells by mixing 25 μL of the same working standards with 225 μL of 15:85 ACN: H_2O. Solutions were prepared in triplicate.

2.3.6-C Plasma calibration curve standards

Five sets of calibration curve standards, made from the five lots of human control plasma used in 2.3.6-B, were prepared for acidic and basic compounds, respectively. Twenty-five μL of the working standards (2.3.5) were pipetted along with 225 μL of human control plasma to obtain calibration standards at: 2, 4, 20, 50, 200, 800 and 1000 nM. Ten μL of 12.5% FA was added to plasma standards containing acidic compounds and 10 μL of 1 M Na_2CO_3 was added to standards containing basic compounds. Then, the standards were mixed with 1 mL of MtBE. After vortexing for 30 sec and centrifuging at 3000 rpm for 2 min, the upper 800 μL of each solution was transferred to a 96-well plate.

The plate was dried under flowing N_2 at 35°C, and the residue was reconstituted in 250 µL of 15:85 ACN:H_2O.

2.3.6-D Plasma GPCho lipid quantification samples

For the five lots of control plasma used for the matrix effect solutions in 2.3.6-B, 200 µL of plasma from each lot was dispensed, 600 µL of ACN was added, and then the solutions were diluted with 1.2 mL of 25:75 ACN:H_2O. These solutions were vortexed, centrifuged, and then 0.5 mL of the supernatant was transferred to a 96-well plate. Quantification standards at 0.5, 1, 5, 10, 25 and 50 µM were prepared by diluting the 50 µM GPCho lipid solutions (2.3.4-C) with 50:50 MeOH:H_2O.

2.3.6-E Chromatography solutions

The 50 µM GPCho lipid solutions (2.3.4-C) were mixed with equal volumes of 2 µM acidic and basic compound working standards (2.3.5), respectively. Mixtures were transferred to 1.5 mL HPLC vials.

2.3.7 HTLC Online Extraction Solutions

2.3.7-A Acidified plasma standards

Appropriate volumes of the primary standards (2.3.1) for A1 and A2 analytes were mixed and diluted with 15:85 ACN:H_2O to obtain a 200 ng/mL neat standard. Similarly, a 200 ng/mL standard containing B1, B2 and B3 analytes was prepared by pipetting the appropriate volumes of the corresponding primary standards and diluting with 15:85 ACN:H_2O.

Plasma standards were prepared by mixing 25 µL of the 200 ng/mL neat standards with 225 µL of pooled human control plasma. For acidic compounds, 10 µL of 12.5% FA, 12.5% acetic acid (HOAc), or 50% HOAc were added to the plasma standards

46

to obtain acidified standards containing 0.5% FA, 0.5% HOAc, or 2% HOAc. The plasma standards for basic compounds containing 0% acid, 0.5% HOAc, or 2% HOAc were prepared similarly by adding 10 µL of H_2O, 12.5% HOAc or 50% HOAc. Five replicates of each plasma standard were prepared.

2.3.7-B Plasma calibration curve standards

A plasma calibration curve was derived from standards at the following concentrations: 2, 4, 20, 50, 200, 800 and 1000 nM. These standards were prepared by adding 25 µL of the working standards (2.3.5) to 225 µL of the human control plasma. Five sets of calibration curve standards, made from the five different lots of human control plasma (2.3.6-B), were prepared for acidic and basic compounds, respectively. Ten µL of 12.5% HOAc were added to the plasma standards containing acidic compounds. The solutions were mixed by vortex.

2.3.8 AQUITY UPLC Analysis Solutions

2.3.8-A Neat A1 standards

The 100 µM analyte A1 secondary standard (2.3.2) was diluted with 15:85 ACN:H_2O to prepare neat A1 standards at 2, 4, 20, 50, 200, 800 and 1000 nM.

2.3.8-B Flow rate effect solutions

The 100 µM A1 and B3 secondary standards (2.3.2) were diluted with 35:65 ACN:0.5% HOAc and 75:25 ACN:10 mM NH_4OAc, respectively, to prepare neat A1 and B3 standards at 1 µM.

2.3.8-C Matrix effect solutions

For each of the five human control plasma lots (same as 2.3.6-B), 225 µL were dispensed into 5 mL glass centrifuge tubes containing 25 µL of 15:85 ACN:H_2O. After

adding 750 μL of ACN, the solutions were vortexed and centrifuged at 3000 rpm for 5 min. Then, the upper 800 μL of the supernatants were transferred to a 96-well plate and the plate was dried under flowing N_2 flow at 35^oC. Separately, 25 μL of acidic and basic compound working standards at 0.04, 0.5 and 8.0 μM (2.3.5) were pipetted into the dry wells. The standards were diluted with 225 μL with 15:85 ACN:H_2O. A neat standard set was prepared in clean wells by pipetting 25 μL of same working standards along with 225 μL of 15:85 ACN:H_2O. The solutions were prepared in triplicate.

2.3.8-D Plasma calibration curves standards

Five sets of calibration curve standards, made from the five human control plasma lots used in 2.3.6-B, were prepared for the acidic and basic compounds, respectively. Twenty-five μL of the working standards (2.3.5) and 225 μL of human control plasma were pipetted to obtain calibration standards at: 2, 4, 20, 50, 200, 800 and 1000 nM. To these plasma standards, 750 μL of ACN was added. Then, the solutions were vortexed and centrifuged at 3000 rpm for 5 min. The upper 800 μL of the supernatants were transferred to a 96-well plate. The plate was dried under flowing N_2 at 35^oC and the residue was reconstituted in 250 μL of 15:85 ACN:H_2O.

2.4 Sample Preparation for Chapter 5: Elucidation of Analyte Ionization Suppression Effects

2.4.1 Single Analyte Solutions

Appropriate volumes of the B1, B2, B3, and 16:0 LPC secondary stock solution standards (2.3.2) were pipetted into 10 mL volumetric flasks and a series of dilutions was performed as indicated in Table 2-4. Solutions were diluted to the mark with 50:50

ACN:H_2O and mixed well.

Table 2-4. Single analyte solutions

	Analyte Conc. (M)	Vol. of Transf. Std. (µL)	Conc. of Transf. Std. (M)	Dil. Vol. (mL)
II-1 a	1.0E-05	1000	1.0E-04 (2.3.2)	10
II-1 b	2.0E-06	200	1.0E-04 (2.3.2)	10
II-1 c	5.0E-07	500	1.0E-05 (II-1 a)	10
II-1 d	1.0E-07	100	1.0E-05 (II-1 a)	10
II-1 e	2.0E-08	20	1.0E-05 (II-1 a)	10
II-1 f	5.0E-09	500	1.0E-07 (II-1 d)	10
II-1 g	1.0E-09	100	1.0E-07 (II-1 d)	10

2.4.2 Single Analyte with Buffer Solutions

A series of 10-fold dilutions were performed using water for each of the 1 M buffers (2.3.3): ammonium acetate, formic acid, and ammonium hydroxide, to prepare buffer solutions ranging from 1.0 x 10^{-1} to 1.0 x 10^{-5} M. Crossover preparations, for which each compound (B1, B2, B3, and 16:0 LPC) was sequentially mixed with the three buffers in 5 mL volumetric flasks, were prepared according to Table 2-5. Solutions were diluted to the mark with 50:50 ACN:H_2O and mixed well.

2.4.3 Binary Analyte Solutions

Binary solutions were designated as containing an analyte and a co-analyte. The concentration of analyte remained constant and the co-analyte concentration varied. B1, B2 and B3 were used as analytes, and B1, B2, B3 and 16:0 LPC were used as co-analytes. The analytes were separately mixed with each co-analyte in 5 mL volumetric flasks, as indicated in Table 2-6. For example, analyte B1 was mixed with co-analyte B2, B3 and 16:0 LPC, respectively. Solutions were diluted to the mark with 50:50 ACN:H_2O and mixed well.

Table 2-5. Single analyte with buffer solutions

	Buf. Conc. (M)	Vol. of Transf. Buf. (µL)	Conc. of Transf. Buf. (M)	Dil. Vol. (mL)
II-2 a	1.0E-01	1000	1.0E-00 (2.3.3)	10
II-2 b	1.0E-02	1000	1.0E-01 (II-2 a)	10
II-2 c	1.0E-03	1000	1.0E-02 (II-2 b)	10
II-2 d	1.0E-04	1000	1.0E-03 (II-2 c)	10
II-2 e	1.0E-05	1000	1.0E-04 (II-2 d)	10

	Analyte_Buf. Conc. (M)	Vol. of Anal. (µL)	Conc. of Anal. (M)	Vol. of Buf. (µL)	Conc. of Buf. (M)	Dil.Vol. (mL)
	1.0E-07_1.0E-02	250	2.0E-06 (II-1 b)	50	2.3.3	5
II-2 h	1.0E-07_1.0E-03	250	2.0E-06 (II-1 b)	50	II-2 a	5
II-2 i	1.0E-07_1.0E-04	250	2.0E-06 (II-1 b)	50	II-2 b	5
II-2 j	1.0E-07_1.0E-05	250	2.0E-06 (II-1 b)	50	II-2 c	5
II-2 k	1.0E-07_1.0E-06	250	2.0E-06 (II-1 b)	50	II-2 d	5
II-2 l	1.0E-07_1.0E-07	250	2.0E-06 (II-1 b)	50	II-2 e	5
II-2 m	1.0E-07_0	250	2.0E-06 (II-1 b)	---	---	5

Table 2-6. Two analyte solutions

	Analyte_Co-Anal. Conc. (M)	Vol. of Anal. (µL)	Conc. of Anal. (M)	Vol. of Co-Anal. (µL)	Conc. of Co-Anal. (M)
	1.0E-07_1.0E-04	250	2.0E-06 (II-1 b)	to be calc.	(2.3.1)
II-3 a	1.0E-07_1.0E-05	250	2.0E-06 (II-1 b)	500	1.0E-04 (2.3.2)
II-3 b	1.0E-07_1.0E-06	250	2.0E-06 (II-1 b)	500	1.0E-05 (II-1 a)
II-3 c	1.0E-07_1.0E-07	250	2.0E-06 (II-1 b)	50	1.0E-05 (II-1 a)
II-3 d	1.0E-07_1.0E-08	250	2.0E-06 (II-1 b)	500	1.0E-07 (II-1 d)
II-3 e	1.0E-07_1.0E-09	250	2.0E-06 (II-1 b)	50	1.0E-07 (II-1 d)
II-3 f	1.0E-07_0	250	2.0E-06 (II-1 b)	---	---

2.4.4 Single Analyte with 16:0 LPC and Buffer Solutions

B1, B2 and B3 analytes were separately mixed with 16:0 LPC and the mixture was diluted with buffered and non-buffered solutions, respectively. Aliquots (250 µL) of

analyte at 2.0 x 10^{-6} M (II-1 b) were mixed with appropriate volumes of the 16:0 LPC standard solution in 5 mL volumetric flasks as indicated in Table 2-7. The three buffers (ammonium acetate, formic acid, and ammonium hydroxide) at 0.1 M were separately added (50 µL) to prepare solutions designated as series II-4 a to II-4 g. A similar series (II-4 h to II-4 n) without buffer was also prepared. Solutions were diluted to the mark with 50:50 ACN:H_2O and mixed well.

Table 2-7. Single analyte with 16:0 LPC and buffer solutions

	Analyte_Buf._LPC Conc. (M)	Vol. of Buf. (µL)	Conc. of Buf. (M)	Vol. of LPC (µL)	Conc. of LPC (M)
II-4 a	1.0E-07_1.0E-03_1.0E-04	50	1.0E-01 (II-2 a)	to be calc.	(2.3.1)
II-4 b	1.0E-07_1.0E-03_5.0E-05	50	1.0E-01 (II-2 a)	2500	1.0E-04 (2.3.2)
II-4 c	1.0E-07_1.0E-03_2.0E-05	50	1.0E-01 (II-2 a)	1000	1.0E-04 (2.3.2)
II-4 d	1.0E-07_1.0E-03_1.0E-05	50	1.0E-01 (II-2 a)	500	1.0E-04 (2.3.2)
II-4 e	1.0E-07_1.0E-03_5.0E-06	50	1.0E-01 (II-2 a)	250	1.0E-04 (2.3.2)
II-4 f	1.0E-07_1.0E-03_2.5E-06	50	1.0E-01 (II-2 a)	125	1.0E-04 (2.3.2)
II-4 g	1.0E-07_1.0E-03_1.0E-06	50	1.0E-01 (II-2 a)	50	1.0E-04 (2.3.2)
II-4 h	1.0E-07_0_1.0E-04	---	---	to be calc.	(2.3.1)
II-4 i	1.0E-07_0_5.0E-05	---	---	2500	1.0E-04 (2.3.2)
II-4 j	1.0E-07_0_2.0E-05	---	---	1000	1.0E-04 (2.3.2)
II-4 k	1.0E-07_0_1.0E-05	---	---	500	1.0E-04 (2.3.2)
II-4 l	1.0E-07_0_5.0E-06	---	---	250	1.0E-04 (2.3.2)
II-4 m	1.0E-07_0_2.5E-06	---	---	125	1.0E-04 (2.3.2)
II-4 n	1.0E-07_0_1.0E-06	---	---	50	1.0E-04 (2.3.2)

2.5 References

[1] *API 4000 LC-MS/MS Hardware Manual,* Applied Biosystems, MDS Sciex, May 2002

[2] Watson, J. T. *Introduction to Mass Spectrometry* 3rd ed*.,* Lippincott Williams and Wilkins, Now York, 1997

[3] Hoffmann, E. De; Charette, J.; Stroobant, V. *Mass Spectrometry: Principles and Applications,* Wiley, Now York, 1998

[4] Bernard, P. S.; Wallace, J. M. *Turbulent Flow: Analysis, Measurement, and Prediction,* Wiley, Now York, 2002

[5] *Unified Chromatography,* Parcher, J. F.; Chester, T. L. (ed.), Oxford University Press, 2000

[6] *Pump Handbook,* 3rd ed., Karassik, I. J.; Messina, J. P.; Paul, C.; Heald, C. C. (ed.), McGraw-Hill I, 2001

[7] Patel, D. *Liquid Chromatography: Essential Data*, Wiley, Now York, 1997

CHAPTER 3

EXPERIMENTAL CONDITIONS AND RESULTS

3.1 Procedures for Reducing Matrix Effects and Investigation of the Role of Glycerophosphocholine Lipid Endogenous Interferences

3.1.1 Mass Spectrometry Measurements

3.1.1-A Plasma supernatant

The control plasma supernatant (2.3.4-A) was directly infused into the TIS source at 100 µL/min to obtain a Q1 scan spectrum. The full scan was conducted over a mass range of 150 to 1000 amu with a step of 1 amu under the following source parameters: Gas 1 and Gas 2: 55, curtain gas: 30, ion spray voltage: 5500, source temperature: 600, declustering potential: 140, and entrance potential: 10. The parameters units are arbitrary numbers. The predominant signals at *m/z* values of 519, 543, 782 and 805 were scanned with a step of 0.1 amu (Q1 center scan) to obtain accurate masses under the same operating conditions (Fig. 4-3). The Q1 center scan identified ions were individually scanned for fragmentation patterns with collision gas at 7, collision energy at about 40 and collision cell exit potential at 12. The product ion spectra for the ions at *m/z* 518.2, 542.3, 544.3 and 546.3 are shown in Figure 4-4 and product ion spectra for ions at *m/z* 780.6, 804.7 and 806.7 are shown in Figure 4-5. A precursor ion scan for the common product ion at *m/z* 147.1 was also conducted and that spectrum is shown in Figure 4-5.

3.1.1-B Glycerophosphocline (GPCho) lipids

The GPCho lipid secondary standards (2.3.2) were separately introduced into the TIS source at 20 µL/min through a tee with 65:35 ACN:H_2O solvent flowing at 0.2

mL/min to obtain Q1 full scans, Q1 center scans and product ion scans. The resulting spectra are shown in Figures 4-6 to 4-9 for 16:0, 18:1, 18:0 LPC and 16:0-18:2 PC, respectively. The corresponding acquisition parameters were optimized for each lipid and the optimized conditions and MRM transitions for quantification are listed in Table 3-1.

Table 3-1. Optimized mass spectrometer acquisition parameters for GPCho lipids

	16:0 LPC	18:1 LPC	18:0 LPC	16:0-18:2 PC
Gas 1:	60	60	60	60
Gas 2:	40	40	40	40
Curtain gas (CUR):	30	30	30	30
Collision gas (CAD):	7	7	7	7
Ion spray voltage (IS):	5500	5500	5500	5500
Temperature (TEM):	600	600	600	600
Declustering potential (DP):	160	170	180	250
Entrance potential (EP):	10	10	10	10
Collision energy (CE):	35	35	35	43
Collision cell exit potential (CXP):	12	12	12	12
Interface heater:	on	on	on	on
Precursor ion monitored:	496.2	522.3	524.3	758.6
Product ion monitored:	184.2	184.2	184.2	184.2
Dwell time:	150 ms	150 ms	150 ms	150 ms
Resolution of Q1:	Unit			
Resolution of Q3:	Unit			
Pause time:	5 ms			
Deflector (DF):	-200			
Channel electron multiplier (CEM):	2000			

3.1.1-C Analytes

The mass spectrometer was operated with the electrospray ionization TIS source in the positive ionization mode. The 1 µM tuning solutions (2.3.4-B) for acidic and basic compounds were separately infused into the TIS source at 200 µL/min. Q1 scans and product ion scans were performed in order to identify the proper ion transition channel

for quantification. The resulting full scan Q1 spectra and product ion scan spectra are shown in Figures 4-10 and 4-11 for acidic and basic compounds, respectively. The Q1 scan parameters including Gas 1, Gas 2, curtain gas, ion spray voltage, source temperature, declustering potential, and entrance potential were optimized to favor the formation of protonated ions. Under unit resolution for both Q1 and Q3, product ion scans were performed for each protonated ion, and collision gas, collision energy, and collision cell exit potential were appropriately optimized to attain sensitive and stable detection conditions. The optimized parameters and MRM transitions for quantification are listed in Table 3-2.

Table 3-2. Optimized mass spectrometer acquisition parameters for analytes

	A1	A2	B1	B2	B3
Gas 1:	55	55	55	55	55
Gas 2:	50	50	50	50	50
Curtain gas (CUR):	25	25	25	25	25
Collision gas (CAD):	7	7	7	7	7
Ion spray voltage (IS):	5500	5500	5500	5500	5500
Temperature (TEM):	650	650	600	600	600
Declustering potential (DP):	36	70	80	65	100
Entrance potential (EP):	9	9	8	8	8
Collision energy (CE):	17	31	32	25	38
Collision cell exit potential (CXP):	12	12	10	12	12
Interface heater:	on	on	on	on	on
Precursor ion monitored:	194.3	283.1	291.3	260.2	472.2
Product ion monitored:	176.2	265.2	230.2	183.2	436.4
Dwell time:	200 ms	200 ms	200 ms	200 ms	200 ms
Resolution of Q1:	Unit				
Resolution of Q3:	Unit				
Pause time:	5 ms				
Deflector (DF):	-200				
Channel electron multiplier (CEM):	2000				

3.1.2 Post-column Infusion

   Post-column infusion was performed with the apparatus shown below (Fig. 3-1). The Aria[TM] HTLC system was reconfigured to bypass the two six-port valves (Fig. 3-2, position 1). By connecting the outlet of the eluting pump to the autosampler, the injected sample was directly transferred to the analytical column. GPCho lipid separations were performed by using an XTerra® RP18 (2.1 x 50 mm, 5 µm) analytical column from Waters Corporation with the LC conditions listed in Table 3-3. The GPCho lipid solution (2.3.4-C) was injected onto the column with the syringe pump off, and the MRM transitions for the GPCho lipids were monitored by using the parameters listed in Table 3-1. The resulting chromatograms are shown in Figure 4-12. Afterwards, the mass spectrometer acquisition parameters were changed to the Table 3-2 conditions in order to monitor the MRM transitions for the analytes. Solution containing analytes (2.3.4-C) was infused with the syringe pump at 20 µL/min. The GPCho lipid solution was injected again with the same chromatographic conditions. As a comparison, a solvent (50:50 ACN:H_2O) was also injected. The infusion spectra of the analytes after injection of the GPCho lipids and solvent are shown in Figures 4-13 and 4-14, respectively.

Figure 3-1. Schematic of the post-column infusion apparatus
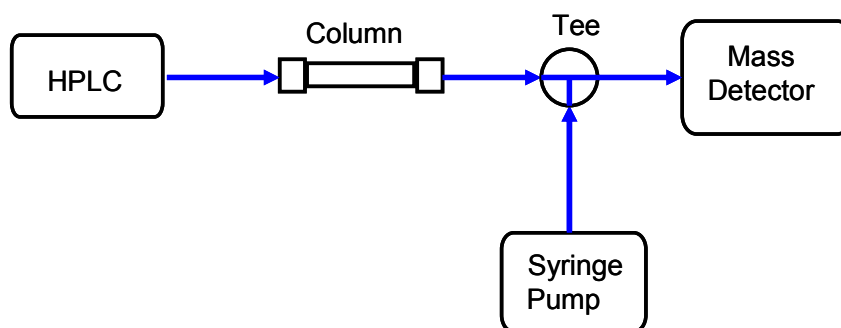
Table 3-3. LC method for GPCho lipid analysis

Step	Time (sec)	Flow (mL/min)	Gradient	%A	%B
1	180	0.3	step	50	50
2	180	0.3	step	5	95
3	60	0.4	step	50	50
4	40	0.3	step	50	50

A: 10 mM NH_4OAc in H_2O; B: 100% ACN

3.1.3 Liquid-liquid Extraction (LLE)

3.1.3-A Chromatography and detection conditions

The Aria[TM] HTLC system was reconfigured for HPLC analysis by connecting the outlet of the eluting pump to the autosampler (Fig. 3-2, position 1). Analyte separations were performed at ambient temperature by using a BDS Hypersil C_{18} (2.1 x 30 mm, 3 µm) analytical column from ThermoElectron (Bellefonte, PA, USA). The LC method for determining LLE processed analytes is listed in Table 3-4. The GPCho lipid samples were analyzed by using the chromatographic conditions listed in Table 3-3. The autosampler compartment was set at $5^{o}C$ and the injection volume was 5 µL. The analytes and GPCho lipids were detected by using the acquisition parameters listed in Tables 3-2 and 3-1, respectively.

3.13-B Recovery of analytes and GPCho lipids

Extracted analyte and GPCho lipid standards (2.3.6-A) were analyzed along with the original un-extracted standards and the percentage of extraction (% Recovery) was calculated based on the mean peak area of the extracted standard relative to the directly injected standard. Because the original 250 µL of standard was reconstituted in 200 µL of solvent, the material loss during the LLE transfer step (transfer 800 µL of extraction

solvent from 1 mL) was accounted for. The extraction recoveries for acidic and basic compounds and GPCho lipids are given in Figures 4-15, 4-16 and 4-19, respectively.

Table 3-4. LC method for analyte analysis

Step	Time (sec)	Flow (mL/min)	Gradient	%A	%B
1	50	0.2	step	70	30
2	20	0.2	ramp	65	35
3	16	0.2	ramp	60	40
4	40	0.2	ramp	50	50
5	32	0.2	ramp	30	70
6	32	0.2	ramp	5	95
7	15	0.2	step	5	95
8	40	0.2	ramp	50	50
9	15	0.2	ramp	70	30
10	115	0.2	step	70	30

Acidic compounds: A: 0.5% HOAc in H_2O; B: 100% ACN
Basic compounds: A: 10 mM NH_4OAc in H_2O; B: 100% ACN

3.1.3-C Absolute matrix effects

Analyte standards prepared with the plasma extract residue and clean solvent (2.3.6-B) were analyzed by using the corresponding conditions for acidic and basic compounds. The peak areas of the two types of standards were compared and the variations of the five lots of control plasma were calculated (Tables 4-2 and 4-3).

3.1.3-D Plasma standard curves

Plasma standard curve samples prepared by LLE (2.3.6-C) were analyzed on the reconfigured system by using the same conditions for absolute matrix effects experiments (3.1.3-C). The analyte chromatographic peaks were integrated by using the Analyst software. Calibration curve linear regressions and relative standard deviation (%RSD) calculations were accomplished by using Microsoft Excel. The regression results and the

RSD (%) values for the slopes are shown in Figures 4-17 and 4-18 for acidic and basic compounds, respectively.

3.1.3-E Plasma GPCho lipid quantification

The plasma samples and quantification standards (2.3.6-D) were analyzed by using the chromatographic and detection conditions specified for GPCho lipids. The quantification data are shown in Table 4-4.

3.1.3-F Chromatograms

Solutions containing analytes and GPCho lipids (2.3.6-E) were separated by using the analyte analysis LC conditions specified in Table 3-4. The MRM transitions for analytes and GPCho lipids were simultaneously monitored and the chromatograms are shown in Figure 4-20.

3.1.4 HTLC Online Extraction

3.1.4-A Columns and mobile phases

A turbulent flow HTLC extraction column, Cyclone (0.5 x 50 mm, 60 μm) from Cohesive Technology Inc., was used to isolate compounds from injected samples. Analyte separations were performed at ambient temperature by using the BDS Hypersil C_{18} (2.1 x 30 mm, 3 μm) analytical column and the XTerra® RP18 column (2.1 x 50 mm, 5 μm) was used for GPCho lipid separations. The autosampler compartment was set at $5^{o}C$ and the injection volume was 5 μL. The mobile phases delivered to the extraction column by the loading pump consisted of A (0.5% HOAc in H_2O), B (0.5% HOAc in ACN), C (15% HOAc in H_2O) and D (100% Acetone). The mobile phases that were delivered to the analytical column by the eluting pump were 0.5% HOAc in H_2O (A) and 100% ACN (B) for acidic compounds, and 10 mM NH_4OAc in H_2O (A) and 100% ACN

(B) for basic compounds and GPCho lipids.

3.1.4-B Procedures

Flow diagrams for the quick elute online extraction mode are shown in Figure 3-2. Samples were injected by the autosampler and immediately loaded onto the extraction column via the flow provided by the loading pump (loading position). The loaded sample was washed with aqueous loading solvents A and C in the sequential order of A-C-A under turbulent flow conditions. During this period, analytes were retained on the narrow-bore extraction column while macromolecules in the matrix were rapidly washed away to waste. The two six-port switching valves (A and B) were then activated at the same time, causing the mobile phase from the eluting pump to be diverted to the extraction column and the mobile phase from loading pump to be switched to waste (transfer position). The analytes were transferred from the extraction column onto the analytical column via the eluting mobile phase. After analyte transfer, valve (B) was switched back and the eluting mobile phase was directed to the analytical column in order to perform the chromatographic separation (position 3). The extraction column was washed in both directions with a combination of loading mobile phases by switching the loading valve (A). Prior to the next injection, the extraction and analytical columns were equilibrated to the initial loading conditions.

3.1.4-C Analyte loading and transfer

The acidified plasma standards (0.5% HOAc) containing acidic and basic compounds (2.3.7-A) were separately injected onto the HTLC/LC-MS/MS system. The columns, mobile phases, and the acquisition conditions for the mass spectrometer were correspondingly set for acidic and basic compounds. While keeping constant transfer

60

Figure 3-2. Flow diagrams for the HTLC/LC-MS/MS system quick elute mode

(1) Loading Position
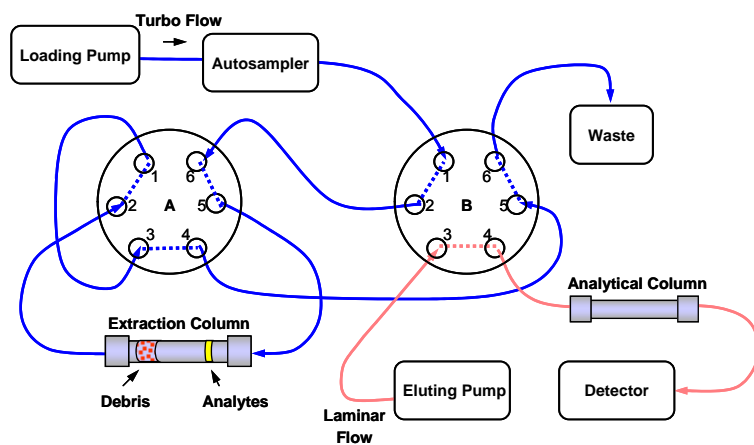
(2) Transferring Position
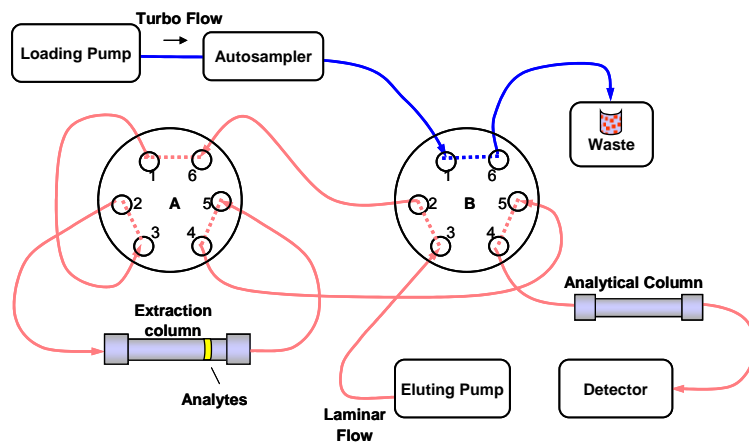
(3) Wash and Equilibrium Position
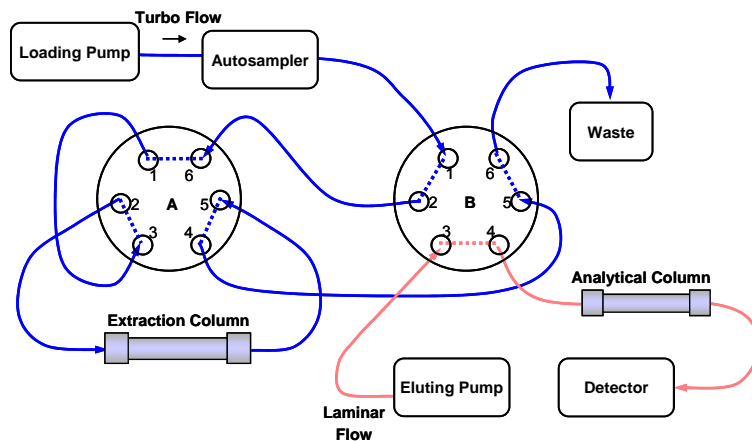
conditions (elution with 70:30 A:B for 25 sec at 0.2 mL/min), loading conditions of 30-5, 45-5, 45-10, 60-5, 60-10 and 60-15 second were separately tested; where 30-5 second represents a total of 30 sec loading for sequential wash using mobile phases A-C-A and the mobile phase C wash time was 5 sec. The other loading condition designations had the same meaning as that for the 30-5 sec designation. Then, for the same loading conditions (30-5 sec), transfer conditions with various compositions of eluting mobile phases (A:B from 85:15 to 60:40) were assessed by using the same plasma standards. The subsequent elution programs were same as for the LC method used in LLE (Table 3-4) in order to reproduce the separation conditions. The mobile phase composition, flow rate and valve switching for the HTLC system were controlled by the LC method. The analysis method is listed in Table 3-5 with conditions for the 30-5 sec loading and 70:30 A:B transfer. The step 1 time determined the total loading time and the step 14 time controlled the mobile phase C wash time. Loading conditions were varied by changing the durations of these steps. The ratio of the two eluting solvents could be varied for both steps 1 - 2 and steps 12 - 15 to test various transfer conditions (A:B 85:15, 80:20, 70:30 and 60:40). The effects of loading and transfer conditions on acidified plasma standards are summarized by Figure 4-21.

3.1.4-D Acid effects

The acidic and basic compound plasma standards (2.3.7-A) were separately analyzed by using the LC method listed in Table 3-5 and the acquisition conditions listed in Table 3-2. With the 30-5 sec loading condition, transfer conditions for different eluting solvent ratios (A:B of 85:15, 80:20, 70:30 and 60:40) were used to examine the effects of acid content on assay performance. The results are summarized in Table 4-5.

Table 3-5. LC method for analysis by using the HTLC system

		Loading Pump							Eluting Pump			
Step[a]	Time	Flow	%A	%B	%C	%D	Pos.[b]	CD[c]	Flow	Grad.	%A	%B
	sec	mL/min							mL/min			
1	30	1.5	100	–	–	–	1	←	0.2	step	70	30
2	25	1.2	–	–	–	100	2	→	0.2	step	70	30
3	20	1.5	100	–	–	–	3	→	0.2	step	70	30
4	20	1.5	100	–	–	–	3	→	0.2	ramp	65	35
5	16	1.5	–	100	–	–	3	→	0.2	ramp	60	40
6	20	1.5	–	–	–	100	3	→	0.2	ramp	55	45
7	20	1.5	–	–	100	–	3	→	0.2	ramp	50	50
8	32	1.5	100	–	–	–	3	→	0.2	ramp	30	70
9	32	1.5	–	–	–	100	3	→	0.2	ramp	5	95
10	15	0.2	100	–	–	–	1	←	0.2	step	5	95
11	40	1.5	–	–	–	100	1	←	0.2	ramp	50	50
12	15	0.2	–	100	–	–	1	←	0.2	ramp	70	30
13	80	1.5	100	–	–	–	1	←	0.2	step	70	30
14	5	1.5	–	–	100	–	1	←	0.2	step	70	30
15	30	1.5	100	–	–	–	1	←	0.2	step	70	30

Loading: A: 0.5% HOAc in H_2O; B: 0.5% HOAc in ACN; C: 15% HOAc in H_2O; D: 100% Acetone

Eluting: A: 0.5% HOAc in H_2O ; B: 100% ACN for acidic compounds

Eluting: A: 10 mM NH_4OAc in H_2O; B: 100% ACN for basic compounds

[a] The loading mobile phase was changed by step gradient at each step.

[b] Positions of the two six-port valves shown in Figure 3-2.

[c] Direction of extraction column flow.

3.1.4-E Plasma standard curves

The acidic and basic compound plasma curve standards (2.3.7-B) were separately injected onto the HTLC/LC-MS/MS system and analyzed by the corresponding LC method indicated in Table 3-5 and MS operating conditions listed in Table 3-2. Representative chromatograms are shown in Figure 4-22. The regressed plasma standard curves with the corresponding RSD (%) for the slopes are shown in Figures 4-23 and 4-24 for the acidic and basic compounds, respectively.

3.1.4-F Loading and transfer of GPCho lipids

The 50 µM GPCho lipid solution (2.3.4-C) was injected in triplicate onto the HTLC/LC-MS/MS system equipped with the mobile phases and columns specified for GPCho lipids. The mass spectrometer was set to the parameters listed in Table 3-1. For the same transfer conditions (elution with 50:50 A:B at 0.3 mL/min for 25 second), loading conditions of 30-5, 45-5, 45-10, 60-5, 60-10 and 60-15 second were examined. Afterwards, for the same loading condition (30-5 sec), transfer conditions with various compositions of eluting mobile phases (A:B from 80:20 to 30:70) were tested. The effects of loading and transfer conditions on GPCho lipids are shown in Figure 4-25. The LC method for lipids analysis is listed in Table 3-6. This method employed a 30-5 sec loading and transfer with 50:50 A:B mobile phase. The total loading time and mobile phase C wash time were changed by varying the durations for steps 1 and 13, respectively. The transfer conditions were modified by changing the eluting A:B ratio in both steps 1 - 2 and steps 12 - 14 to 80:20, 70:30, 60:40, 50:50, 40:60 and 30:70, respectively.

3.1.4-G Direct observation of eluted GPCho lipids

The loading diagram of the HTLC system (Fig. 3-2, position 1) was reconfigured. Instead of connecting to the waste, the outlet of the extraction column was connected to the mass spectrometer. Following the injection of 50 µM GPCho lipids (2.3.4-C), the extraction column was sequentially washed with 0.5% HOAc in H_2O and 100% ACN for 60 second at a flow rate of 1.5 mL/min. The MRM transitions of the GPCho lipids were monitored and the direct wash spectra for GPCho lipids eluting the extraction column are shown in Figure 4-26.

Table 3-6. LC method for GPCho lipid analysis by using the HTLC system

		Loading Pump							Eluting Pump		
Step[a]	Time	Flow	%A	%B	%C	%D	Pos.[b]	CD[c]	Flow	%A	%B
	sec	mL/min							mL/min		
1	30	1.5	100	–	–	–	1	←	0.3	50	50
2	25	1.2	–	–	–	100	2	→	0.3	50	50
3	40	1.5	100	–	–	–	3	→	0.3	50	50
4	76	1.5	–	100	–	–	3	→	0.3	50	50
5	20	1.5	–	–	–	100	3	→	0.3	50	50
6	20	1.5	–	–	100	–	3	→	0.3	5	95
7	32	1.5	100	–	–	–	3	→	0.3	5	95
8	32	1.5	–	–	–	100	3	→	0.3	5	95
9	15	1.5	100	–	–	–	1	←	0.3	5	95
10	40	1.5	–	–	–	100	1	←	0.3	5	95
11	15	1.5	–	100	–	–	1	←	0.3	5	95
12	80	1.5	100	–	–	–	1	←	0.3	50	50
13	5	1.5	–	–	100	–	1	←	0.3	50	50
14	30	1.5	100	–	–	–	1	←	0.3	50	50

Loading: A: 0.5% HOAc in H_2O; B: 0.5% HOAc in ACN; C: 15% HOAc in H_2O; D: 100% Acetone

Eluting: A: 10 mM NH4OAc; B: 100% ACN

[a] The loading and eluting mobile phases were changed by step gradient at each step.

[b] Positions of the two six-port valves shown in Figure 3-2.

[c] Direction of extraction column flow.

3.1.5 AQUITY UPLC Analysis

3.1.5-A Mass scan rate

The A1 neat standards (2.3.8-A) were injected in 5 replicates onto the UPLC system equipped with a BEH Shield RP18 (2.1 x 50 mm, 1.7 μm) UPLC column from Waters. An isocratic elution with mobile phase (35:65 ACN:0.5% HOAc) flowing at 0.6 mL/min was employed for analysis. The mass spectrometer was set with the parameters specified for A1 in Table 3-2 except that the dwell time for the MRM channel was changed from 200 ms to 50 ms and then 100 ms. Two MRM transitions (one for A1 and

one for a blank) were monitored for each dwell time. By using the same integration parameters, the peak areas and peak widths at 50% peak height were obtained with the Analyst software and the data are listed in Table 4-6.

3.1.5-B MS responses at different flow rates

The 1 μM A1 and B3 solutions (2.3.8-B) were separately infused into the TIS source at infusion rates of 50, 100, 300, 600 and 1000 μL/min. The MS parameters were optimized for each flow rate to obtain favored conditions for formation of protonated ions and product ions. The acquisition conditions for the various flow rates are listed in Table 3-7.

Flow analysis was conducted by replacing the UPLC column with 2 meters of peek tubing (ID: 125 μm) and separately injecting 20 μL of the A1 and B3 standards (2.3.8-B) onto the UPLC system. The mobile phases were 35:65 ACN:0.5% HOAc and 75:25 ACN:10 mM NH_4OAc for the A1 and B3 samples, respectively. The MS responses for A1 and B3 at flow rates of 50, 100, 300, 600 and 1000 μL/min were monitored by using the corresponding optimized acquisition parameters (Table 3-7). The effects of flow rate on analyte MS response are shown in Figures 4-27 and 4-28 for A1 and B3 analytes, respectively.

3.1.5-C Chromatography and detection

Chromatographic separations were performed at ambient temperature by using the BEH Shield RP18 (2.1 x 50 mm, 1.7 μm) UPLC column. The elution conditions are listed in Table 3-8. The autosampler compartment was set at $5^{o}C$ and the injection volume was 2 μL. Analyte and lipid combined solutions (2.3.6-E) were separated by using the corresponding UPLC conditions for acidic and basic compounds. The

Table 3-7. Optimized mass spectrometer acquisition parameters at various flow rates

A1	Flow rate (µL/min):	50	100	300	600	1000
	Gas 1:	50	50	60	75	85
	Gas 2:	50	50	55	75	85
	Curtain gas (CUR):	30	30	30	30	30
	Collision gas (CAD):	6	6	6	6	6
	Ion spray voltage (IS):	5500	5500	4500	4000	4000
	Temperature (TEM):	700	700	700	700	700
	Declustering potential (DP):	36	36	36	36	36
	Entrance potential (EP):	8	8	8	8	8
	Collision energy (CE):	17	17	17	17	17
	Collision cell exit potential (CXP):	14	14	14	14	14
	Interface heater:	on	on	on	on	on
	Transition monitored:	m/z 194.3 → 176.2				
	Resolution of Q1:	Unit				
	Resolution of Q3:	Unit				
	Pause time:	1 ms				
	Deflector (DF):	-200				
	Channel electron multiplier (CEM):	2000				

B3	Flow rate (µL/min):	50	100	300	600	1000
	Gas 1:	30	50	55	65	75
	Gas 2:	30	50	55	65	85
	Curtain gas (CUR):	30	30	30	30	30
	Collision gas (CAD):	7	7	7	7	7
	Ion spray voltage (IS):	5500	5500	5000	4500	4500
	Temperature (TEM):	550	550	550	600	600
	Declustering potential (DP):	100	100	100	100	100
	Entrance potential (EP):	8	8	8	8	8
	Collision energy (CE):	38	38	38	38	38
	Collision cell exit potential (CXP):	15	15	15	15	15
	Interface heater:	on	on	on	on	on
	Transition monitored:	m/z 472.2 → 436.4				
	Resolution of Q1:	Unit				
	Resolution of Q3:	Unit				
	Pause time:	1 ms				
	Deflector (DF):	-200				
	Channel electron multiplier (CEM):	2000				

acquisition parameters listed in Table 3-2 were modified to account for the effects of flow rate (Table 3-7). The Gas 1, Gas 2 and TEM values were set at 75, 75 and 700 and 65, 65 and 600, for acidic and basic compounds, respectively. The MRM transitions for the analytes and GPCho lipids were simultaneously monitored and the chromatograms are shown in Figure 4-29.

Table 3-8. LC method for analyte analysis by using the UPLC system

Time (min)	Flow (mL/min)	%A	%B	Gradient
0	0.6	80	20	
2.0	0.6	30	70	ramp
2.2	0.8	1	99	step
2.5	1	1	99	step
3.0	0.6	80	20	ramp

Acidic compounds: A: 0.5% HOAc in H_2O; B: 100% ACN
Basic compounds: A: 10 mM NH_4OAc in H_2O; B: 100% ACN

3.1.5-D Absolute matrix effects

Analyte standards prepared in plasma supernatant and solvent (2.3.8-C) were analyzed by using the specified UPLC conditions for acidic and basic compounds, respectively (Table 3-8). MS detection employed the modified conditions from Table 3-2. The peak areas of the two types of standards were compared and variations between the five lots of control plasma were calculated. The results for acidic and basic compounds are listed in Tables 4-7 and 4-8, respectively.

3.1.5-E Plasma standard curves

Plasma standard curve samples for acidic and basic compounds prepared by protein precipitation (2.3.8-D) were separately injected onto the UPLC system and separated by using the same conditions as were used for the absolute matrix effect

experiments (3.1.5-D). The linear regression results and slope RSD (%) values are shown in Figures 4-30 and 4-31 for acidic and basic compounds, respectively.

3.2 **Elucidation of Analyte Ionization Suppression Effects**

3.2.1 Mass Spectrometry Conditions

The API 4000 mass spectrometer was operated in positive electrospray ionization (ESI) mode with the TIS source set at unit mass resolution. Q1 scans were performed by using the same parameters for all measurements. The scan range was from m/z: 150 to 550 and 10 MCA were acquired with a step of 0.5 amu and scan time of 0.2 sec. The Gas1, Gas 2, CUR, DP, EP and TEM values were set at 30, 50, 50, 80, 8 and 600 arbitrary units, respectively. The ion spray voltage employed three conditions: 3000, 4000, or 5000 V. The CEM was set at 2200 and the deflector was at -200. Solutions were infused at 60 µL/min into the TIS source with a syringe pump to obtain Q1 full scan mass spectra. Protonated positive ions $[M+H]^+$ at m/z values of 291.5, 260.5, 472.5, and 496.5 were monitored for B1, B2, B3, and 16:0 LPC, respectively. All of the results were the average of five measurements.

3.2.2 Simulated Results in Microsoft Excel

Figure 5-2 shows the simulated logarithm surface concentration for a single analyte as a function of concentration. The equations used to calculate the plotted values as well as the individual data are included. Assuming that the concentration of background electrolyte (C_E) was constant at 1.0×10^{-5} M, when the partition coefficient ratio of the analyte relative to electrolyte (K_A/K_E) was varied from 0.1, 1 and 10, the corresponding analyte surface concentrations ($[A^+]_s$) were calculated over a concentration

(C_A) range of 1.0×10^{-10} M to 1.0×10^{-4} M.

Figure 5-3 shows the simulated surface concentrations for two analytes in the same solution at equal concentrations. Assuming that analytes (A and B) have different partition coefficients, $K_A/K_E = 1$ and $K_B/K_E = 10$, and C_E was constant at 1.0×10^{-5} M, the surface concentrations of $[A^+]_s$ and $[B^+]_s$ were calculated over a concentration range of 1.0×10^{-10} M to 1.0×10^{-4} M.

3.2.3 MS Response for a Single Analyte as a Function of Concentration

The series of single analyte solutions prepared in 2.4.1 were infused into the mass spectrometer. A Q1 scan was performed to measure the analyte ion intensities at different concentrations and the logarithm of the results are shown in Figure 5-4.

3.2.4 MS Response for a Single Analyte in a Buffered Solution

Single analyte solutions prepared in three types of buffers over a wide buffer concentration range (2.4.2) were sequentially infused to compare the ion intensities under different buffer conditions. The data for B1, B2, B3, and 16:0 LPC, are shown in Figures 5-5 to 5-8, respectively.

3.2.5 MS Response for Binary Analyte Solutions

Solutions containing two analytes, prepared as described in 2.4.3, were separately infused to measure the effects of co-analytes on analyte ionization. The results for B1 containing co-analyte B2, B3, and 16:0 LPC, respectively are shown in Figure 5-10; B2 with B1, B3, and 16:0 LPC, respectively are shown in Figure 5-11; and B3 with B1, B2, and 16:0 LPC, respectively are shown in Figure 5-12.

3.2.6 Total Ion Current for a Single Analyte as a Function of Concentration

Single analyte solutions were diluted with 50:50 $ACN:H_2O$ to form solutions with

a concentration ranging between 1.0 x 10^{-9} M to 1.0 x 10^{-4} M following a procedure similar to 2.4.1. The total ion current (TIC), which is the summed intensities of detected ions, was measured during infusion. The TIC results for B3 and 16:0 LPC are shown in Figure 5-13.

3.2.7 MS Response for a Single Analyte in Buffered GPCho Lipid Solutions

A series of solutions prepared as described in 2.4.4 were sequentially infused and analyte ion intensities were measured by Q1 scans. The MS responses for analytes in buffered and un-buffered solutions containing 16:0 LPC are shown in Figures 5-14 to 5-16 for B1, B2, and B3, respectively.

3.2.8 TIC for 16:0 LPC in Buffered and Un-buffered Solutions

A series of 16:0 LPC solutions were prepared by following the procedure outlined in Table 2-7 (II-4 a to II-4 g) in 2.4.4 except that no analyte was added. These solutions were infused to obtain the TIC spectra and the results are shown in Figure 5-17.

CHAPTER 4

PROCEDURES FOR REDUCING MATRIX EFFECTS AND INVESTIGATION OF THE ROLE OF GLYCEROPHOSPHOCHOLINE LIPID ENDOGENOUS INTERFERENCES

4.1 Theory and Background

4.1.1 Theory of Turbulent Flow Chromatography

High turbulent flow liquid chromatography (HTLC), which is characterized by high separation efficiency at high flow rate, has been demonstrated to be useful for fast and automated sample pretreatment [1-6]. It has been verified that at ultra high flow rate (linear flow rate > 12 cm/s), the reduced plate height decreases with increasing flow rate [7], which is inconsistent with van Deemter equation predictions. Currently, a quantitative theory describing peak spreading for turbulent flow in a packed column is not available because the flow profile is more complicated than laminar flow and therefore more difficult to model. Based on what is known about conventional packed column LC and exploratory investigations into turbulent flow in open-tubular chromatography [2,3,8,9], the high separation efficiency of turbulent flow chromatography might be attributed to the increased mass transfer inherent in the complex flow pattern, where eddy convection is considerably increased compared to laminar flow.

Chromatographic peak spreading is due to solute velocity inequalities as molecules move through the column [10-12]. Due to the complicated geometry of a packed column, the flow rates of molecules in interstitial channels between particles can be different. The adsorption and desorption processes for molecules at the mobile

phase/stationary phase boundary as well as the diffusion of molecules into different flow-paths and along (up and down) the flow axis cause band broadening. In addition, the parabolic profile of laminar flow causes molecules at the front of the band to exhibit a mass transfer rate that is different from those at the tailing edges. As a consequence, peak broadening arises due to the flow gradient and molecular diffusion. The column efficiency in conventional LC, which is carried out under laminar flow conditions, can be modeled by the van Deemter equation. For a packed column [13]:

$$H = \cfrac{1}{\cfrac{1}{C_e d_p} + \left(\cfrac{1}{(C_m d_p^2 u)/D_m} \right)} + \frac{C_d D_m}{u} + \frac{C_{sm} d_p^2 u}{D_m} = A + B/u + C \cdot u \qquad \text{(I-1)}$$

where H: plate height; d_p: particle diameter; u: linear velocity of the mobile phase; D_m: analyte diffusion coefficient; C_e, C_m, C_d, and C_{sm} are coefficients for eddy diffusion, mobile phase mass transfer, longitudinal diffusion, and mass transfer within a particle, respectively. Term A in the above equation represents the dispersive contribution from the flow profile, and it is considered to be independent of the flow velocity when flow terminates the velocity bias; term B is related to axial molecular diffusion; the mass transfer term, C, is determined by stationary phase adsorption and desorption processes.

In contrast to laminar flow, turbulent flow exhibits a profile with a plug character and yields reduced concentration gradients across the flow-paths. Moreover, the combination of large particles and high flow rates results in the formation of eddies, which greatly enhance mass transfer via convection. Because concentration gradients are quickly eliminated by cross channel mass transfer, peak broadening caused by flow inequalities within interstitial channels is reduced [8,14-16]. The absence of eddy diffusion effects indicates that molecular diffusion within and between eddies is not an

important factor for band spreading in turbulent flow [17]. It would be expected that the partitioning of molecules between stationary and mobile phases would substantially contribute to the separation efficiency in turbulent flow LC whereas the flow and diffusion effects, which are represented by terms A and B in the van Deemter equation for conventional LC, would be reduced [8,10].

In liquid chromatography, separation is achieved by differential adsorption of molecules at the surface of packing materials. Adsorption to and desorption from the surface of the stationary phase requires molecules to cross a stagnant film of mobile phase at the outer surface of the packing material and then pass through mobile phase pools inside the pores that contain reverse phase materials. In conventional LC, these processes are diffusion controlled [18-19]. Although they contribute to peak broadening, the pores must exist in order to ensure sufficient surface area for adequate column capacity. In HTLC, two factors dominate molecular transport. The large particles (50 – 60 μm) employed in turbulent flow columns increase the stagnant mobile phase mass transfer effect due to increased diffusion path lengths in the stagnant films on particle surfaces. Even under turbulent flow conditions, mass transfer in these stagnant zones is speculated to depend mainly on molecular diffusion. On the other hand, mass transfer in turbulent flow chromatography is predominantly achieved by mobile phase convection. Eddies also facilitate molecular transport into and out of the pores. The interplay of these factors determines the efficiency of adsorption/desorption processes in turbulent flow chromatography.

The onset Reynolds number, defined as when the flow changes from laminar to turbulent in a packed column, can vary from 1 to 100 [20-22]. The transition zone

between completely laminar and completely turbulent should be large as indicated by the smooth curve of reduced plate height vs reduced velocity as a function of Reynolds number [7,8]. The Reynolds numbers for turbulent flow columns used in a patent (100 x 4.6 mm, 500 µm) and commercially available (50 x 0.5 mm, 50 µm) were calculated by using a mobile phase density ρ = 0.9 g/cm^3, viscosity η = 1.6 g/m·s, and analyte diffusion coefficient D_m = 1.5 x 10^{-5} cm^2/s. Because the particle size of the former column was ten times larger than that of the other column, the corresponding Reynolds number and reduced velocity were 10-fold higher at comparable linear flow rates. There is a debate regarding whether the flow at Reynolds numbers below 10 should be claimed as turbulent flow or not [4,23-25], but it is generally agreed that even if the flow profile is not completely turbulent, mass transfer is effectively increased and velocity differences are reduced through eddy diffusion.

Table 4-1. Reynolds numbers and reduced velocities for turbulent flow packed columns

Column ID (mm)	Particle size d_p (µm)	Flow rate (mL/min)	Linear flow rate μ (cm/s)	Reduced velocity $v = \mu\, d_p/ D_m$	Reynolds number $Re = \mu\, \rho\, d_p/ \eta$
100 x 4.6	500	80	11.4	3.8E+04	32.1
		100	14.3	4.8E+04	40.2
		120	17.2	5.7E+04	48.4
		140	20.0	6.7E+04	56.3
50 x 0.5	50	1.5	12.7	4.2E+03	3.6

(*Re* for the 100 x 4.6 mm column was calculated based on Fig. 14 in Ref. 7)

A unique feature of turbulent flow LC is that proteins and other endogenous macromolecules can be rapidly washed away while analytes are retained by reverse phase materials [26,27]. The ability of molecules to enter the interior of particles is determined by the sizes of the pores within the particles. When the diameter of a molecule is smaller

than the pore diameter, the molecule can access the particle interior. Among the primary human plasma proteins: serum albumins, globulins and fibrinogen; the serum albumins are the smallest and most abundant [28]. Based on a solid sphere model, serum albumins possess an estimated sphere radius of approximately 40 Å [29]. This size increases about 2-fold when these molecules are denatured [30,31]. The use of small pores (60Å) as well as large particles (50 - 60 μm) coupled with porous end-column frits (~ 20 μm) allows for the separation of small molecules from endogenous macromolecules through a size exclusion mechanism. In addition, the degree to which a molecule follows turbulent fluctuations depends on its size and density. Large molecules would not be expected to behave in the same way as small molecules [17]. Small molecules with high diffusivities are quickly transferred into the particle pores via convection whereas large molecules with relatively low diffusivities require more time to diffuse into the pore areas and are more quickly eluted from the column.

4.1.2 Theory of Liquid-liquid Extraction

Liquid-liquid extraction (LLE) is a common approach for removing analytes from biological samples by selective partitioning between two immiscible phases: aqueous and organic solvent [32-36]. A hydrophobic compound tends to reside in the non-polar organic phase whereas a more hydrophilic compound favors the polar aqueous phase. Thus, sample components are separated according to their polarity preference. The partition coefficient (K), which is equal to the concentration of an analyte in the organic phase divided by its concentration in the aqueous phase, is normally used as a measure of distribution of a species between the two phases [37-39]. The separation efficiency of two components in LLE is quantified by the separation factor (α), which is the distribution

ratio of one species divided by the other. *K* is directly related to the chemical potentials

(μ_i) of an analyte (*i*) in the two partitioning phases ($K = exp(-\Delta\mu_i^0/ RT)$) and μ_i depends

on the intrinsic thermodynamic energy of the analyte in a certain solvent and the dilution

effects of that solvent. When the chemical potentials of the analyte in the two phases are

equal, the partitioning process reaches equilibrium.

4.1.3 Theory of Ultra Performance Liquid Chromatography

The separation process in chromatography can be modeled as a repeated

distribution/equilibration. The goal of separation optimization is to achieve a sufficient

number of theoretical plates (*N*) in a reasonable analysis time. The plate number is an

approximation of the number of distribution/equilibration events that a given analyte

undergoes when eluting from the column ($N \approx t_R/ \tau_{eq}$); where t_R is the analyte retention

time and τ_{eq} is the time for a single equilibrium in the distribution process [40]. The most

important factors that affect the value of τ_{eq} are the diffusion coefficient (D_m) and

diffusion path length (*l*). For a spherical particle packed column, $\tau_{eq} \approx d_p^2/ 30D_m$ and

$N \approx 30D_m\ t_R / d_p^2$ (d_p: particle diameter) [40]. Although these equations only take into

account the separation impedance of mass transfer within the particle, they explain the

fundamental aspects of the chromatographic separation: resolution and analysis time

tradeoff. With a particular mobile phase and stationary phase, decreasing the diffusion

path length, which is proportional to the particle diameter, is one of the most effective

means of improving column performance. The use of a small particle column to perform

fast analyses with better resolution is indicated by the effect of the mass transfer C term

in the van Deemter equation. The equilibrium time is a function of the square of the

particle size. Reducing the particle size leads to a decrease in the mass transfer resistance

and consequently a large decrease in the plate height.

Decreasing the particle size to improve resolving power is limited by the pressure that equipment can withstand. According to Darcy's law, the dependence of back pressure (ΔP) for a solvent on a column with resistance factor ($\emptyset$) is $\Delta P = u\, L\, \eta\, \emptyset / d_p{}^2$; where u: flow rate, η: solvent viscosity and L: column length. The tradeoff between separation time, resolution, and back pressure was pointed out by Knox in 1969 [41,42] and subsequently discussed by many other researchers [40,43-45]. The theoretical performance of a column with various particle sizes can be shown by a Knox curve, which is a plot of plate height versus linear velocity (Fig. 4-1). This plot illustrates that when the particle size is below 2 μm, in addition to an efficiency increase, optimal separation can be maintained for a wider velocity range, which implies that faster separation can be made without significantly compromising resolution. Frontiers in ultra high pressure LC have been investigated in academic research laboratories [46-51]. With high pressure and flow rate, frictional heating of the mobile phase produces uneven

Figure 4-1. Theoretical plate height curves for different particle sizes
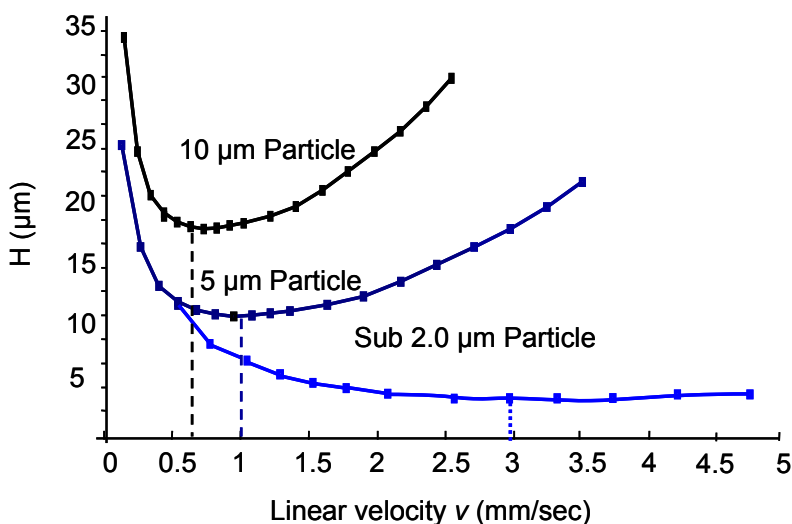
Curves were calculated according to eq. I-1 with A = 1.0, B =1.5 and C = 0.05

temperatures across the column and parameters such as solvent density, viscosity and diffusion coefficient are dependent on the pressure drop [43,44,52,53]. These issues, as well as instrumental requirements for sample introduction and pumping at high pressure, and uniform porous particles capable of withstanding high pressure, have been described in review articles [54,55]. In this research, a recently commercialized UPLC system and a bridged ethylsiloxane/silica hybrid (BEH) 1.7 μm particle column with a pressure limit of up to 15000 psi were employed.

4.1.4 Phospholipids Background

Lipids are present in all organisms and are essential for the functioning of membrane related processes, including energy storage, building structural components of cellular membranes, and serving as precursors for numerous secondary messengers. Phospholipids are a class of lipid formed from four components: fatty acids, a phosphate group, a nitrogen containing alcohol, and a backbone. Phospholipids with a glycerol backbone are known as glycerophosphocholines (GPCho), and are the most abundant phospholipids in plasma [56-58]. The general structure of GPCho lipids is a three carbon backbone molecule with fatty acids esterified at *sn*-1 and *sn*-2 positions and a polar head containing a phosphate ester at the *sn*-3 position (Fig. 4-2). Variations in the head group lead to different GPCho lipid classes, such as phosphatidic acid (PA), phosphatidylcholine (PC), phosphatidylethanolamine (PE), phosphatidylserine (PS), phosphatidylglycerol (PG) and phosphatidylinositol (PI) [59]. The type of bonding, ester or ether (alkyl ether or vinyl ether), between the fatty acid chain and glycerol at the *sn*-1 position determines whether the subclass of the phospholipid is phosphatidyl or plasmalogen. The linkage at the *sn*-2 position is always an ester bond. The ester group

chain may vary from 14 to 22 carbons in length and contain 0 to 6 double bonds [60].

Numerous extraction procedures for separating phospholipids from biological materials

and chromatographic methods for qualitative and quantitative determination of these

substances have been described and are summarized in a recent review [61]. The

application of mass spectrometry to phospholipid analysis has been investigated by using

various ionization methods, including fast atom bombardment (FAB), matrix assisted

laser desorption ionization (MALDI), and electrospray ionization (ESI), and the

mechanisms for product ion formation have been summarized in an article [62].

Figure 4-2. Structures of glycerophosphocholine lipids
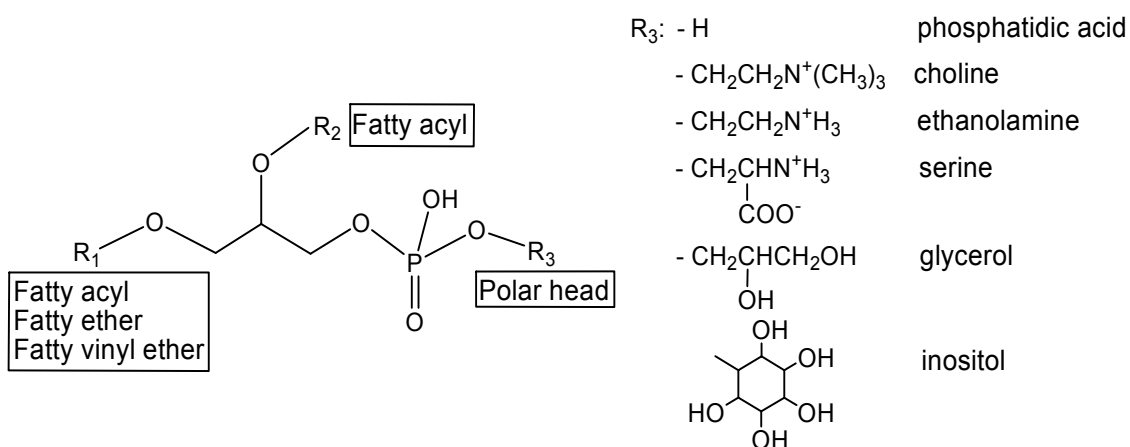
Matrix effects caused by plasma sample endogenous species are known to affect

quantitative analysis and the reliability of an assay is determined to a large extent by the

specifics of the extraction and chromatographic separation processes. The techniques

described previously represent three different approaches used for achieving analysis

specificity. The HTLC method utilizes the high efficiency of turbulent flow mass transfer

to separate target analytes from sample matrix whereas LLE separation is based on

compound polarity. The UPLC approach isolates analytes from matrix components by

using high resolution chromatographic separation. The capabilities of these three methods for eliminating matrix effects in biological sample analysis will be compared. In addition, in order to effectively resolve matrix effect problems, it will be necessary to identify the source of the endogenous species that interfere during analysis. Identifying the main interfering components will be helpful for designing suitable analysis procedures that avoid matrix effect interferences.

4.2 Discussion

4.2.1 MS Detectable Components in Human Plasma

4.2.1-A MS results for protein precipitated plasma samples

The supernatant of pooled human plasma was directly infused into a mass spectrometer to identify the main endogenous components. If the detected components affect analyte analyses, they most likely contribute to matrix effect interferences. The ESI positive ion full scan Q1 mass spectrum for a protein precipitated human plasma sample is shown in Figure 4-3(a). Several abundant signals were observed at *m/z* 305, 519, 543, 782 and 805. These major signals were examined with a higher resolution Q1 center scan to obtain their accurate masses. The ion at *m/z* 305 does not derive from GPCho lipids and was not examined further. The Q1 center scan spectrum for *m/z* 519 indicates that this signal has a single peak with an accurate mass of 518.3. A shoulder peak at 519.3 is due to isotopic effects (Fig. 4-3(b)). The Q1 center scan spectrum for *m/z* 543 shows three peaks with comparable heights at *m/z* 542.3, 544.3 and 546.3. It appears that these peaks originate from endogenous components with similar structures, except for the number of double bonds. The Q1 center scan spectrum for *m/z* 782 and 805 demonstrates

that the former ion is due to a single peak with an accurate mass of 780.6 and the latter

ion appears to consist of peaks at *m/z* 804.7 and 806.7 (Fig. 4-3(c)).

Figure 4-3. Full scan Q1 spectrum (a) and Q1 center scan spectra (b and c) for a protein precipitated human plasma sample
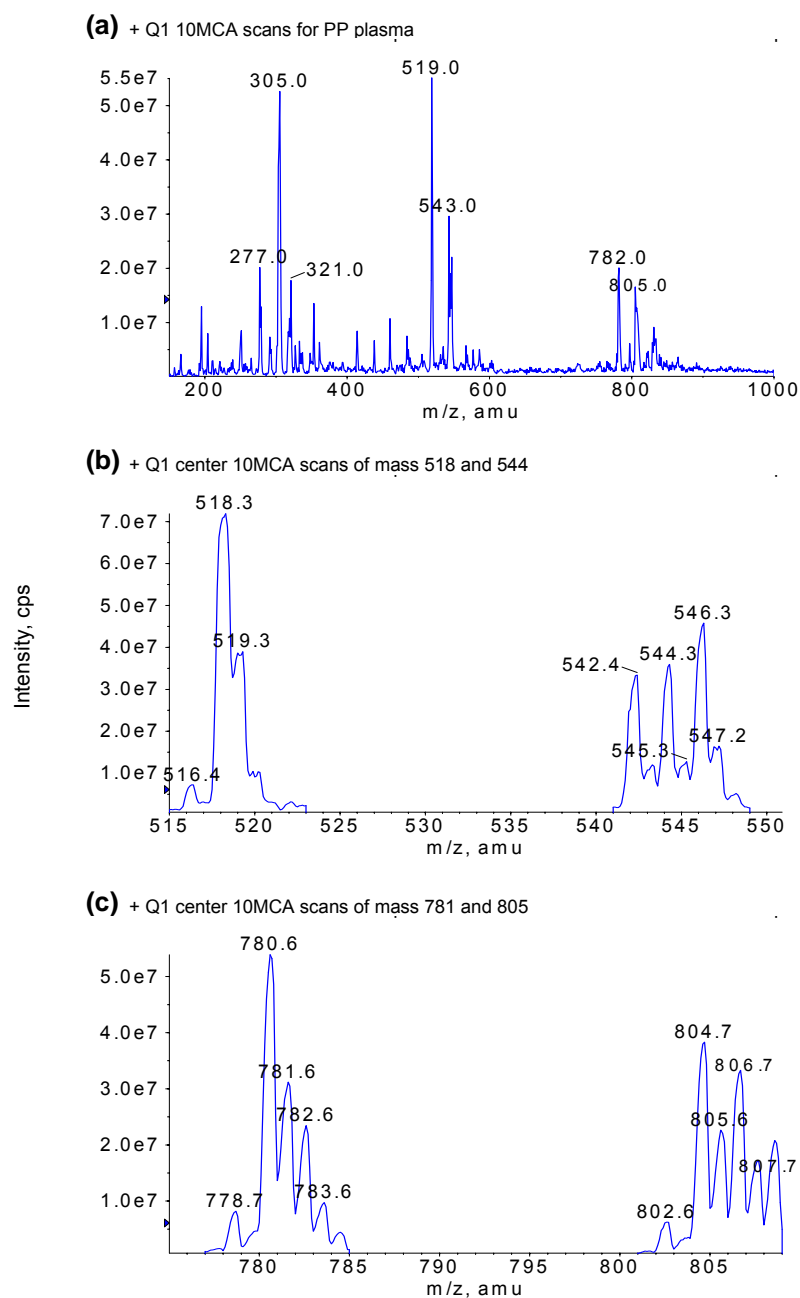
The Q1 center scan identified ions were subjected to product ion scans to investigate their fragmentation pathways, which should be closely associated with their structures. The product ion scan spectra for ions at *m/z* 518.3, 542.3, 544.3 and 546.3 exhibit a similar dissociation pattern where abundant product ions corresponding to *m/z* 147, [M-205]$^+$ and [M-59]$^+$ were formed and the most intense ion was [M-59]$^+$ (Fig. 4-4). The spectra of ions at *m/z* 780.6, 804.7 and 806.7 exhibit abundant fragment ions at *m/z* 147, [M-205]$^+$, [M-183]$^+$ and [M-59]$^+$ with signal intensities distributed in a similar pattern (Fig. 4-5). The base signal was [M-183]$^+$, which was barely observed in the product ion spectra of *m/z* 518.3, 542.3, 544.3 and 546.3 under the specified collision induced dissociation conditions. Since all of the identified ions yielded a common ion at *m/z* 147, the precursor ion scan was utilized to confirm the above results obtained from the Q1 scans (Fig. 4-5(d)). The obtained spectrum is very similar to Figure 4-3(a), except for the disappearance of the ion at *m/z* 305, which indicates that: (1) the endogenous components of human plasma that can produce a relatively intense *m/z* 147 moiety during fragmentation are included in the Q1 scan identified ions; and (2) the ion at *m/z* 305 does not fit in the category to which the identified ions belong.

Phospholipids are one of the major components of human plasma and mass spectrometry studies for lipids indicate that in positive ionization, sodiated GPCho lipid ions produce fragment ions at *m/z* 147, [M+Na-205]$^+$, [M+Na-183]$^+$ and [M+Na-59]$^+$ [66-68]. Further characterization of the subclasses of GPCho lipids indicated that lysophosphatidylcholine (LPC), plasmanyl-PC, and plasmenyl-PC yielded the most abundant [M+Na-59]$^+$ product ion, which can be used to distinguish them from PC, which produces a prominent ion for [M+Na-183]$^+$ [69-71]. The fragmentations of

Figure 4-4. Product ion scan spectra for ions at *m/z* 518.3 (a), 542.3 (b), 544.3 (c) and 546.3 (d) from a protein precipitated human plasma sample
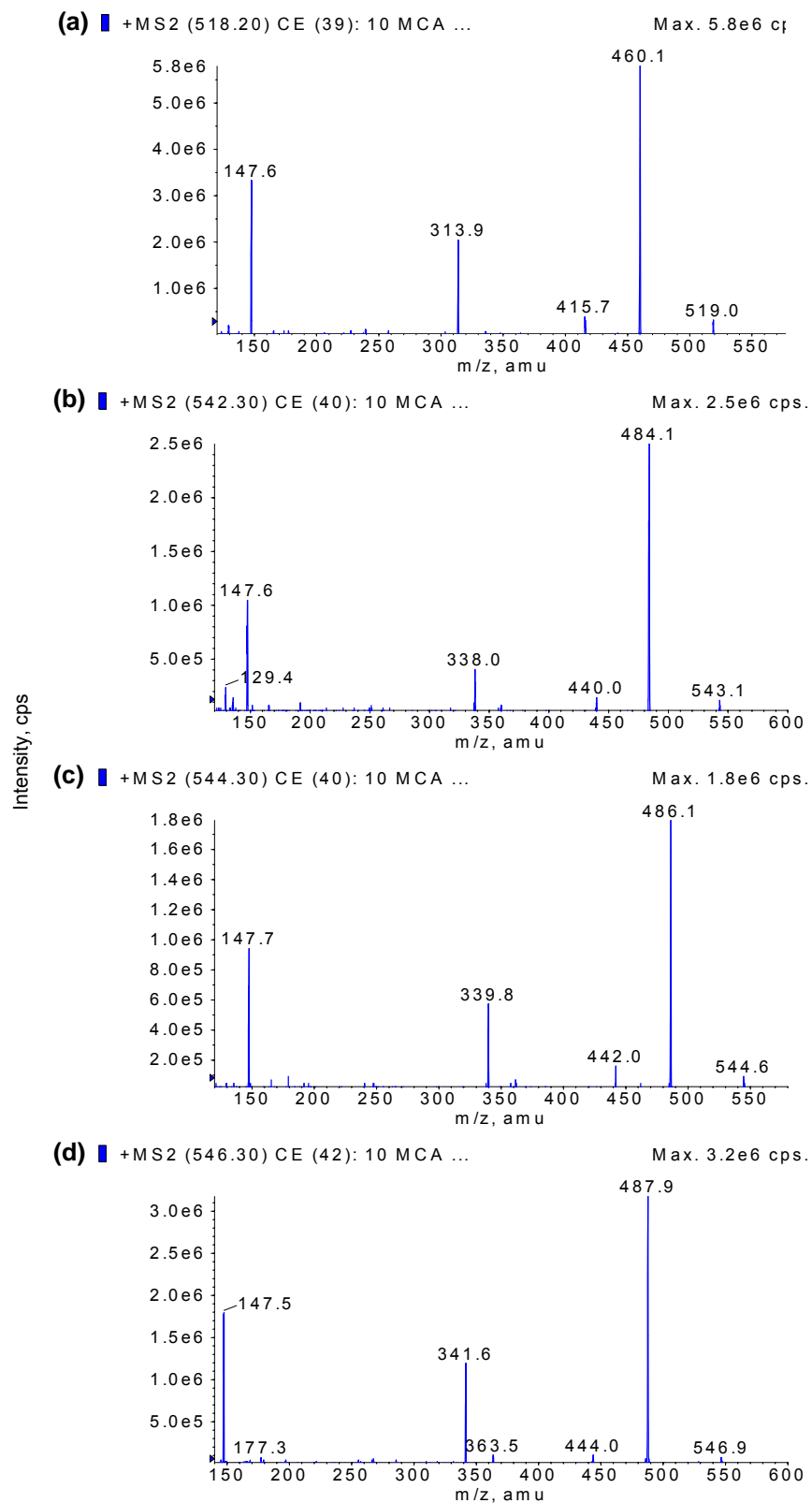
Figure 4-5. Product ion scan spectra for *m/z* 780.6 (a), 804.7 (b) and 806.7 (c) as well as a precursor ion spectrum of *m/z* 147.1 (d) from a protein precipitated human plasma sample
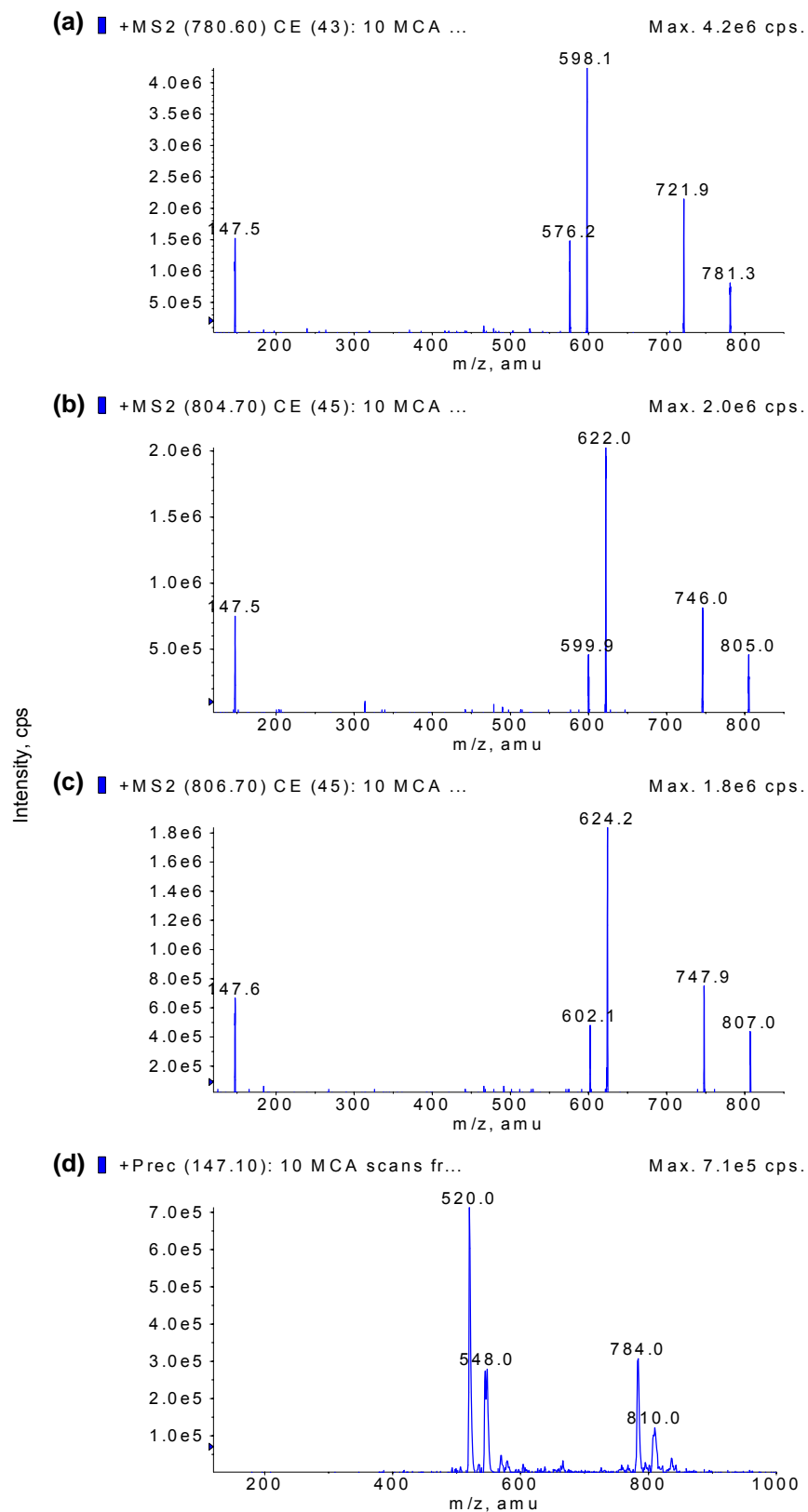
plasmanyl-PC and plasmenyl-PC are analogous to that of LPC except for an additional loss of R_2COOH from the $[M+Na-205]^+$ ion. Differentiation of LPC regioisomers is based on the relative abundance of the product ions; *sn*-1-LPC forms an abundant ion at *m/z* 147 whereas the base signal for *sn*-2-LPC corresponds to $[M+Na-59]^+$ [72]. The observed dissociation pattern for ions at *m/z* 518.3, 542.3, 544.3 and 546.3 is consistent with the fragmentation features of *sn*-2-LPC, therefore, these ions are suspected to be sodiated *sn*-2-LPC. The identity of these ions was confirmed by analysis of synthetic LPC standards. Based on the mass of each molecule, which is calculated as the mass of the detected ion minus the mass of sodium, 16:0, 18:1 and 18:0 LPC standards were selected. The ion at *m/z* 542.3, which was probably due to 18:2 LPC, was not examined because a standard was unavailable. The ions at *m/z* 780.6, 804.7 and 806.7 exhibit dissociations similar to PC, but to determine their identities (e.g. carbon number of each acyl chain and location of double bonds) and the positions of the fatty acid substituents, deuterium labeled analogues and CAD mass spectrometry would be needed. Because of the structural and polarity similarities of the PC type lipids, the synthetic 16:0-18:2 PC standard, which forms sodium adduct ions at *m/z* 780.6, was used to represent the PC lipids detected in human plasma samples.

4.2.1-B MS results for synthetic LPC and PC standards

To confirm the identity of the Q1 scan signals in the protein precipitated plasma sample, 16:0, 18:1 and 18:0 LPC and 16:0-18:2 PC standards were separately infused into the mass spectrometer under conditions that were identical to those used for the plasma supernatant. Corresponding spectra for Q1 full scan, Q1 center scan, and product ion scans are shown in Figures 4-6 to 4-9. The full scan Q1 spectra indicate that each
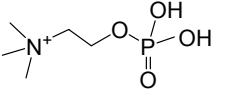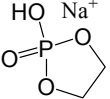
GPCho lipid standard yielded a protonated ion [M+H]$^+$ and a sodium adduct [M+Na]$^+$. The [M+H]$^+$ peak assignment was justified by the correspondence of the calculated exact mass of the molecule to the accurate mass of the protonated ion in the Q1 center scan. The [M+H]$^+$ ions, with accurate masses of 496.2, 522.2, 524.2 and 758.6, produced predominately a single fragment ion at m/z 184. This dissociation is a characteristic fragmentation of protonated GPCho lipids and the m/z 184 ion is the protonated phosphocholine moiety ( ) from the polar head. The corresponding sodium adducts for 16:0, 18:1 and 18:0 LPC standards, with accurate masses at m/z of 518.3, 544.3 and 546.3, produced major fragment ions at m/z 147, [M+Na-205]$^+$ and [M+Na-59]$^+$ with the base peak at [M+Na-59]$^+$. The [M+Na]$^+$ for 16:0-18:2 PC at m/z 780.7 yielded an additional fragment ion at m/z [M+Na-183]$^+$, which was the base peak. These sodium adducts yielded identical fragmentation patterns to those for plasma endogenous species with the same masses. The fragment ion at m/z 147 corresponds to ( ) a sodiated, five-membered cyclophosphane ring. The [M+Na-59]$^+$ ion was due to a neutral loss of trimethylamine, and the [M+Na-183]$^+$ and [M+Na-205]$^+$ ions resulted from the loss of non-sodium and sodium phosphocholine, respectively. Preliminary results for the synthetic LPC and PC standards have verified that the Q1 scan signals at m/z 518.3, 544.3, 546.3 and 780.7 for the plasma supernatant were from the sodium adduct ions of endogenous GPCho lipids. This confirmation also supports the conclusion that ions at m/z 542.3, 804.7 and 806.7 were also formed by endogenous GPCho lipids. The reason why GPCho lipids in plasma only form sodium adducts whereas the synthetic lipids yielded principally protonated ions was due to the fact that the sodium content in plasma is much higher than in a solvent. Detailed fragmentation

Figure 4-6. MS spectra for the 16:0 LPC standard: Q1 scan (a), Q1 center scan (b) and product ion scans (c and d)

(a) +Q1: 10 MCA scans from Sample...   Max. 6.8e7 cps.

497.0 [M + H]⁺
519.0 [M + Na]⁺
216.0

(b) +Q1: 10 MCA scans from Sample...   Max. 7.2e7 cps.

496.2
497.2
498.2
518.3
519.3
520.3

(c) +MS2 (496.20) CE (40): 10 MCA ...   Max. 2.8e7 cps.

184.2
125.1
313.5

(d) +MS2 (518.30) CE (40): 10 MCA...   Max. 6.4e6 cps.

459.7
147.4
313.7
177.3
415.7
518.5
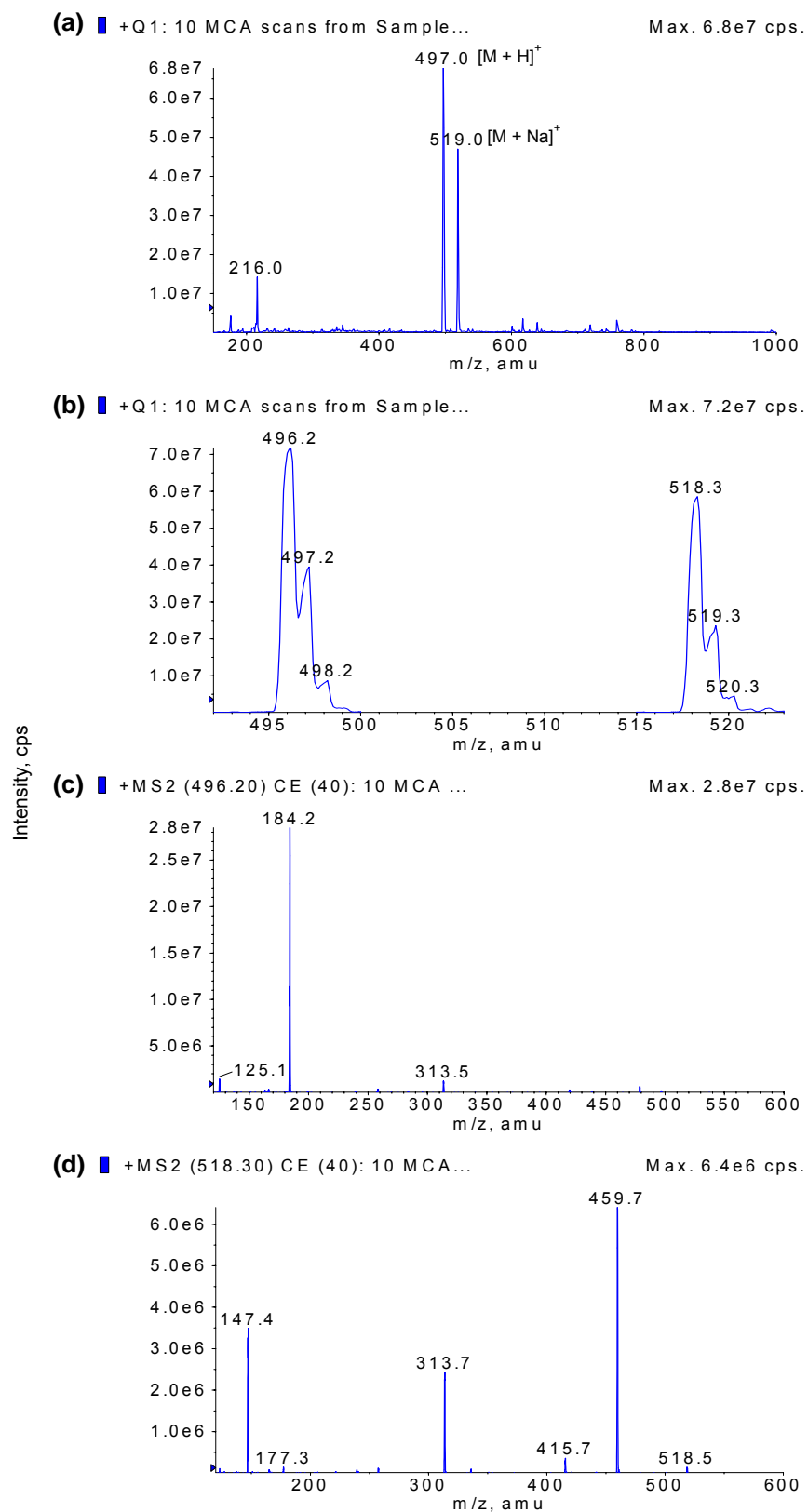
Figure 4-7. MS spectra for the 18:1 LPC standard: Q1 scan (a), Q1 center scan (b) and product ion scans (c and d)
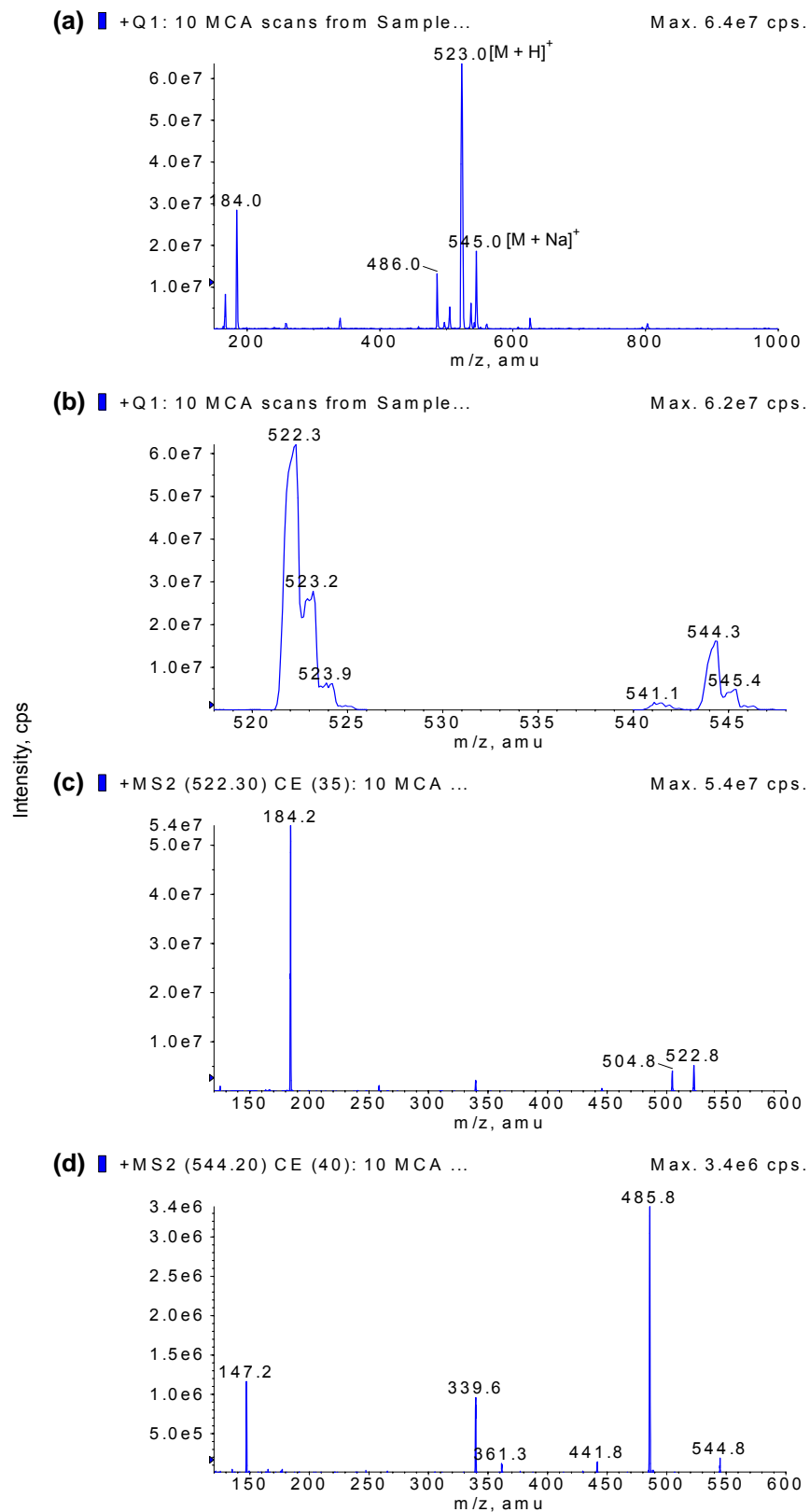
Figure 4-8. MS spectra for the 18:0 LPC standard: Q1 scan (a), Q1 center scan (b) and product ion scans (c and d)
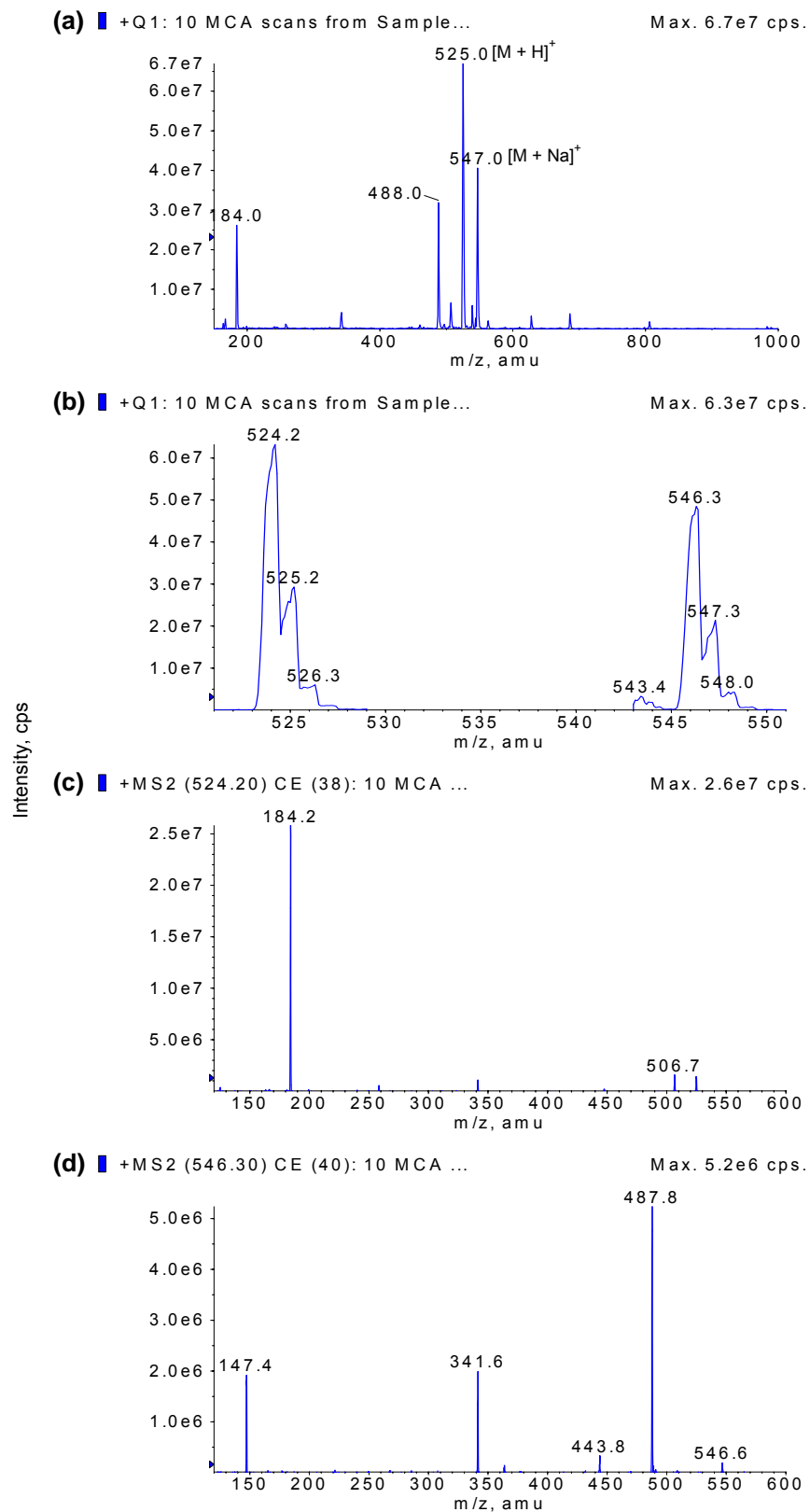
Figure 4-9. MS spectra for the 16:0-18:2 PC standard: Q1 scan (a), Q1 center scan (b) and product ion scans (c and d)
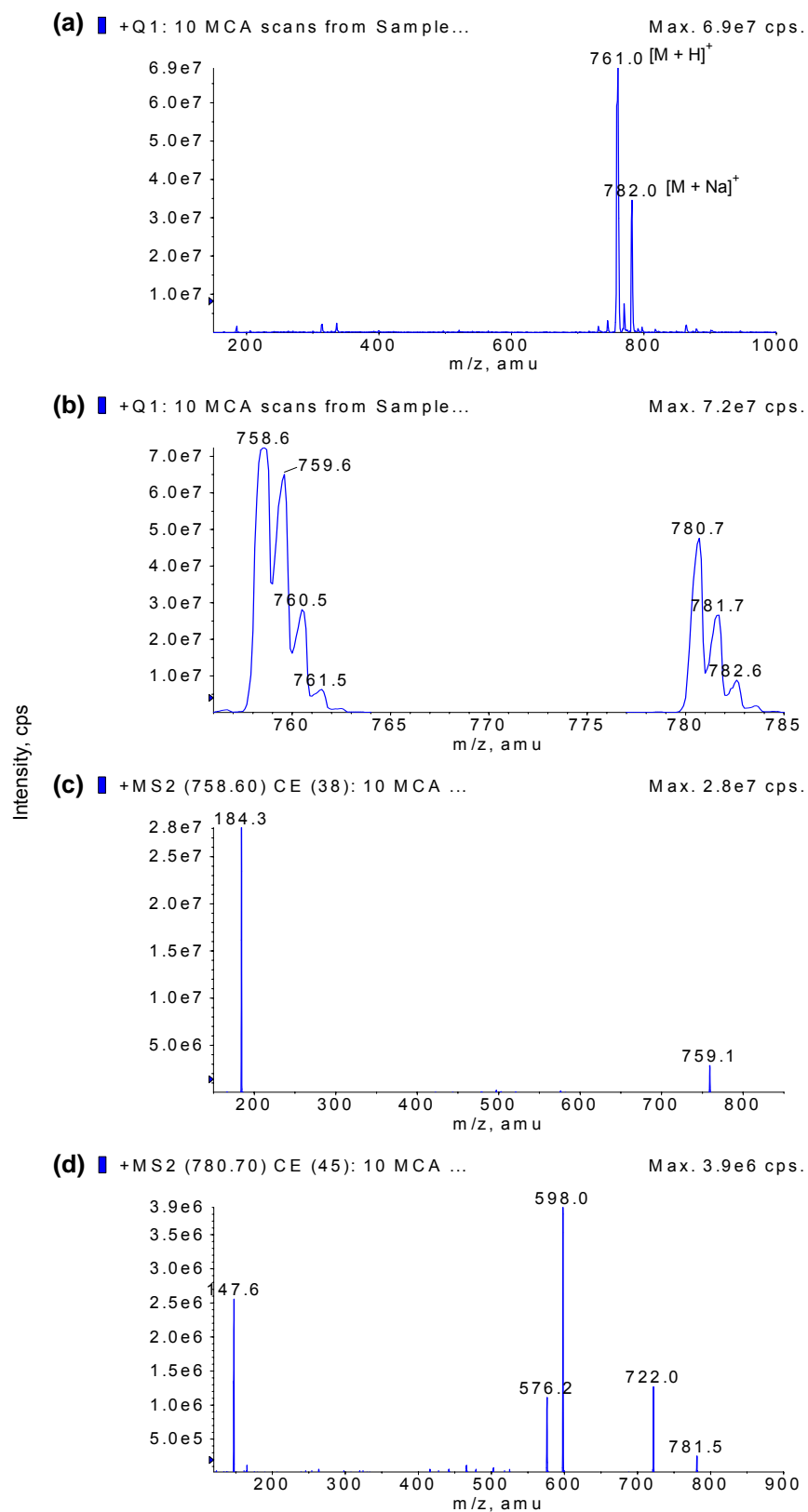
pathways for sodiated GPCho lipids in positive ionization mode have been proposed [66-67,72] and the dramatic differences in fragmentation patterns for [M+H]$^+$ and [M+Na]$^+$ ions were attributed to a cationization change. Sodium seems to stabilize the phosphate group and inhibits proton transfer in the rearrangement that leads to the formation of the phosphocholine moiety (*m/z* 184). Thus, the dissociation reaction prefers to initiate at the amine group and results in the formation of the [M+Na-59]$^+$ ion [67].

4.2.1-C Analyte monitoring

To investigate the effects of endogenous GPCho lipids on analyte ionization, a group of acidic and basic compounds with a wide polarity range were selected for study. Because these analytes possess various properties, different analysis conditions were needed. Therefore, matrix effects could be studied under different conditions and the influence of mobile phase composition and solvent pH on matrix effects was also examined. Analytes were tuned in positive ESI mode and the spectra for the acidic and basic compounds are shown in Figures 4-10 and 4-11, respectively. For A1 and A2 analytes, in addition to formation of protonated ions [M+H]$^+$, relatively intense sodium adduct ions [M+Na]$^+$ were produced. Because the abundance of sodium adduct ions varied with the sodium content in ionizing solution, and the content of sodium that originates from methanol and glass containers cannot be controlled, the [M+Na]$^+$ ion was not employed to monitor the target analytes [63-65]. Thus, the protonated A1 and A2 ions, with corresponding *m/z* values at 194 and 283, were selected as precursor ions for product ion scans. Moreover, to enhance the formation of protonated ions, a solvent containing less sodium was used for the mobile phase. It was observed that the intensities of sodium adduct ions were significantly reduced when acetonitrile rather than methanol

was used for infusion. The precursor ions for both A1 and A2 yielded predominantly the $[M+H-H_2O]^+$ ion, which is a common product ion for acidic compounds. The MRM transitions of m/z 194 → 176 and m/z 283 → 265 were utilized for quantitative determinations of A1 and A2, respectively.

The basic compounds were tuned similarly. The predominate signals in the Q1 spectrum were at m/z 291, 260 and 472, which corresponded to the protonated ions of analytes B1, B2 and B3, respectively. When these $[M+H]^+$ ions were scanned for product ions, multiple fragment ions were observed. Parameters for the major fragment ions were separately optimized in order to obtain the most abundant product ion for analyte quantification. Fragment ions at m/z 230, 183 and 436, which correspond to $[B1+H-OCH_2OCH_3]^+$, $[B2+H-H_2O-NH_2CHCH_3CH_3]^+$ and $[B3+H-2H_2O]^+$, were the most intense product ions for B1, B2 and B3 analytes, respectively. The corresponding MRM transitions used for quantitative determinations were m/z 192 → 230, m/z 260 → 183, and m/z 472 → 436.

4.2.1-D Effects of GPCho lipids on analyte ionization

The influence of GPCho lipids on analyte ionization was explored by using the widely accepted post-column infusion method. A constant amount of analyte was delivered to the ion source of the mass spectrometer by using a mixing tee with one inlet connected to an HPLC column. When the extracted control sample was injected onto the HPLC column, any endogenous components that affect the ionization of the infused analyte caused a variation of analyte response at their elution times. Standards of synthetic lipids were examined in order to determine the influence of specific endogenous components.

Figure 4-10. Full scan Q1 spectrum (a) and product ion scan spectra for A1 (b) and A2 (c) analytes in positive ionization mode
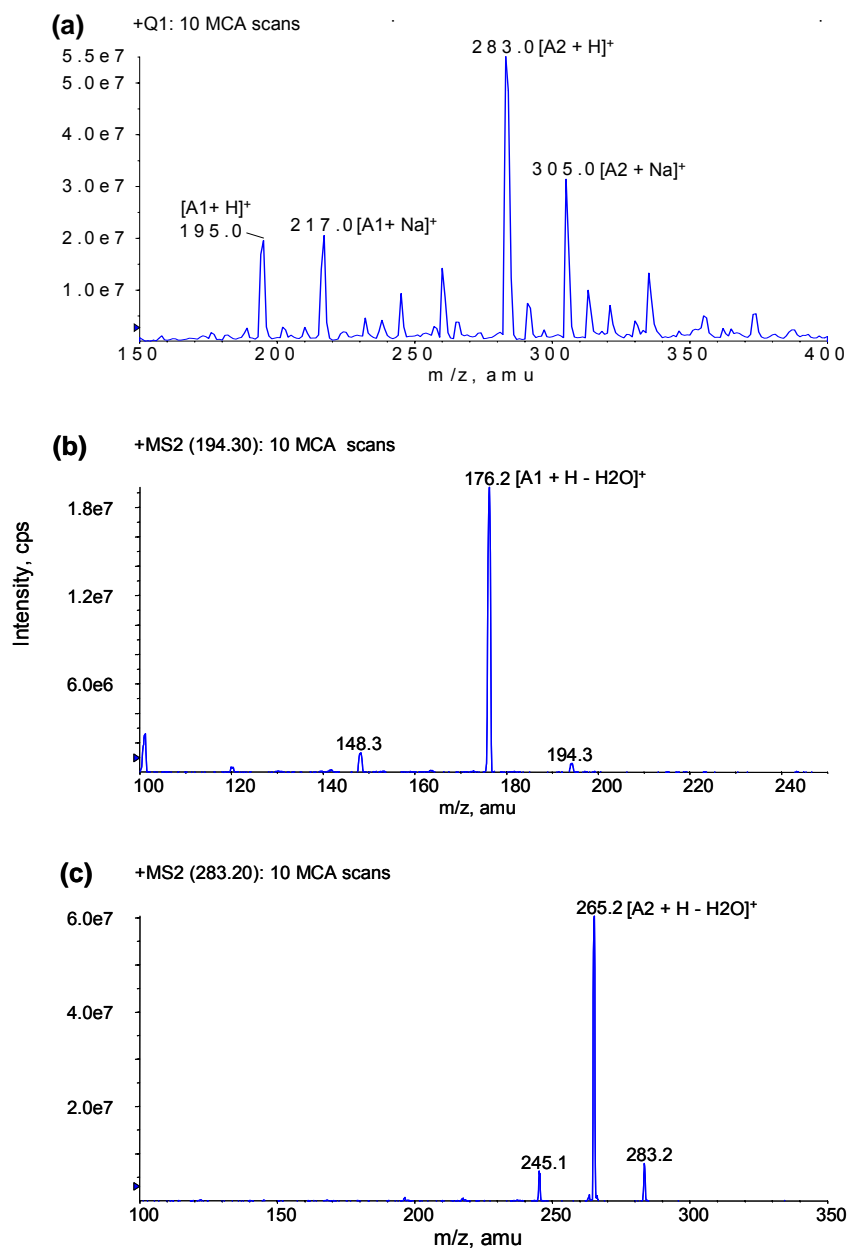
Figure 4-11. Full scan Q1 spectrum (a) and product ion scan spectra for B1 (b), B2 (c) and B3 (d) analytes in positive ionization mode
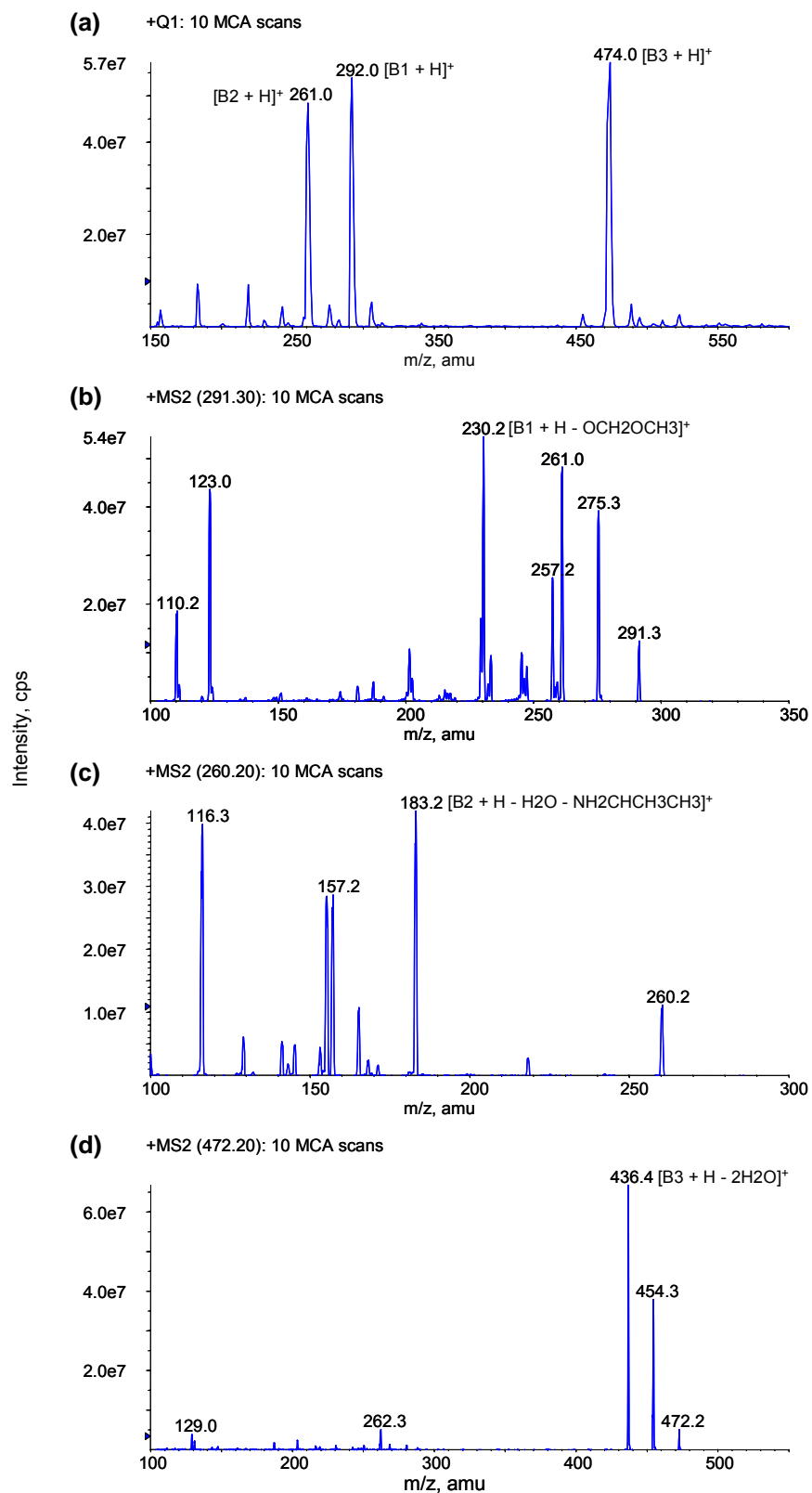
To increase the reliability of post-column infusion experiments and minimize variations from other sources, such as co-eluting components and mobile phase gradients, the chromatographic conditions for the synthetic LPC and PC were extensively examined with respect to peak shape, MS response, and elution time. GPCho lipids are hydrophobic compounds and it was expected that they would require relatively long elution times with reversed phase HPLC. Organic solvent, acetonitrile, methanol and their combinations in different ratios as well as aqueous solvent at pH ranging from 3 to 7 containing 0.1% formic acid, 0.1% acetic acid and 10 mM ammonium acetate were assessed in various compositions. Several HPLC columns: BDS Hypersil C_{18} from ThermoElectron, Luna C_{18} and Synergi Fusion RP C_{18} from Phenomenex, and XTerra RP18 from Waters were tested with the various mobile phases. Varying the pH had no obvious effect on the retention times of the LPC and PC standards. Changing the composition of the organic solvent affected the retention time and symmetry of the three LPC peaks but not the 16:0-18:2 PC peak, which had a peak shape and retention time that appeared to depend primarily on the properties of the column stationary phase. Although all of the columns were reversed phase C_{18}, the behavior of the 16:0-18:2 PC standard on these columns was significantly different. Only the XTerra RP18 column yielded an acceptable peak shape. The other columns exhibited either a hump or a broadened peak. The reason for these different behaviors requires further investigation, but that issue is not addressed here.

Representative chromatograms for the GPCho lipid standards were obtained by using the optimized chromatographic conditions and are shown in Figure 4-12. The retention times for 16:0, 18:1, 18:0 LPC and 16:0-18:2 PC were about 1.9, 2.4, 3.7 and

5.5 min, respectively. While the target analytes were infused and constant MRM signals were acquired, the GPCho lipid standards were injected to examine their ionization suppression effects. Four dips at the corresponding elution times for 16:0, 18:1, 18:0 LPC and 16:0-18:2 PC were observed in all of the MRM transitions for the target analytes (Fig. 4-13). The first dip at 0.4 min was due to column void. The other dips were caused by the GPCho lipids. When the lipid standards eluted from the column, they suppressed analyte ionization, which reduced the detected signal. To verify this hypothesis, the same experiment was repeated with an injection of solvent for comparison (Fig. 4-14). As expected, the spectra with solvent injection exhibit steady analyte signals. The variation at about 3.3 min was caused by changing the mobile phase composition via a step gradient. Since the only difference between these experiments was the material injected and the times associated with the dips corresponded to the elution times of the GPCho lipid standards, it was concluded that analyte signal suppression was caused by the GPCho lipids. Because the suppression affected all analytes, it appears that this effect is not restricted to a specific compound, but can affect a wide variety of analytes.

The infusion spectra show that analyte MS responses were highly matrix dependent. Undetected but co-eluting endogenous molecules alter the ionization environments for analytes of interest and result in a variation of the MS response. In clinical studies, biological samples come from a large number of subjects and even the same subject may exhibit sample variations due to food effects or drug interactions, etc. The composition of the endogenous components in the biofluids (e.g. plasma) can change dramatically. Therefore, when different subjects are analyzed by methods that present matrix effects, the signal intensity of an analyte does not necessarily reflect the amount of

Figure 4-12. MRM chromatograms for 16:0, 18:1 and 18:0 LPC and 16:0-18:2 PC standards
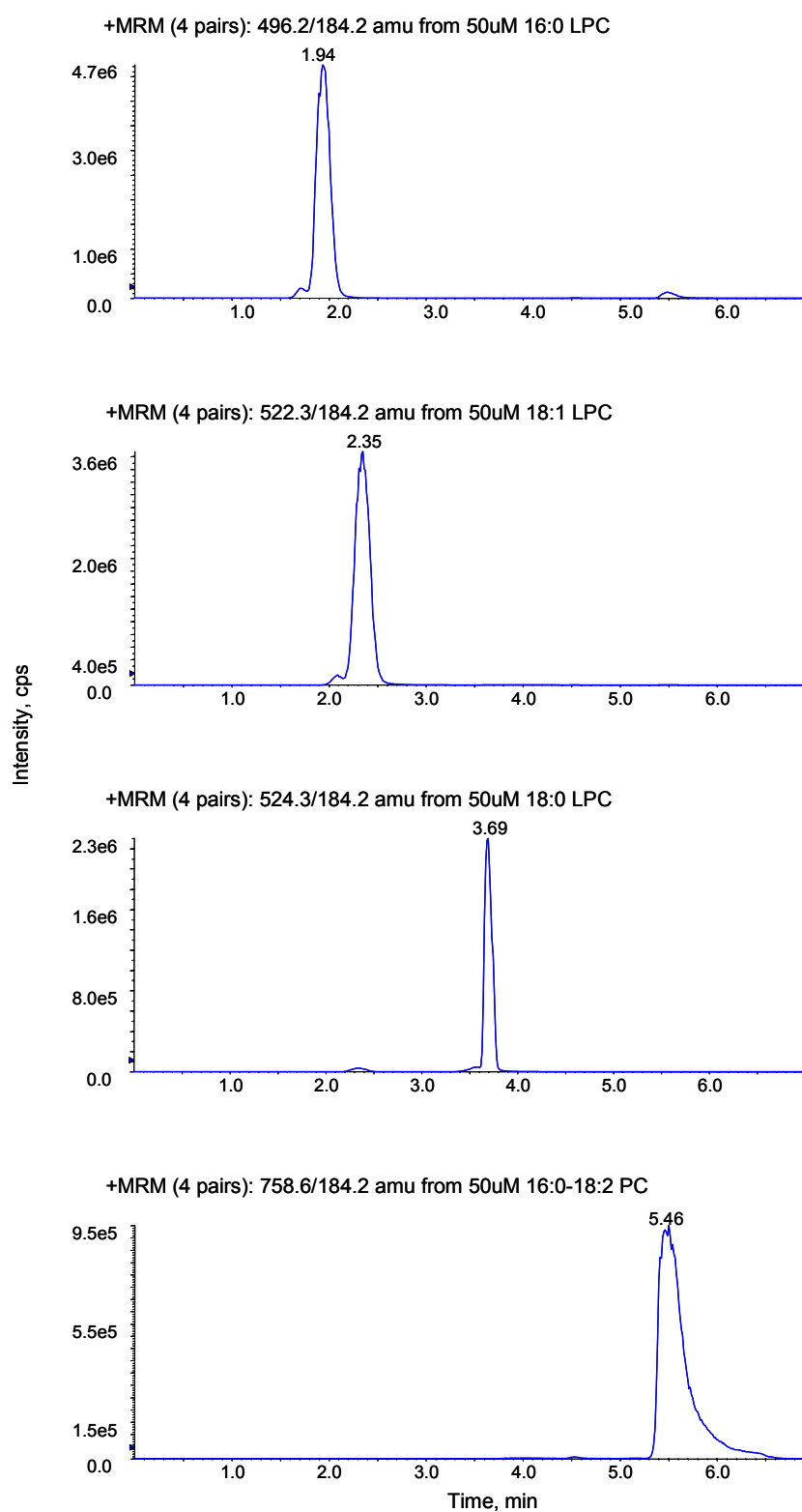
Figure 4-13. Post-column infusion spectra for five analytes after injection of GPCho lipid standards
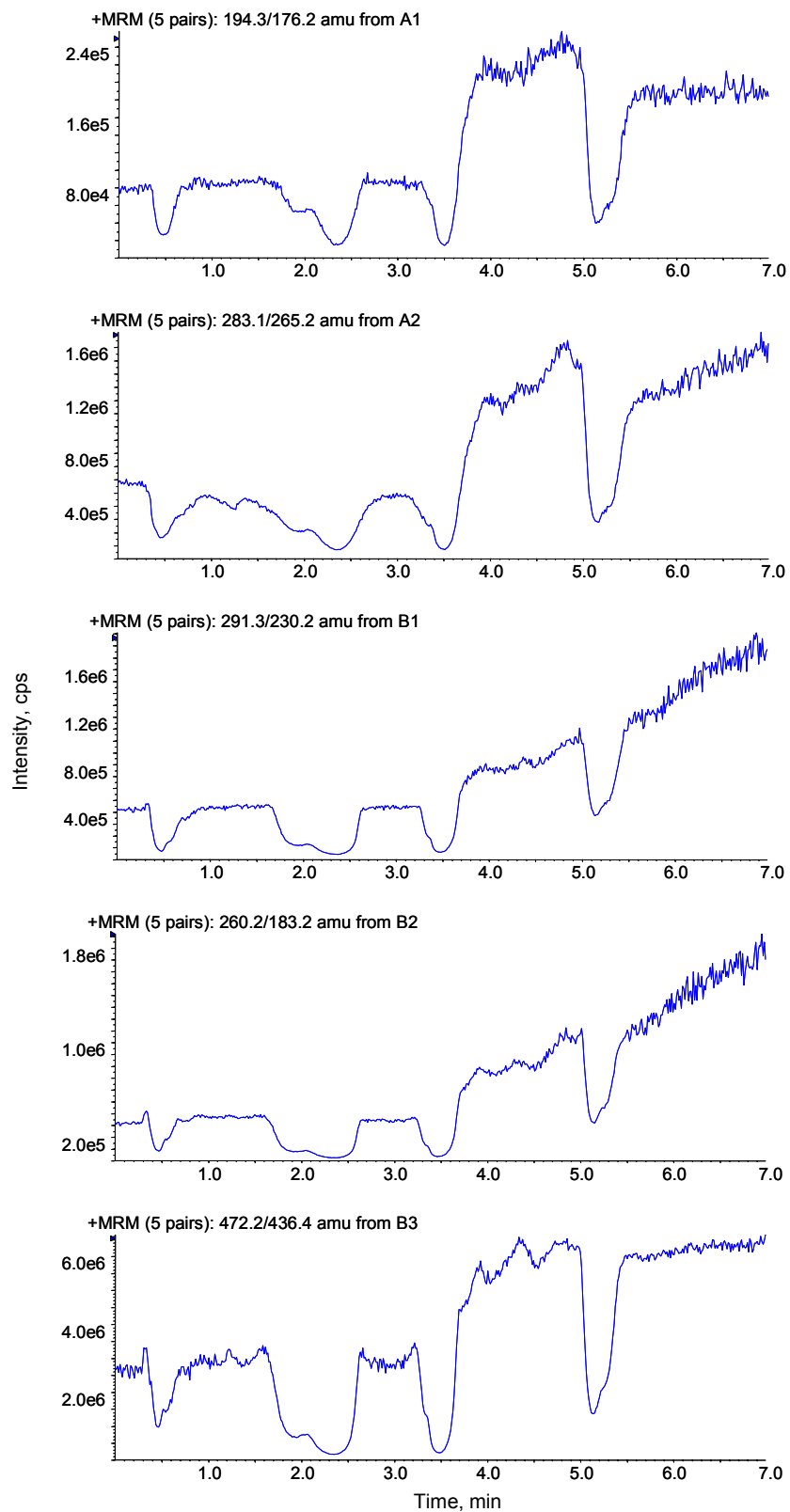
Figure 4-14. Post-column infusion spectra for five analytes after injection of solvent
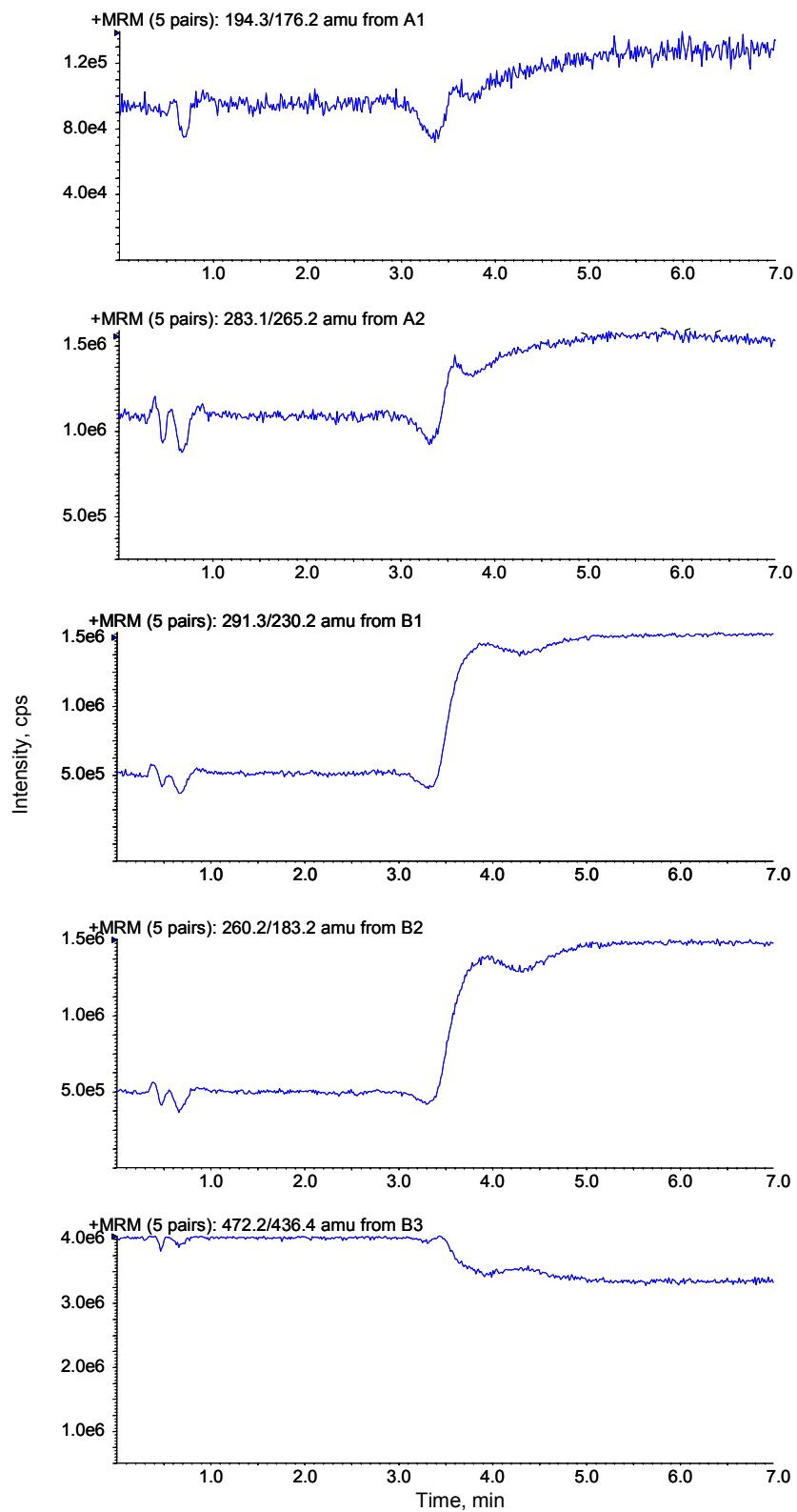
that analyte in the sample. Elimination of these interferences is important for developing a reproducible and accurate quantitative assay for biological samples. The novel HTLC online sample preparation and UPLC analysis were compared with the classic LLE method with regard to their efficiencies for reducing matrix effects caused by endogenous species in biological samples. The GPCho lipids identified by the Q1 scan were also studied by these methods to verify that they were a major source of matrix effect interferences.

4.2.2 Matrix Interference Reduction by using LLE

4.2.2-A Optimization of LLE conditions

To ensure an accurate assessment of matrix effect interferences, sample analysis conditions for using LLE were optimized. The chromatographic conditions were selected based on the principles of reversed phase HPLC. A suitable analytical column should be able to balance the needs of various compound properties and perform separations for all of the analytes. The hydrophilic A1 and B1 analytes need to have reasonable retention times with an ESI acceptable mobile phase, in which a certain amount of organic solvent is needed to improve ionization efficiency. The basic B1, B2 and B3 analytes should yield relatively symmetric peaks. Since peak tailing for basic compounds in most cases is due to interactions with silanol groups inside the column, polar endcapped LC/MS columns such as Aquasil C_{18} and BDS Hypersil C_{18} from ThermoElectron, Synergi Hydro-RP 18 from Phenomenex, and SymmetryShield RP 18 from Waters were evaluated. It was found that the BDS Hypersil C_{18} column yielded the best performance in terms of interday reproducibility, analyte response, peak shape and retention times. The mobile phase was programmed with a gradient elution in order to elute the

hydrophobic A2 and B3 analytes in a reasonable time while still providing adequate separation for all of the analytes.

Extraction conditions were selected based on analyte recovery studies, in which various extraction solvents and solvent combinations at different pH values were examined (Fig. 4-15 and 4-16).

Figure 4-15. Recovery of A1 and A2 by using LLE with various solvent and pH conditions
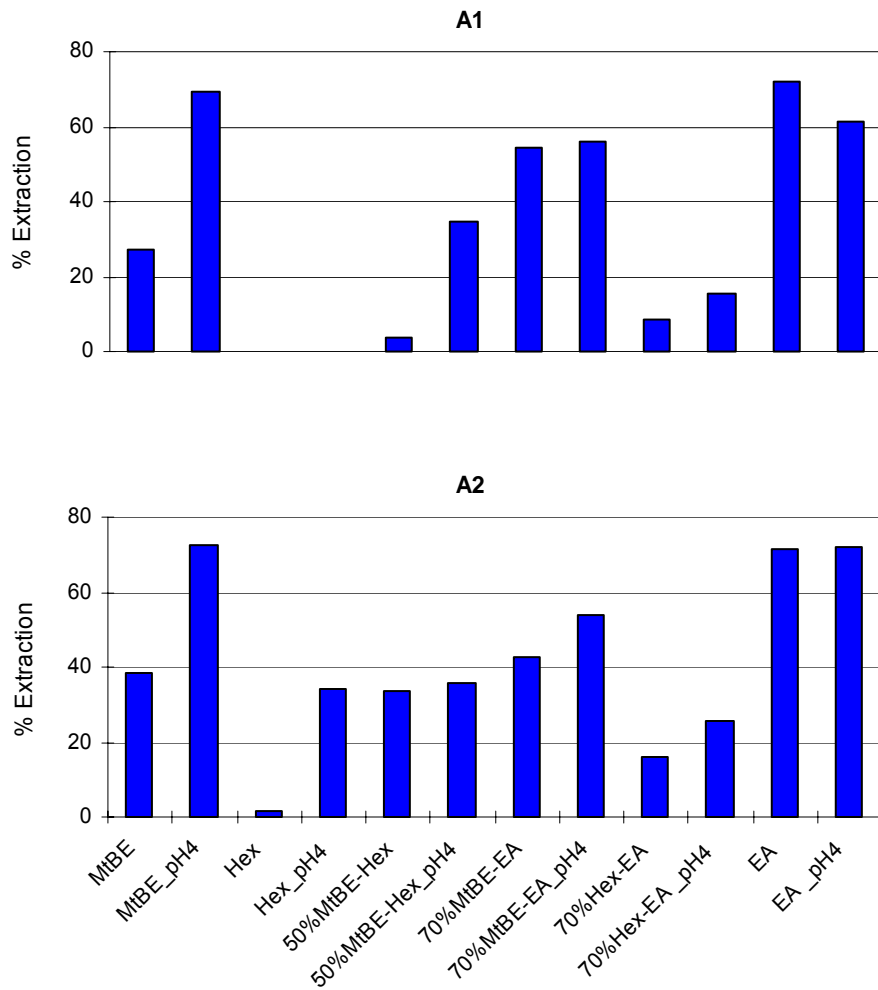
Figure 4-16. Recovery of B1, B2 and B3 by using LLE with various solvent and pH conditions
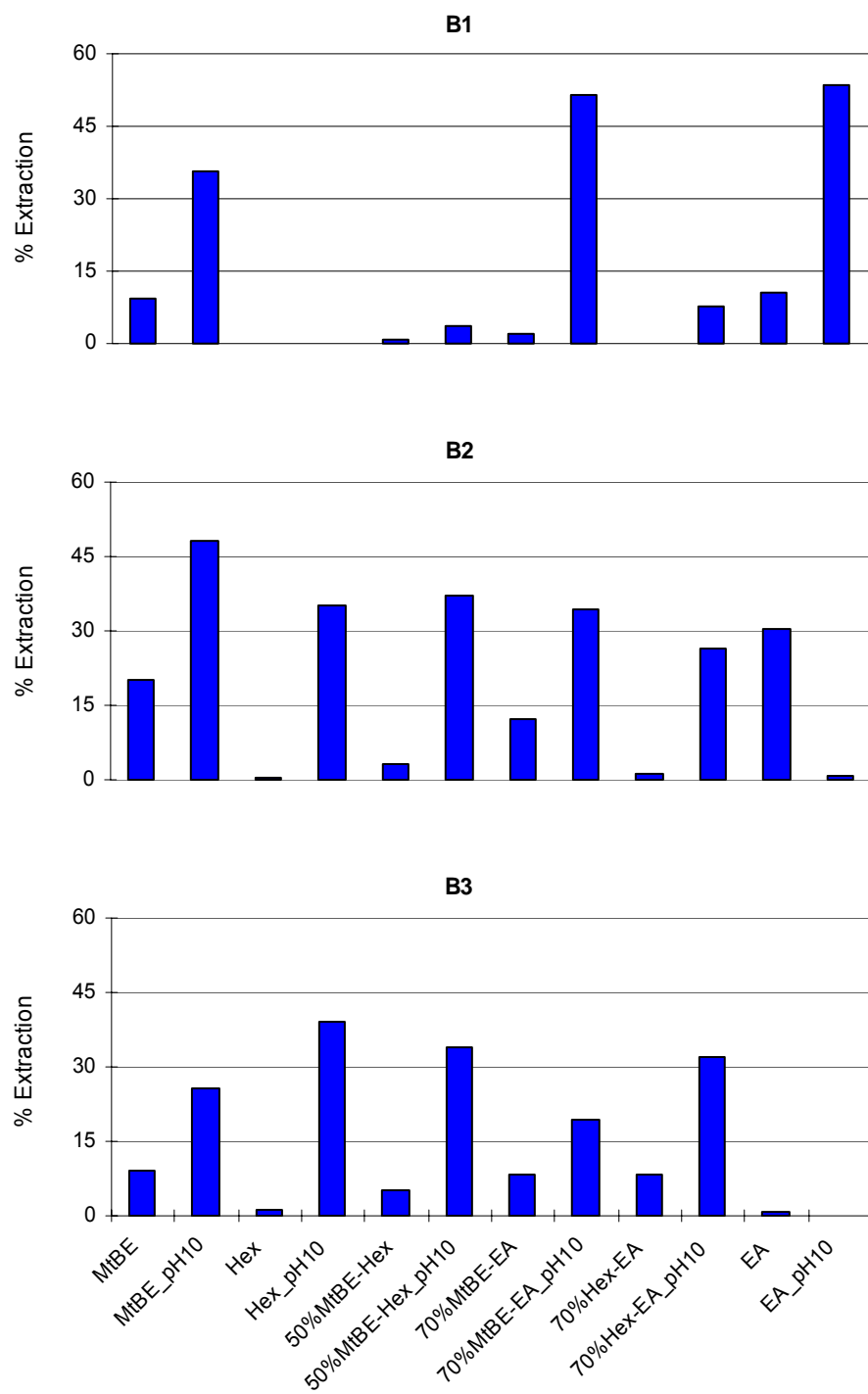
The extraction percentage was calculated as the peak area ratio of LLE processed standard to original (without extraction) standard. The results indicated that acidified conditions generally yielded higher recovery for the acidic compounds and basified conditions were more suitable for the basic compounds, which is a typical situation for LLE experiments. MtBE was selected for extracting analytes because it gave acceptable extraction recovery for all of the analytes at the proper pHs.

4.2.2-B Matrix effect measurements for LLE

A widely accepted method for studying matrix effect interferences is by computing the absolute matrix effect, which is defined as the peak area ratio for an analyte prepared from a control biofluid extract to the same analyte contained in neat solvent [77,78]. A ratio of 100% indicates that the responses for the analyte in the control extract and in the neat solvent are the same. Because the control extract is obtained by using a real sample extraction procedure, a value of 100% suggests an absence of matrix effects. The absolute matrix effects for LLE were obtained by extracting control plasma with MtBE in a 1 to 4 ratio with the pH adjusted to 4 or 10 depending on whether the analytes were acidic or basic. The measurements were conducted at three concentrations in five different plasma lots and the results are shown in Tables 4-2 and 4-3. The average absolute matrix effects for the three concentrations were 103% and 94% for A1 and A2, and 101%, 95% and 45% for B1, B2 and B3, respectively. The corresponding average precision (%RSD) for the A1, A2, B1, B2 and B3 analyses for the five plasma lots were 2.9%, 6.5%, 2.7%, 4.3% and 33%. The B3 analyte, which exhibited significant absolute matrix effects, produced the largest inter-batch variation whereas A2, and A1, B1 and B2, which exhibited moderate to small ionization suppressions, respectively, yielded much

better precisions. These results indicate that matrix effects significantly affect the analyte analysis. A compound analysis method may have a large deviation with less sensitivity due to this adverse effect. In addition, the extent of ionization suppression was correlated with batch-to-batch variations. This correlation is logical because the absolute matrix effect is derived from the influences of co-eluting endogenous components. Therefore, endogenous component differences lead to variations in the absolute matrix effect.

Table 4-2. Absolute matrix effects for A1 and A2 by using LLE analysis

Analyte		Peak area and matrix effects[a]					
		4 nM		50 nM		800 nM	
A1	PL Lot1	4.98E+03	92.0	6.34E+04	105.4	1.03E+06	101.0
	PL Lot2	5.07E+03	93.8	6.31E+04	105.0	1.05E+06	102.6
	PL Lot3	4.92E+03	91.0	6.47E+04	107.5	1.02E+06	100.0
	PL Lot4	5.11E+03	94.5	6.60E+04	109.8	1.03E+06	100.3
	PL Lot5	5.62E+03	103.9	6.47E+04	107.6	1.01E+06	98.7
	Neat Std	5.41E+03		6.01E+04		1.02E+06	
	Mean		95.0		107.1		100.5
	%RSD[b]		5.4		1.8		1.4
A2	PL Lot1	2.12E+04	92.4	2.35E+05	83.6	3.94E+06	83.5
	PL Lot2	2.34E+04	102.0	2.75E+05	97.6	4.51E+06	95.6
	PL Lot3	2.23E+04	97.2	2.69E+05	95.5	4.34E+06	92.0
	PL Lot4	2.52E+04	109.7	2.49E+05	88.5	3.94E+06	83.5
	PL Lot5	2.23E+04	97.0	2.66E+05	94.6	4.48E+06	94.9
	Neat Std	2.29E+04		2.82E+05		4.72E+06	
	Mean		99.6		92.0		89.9
	%RSD[b]		6.6		6.3		6.7

[a] Calculated as (peak area in plasma extract/ peak area of neat std) x 100%.
[b] Relative standard deviation of peak areas for five lots of plasma extract.

Table 4-3. Absolute matrix effects for B1, B2 and B3 by using LLE analysis

Analyte		Peak area and matrix effects[a]					
		4 nM		50 nM		800 nM	
B1	PL Lot1	2.56E+04	97.8	3.32E+05	100.6	4.96E+06	98.8
	PL Lot2	2.68E+04	102.4	3.33E+05	100.9	4.95E+06	98.7
	PL Lot3	2.77E+04	105.8	3.47E+05	105.1	4.92E+06	98.1
	PL Lot4	2.71E+04	103.7	3.45E+05	104.5	5.17E+06	103.0
	PL Lot5	2.56E+04	97.8	3.28E+05	99.3	4.99E+06	99.5
	Neat Std	2.61E+04		3.30E+05		5.01E+06	
	Mean		101.5		102.1		99.7
	%RSD[b]		3.6		2.5		2.0
B2	PL Lot1	1.61E+04	92.9	2.04E+05	86.0	3.60E+06	96.1
	PL Lot2	1.69E+04	97.5	2.16E+05	91.0	3.59E+06	95.7
	PL Lot3	1.75E+04	101.0	2.29E+05	96.5	3.57E+06	95.3
	PL Lot4	1.78E+04	102.4	2.41E+05	101.5	3.65E+06	97.4
	PL Lot5	1.58E+04	90.9	2.17E+05	91.2	3.52E+06	93.8
	Neat Std	1.73E+04		2.37E+05		3.75E+06	
	Mean		96.9		93.2		95.7
	%RSD[b]		5.2		6.4		1.4
B3	PL Lot1	9.27E+04	37.6	1.19E+06	37.8	1.73E+07	38.2
	PL Lot2	9.27E+04	37.6	1.63E+06	51.7	2.32E+07	51.3
	PL Lot3	1.34E+05	54.5	1.31E+06	41.4	2.23E+07	49.3
	PL Lot4	5.34E+04	21.7	6.08E+05	19.3	1.82E+07	40.3
	PL Lot5	1.48E+05	59.8	1.96E+06	62.1	3.22E+07	71.3
	Neat Std	2.47E+05		3.16E+06		4.52E+07	
	Mean		42.2		42.5		50.1
	%RSD[b]		36.0		37.8		26.2

[a] Calculated as (peak area in plasma extract/ peak area of neat std) x 100%.
[b] Relative standard deviation of peak areas for five lots of plasma extract.

Matrix interferences for the LLE method were also evaluated by examining the relative matrix effect, which is based on the variation of matrix effect. Because of difficulties in conducting the absolute matrix effect measurements with HTLC online extraction (i.e. the control biofluid extract after loading must be directly transferred to the analytical column), an alternative approach was needed in order to have a way to directly compare the analytical techniques. The relative matrix effect was determined by the precision of slopes for five calibration curves derived from five different control plasma lots [73]. Using the slope rather than individual measurements was preferred because contributions from random variations in sample preparation, chromatographic separation, and MS response were considerably reduced by computing linear regressions. Moreover, in order to demonstrate the influence of the matrix, calculations were based on peak area rather than the peak area ratio of analyte to an internal standard. The purpose of an internal standard is to account for variations in analyte concentration during various steps in the sample analysis process and to compensate for matrix effects, which was not desired for these studies.

Five plasma calibration curves were obtained by using the same procedure as was used for studies of the absolute matrix effect. The only difference was that analytes were spiked with control plasma before conducting LLE whereas for the absolute matrix effect studies, analytes were spiked with the LLE processed control plasma extract. The LLE relative matrix effects for target analytes are presented in Figures 4-17 and 4-18 for acidic and basic compounds, respectively. The %RSD of the five slopes was 2.9%, 5.5%, 4.3%, 4.5% and 16.8% for A1, A2, B1, B2 and B3, respectively. The trend in these data was consistent with the absolute matrix effect results. The A1, A2, B1, and B2 analytes,

Figure 4-17. Plasma calibration curves for A1 and A2 determined by using LLE
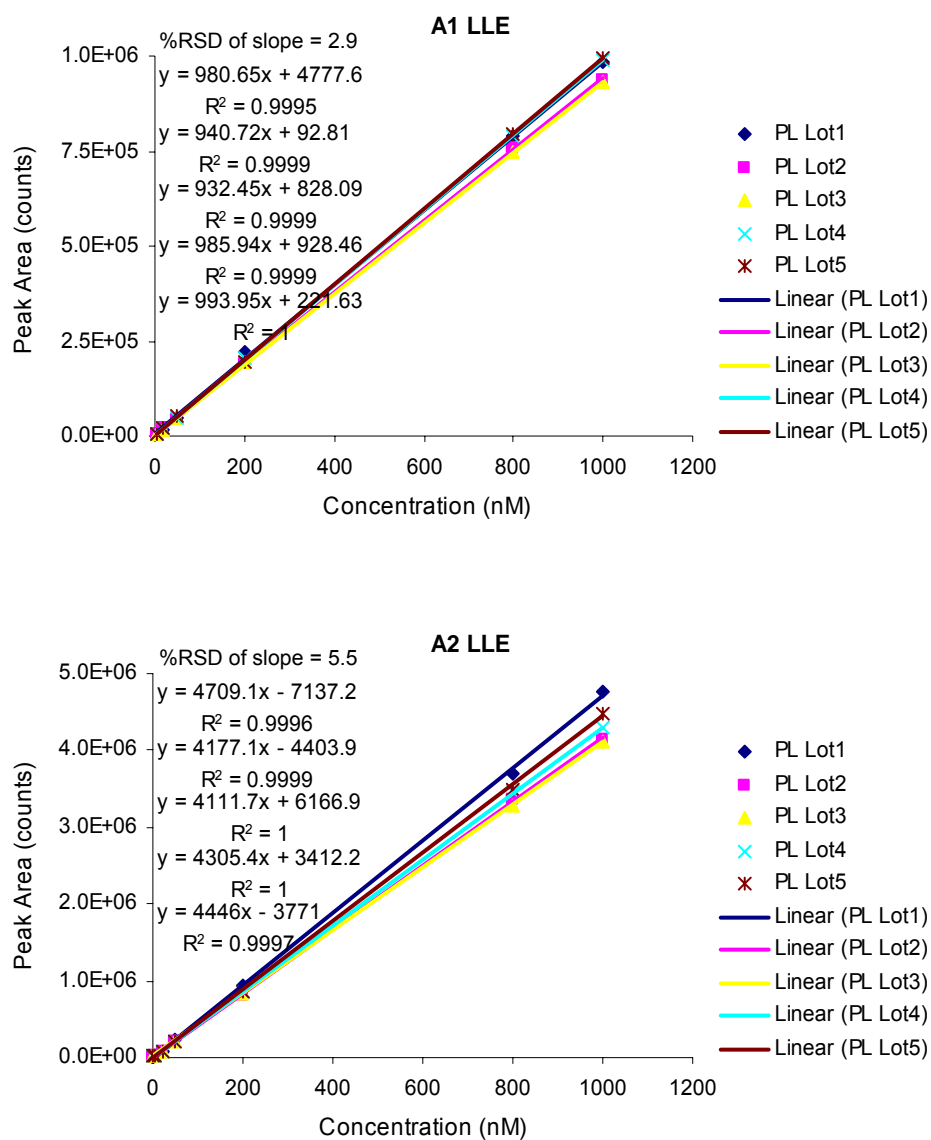
Figure 4-18. Plasma calibration curves for B1, B2 and B3 determined by using LLE

B1 LLE

%RSD of slope = 4.3
y = 2561.9x + 16951
R^2 = 0.998
y = 2303.3x + 18450
R^2 = 0.9953
y = 2543.9x - 811.6
R^2 = 0.9997
y = 2539.8x + 5118.4
R^2 = 1
y = 2483.5x + 11796
R^2 = 0.9992

B2 LLE

%RSD of slope = 4.5
y = 2382.2x + 14197
R^2 = 0.9985
y = 2095.8x + 9722.1
R^2 = 0.9962
y = 2237.7x + 227.02
R^2 = 0.9998
y = 2247.7x + 5768.7
R^2 = 0.998
y = 2230.6x + 496.53
R^2 = 0.9975

B3 LLE

%RSD of slope = 16.8
y = 4252.7x - 86684
R^2 = 0.9955
y = 6703.1x - 131162
R^2 = 0.9956
y = 5773.9x - 133423
R^2 = 0.9845
y = 5074.8x - 73829
R^2 = 0.9986
y = 6002.6x - 155932
R^2 = 0.9916
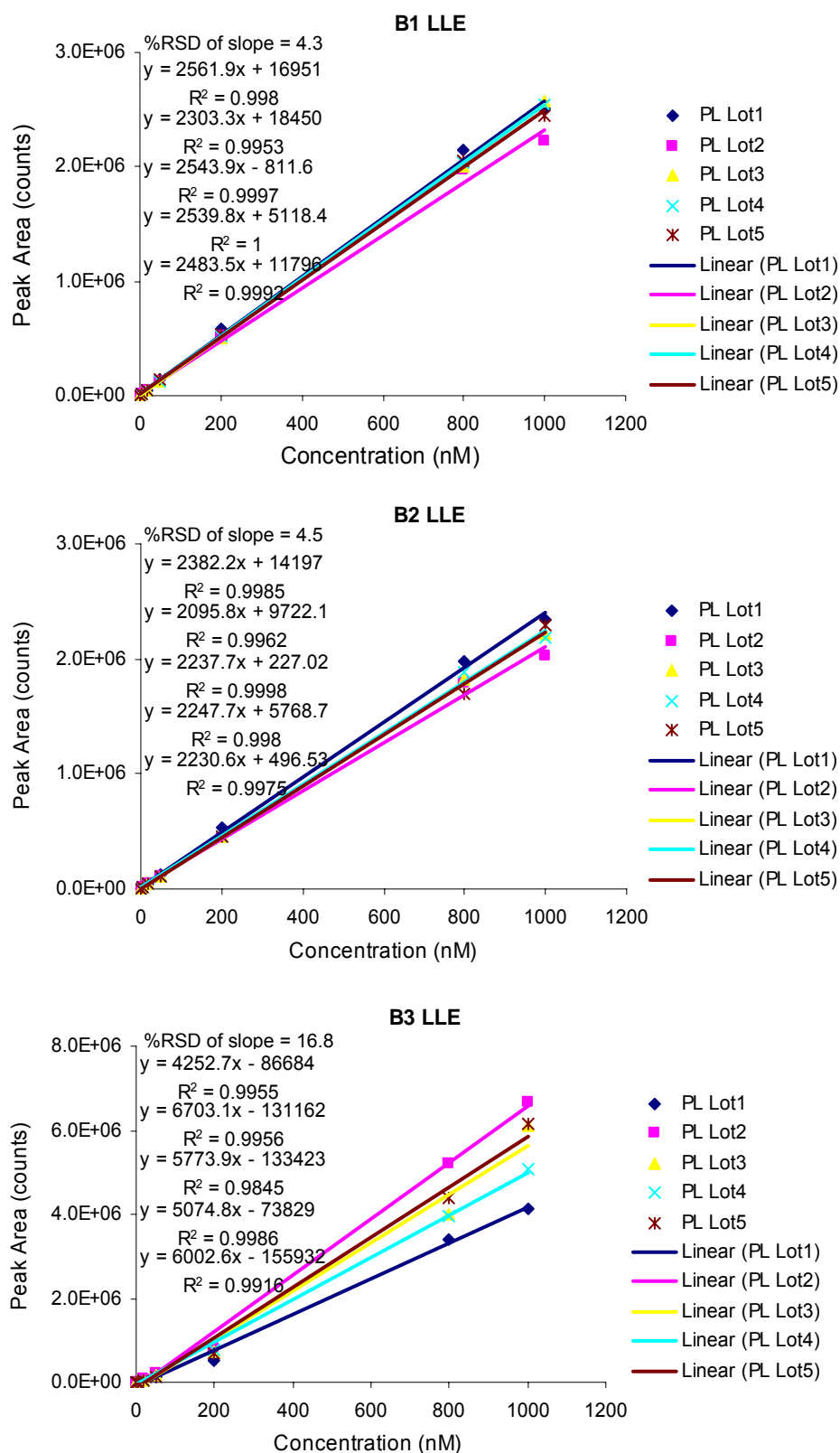
which exhibited relatively small absolute matrix effects, exhibited small slope variations. Results for B3, which exhibited a serious analyte ionization suppression problem, exhibited a much larger relative deviation.

It should be pointed out that the five slope precision calculations reflected contributions from matrix effects and recovery. Compared to a directly analyzed neat standard, results for extracted plasma standards exhibited not only the impact of endogenous components on analyte ionization, but also the impact of material loss during extraction. However, the effects of recovery on slope variations should not be an issue because the primary factor that determined recovery was the polarity similarity between the analytes and extraction solvent, which was dictated by analyte properties. In addition, the good correlation between the relative matrix effect and the absolute matrix effect results indicated that the influence of recovery on batch-to-batch variability was not significant.

4.2.2-C Removal of GPCho lipids by LLE

To assess the relationship between the observed matrix effect and the endogenous GPCho lipids detected by the Q1 scan, the LLE efficiency for removing GPCho lipids was examined by using the LPC and PC standards. Although the post-column infusion experiment had verified the suppression effects of the GPCho lipids on analyte ionization, if these lipids were eliminated during the extraction step, the observed matrix effects would have to be attributed to other factors. The extraction recoveries for GPCho lipid standards under various extraction solvents and pH conditions are shown in Figure 4-19. Generally, these lipids did not favor hexene but preferred ethyl acetate; the universal extraction solvent, MtBE, yielded more than 50% recovery for them. Changing

Figure 4-19. Recovery of GPCho lipid standards by using LLE with various solvents and pH conditions

111
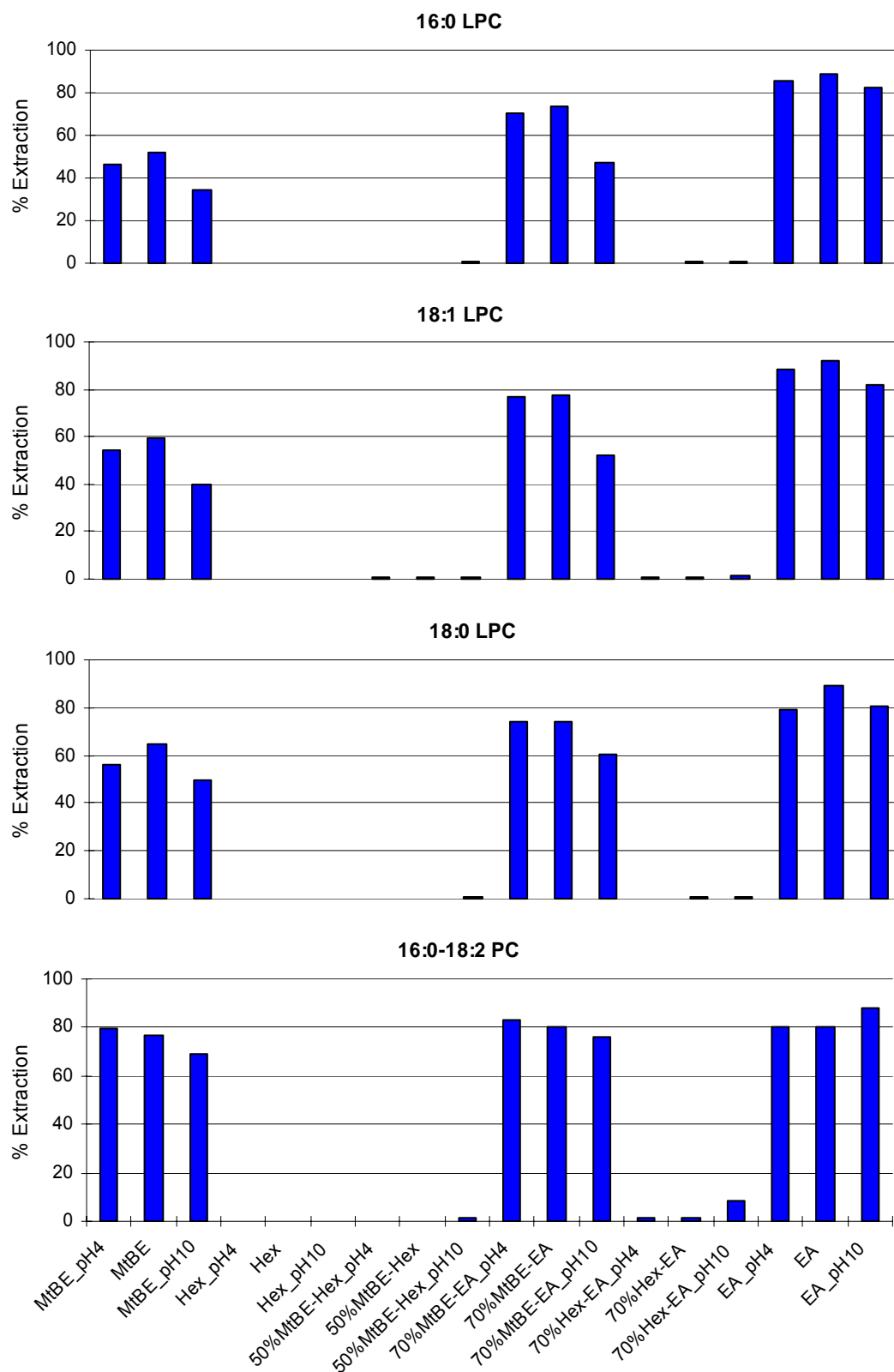
the pH conditions had no significant effect on the extractions of LPC and PC, which was likely due to the opposite charges on N^+ and P^- in the polar head of the GPCho lipids. Under the LLE conditions used for plasma samples, considerable amounts of endogenous GPCho lipids were extracted along with the analytes. It therefore appears that the observed matrix effects might be related to the presence of these GPCho lipids.

In order to investigate the role of GPCho lipids in the plasma matrix effects observed during analyte determinations, the concentrations of endogenous GPCho lipids were quantified for the five control plasma lots used in this research. The concentration of endogenous 16:0, 18:1, 18:0 LPC and 16:0-18:2 PC were about 115, 20, 32, and 233 µg/mL, respectively and the corresponding lot-to-lot variation (%RSD) was about 30% for LPC and 14% for PC (Table 4-4). The concentrations of endogenous lipids were much higher than analyte concentrations and the batch-to-batch variation was significant, thus endogenous GPCho lipids have the potential to be major contributors to the observed matrix interferences.

Table 4-4. Quantification results for endogenous GPCho lipids in human plasma

	Concentration (µM)[a]			
	16:0 LPC	18:1 LPC	18:0 LPC	16:0-18:2 PC
PL Lot1	155	27	49	263
PL Lot2	91	16	24	209
PL Lot3	102	17	33	215
PL Lot4	151	24	38	271
PL Lot5	75	14	19	206
Mean	115	20	32	233
%RSD[b]	31.5	28.4	36.2	13.6

[a] Obtained from 3 replicate protein precipitated control plasma samples.
[b] Relative standard deviation of peak areas in five lots of plasma.

Another prerequisite for causing a matrix interference is that the interfering components co-elute with the analytes, thus, the MRM transitions for the LPC and PC standards were simultaneously monitored along with those for the analytes in order to assess the behavior of endogenous GPCho lipids under specific chromatographic conditions. The chromatograms for LPC and PC standards obtained by using the HPLC conditions for the acidic and basic compounds are shown in Figure 4-20. The elution results for the GPCho lipids are consistent with the matrix effect study results. The A1, B1 and B2 analytes were completely separated from the GPCho lipid standards, thus, variations in their plasma calibration curve slopes were the smallest of all the analytes. A2 was not quite separated from the lipid standards, consequently the influence of the matrix on the variations of the plasma calibration curve slopes for A2 was slightly higher than for A1, B1 and B2. The worst case was for the B3 analyte. Because 16:0 and 18:1 LPC eluted at its retention time, this compound exhibited the largest ionization suppression and greatest inter-batch variations. Based on the facts that the GPCho lipids suppress analyte ionization; concentrations of endogenous GPCho lipids are relatively high and inter-batch variations were large; and that the analyte exhibited serious matrix interferences when it co-eluted with lipids; it was concluded that the GPCho lipids detected by the Q1 scan were likely a major factor affecting plasma sample quantification measurements. However, one possibility that should not be ignored is the influence of other endogenous components. Undetected endogenous species may also be extracted and affect analyte determinations. To verify that GPCho lipids were the primary cause of the observed matrix effects, and to assess the ability of turbulent flow separations to eliminate this adverse effect, the HTLC online extraction method was employed.

Figure 4-20. Representative Chromatograms for analytes and GPCho lipids by using LLE
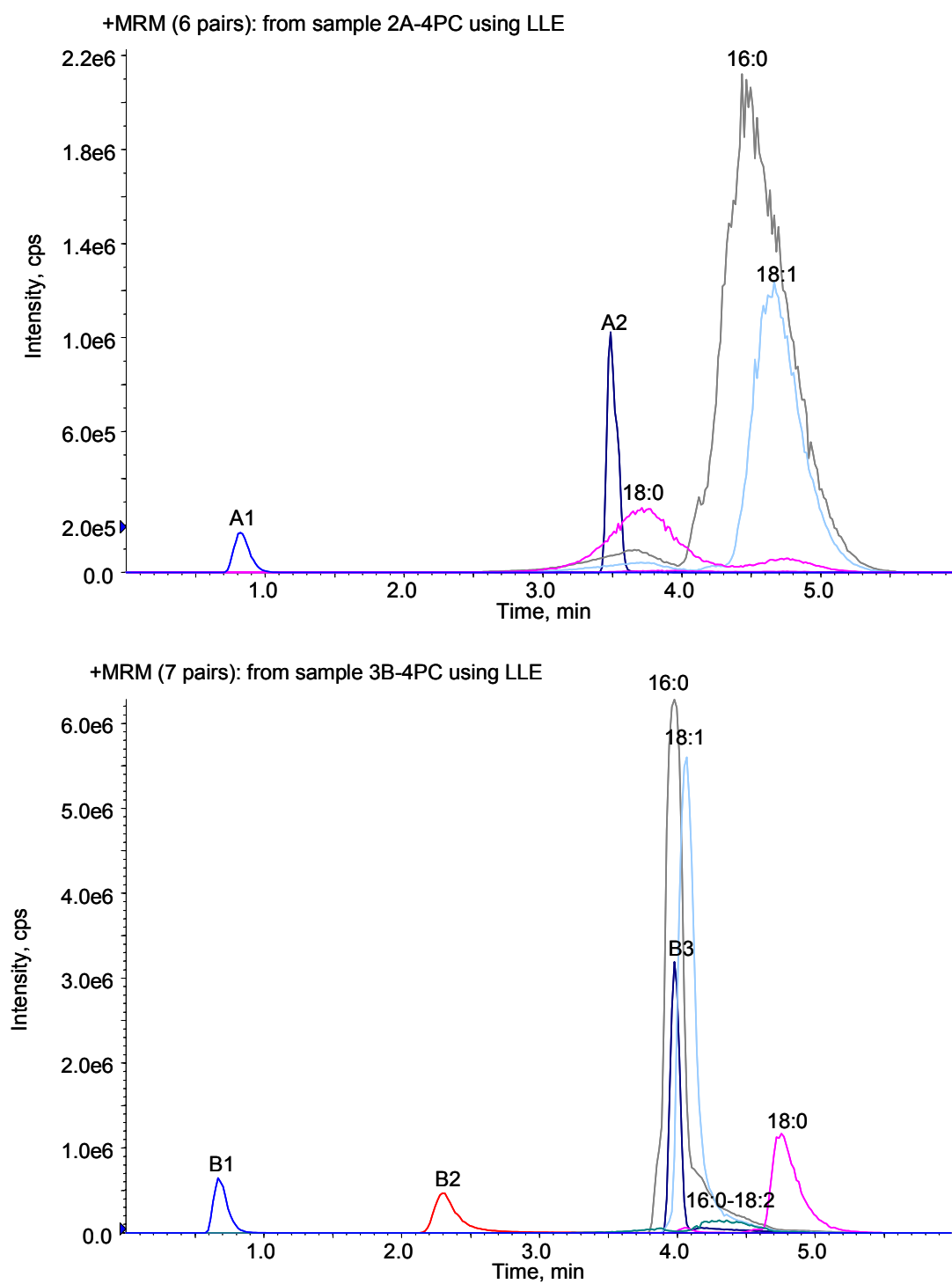
4.2.3 Matrix Interference Reduction by using HTLC Online Extraction

4.2.3-A Optimization of the HTLC online extraction conditions

For online HTLC, extraction steps involving analyte loading, transfer, washing, and equilibration determine the analysis reproducibility. A reliable extraction is essential because problems with the extraction process might be incorrectly attributed to matrix interferences. An optimized loading step sufficiently removes matrix materials from the extraction column and limits interferences without compromising analyte recovery. To avoid build up of macromolecules on the extraction column, a solvent that is capable of denaturing proteins in reversed phase separations was selected for loading plasma samples. Acidified aqueous solvent was used here. Sometimes the aqueous loading solvent is not sufficient to completely wash away all of the human plasma matrix components [6,74]. The remaining matrix residue might be transferred to the analytical column and would gradually accumulate on the surface of the stationary phase. Consequently, the loading efficiency of the extraction column and separation efficiency of analytical column would both decrease. Acids, such as trifluoroacetic acid, acetic acid, and phosphoric acid, are commonly used in reversed phase protein separations to improve solubility [75,76]. Taking into account that the mobile phase must be compatible with mass spectrometry, a 15% HOAc solution was used to dissolve matrix residues. A combination of loading solvent and acid was used to clean the extraction column following each loading. Various loading conditions were evaluated and the results are shown in Figure 4-21(a). The effect of loading solvent on the acidic compounds was not significant. When the total loading time increased from 30 to 60 sec, no obvious peak area decrease was observed. However, increasing the washing time with 15% HOAc

from 5 to 15 second resulted in a peak area decrease. For the basic compounds, a decreasing trend in peak area was observed when the washing time of either the loading solvent or the 15% HOAc was increased. Although the additional wash with 15% HOAc extends the extraction and analytical column lifetimes, analyte recovery is compromised. A loading program of 30-5 sec was thus employed for subsequent studies.

The transfer step involves moving analytes from the extraction column to the analytical column for chromatographic separation. A transfer time of 25 second was suitable because the flow volume corresponding to 25 sec at 0.2 mL/min was about 9 times the extraction column void volume (ID: 0.5 x 50 mm), which should be sufficient to transfer the partitioned analytes. A longer transfer time did not significantly improve analyte recovery, but did cause peak shape broadening. The subsequent eluting conditions were the same as those described for the LLE chromatographic conditions in order to ensure retention time consistency. Under the selected loading conditions, various transfer conditions were assessed and the results are shown in Figure 4-21(b). The manner in which the solvent composition affects transfer is consistent with the retention mechanism in reversed phase chromatography. With increasing organic content, more analyte species are moved from the extraction column to analytical column. The decreased peak areas for B1 and B2 might have been caused by column break-through. Due to the strong hydrophobicity of the transfer solvent, hydrophilic analytes were not well focused at the head of the analytical column. Because increasing the organic content may also favor the transfer of endogenous interferences and enhances the potential of matrix interferences, a transfer solvent containing 30% acetonitrile was used as a compromise between acceptable recovery and minimal interference.

Figure 4-21. Effects of loading and transfer conditions on analyte MS response for HTLC online extraction

(a) **Effects of loading conditions on analytes**

(b) **Effects of transfer conditions on analytes**
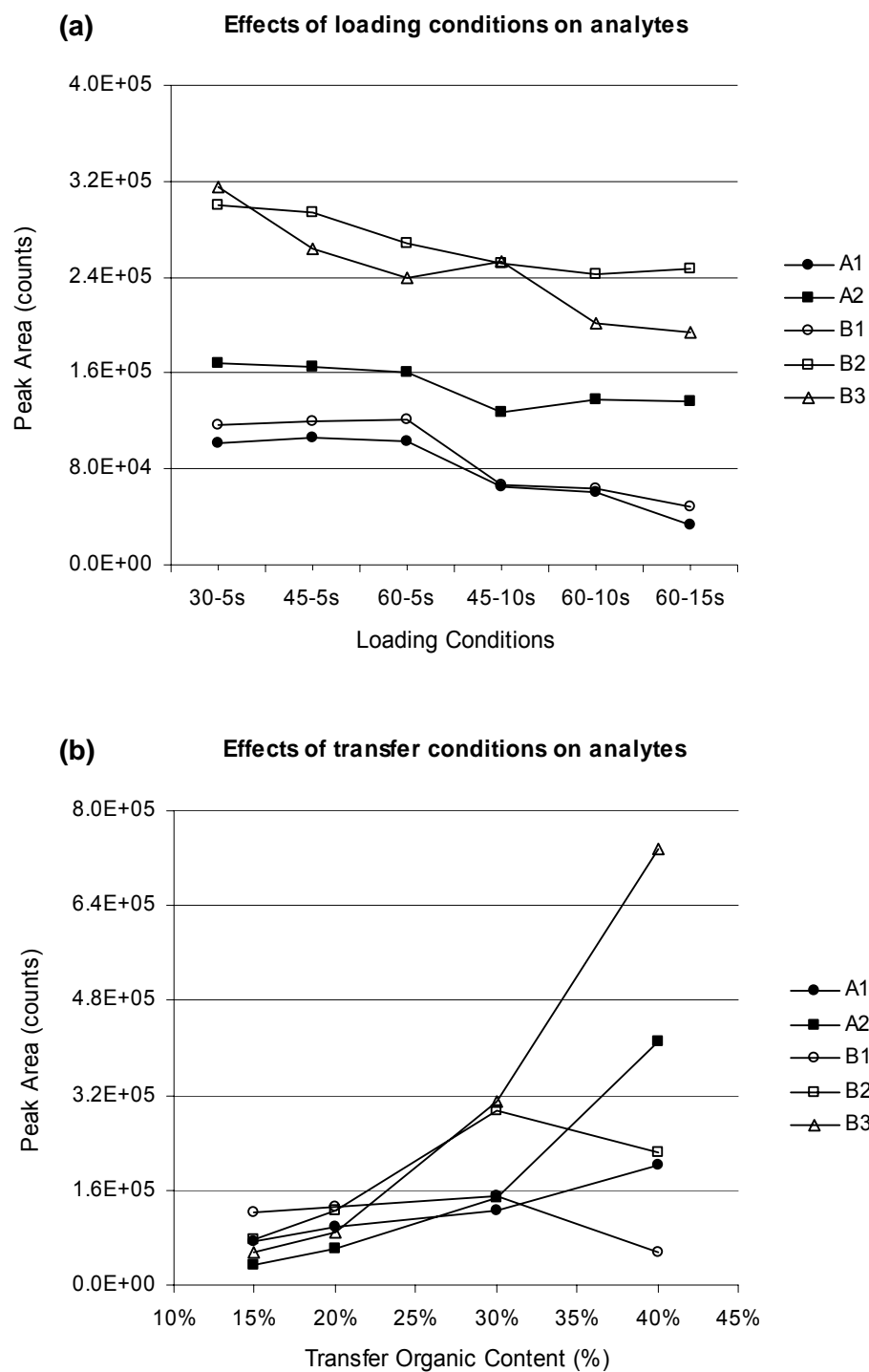
After analyte transfer, the extraction column was extensively cleaned with various combinations of the loading solvents in order to minimize carryover effects. It has been found that alternating washes using high organic and low organic content solvent is helpful for reducing carryover [77]. The reason for this may be that a sequential change between hydrophobic and hydrophilic solvent causes a stretching out and drawing back of stationary phase materials and these movements assist in the diffusion of analyte molecules within stagnant regions.

A critical factor for conducting HTLC online extractions is to ensure that the desired solvents are delivered to the extraction column during each step. A delivery delay caused by the void volume of the loading pump must be accurately measured. The void volume of the system used in this study was about 1.2 mL and the delay time was about 50 sec at a flow rate of 1.5 mL/min. Representative chromatograms for the acidic and basic compounds obtained by using optimized HTLC online extraction conditions are shown in Figure 4-22.

Because plasma sample pH may also affect the measurement reliability, the influence of acid content on analysis reproducibility was examined. Plasma standards were prepared containing 0.5% FA, 0.5% HOAc or 2% HOAc and measured by using a 30-5 second loading with different transfer solvents. The effects of sample acidifying conditions on analyte MS response are summarized in Table 4-5. The precisions of A1 and A2 measurements in 0.5% HOAc were better than in 0.5% FA and 2% HOAc whereas the peak areas for the three acidifying conditions were comparable. Analytes B1 and B2 were not affected by the acid content, but B3 demonstrated a relatively poor response in acidified plasma compared to neutral plasma. Therefore, acidic compounds

Figure 4-22. Representative Chromatograms for the analytes obtained under optimized HTLC online extraction conditions
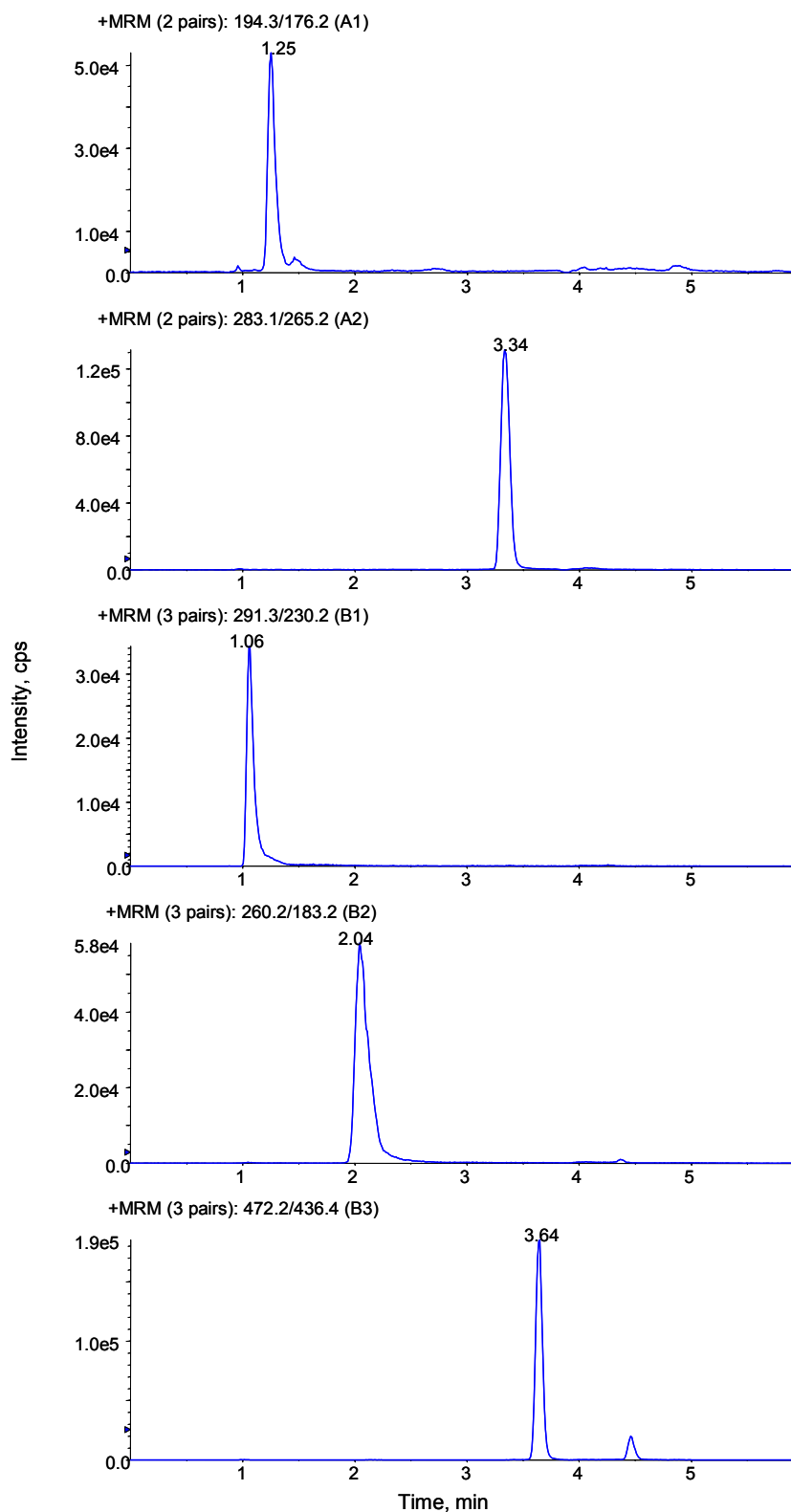
Table 4-5. Acid effects on analyte MS response and precision for HTLC online extraction

Analytes	Acid in plasma (% v/v)	Response (peak area) and precision [%RSD, n=5]			
		Organic content of transfer solvent			
		15% ACN	20% ACN	30% ACN	40% ACN
A1	0.5%FA	6.44E+04 [6.6]	9.26E+04 [7.7]	1.22E+05 [4.7]	1.77E+05 [2.8]
	0.5%HOAc	7.43E+04 [1.2]	9.76E+04 [1.9]	1.26E+05 [1.9]	2.03E+05 [3.7]
	2%HOAc	6.80E+04 [9.3]	9.13E+04 [3.5]	1.16E+05 [2.2]	1.79E+05 [3.0]
A2	0.5%FA	3.51E+04 [7.6]	7.88E+04 [8.3]	1.82E+05 [3.8]	4.80E+05 [2.7]
	0.5%HOAc	3.29E+04 [3.9]	6.07E+04 [5.6]	1.47E+05 [3.2]	4.11E+05 [2.7]
	2%HOAc	3.34E+04 [9.4]	6.25E+04 [7.1]	1.44E+05 [3.5]	4.53E+05 [4.1]
B1	0%HOAc	1.23E+05 [1.7]	1.31E+05 [3.7]	1.49E+05 [2.9]	5.55E+04 [2.2]
	0.5%HOAc	1.29E+05 [0.8]	1.32E+05 [4.8]	1.60E+05 [2.2]	6.60E+04 [2.3]
	2%HOAc	1.07E+05 [2.4]	1.23E+05 [5.2]	1.07E+05 [1.2]	6.23E+04 [1.5]
B2	0%HOAc	7.52E+04 [1.1]	1.25E+05 [1.8]	2.94E+05 [1.2]	2.24E+05 [2.6]
	0.5%HOAc	7.12E+04 [3.3]	1.15E+05 [2.3]	2.61E+05 [1.9]	2.15E+05 [3.2]
	2%HOAc	5.78E+04 [2.2]	1.17E+05 [6.4]	1.91E+05 [1.0]	2.24E+05 [1.1]
B3	0%HOAc	5.58E+04 [2.6]	8.78E+04 [3.0]	3.10E+05 [3.0]	7.35E+05 [4.1]
	0.5%HOAc	4.25E+04 [3.5]	5.89E+04 [5.7]	2.30E+05 [2.5]	5.24E+05 [2.0]
	2%HOAc	3.98E+04 [2.9]	7.15E+04 [4.7]	2.11E+05 [2.2]	6.65E+05 [1.4]

were prepared in plasma containing 0.5% HOAc and basic compound samples contained no acid. The precision results of less than 5% RSD for five replicate samples indicated that the analytical procedure was reliable with the selected conditions.

4.2.3-B Matrix effect measurements for HTLC online extraction

Due to the inherent difficulties in calculating the absolute matrix effect for the online HTLC system, relative matrix effect measurements were made. Analyte plasma curve samples prepared with the five control plasma lots were measured by using the optimized HTLC online extraction conditions and results are shown in Figures 4-23 and 4-24 for the acidic and basic compounds, respectively. The slope %RSD values for A1, A2, B1, B2 and B3 measurements were 2.1%, 3.7%, 4.0%, 2.2% and 8.0%, respectively. Compared to the other analytes, B3 exhibited a relatively large slope variation. The previous analysis results during procedure optimization indicated that an RSD value of less than 5% for five replicates plasma standards should be obtained, and the results for A1, A2, B1 and B2 were comparable and precise. Therefore, the relatively large variation among the five B3 curves was attributed to the effects of endogenous components. Although this variation included the influence of recovery, that effect should have been minimal because recovery is determined by the interactions between analytes and the stationary phase of extraction column. Compared to the relative matrix effect results for LLE, the slope precisions for the five analytes were better, especially for A2 and B3. Because the chromatographic elution conditions for the two approaches were the same, the improved precision indicated that online HTLC extraction was more efficient for reducing endogenous interfering components than LLE. If the GPCho lipids were indeed a major cause of matrix interferences, these effects should be more effectively reduced by

Figure 4-23. Plasma calibration curves for A1 and A2 determined by using HTLC online extraction

A1 Online extraction

%RSD of slope = 2.1
y = 1285.4x - 3449.7
R^2 = 0.9987
y = 1316.1x + 1325.1
R^2 = 1
y = 1359.1x - 4824.3
R^2 = 0.9999
y = 1344.5x - 3805.5
R^2 = 0.9999
y = 1322.9x + 1176.5
R^2 = 0.9999

Legend:
- ◆ PL Lot1
- ■ PL Lot2
- ▲ PL Lot3
- ✕ PL Lot4
- ✴ PL Lot5
- — Linear (PL Lot1)
- — Linear (PL Lot2)
- — Linear (PL Lot3)
- — Linear (PL Lot4)
- — Linear (PL Lot5)

X-axis: Concentration (nM)
Y-axis: Peak Area (counts)

A2 Online extraction

%RSD of slope = 3.7
y = 3730.4x - 1556.5
R^2 = 0.9995
y = 3967.3x - 9220.6
R^2 = 0.9996
y = 3616.5x + 28274
R^2 = 0.9991
y = 3767.7x + 4883.7
R^2 = 0.9972
y = 3902.6x + 3837.1
R^2 = 0.9999

Legend:
- ◆ PL Lot1
- ■ PL Lot2
- ▲ PL Lot3
- ✕ PL Lot4
- ✴ PL Lot5
- — Linear (PL Lot1)
- — Linear (PL Lot2)
- — Linear (PL Lot3)
- — Linear (PL Lot4)
- — Linear (PL Lot5)

X-axis: Concentration (nM)
Y-axis: Peak Area (counts)

Figure 4-24. Plasma calibration curves for B1, B2 and B3 determined by using HTLC online extraction

B1 Online extraction

%RSD of slope = 4.0
y = 757.39x + 973.59
R^2 = 0.9998
y = 788.92x - 1268.7
R^2 = 0.9999
y = 775.75x - 1146.3
R^2 = 0.9997
y = 751.51x + 1344.7
R^2 = 0.9996
y = 830.3x + 16607
R^2 = 0.999

B2 Online extraction

%RSD of slope = 2.2
y = 2370.7x + 5826.3
R^2 = 0.9999
y = 2375.7x + 943.94
R^2 = 0.9997
y = 2469.4x + 4417.9
R^2 = 0.9996
y = 2489x + 1005.8
R^2 = 1
y = 2417.1x + 5043.2
R^2 = 0.9989

B3 Online extraction

%RSD of slope = 8.0
y = 3721x + 3736.3
R^2 = 0.9998
y = 4622.8x - 14352
R^2 = 0.9996
y = 4234x - 6363.7
R^2 = 0.9999
y = 4023x + 15550
R^2 = 0.9967
y = 4269.9x - 1549.2
R^2 = 0.9997

Legend for all three charts:
PL Lot1, PL Lot2, PL Lot3, PL Lot4, PL Lot5, Linear (PL Lot1), Linear (PL Lot2), Linear (PL Lot3), Linear (PL Lot4), Linear (PL Lot5)

using online HTLC extraction than LLE.

4.2.3-C Removal of GPCho lipids by HTLC online extraction

To prove that the B3 measurement variation was caused by the endogenous GPCho lipids, the efficiency of turbulent flow extraction for eliminating GPCho lipids was examined by using the same conditions that were used for analyte analysis. Effects of loading conditions on removal of GPCho lipid standards (Fig. 4-25(a)) indicated that the analyte loading step had no obvious influence on these lipids. Changing the flow time of either aqueous solvent or acid did not affect the lipid peak areas significantly. In contrast, the transfer conditions significantly affected the lipid extraction efficiency (Fig. 4-25(b)). When the organic content of the transfer solvent was increased, the amount of transferred lipids increased dramatically. The 16:0, 18:1 and 18:0 LPC lipids reached their highest extraction yields of 90%, 90% and 65%, respectively with 50% acetonitrile, whereas the maximum extraction yield for 16:0-18:2 PC required at least 70% acetonitrile. To confirm that turbulent flow loading, during which macromolecules are effectively flushed, is not very effective for eliminating small molecules such as GPCho lipids, the eluates from extraction column were directly measured after a wash with aqueous loading solvent and with 100% acetonitrile under turbulent flow conditions (Fig. 4-26). Comparing the peak areas measured for the aqueous eluate (0.07 min) to the acetonitrile eluate (1.29 min), it was concluded that the removal of the GPCho lipids during the loading step is very limited and that the efficiency of lipid reduction is heavily dependent on the organic content of the transfer solvent. This comparison is not quite accurate because ionization efficiencies in aqueous and organic solvents are different, but clearly there are large amounts of LPC and PC lipids that remain after aqueous loading.

Figure 4-25. Effects of loading and transfer conditions on GPCho lipids during HTLC online extraction

(a) Effects of loading conditions on GPCho lipids

- 16:0 LPC
- 18:1 LPC
- 18:0 LPC
- 16:0-18:2 PC

(b) Effects of transfer conditions on GPCho lipids

- 16:0 LPC
- 18:1 LPC
- 18:0 LPC
- 16:0-18:2 PC
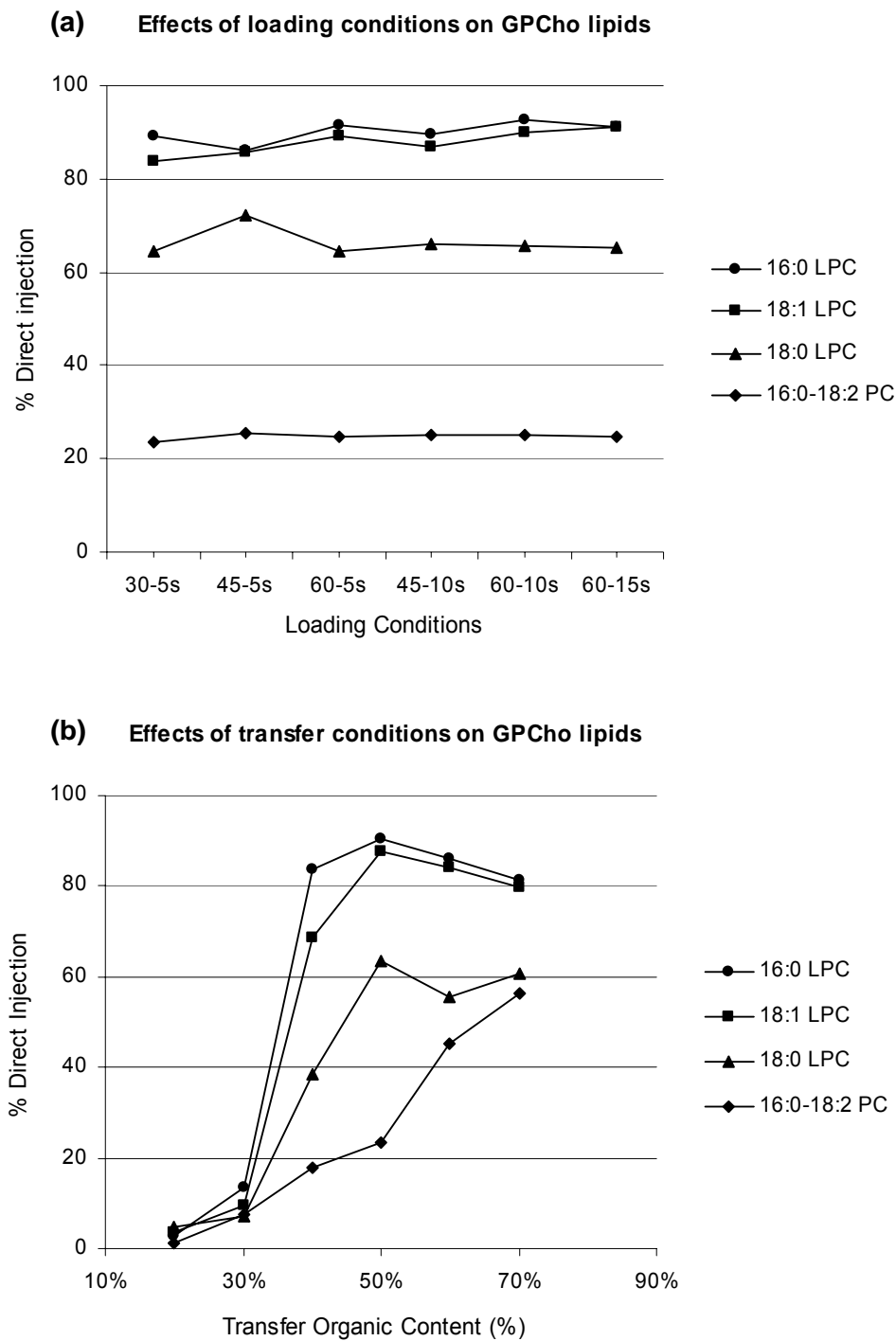
Figure 4-26. MRM spectra of directly eluted GPCho lipids after turbulent flow extraction
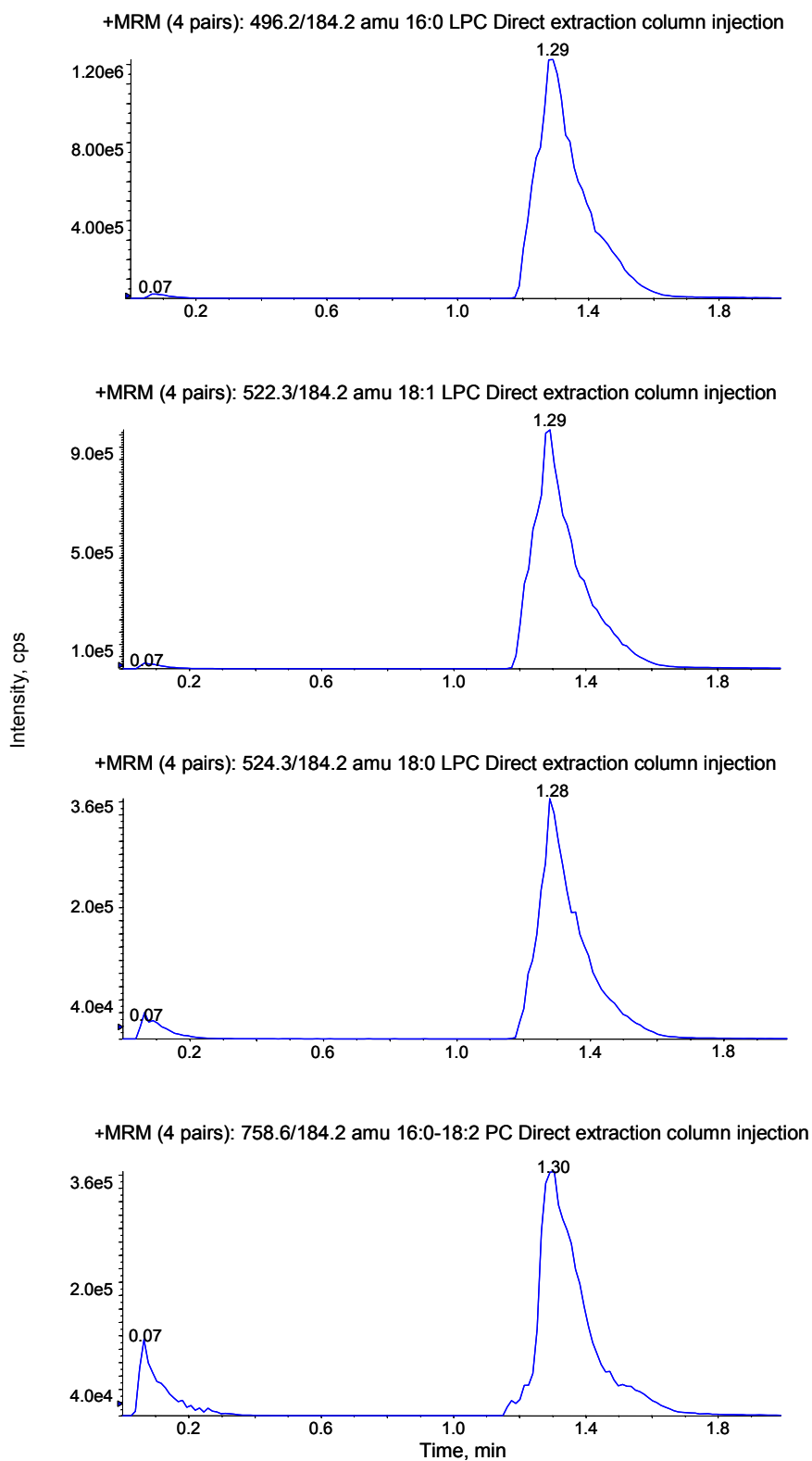
Under the extraction conditions used for analyte analysis (30-5 sec loading and 30% acetonitrile transfer), about 10% of the endogenous GPCho lipids were transferred to the analytical column along with the analytes. Due to the large amount of endogenous GPCho lipids in plasma, 10% of the initial concentration is still much higher than the analyte concentrations.

Comparing HTLC extraction to LLE, the efficiency of these two methods for removing GPCho lipids is represented by the precisions of the results obtained by using the corresponding approaches. With optimized HTLC extraction conditions, about 90% of the LPC and PC standards were separated from analytes, whereas under optimized LLE conditions, the separation efficiency was about 50%. When plasma calibration curves were generated by using both methods, the slope precision for A2 and B3, which slightly and completely co-eluted with the GPCho lipids, respectively, changed from 5.5% and 16.8% when using LLE to 3.7% and 8.0% when using HTLC extraction. For A1, B1 and B2, which were chromatographically separated from the lipids, the relative matrix effects were not significantly affected by the extraction conditions, even though the mechanisms of the two approaches were quite different. The correlation between the efficiency for GPCho lipid removal and plasma calibration curve variability is persuasive evidence that GPCho lipids are major sources of the observed matrix interferences.

4.2.4 Matrix Interference Reduction by using UPLC Analysis

4.2.4-A Characterization of UPLC analysis

To confirm that the reason that the analyses of samples containing A2 and B3 exhibited more variation than the other analytes was because they co-eluted with GPCho lipids, UPLC analysis, which is characterized by greater chromatographic resolution than

127

conventional HPLC, was an ideal approach to employ. Assuming that the GPCho lipids were the major cause of the matrix effects, if they are separated from the target analytes by chromatography, the matrix effect should be greatly reduced. A protein precipitation method was used in combination with UPLC analysis because it allowed retention of the endogenous materials to the greatest extent. When GPCho lipids are chromatographically separated from analytes, the results of matrix effect measurements should reflect the influence of all interfering endogenous components except for the GPCho lipids. An acceptable measurement precision under such conditions would not only confirm that the GPCho lipids are major sources of the matrix effects, but would also provide information regarding the extent to which they contribute to these adverse effects.

Prior to using this method, it was necessary to evaluate the reliability of UPLC-MS/MS for quantitative analysis. One of the features of fast UPLC is that narrow chromatographic peaks are obtained (baseline peak width < 0.1 min). The mass spectrometer scan rate must be fast enough to acquire a sufficient number of data points during the short elution time of each analyte. If an insufficient number of data points are measured for LC peaks, the peak shape will be distorted and peak area quantification will be unreliable. The effects of mass spectrometer scan rate on chromatographic peak shapes were evaluated by using A1 solutions. The maximum scan rate of the API 4000 for MRM monitoring was 50 ms per channel. If multiple analytes are simultaneous measured, the data acquisition rate will be the number of analytes multiplied by 50 ms per analyte plus the delay time involved in switching between channels. Neat A1 standard solutions were analyzed by using two-channel MS/MS monitoring with scan times of 50 and 100 ms, respectively. The precision of five replicate injections and the average

number of data points above 50% peak height are listed in Table 4-6. The peak area precisions for scan rates of 50 and 100 ms were comparable for the same analyte concentration, ranging from 1.1% to 6.7%. The deviation at low concentration was relatively larger than at high concentration due to lower signal-to-noise. At the faster scan rate, the peaks were acquired with less filtering, which yielded higher noise. The number of data points at or above 50% peak height was 16 and 7 for scan times of 100 and 200 ms, respectively. The manufacturer suggested minimum number of data points for a chromatographic peak is 13. Thus, the 200 ms scan time was sufficient to maintain chromatographic peak shapes.

Another concern for UPLC analysis is the higher flow rate employed (> 0.6 mL/min), because a high flow rate is not favorable for ESI ionization. The relationship between flow rate, mobile phase composition and analyte sensitivity has been explored. A1 and B3 were separately prepared in solvents with high aqueous content and high organic content in order to simulate mobile phase compositions that were used to elute them from the analytical column. Flow injection was conducted by using a 2-meter length of peek tubing (ID: 125 μm), which was able to store an injection volume of 20 μL. The solution cylinder formed by the tubing was pushed into the mass spectrometer by mobile phase at different flow rates. Due to the long length of the solution cylinder, mobile phase dilution caused by molecular diffusion at each end of the cylinder was minimized. The MS responses for A1 and B3 at flow rates of 50, 100, 300, 600 and 1000 μL/min are shown in Figures 4-27 and 4-28, respectively. When the solution contained less organic phase (35% acetonitrile for A1), a decrease in MS response with increasing flow rate was observed. A decrease of 20% was considered to be tolerable when the flow rate increased

Table 4-6. The effects of data acquisition rate on A1 MS response

Scan rate	Peak area (counts)						
	2 nM	4 nM	20 nM	50 nM	200 nM	800 nM	1000 nM
50 ms	2.96E+03	5.29E+03	2.63E+04	6.16E+04	2.56E+05	1.02E+06	1.28E+06
	2.81E+03	5.94E+03	2.66E+04	6.23E+04	2.58E+05	1.06E+06	1.33E+06
	2.55E+03	5.60E+03	2.57E+04	6.34E+04	2.55E+05	1.05E+06	1.36E+06
	2.66E+03	5.76E+03	2.66E+04	6.45E+04	2.60E+05	1.04E+06	1.37E+06
	2.86E+03	5.98E+03	2.60E+04	6.26E+04	2.63E+05	1.05E+06	1.34E+06
Mean	2.77E+03	5.71E+03	2.62E+04	6.29E+04	2.59E+05	1.04E+06	1.34E+06
%RSD	5.8	4.9	1.4	1.8	1.2	1.5	2.6
100 ms	3.78E+03	7.14E+03	2.68E+04	6.32E+04	2.58E+05	1.02E+06	1.28E+06
	3.91E+03	7.21E+03	2.70E+04	6.36E+04	2.62E+05	1.05E+06	1.31E+06
	3.51E+03	7.00E+03	2.63E+04	6.52E+04	2.65E+05	1.07E+06	1.37E+06
	3.28E+03	6.65E+03	2.67E+04	6.57E+04	2.75E+05	1.07E+06	1.35E+06
	3.65E+03	6.09E+03	2.69E+04	6.40E+04	2.69E+05	1.08E+06	1.37E+06
Mean	3.63E+03	6.82E+03	2.67E+04	6.44E+04	2.66E+05	1.06E+06	1.34E+06
%RSD	6.7	6.7	1.1	1.7	2.5	2.1	3.0

Scan rate	Peak width at 50% peak height (min)						
	2 nM	4 nM	20 nM	50 nM	200 nM	800 nM	1000 nM
50 ms	0.021	0.025	0.027	0.027	0.027	0.027	0.027
	0.028	0.028	0.026	0.027	0.028	0.028	0.028
	0.028	0.024	0.027	0.027	0.027	0.027	0.027
	0.032	0.030	0.029	0.028	0.027	0.027	0.028
	0.028	0.026	0.028	0.028	0.027	0.027	0.028
Mean	0.027	0.027	0.027	0.027	0.027	0.027	0.028
Points[a]	16	16	16	16	16	16	17
100 ms	0.022	0.022	0.023	0.023	0.023	0.023	0.023
	0.022	0.023	0.023	0.023	0.022	0.023	0.023
	0.025	0.022	0.022	0.022	0.023	0.023	0.023
	0.022	0.023	0.022	0.022	0.023	0.023	0.022
	0.024	0.022	0.023	0.023	0.023	0.023	0.023
Mean	0.023	0.023	0.023	0.023	0.023	0.023	0.023
Points[b]	7	7	7	7	7	7	7

[a] Calculated as: mean peak width * 60/ 0.1 (sum of two scan channels)

[b] Calculated as: mean peak width * 60/ 0.2 (sum of two scan channels)

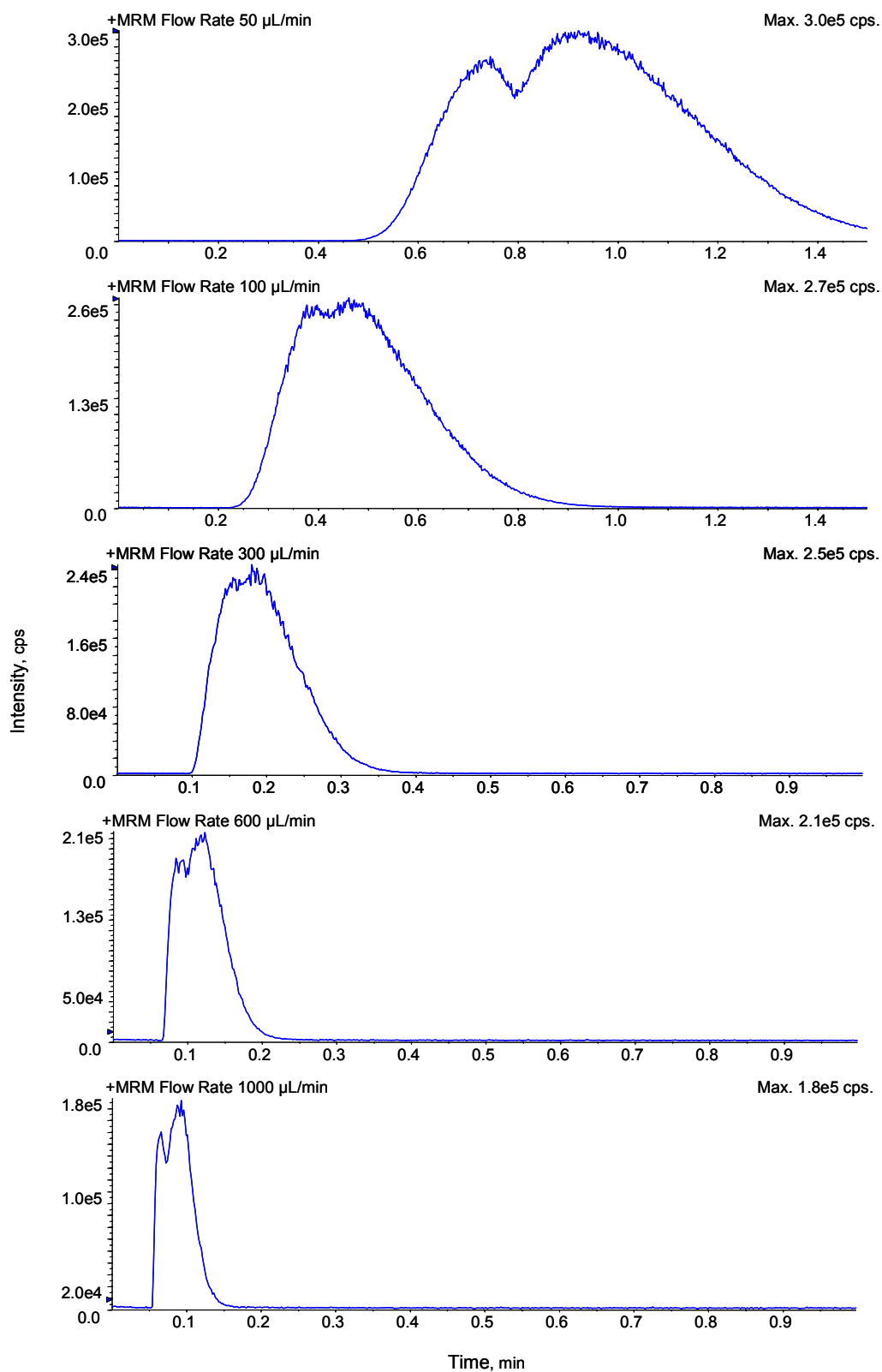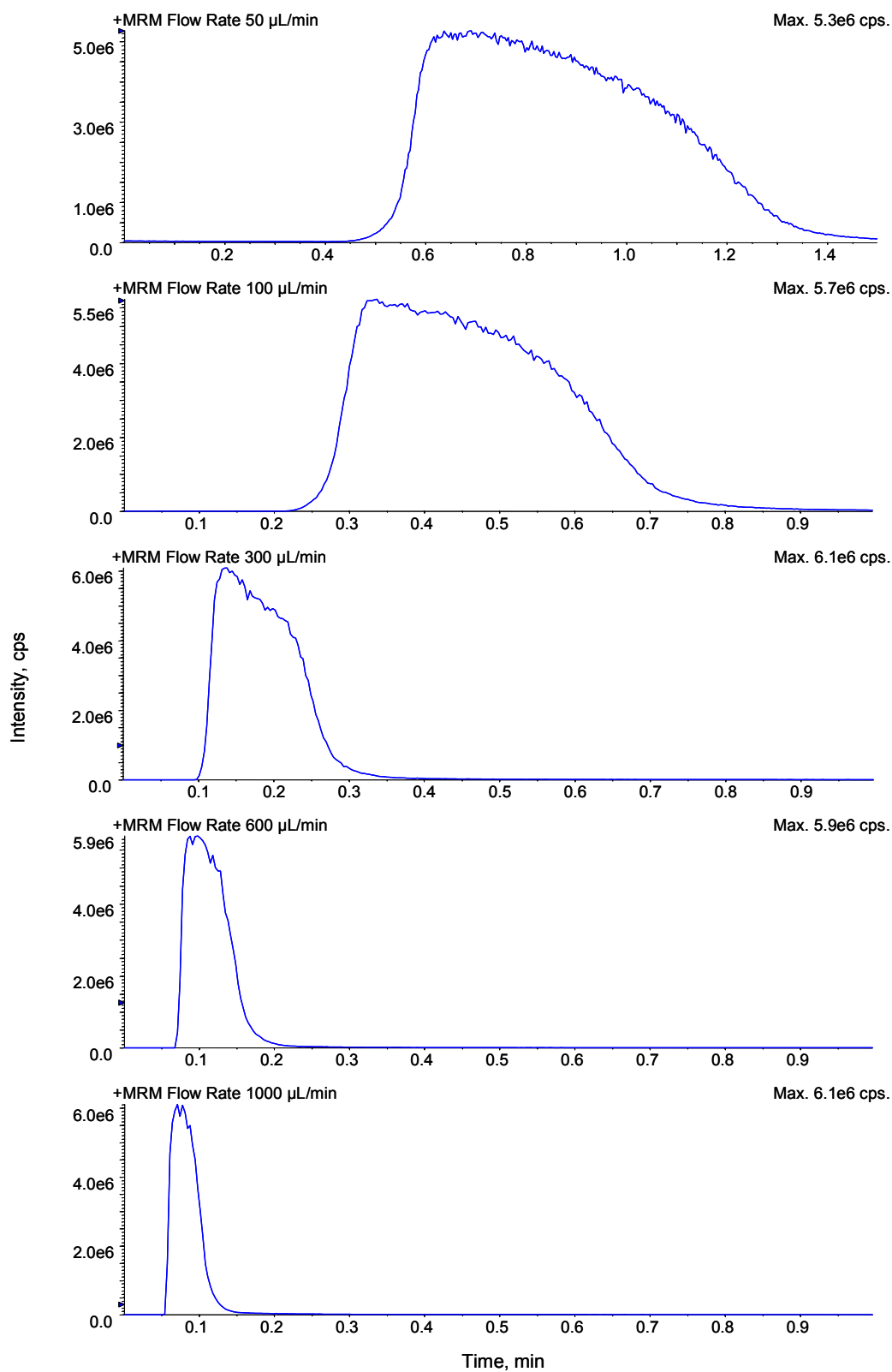Figure 4-27. MRM spectra for A1 at different flow rates with optimized MS acquisition conditions

Figure 4-28. MRM spectra for B3 at different flow rates with optimized MS acquisition conditions

from 100 to 600 µL/min. In the case of higher organic content solutions (75% acetonitrile for B3), the MS response was not significantly affected by the flow rate.

4.2.4-B Optimization of UPLC analysis conditions

Chromatographic peak shape, peak area, precision, and flow rate evaluations suggested that UPLC-MS/MS was a reliable technique and could be utilized to quantify the target analytes for matrix effect studies. To attain separations for solutions containing analytes and LPC and PC standards, the BEH C_{18} and Shield RP 18, 1.7 µm, UPLC columns were tested with various mobile phase gradient programs. The optimized chromatographic conditions not only separated all analytes from the GPCho lipids, but also produced acceptable analyte peak shapes (Fig. 4-29). The MS acquisition parameters were also optimized for the increased flow rate at 0.6 mL/min.

4.2.4-C Matrix effect measurements for UPLC analysis

Analyte solutions prepared by using protein precipitated control plasma and neat solvent were analyzed at three different concentrations by using the optimized separation conditions. The absolute matrix effect and precision for the five plasma lots are summarized in Tables 4-7 and 4-8 for the acidic and basic compounds, respectively. The average absolute matrix effect and precision (%RSD) for the three concentrations were 101% (6.3%) and 101% (5.8%) for A1 and A2, respectively. The corresponding results for the B1, B2 and B3 measurements were 94% (1.4%), 94% (5.0%) and 81% (4.5%). There was no obvious matrix effect for A1 and A2, because peak areas obtained from measurements of solutions derived from protein precipitated plasma and solvent were comparable. However, despite the absence of matrix effects, the more than 5% batch-to-batch variation seemed to be high. Because of the rapid scan rates required for UPLC-

133

Figure 4-29. Representative Chromatograms for analytes and GPCho lipids by using UPLC-MS/MS analysis
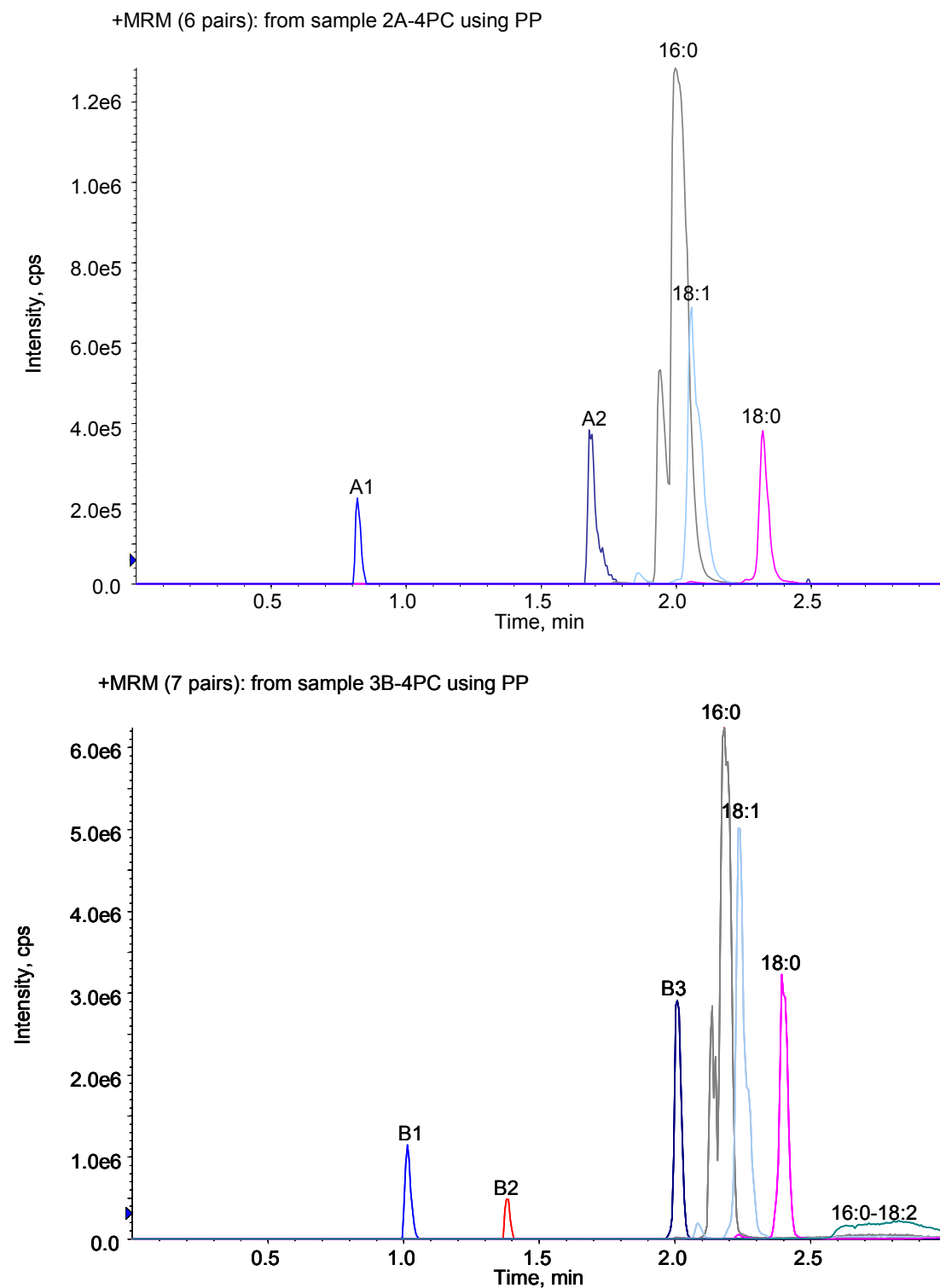
Table 4-7. Absolute matrix effects for A1 and A2 by using protein precipitation with UPLC-MS/MS

Analyte		Peak area and matrix effects[a]					
		4 nM		50 nM		800 nM	
A1	PL Lot1	5.47E+03	98.8	7.10E+04	110.6	9.74E+05	104.9
	PL Lot2	5.05E+03	91.2	7.10E+04	110.6	9.14E+05	98.5
	PL Lot3	6.01E+03	108.7	6.34E+04	98.8	9.30E+05	100.2
	PL Lot4	5.73E+03	103.5	6.31E+04	98.4	8.38E+05	90.2
	PL Lot5	5.97E+03	108.0	6.35E+04	99.0	9.00E+05	97.0
	Neat Std	5.53E+03		6.42E+04		9.29E+05	
	Mean		102.0		103.5		98.2
	%RSD[b]		7.1		6.3		5.4
A2	PL Lot1	8.70E+03	100.7	1.29E+05	107.9	1.96E+06	96.4
	PL Lot2	8.44E+03	97.7	1.31E+05	109.6	1.83E+06	90.0
	PL Lot3	1.01E+04	116.9	1.18E+05	98.8	2.04E+06	100.5
	PL Lot4	9.18E+03	106.3	1.20E+05	100.3	1.99E+06	98.2
	PL Lot5	8.60E+03	99.5	1.14E+05	95.5	1.94E+06	95.4
	Neat Std	8.64E+03		1.20E+05		2.03E+06	
	Mean		104.2		102.4		96.1
	%RSD[b]		7.5		5.9		4.1

[a] Calculated as (peak area in plasma supernatant/ peak area of neat std) x 100%.

[b] Relative standard deviation of peak areas in five lots of plasma.

Table 4-8. Absolute matrix effects for B1, B2 and B3 by using protein precipitation with UPLC-MS/MS

Analyte		Peak area and matrix effects[a]					
		4 nM		50 nM		800 nM	
B1	PL Lot1	2.06E+04	97.6	2.45E+05	94.5	3.68E+06	93.2
	PL Lot2	1.94E+04	91.7	2.39E+05	92.0	3.67E+06	93.0
	PL Lot3	2.01E+04	95.1	2.38E+05	91.8	3.69E+06	93.4
	PL Lot4	1.97E+04	93.2	2.43E+05	93.6	3.66E+06	92.6
	PL Lot5	2.05E+04	96.9	2.43E+05	93.8	3.69E+06	93.4
	Neat Std	2.11E+04		2.59E+05		3.95E+06	
	Mean		94.9		93.1		93.1
	%RSD[b]		2.6		1.3		0.4
B2	PL Lot1	9.03E+03	99.7	9.06E+04	81.6	1.62E+06	92.4
	PL Lot2	8.75E+03	96.6	1.01E+05	90.8	1.74E+06	99.3
	PL Lot3	9.87E+03	108.9	1.06E+05	95.4	1.69E+06	96.1
	PL Lot4	8.86E+03	97.8	9.82E+04	88.5	1.69E+06	96.1
	PL Lot5	8.26E+03	91.2	9.78E+04	88.1	1.64E+06	93.5
	Neat Std	9.06E+03		1.11E+05		1.76E+06	
	Mean		98.9		88.9		95.4
	%RSD[b]		6.5		5.6		2.8
B3	PL Lot1	8.86E+04	77.9	1.18E+06	81.4	1.60E+07	81.0
	PL Lot2	9.22E+04	81.1	1.30E+06	89.7	1.65E+07	83.5
	PL Lot3	9.74E+04	85.6	1.13E+06	77.7	1.70E+07	85.7
	PL Lot4	8.76E+04	77.1	1.19E+06	82.1	1.60E+07	80.8
	PL Lot5	8.71E+04	76.6	1.12E+06	77.2	1.59E+07	80.5
	Neat Std	1.14E+05		1.45E+06		1.98E+07	
	Mean		79.7		81.6		82.3
	%RSD[b]		4.7		6.1		2.7

[a] Calculated as (peak area in plasma supernatant/ peak area of neat std) x 100%.
[b] Relative standard deviation of peak areas in five lots of plasma.

MS/MS analysis, the chromatographic baseline noise increased, and this resulted in decreased reproducibility, especially when peak areas were less than 10^4 counts. The decreased reproducibility for UPLC peaks was demonstrated by the more than 5% RSD for the five replicate injections of A1 measurements (Table 4-6). Results from the B1 and B2 samples indicated that they were not significantly influenced by the endogenous matrix. Although B3 measurements were affected by matrix components to some extent, a more than 80% correlation with the neat solvent results can be considered to mean that the analyte was effectively removed from the main sources of interference. The slight suppression might have been due to unidentified lipids or other endogenous components.

The plasma calibration curves for the target analytes were obtained by using the same protein precipitation procedure and chromatographic conditions as were used for the absolute matrix effect studies. The results are shown in Figures 4-30 and 4-31. The 6.6% and 5.7% slope variations for A1 and A2 measurements were in accordance with their absolute matrix effect precision results. The slope variation among the five plasma lots might have been due to the combined effects of UPLC peak reproducibility and endogenous matrix. The slope precisions for B1, B2 and B3 measurements were 4.3%, 4.0% and 6.7%, respectively. This confirms the absolute matrix effect findings. B1 and B2, with no obvious matrix effects, exhibited precise inter-batch deviations, whereas B3, because of some matrix effects, yielded a slightly larger slope variation.

4.2.4-D Removal of GPCho lipids by UPLC analysis

The GPCho lipids were chromatographically separated from the target analytes by virtue of the high resolving power of UPLC. Although the protein precipitated plasma

Figure 4-30. Plasma calibration curves for A1 and A2 determined by using UPLC-MS/MS

A1 UPLC

%RSD of slope = 6.6
$y = 1420.1x + 5405.6$
$R^2 = 0.9991$
$y = 1462.7x + 11538$
$R^2 = 0.9994$
$y = 1259.4x + 21993$
$R^2 = 0.996$
$y = 1280.8x + 5505.4$
$R^2 = 0.9987$
$y = 1312.8x + 3032.1$
$R^2 = 0.9989$

- PL Lot1
- PL Lot2
- PL Lot3
- PL Lot4
- PL Lot5
- Linear (PL Lot1)
- Linear (PL Lot2)
- Linear (PL Lot3)
- Linear (PL Lot4)
- Linear (PL Lot5)

A2 UPLC

%RSD of slope = 5.7
$y = 2635.9x + 4959.9$
$R^2 = 0.9998$
$y = 2794.2x + 10190$
$R^2 = 0.9997$
$y = 2558.6x + 31359$
$R^2 = 0.9972$
$y = 2631.8x + 8869.5$
$R^2 = 0.9983$
$y = 2942x + 3311.1$
$R^2 = 0.9988$

- PL Lot1
- PL Lot2
- PL Lot3
- PL Lot4
- PL Lot5
- Linear (PL Lot1)
- Linear (PL Lot2)
- Linear (PL Lot3)
- Linear (PL Lot4)
- Linear (PL Lot5)

Figure 4-31. Plasma calibration curves for B1, B2 and B3 determined by using UPLC-MS/MS

B1 UPLC

%RSD of slope = 4.3
y = 3815.9x + 5263.7
R^2 = 1
y = 3923.9x + 19361
R^2 = 0.9991
y = 3885.9x + 57556
R^2 = 0.995
y = 4049.6x + 31674
R^2 = 0.9983
y = 4255.5x + 18026
R^2 = 0.9997

Peak Area (counts)

Concentration (nM)

- PL Lot1
- PL Lot2
- PL Lot3
- PL Lot4
- PL Lot5
- Linear (PL Lot1)
- Linear (PL Lot2)
- Linear (PL Lot3)
- Linear (PL Lot4)
- Linear (PL Lot5)

B2 UPLC

%RSD of slope = 4.0
y = 1767.6x + 10873
R^2 = 0.9978
y = 1758.2x - 6485.6
R^2 = 0.9981
y = 1721.4x - 952.34
R^2 = 0.9977
y = 1800.5x - 11166
R^2 = 0.9963
y = 1910x - 25376
R^2 = 0.9843

Peak Area (counts)

Concentration (nM)

- PL Lot1
- PL Lot2
- PL Lot3
- PL Lot4
- PL Lot5
- Linear (PL Lot1)
- Linear (PL Lot2)
- Linear (PL Lot3)
- Linear (PL Lot4)
- Linear (PL Lot5)

B3 UPLC

%RSD of slope = 6.7
y = 16518x + 126262
R^2 = 0.9993
y = 16559x + 113326
R^2 = 0.9994
y = 14456x + 269931
R^2 = 0.9941
y = 16383x - 3825.5
R^2 = 0.9996
y = 14680x + 62954
R^2 = 0.9997

Peak Area (counts)

Concentration (nM)

- PL Lot1
- PL Lot2
- PL Lot3
- PL Lot4
- PL Lot5
- Linear (PL Lot1)
- Linear (PL Lot2)
- Linear (PL Lot3)
- Linear (PL Lot4)
- Linear (PL Lot5)

samples contained the maximum amounts of endogenous components, the measured analyte matrix effects were acceptable, and the results for B3 were significantly better when compared to LLE and HTLC extraction analysis. In addition, comparing the basic mechanisms involved in the three sample analysis techniques, UPLC separates GPCho lipids from the analytes, whereas the LLE and HTLC online extraction methods reduce lipid concentration based on polarity and hydrophobility preferences. Although the mechanisms for these three approaches are different, the goals are same: to decrease the co-eluted endogenous GPCho lipid species and generate a less interfering environment for analyte ionization inside the mass spectrometer. The efficiencies for removing GPCho lipid interferences were about 100%, 90% and 50% for UPLC analysis, HTLC online extraction, and LLE, respectively. The B3 analyte, which exhibited the worst matrix effects, yielded slope %RSD values for the five plasma calibration curves of 6.7%, 8.0% and 16.8% for UPLC analysis, HTLC online extraction, and LLE, respectively. The correlation between plasma calibration curve variations and GPCho lipid removal efficiency for these analytical methods confirms that GPCho lipids were a major contributor to the matrix interferences.

Compared to the other techniques, the analyte samples prepared for UPLC analysis contained the largest amount of endogenous components. Even with this high endogenous content, the MS responses for A1, A2, B1 and B2 were within 10% of those for samples prepared with neat solvent, and B3, which was highly susceptible to matrix effects because it has a hydrophobic nature that is similar to the endogenous interferences, was within 20%. These results suggest that separation of the GPCho lipids from target analytes will significantly reduce the effects of plasma endogenous

interferences. Because the selected analytes had substantially different properties, they might be useful representatives for general drug candidates, for which assay methods could be developed by studies similar to those described here.

4.2.5 Conclusions

Practical approaches for identifying, monitoring and eliminating matrix interferences in biological sample assays were investigated by using three analytical techniques: classical LLE, novel HTLC online extraction, and UPLC analysis. The large MS signals detected for control plasma samples were verified to be GPCho lipids, mainly 16:0, 18:1, 18:0 LPC and 16:0-18:2 PC lipids. The correlation between the observed plasma matrix interferences and the efficiency of removing lipid standards from synthetic samples suggested that GPCho lipids were a major source of matrix effect interferences that result in plasma sample analysis variations. A dramatic improvement in quantification reproducibility was demonstrated when these lipids were separated from analytes. Detailed studies of the analyte ionization suppression mechanism, which was responsible for the observed matrix interferences, are described in the next chapter.

4.3 References

[1] Herman, J. L. *Rapid Commun. Mass Spectrom*. **2005**, 19, 696

[2] Fairhurst, R. E.; Chassaing, C.; Venn, R. F.; Mayes, A. G. *Biosens. Bioelectron.* **2004**, 20, 1098

[3] Ayrton, J.; Dear, G. J.; Leavens, W. J.; Mallett, D. N.; Plumb, R. S. *Rapid Commun. Mass Spectrom.* **1997**, 11, 1953

[4] Ayrton, J.; Dear, G. J.; Leavens, W. J.; Mallett, D. N.; Plumb, R.S. *J. Chromatogr. A.* **1998**, 828, 199

[5] Lieseneer, A.; Karst, U. *J. Sep. Sci.* **2005**, 28, 1658

[6] Du, L.; Musson, D. G.; Wang, A. Q. *Rapid Commun. Mass Spectrom.* **2005**, 19, 1779

[7] Quinn, H. M.; Takarewski J. J. **1997**, WO97/16724

[8] Knox, J. H. *Anal. Chem.* **1966**, 38, 253

[9] Pretorius, V.; Smuts, T. W. *Anal. Chem.* **1966**, 38, 274

[10] Knox, J. H. *J. Chromatogr. A* **1999**, 831, 3

[11] Knox, J. H.; Scott, H. P. *J. Chromatogr.* **1983**, 282, 297

[12] Knox, J. H. *J. Chromatogr. A* **2002**, 960, 7

[13] Giddings, J. C. *Unified Separation Science,* Wiley, New York, 1991

[14] van Kreveld, M. E.; van den Hoed, N. *J. Chromatogr.* **1978**, 149, 71

[15] Martin, M.; Guiochon, G. *Anal. Chem.* **1982**, 54, 1533

[16] Lin, C. S.; Moulton, R. W.; Putnam, G. L. *Ind. Eng. Chem.* **1953**, 45, 636

[17] Gerard, P. L. *Ind. Eng. Chem. Fundam.* **1973**, 12, 268

[18] Majors, R. E. *Anal. Chem.* **1972**, 44, 1722

[19] Unger, K. K.; Kern, R.; Ninov, M. C.; Krebs, K.F. *J. Chrotmtogr.* **1974**, 99, 435

[20] Collins, R. E. *Flow of Fluids through Porous Media,* Reinhold, New York, 1961

[21] Seguin, D.; Montillet, A.; Comiti, J.; Huet, F. *Chem. Eng. Sci.* **1998**, 53, 3897

[22] Jolls, K. R.; Hanratty, T. J. *Chem. Eng. Sci.* **1966**, 21, 1185

[23] Asperger, A.; Efer, J.; Engewald, W.; Koal, T. *J. Chrotmtogr.* A **2002**, 960, 109

[24] Grant, P. R.; Cameron, C.; Mackenzie-McMurter, S. *Rapid Commun. Mass Spectrom.* **2002**,   16, 1785

[25] Vintiloiu, A.; Mullett, W. M.; Papp, R.; Lubda, D.; Kwong, E. *J. Chrotmtogr.* A **2005**, 1082, 150

[26] Wu, J. T.; Zeng, H.; Qian, M.; Borgdon, B. L.; Unger, S. E. *Anal. Chem.* **2000**, 72, 61

[27] Jemanl, M.; Xia, Y .Q.; Whigan, D. B. *Rapid Commun. Mass Spectrom.* **1998**, 12, 1389

[28] Low, B. *J. Am. Chem. Soc.*, **1952**, 74, 4830

[29] Yau, W. W.; Kirkland, J. J.; Bly, D. D. *Modern Size-Exclusion Liquid Chromatograpgy,* Wiley, New York, 1979

[30] Ghrist, B. F. D.; Stadalius, M. A.; Snyder, L. R. *J. Chrotmtogr.* **1987**, 387, 1

[31] Stadalius, M. A.; Ghrist, B. F. D.; Snyder, L. R. *J. Chrotmtogr.* **1987**, 387, 21

[32] Peng, S. X.; Branch, T. M.; King, S. L. *Anal. Chem.* **2001**, *73*, 708

[33] Rezk, N. L.; Brown, K. C.; Kashuba, A. D. M. *J. Chrotmtogr.* B **2006**, 844, 314

[34] Wang, P. G.; Wei, J. S.; Kim, G.; Chang, M.; El-Shourbagy, T. *J. Chrotmtogr.* A **2006**, 1130, 302

[35] Bahrami, G.; Mohammadi, B. *Clinica Chimica Acta,* **2006**, 370, 185

[36] Oshima, T.; Higuchi, H.; Ohto, K.; Inoue, K.; Goto, M. *Langmuir* **2005**, 21, 7280

[37] Meloan, C. E. *Chemical Separations: Principles, Techniques, and Experiments: a Combined Text, Laboratory Manual, and Reference,* Wiley, New York, 1999

[38] King, C. J. *Separation Process*, McGraw-Hill, New York, 1971

[39] Martire, D. E.; Boehm, R. E. *J. Phys. Chem.* **1987**, 91, 2433

[40] Poppe, H. *J. Chrotmtogr.* A **1997**, 778, 3

[41] Knox, J. H.; Saleem, M. *J. Chrotmtogr. Sci.* **1969**, 7, 614

[42] Knox, J. H. *J. Chrotmtogr. Sci.* **1977**, 15, 352

[43] Halász, I.; Endele, R.; Asshauer, J. *J. Chromatogr.* **1975**, 112, 37

[44] Martin, M.; Eon, C.; Guiochon, G. *J. Chromatogr.* **1975**, 110, 123

[45] Katz, E.; Scott, R. P. W. *J. Chromatogr.* **1982**, 253, 159

[46] Bidlingmeyer, B.A.; Rogers, L. B. *Sep. Sci.* **1972**, 7, 131

[47] MacNair, J. E.; Lewis, K. C.; Jorgenson, J. W. *Anal. Chem.* **1997**, 69, 983

[48] Jerkovich, A. D.; Mellors, J. S.; Jorgenson, J. W. *LC-GC Europe* **2003**, 16, 20

[49] Wu, N.; Lippert, J. A.; Lee, M. L. *J. Chromatogr. A* **2001**, 911, 1

[50] Wu, N.; Collins, D. C.; Lippert, J. A.; Xiang, Y.; Lee, M. L. *J. Microcol. Sep.* **2000**, 12, 462

[51] Xiang, Y.; Yan, B.; McNeff, C. V.; Carr, P. W.; Lee, M. L. *J. Chromatogr. A* **2003**, 1002, 71

[52] Colón, L. A.; Cintron, J. M.; Anspach, J. A.; Fermier, A. M.; Swinney, K. A. *The Analyst* **2004**, 129, 503

[53] de Villiers, A.; Lestremau, F.; Szucs, R.; Gélébart, S.; David, F.; Sandra, P. *J. Chromatogr. A* **2006**, 1127, 60

[54] Nguyen, D. T.; Guillarme, D.; Rudaz, S.; Veuthey, J. *J. Sep. Sci.* **2006**, 29, 1836

[55] Philip, R. T.; Romanyshyn, L. A.; Neue, U. D. *Anal. Bioanal. Chem.* **2003**, 377, 788

[56] Berg, J. M.; Stryer, L.; Tymoczko, J. L. *Biochemistry* 5th ed. W.H. Freeman, New York, 2002

[57] Geigy Scientific Tables. Vol. 3: *Physical Chemistry; Composition of Blood; Hematology; Somatometric Data* 8th ed., 1981

[58] Myher, J. J.; Kuksis, A.; Pind, S. *Lipids* **1989**, 24, 408

[59] IUPAC-IUB Commission on Biochemical Nomenclature, *Biochem. J.* **1978**, 171, 21

[60] Schiller, J.; Suss, R.; Arnhold, J.; Fuchs, B.; Lessig, J.; Muller, M; Petkovic, M. etc. *Prog. Lipid Res.* **2004**, 43, 449

[61] Peterson, B. L.; Cummings, B. S. *Biomed. Chromatogr.* **2006**, 20, 227

[62] Pulfer, M.; Murphy, R. C. *Mass Spectrom. Rev.* **2003**, 22, 332

[63] Gao, S.; Zhang, Z.; Edinboro, L. E.; Ngoka, L. C.; Karnes, H. T. *Biomed. Chromatogr.* **2006**, 20, 683

[64] Mortier, K. A.; Zhang, G.; Van Peteghem, C. H.; Lambert, W. E. *J. Am. Soc. Mass Spectrom.* **2004**, 15, 585

[65] Zhao, J. J.; Xie, I. H.; Yang, A. Y.; Roadcap, B. A.; Rogers, J. D. *J. Mass Spectrom.* **2000**, 35, 1133

[66] Han, X.; Gross, R. W. *J. Am. Soc. Mass Spectrom.* **1995**, 6, 1202

[67] Domingues, P.; Domingues, M. R. M.; Amado, F. M. L.; Correia, A. J. F. *Rapid Commun. Mass Spectrom.* **2001**, 15, 799

[68] Hsu, F.; Turk, J.; Thukkani, A. K.; Messner, M. C.; Wildsmith, K. R.; Ford, D. A. *J. Mass Spectrom.* **2003**, 38, 752

[69] Hsu, F.; Borher, A.; Turk, J. *J. Am. Soc. Mass Spectrom.* **1998**, 9, 516

[70] Hsu, F.; Turk, J. *J. Am. Soc. Mass Spectrom.* **2003**, 14, 352

[71] Murphy, R. C.; Fiedler, J.; Hevko, J. *Chem. Rev.* **2001**, 101, 479

[72] Han, X.; Gross, R. W. *J. Am. Chem. Soc.* **1996**, 118, 451

[73] Matuszewski, B. K.; Constanzer, M. L.; Chavez-Eng, C. M. *Anal. Chem.* **2003**, 75, 3019

[74] Zeng, W.; Fisher, A. L.; Musson, D. G.; Wang, A. Q. *J. Chromatogr. B* **2004**, 806, 177

[75] Snyder, L. R.; Kirkland, J. J.; Glaich, J. L. *Practical HPLC Method Development* 2nd ed., Wiley, New York, 1997

[76] Guyton, A. C.; Hall, J. E. *Textbook of Medical Physiology* 9th ed., W. B. Saunders Co., Philadelphia, 1996

[77] Zeng, W.; Musson, D. G.; Fisher, A. L.; Wang, A. Q. *Rapid Commun. Mass Spectrom.* **2006**, 20, 635

[78] Buhrman, D.; Price, P.; Rudewicz, P. *J. Am. Soc. Mass Spectrom.* **1996**, 7, 1099

CHAPTER 5

ELUCIDATION OF ANALYTE IONIZATION SUPPRESSION EFFECTS

5.1 Theory and Simulation

5.1.1 A Brief Review of the Electrospray Ionization Process

Electrospray ionization (ESI) is a technique for creating gas phase ions from solution species. The combination of an ESI source with mass spectrometric detection is known as electrospray mass spectrometry (ES-MS) [1]. Because analyte molecules interact strongly with solvent molecules in solution, the energy required to extract analyte ions from the liquid to gas phase is larger than that required to break a C-C bond. Compared to other ionization methods, such as fast atom bombardment and plasma desorption [2-7], ESI is a softer technique because the degree of fragmentation during the ion generation process is minimal. Since the introduction of ES-MS in 1984 [8], the technique has revolutionized the field of bioanalytical mass spectrometry.

The process of generating gas phase ions by using ESI involves three stages: production of a stream of charged droplets at the solution emitter where a high voltage is applied; formation of sub-droplets through solvent evaporation and Coulomb fission; creation of gas phase ions from the very small and highly charged sub-droplets. Typically, samples are introduced into the ESI source through a metal capillary held at a high voltage (3 - 6 kV). A planar counter electrode is located a short distance from the capillary. The high electric field between the capillary tip and the counter electrode causes electrolytes in the solution to undergo electrophoretic movement to counteract the imposed electric field. In the positive ionization mode (the capillary is the positive

146

electrode), positive ions migrate away from the capillary tip and concentrate at the liquid surface whereas negative ions are driven in the opposite direction. Positive ion repulsion and the attractive force due to the electric field are counterbalanced by the surface tension of the liquid. At sufficiently high voltage, the liquid at capillary tip is expanded into a dynamic cone (Taylor cone) [9]. The least stable point at the tip of the cone elongates into a filament, which breaks apart into positively charged droplets [10-16]. The net charge results from an excess of positive ions relative to negative ions at the cone surface. As charged droplets are emitted from the tip, they become relatively stable because the charges are dispersed on a larger surface area through the fission. Due to solvent evaporation, these charged droplets shrink. At certain shrinkage, the next fission occurs.

The electric field (E) at the capillary tip can be represented by: $E_c = \dfrac{2V_c}{r_c \ln(4d / r_c)}$ [10]

and the electric field required for the formation of a charged jet is: $E_{on} \approx (\dfrac{2\gamma \cos 49°}{\varepsilon_0 r_c})^{1/2}$

[11]. The rate at which charges leave the tip in the form of charged droplets is equal to the current at the electrospray capillary. Based on theoretical equations [10], a modified form for the capillary current is expressed as: $I = H \kappa^n v_f^{\ v} E_c^{\ \sigma}$ [15,16]. Based on experimental measurements of current, droplet size, and charge, an empirical equation for current has also been proposed: $I \approx f(\gamma \kappa v_f \dfrac{\varepsilon}{\varepsilon_0})^{1/2}$. The radius (R) and charge (q) of the initially formed droplets are expressed as: $R \approx (v_f \varepsilon / \kappa)^{1/3}$ and $q \approx 0.7[8\pi(\varepsilon_0 \gamma R^3)]^{1/2}$

[14]. In the above equations, V_c: applied voltage, r_c: radius of the capillary, d: distance from capillary tip to counter electrode, ε and ε_0: permittivity of solvent and vacuum, γ: surface tension of the solution, cos 49°: half-angle of the Taylor cone, H: surface tension

and dielectric related constant, κ: conductivity of solution, v_f: flow rate, f: constant, exponents in the equation (n, v, and σ): small numbers ($\sim$ 0.5) associated with experimental conditions.

To compensate for the continuous loss of ions of one polarity and to complete the electrical circuit for charge flow, an electrochemical reaction must take place. The ESI process can therefore be described as a special electrolytic flow cell where part of the electrical circuit involves an oxidation reaction at the positive electrode (capillary tip) and occurs in the gas phase [17-22]. Evidence for the occurrence of electrochemical reactions has been provided by several experiments in which metal ions released from the capillary were detected in solution [19]; oxidation reaction sequence was found to be affected by the addition of electrolytes with different redox potentials [23-25]; and analyte electrolysis was found to change when the metal capillary was replaced with a fused silica capillary [26]. Although the solution sprayed from the capillary tip is an electrolytically altered solution, in many cases, the discrepancy between gas phase ion intensity observed in a mass spectrum and the solution concentration for the same ion has been attributed to the droplet formation process occurred in the gas phase [27-30].

After being formed at the capillary tip, charged droplets shrink in size due to solvent evaporation assisted by heated air whereas the amount of charge on each drop remains constant [31-33]. The charge is expected to remain at the droplet surface because the transmission of charge from solution to the gas phase is a highly endoergic process and repulsion between like charges causes them to achieve maximum dispersion. A decrease in the droplet radius with the charge remaining constant leads to an increase in electrostatic repulsion between like charges. When this repulsion force is equal to the

droplet cohesive force derived from surface tension, the Rayleigh stability limit is reached $q_R = 8\pi(\varepsilon_0 \gamma R^3)^{1/2}$ [34]. To relieve the stress caused by continuous shrinkage, droplets undergo fragmentation (Coulomb fission) and smaller offspring droplets are created. Upon reaching the Rayleigh limit, parent droplets distort from a spherical to a raindrop shape and a stream of much smaller droplets is emitted from the small end of parent droplets [33]. The process of producing generations of droplets through evaporative shrinkage and Coulomb fission continues until the droplets are very small. Coulomb fission in a charged droplet is uneven; the relative mass loss of the parent droplet is much smaller than its relative charge loss [16,33,35-36]. The time required for emission of offspring droplets is short comparing to the parent droplet solvent evaporation process. The duration for rapid reduction of droplet size and charge is in the range of hundreds of microseconds [16,33,35-36].

Two principle mechanisms have been proposed to explain the formation of gas phase ions from the small and highly charged offspring droplets. The charge residue model (CRM) suggests that jet fission of droplets continues to a point where extremely small offspring droplets, which contain only one ion, are formed and solvent evaporation from such ions produces gas phase ions [37-40]. The other mechanism, known as the ion evaporation model (IEM), predicts that when solvent evaporation and Coulomb fission have reduced the size of the charged droplets to a suitable radius R (10 - 20 nm), solvated ions are directly emitted to the gas phase [41-44]. Because the required charge for ion evaporation is lower than for Coulomb fission, ion evaporation replaces Coulomb fission as a means of overcoming repulsion between charged ions. The threshold for ion evaporation depends on opposing electrostatic forces, the repulsion between the escaping

ion and the remaining charges on the droplet, and attraction caused by similar polarizabilities. The rate constant (k_I) for ion evaporation has been proposed to be:

$$k_I = \frac{k_B T}{h} e^{-\Delta G^{\neq}/kT}$$, where k_B: Boltzmann's constant, h: Planck's constant, T: temperature

of the droplet, and $\Delta G^{\neq}$: the energy difference of defined transition and initial state [41].

Various attempts have been made to examine the way by which gas phase ions are formed in light of these different mechanisms [45-52]. From the results of cationized polyethylene glycols, Fenn et al concluded that evaporation of molecules with linear dimensions significantly larger than the resided droplets was through CRM [47,48]. With a different approach, in which the difficulty of direct measuring the radius and charge of very small droplets was avoided, the size and charge of solid residues formed after the last solvent evaporation were determined by Fernandez de la More. The charge determined by this experiment was lower than that required for the Rayleigh stability limit. These results were considered as evidence that small ions are formed by IEM [49]. Using a further developed methodology, the maximum charge state on several globular proteins were investigated by the same researcher and the conclusion that CRM was applicable to molecules with mass at least 3300 Da was drawn [50]. Contrary to these results, a recently reported phenomenon provides evidence that multiply charged small organic ions might be formed by CRM. These results were obtained by investigating the extent of dendrimer charging from solutions with different compositions [51]. The debate about the mechanism of ion transition from droplets to the gas phase in ESI will probably continue even though it is widely believed that IEM is more likely responsible for the formation of small organic ions and CRM is probably for the formation of macro ions.

It is generally agreed that the initially formed gas phase ions are highly solvated regardless of the formation mechanism [53-58]. Instead of generating a naked ion (M^+), ESI produces ions surrounded by a solvent shell, $M^+(sol)_n$. These solvent molecules can be removed by heating or collision induced dissociation in the ion source [53,54]. As the ions proceed to the mass analyzer region, gas phase modification reactions, such as proton transfer and rearrangements, may occur. Because the gas phase environment differs from that of a liquid phase, the ions can be altered and this modification also affects the signal intensity of gas phase ions. For example, the basicity order of compounds in solution differs from that in the gas phase [59-62], thus, a competition for gas phase protons among analyte ions and electrolytes results in proton transfer from a weak gas phase base to a stronger base. Therefore, higher gas phase basicity analytes would be expected to suppress the MS response for a co-analyte having a lower gas phase basicity [59,62]. The investigation of gas phase modification reactions, which involve both solution and the gas phase studies, has attracted the interest of many researchers in order to elucidate ionization mechanisms.

5.1.2 Existing Models for Predicting Analyte ESI MS Response

Despite the desire to determine the correlation between the ESI MS response of an analyte and its concentration in solution, the dependence of the detected analyte ion intensity on its concentration is still not very clear. The gas phase ion signal intensity is not directly proportional to solution concentration. It depends on the chemical nature of the analyte, the presence of other electrolytes, and the ionization environment. Therefore, it is difficult to quantitatively predict the effects of solvent and electrolyte on the signal intensity of an analyte in an ESI mass spectrum. The model for describing the

relationship between analyte concentration and MS signal intensity was initially proposed by Kebarle and Tang [16,44]. Here, ion evaporation was decided as the principle factor affecting the ability of an analyte to form gas phase ions. When a droplet is produced from a solution containing two components, A^+X^- and B^+Y^-, both A^+ and B^+ ions are the excess positive ions that constitute the charges of the droplet. Ion A^+ competes with B^+ for the excess charges on the droplet surface. Depending on the competition mechanism, a quantitative equation for predicting analyte MS response was suggested. Because the reagents used contain electrolyte impurities, a solution containing a dissolved analyte is actually a two components system, analyte (A) and electrolyte impurities (E).

$$I_{A+} = pf \frac{C_A k_A}{C_A k_A + C_E k_E} I \qquad\qquad (I\text{-}1)$$

For a solution with two analytes, A and B,

$$I_{A+} = pf \frac{C_A k_A}{C_A k_A + C_B k_B + C_E k_E} I \qquad\qquad (I\text{-}2)$$

The coefficient k, which represents the efficiency of transferring ions to gas phase, is expected to depend on the ion formation mechanism. If the IEM mechanism is responsible for ionization, the coefficient will depend on the ion's surface activity and the evaporation rate. If the CRM model is more appropriate, the surface activity constant alone will determine the coefficients. In the above equations, I_{A+} is the measured ion current; C_A, C_B and C_E are the molar concentrations of analytes and electrolytes in solution; I is the total electrospray current at the metal capillary; f is the fraction of charged ions on the droplets that are converted to gas phase ions; and p is a constant corresponding to the sampling efficiency of the mass spectrometer for detecting gas phase ions. Both p and f depend on the instrumental operating conditions.

According to these equations, the MS response ratio for equal concentration of analytes A and B should equal the ratio of their coefficients (k_A/k_B) and this ratio should be constant if their concentrations are increased by the same amount.

$$\frac{I_{A+}}{I_{B+}} = \frac{C_A k_A}{C_B k_B} \, , \qquad \text{when } C_A = C_B \, , \qquad \frac{I_{A+}}{I_{B+}} = \frac{k_A}{k_B} \qquad \text{(I-3)}$$

Experimentally measured MS responses for such solutions do not fit equation I-3 over a wide concentration range [44]. A good fit with a constant k_A/k_B was observed only for $C_A = C_B > 10^{-5}$ M. At low concentrations ($C_A = C_B < 10^{-5}$ M), the measured response deviated from the predicted response curve; the response ratio I_{A+}/I_{B+} gradually decreased to close to unity. This variable ratio was attributed to a depletion phenomenon. According to the ion evaporation model, the sources of gas phase ions were charged ions at the droplet surface and the charge balance ions in the droplet interior. Ions evaporated from the surface were replaced by those from the droplet interior. When the analyte concentration is low, the droplet charges are mainly due to impurity electrolyte ions, and almost all analyte ions are at the droplet surface due to their larger coefficients. Thus, the analyte concentration in the droplet interior is much smaller than the initial concentration. The low analyte concentration and its high surface activity result in a concentration difference between the droplet surface and solution. Therefore, the analyte ion intensity no longer depends on the coefficient, and instead becomes mass dependent. When the available amounts of two analytes are equal, the ion intensity ratio is unity. However, the effects of analyte surface activity, which lead to the concentration depletion, were not included in the above equations. The response for analytes at low concentration, which is the most useful region for quantitative analysis, still cannot be predicted.

Subsequently, an equilibration model was proposed to predict analyte MS responses by taking into account the mass balance between the charged surface and neutral interior of the ESI droplet [63-67]. This model defines the surface and interior of a droplet as two distinct phases and ions partition between these two phases to establish equilibrium. It is assumed that there is a fixed amount of excess charges at the surface of the droplet. Once an ESI droplet is formed, the partition equilibrium is quickly established and the concentration of excess charge remains relatively constant throughout the evaporation process. The MS response of an analyte is proportional to the number of excess charge carrying ions on the surface. For a solution with a single analyte (A) dissolved in electrolyte (E), cations of A^+ and E^+ rapidly partition between the surface and interior phases and reach an equilibrium state.

$$(A^+X^-)_i \leftrightharpoons (A^+)_s + (X^-)_i \qquad (E^+X^-)_i \leftrightharpoons (E^+)_s + (X^-)_i \qquad (\text{II-1})$$
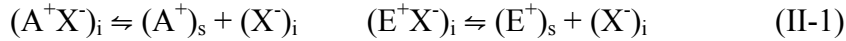
The corresponding equilibrium constants are expressed as:

$$K_A = [A^+]_s [X^-]_i / [A^+X^-]_i \qquad K_E = [E^+]_s [X^-]_i / [E^+X^-]_i \qquad (\text{II-2})$$

Where X^- represents the counter ions, and subscripts s and i represent surface and interior phases. The initial analyte concentration equals the sum of the surface and interior phase concentrations.

$$C_A = [A^+]_s + [A^+X^-]_i \qquad C_E = [E^+]_s + [E^+X^-]_i \qquad (\text{II-3})$$

A significant advance in the equilibrium model was the introduction of the equivalence of excess charge concentration [Q]. Because production of excess charge is directly proportional to the ion spray current, the production rate can be expressed as excess charge concentration.

$$[Q] = I / F v \qquad (\text{II-4})$$

154

Where I is the electrospray current (C/s); F is the Faraday constant (C/mol); and v is the flow rate (L/s). The excess charge is composed of all charged ions on the droplet surface. For a single analyte solution, excess charge concentration is the sum of the surface concentrations for A^+ and E^+.

$$[Q] = [A^+]_s + [E^+]_s \qquad\qquad\qquad (II-5)$$

Therefore, $\dfrac{K_A}{K_E} = \dfrac{[A^+]_s[E^+X^-]_i}{[E^+]_s[A^+X^-]_i} = \dfrac{[A^+]_s(C_E - [E^+]_s)}{[E^+]_s(C_A - [A^+]_s)} = \dfrac{[A^+]_s(C_E - [Q] + [A^+]_s)}{([Q] - [A^+]_s)(C_A - [A^+]_s)}$ (II-6)

By substituting the mass balance and charge balance equations, the analyte surface concentration $[A^+]_s$ can be calculated from C_A, C_E, K_A/K_E and $[Q]$ in a quadratic equation. For a two analyte solution, $[Q] = [A^+]_s + [B^+]_s + [E^+]_s$, a cubic equation for $[A^+]_s$ can be deduced using C_A, C_B, C_E, K_A, K_B, K_E and $[Q]$. These quadratic and cubic equations can be fit to the experimental MS response curves published by Kebarle and Tang [44] by using simulated parameters [63].

   An experimental result that was in contrast to the equilibrium model prediction was the effect of electrolyte concentration on the analyte MS response [64]. In this experiment, the concentration of analyte (tetrapentylammonium, TPA) ranged from 10^{-9} to 10^{-3} M and that for the electrolyte (NaCl) varied from 10^{-3} to 10^{-6} M. The MS responses (R_{TPA}) for a series of C_{TPA} solutions at various C_{NaCl} levels were measured. The author predicted that the analyte response should decrease as C_{NaCl} concentration increased based on the quadratic equation. However, the experimental results did not follow this prediction. The R_{TPA} increased with increasing C_{NaCl} when $C_{NaCl} < 10^{-4}$ M and decreased at $C_{NaCl} = 10^{-3}$ M. The discrepancy between the measured and predicted responses was explained as disproportional distribution of excess charge in the interior of

droplet. Instead of having all excess charges at the droplet surface, as the model assumed, some of the excess charge was thought to be in the droplet interior. The fraction of surface excess charges was related to the ionic strength of the solvent. A higher ionic strength solvent (high salt concentration) contained a higher fraction of excess charge at the surface and thus, higher analyte MS responses were observed. The simulated experimental results are shown in Figure 5-1. Similar observations for the measured response have been reported by other researchers [29,68].

Figure 5-1. Simulated results for the effects of C_{NaCl} on TPA MS response
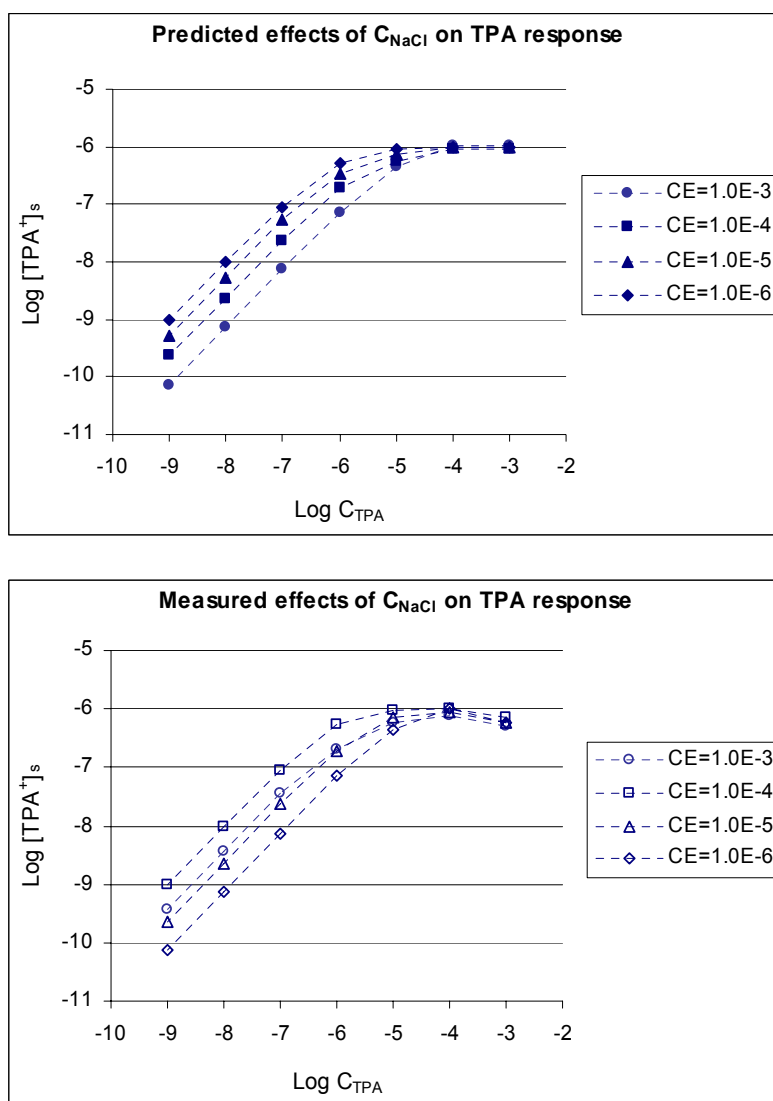
These explanations for the results are not persuasive because the equilibrium model is based on the assumption of charge balance. If some of the excess charges are carried by ions in the droplet interior, the charge balance equation would have to be modified to be: $[Q] = [A^+]_s + [A^+]_i + [E^+]_s + [E^+]_i$. This modification will change all the relevant equations.

5.1.3 Improved Model for Explaining Analyte MS Response

The purpose of the research in this section is to modify some of the concepts defined in the equilibration model and to derive improved linear equations for quantitative prediction of analyte surface concentrations. The derived equations are then used to explain measured analyte MS responses under typical ESI conditions. If the equations fit experimental results over a wide concentration range with constant coefficients, it may be concluded that the proposed approach is valid for quantitatively predicting analyte ESI responses. In the experiments, the mutual interactions of analytes, buffers, and GPCho lipids during ESI process were investigated. No such research has been conducted previously. The B1, B2 and B3 basic compounds were selected to represent single protonated analytes. The A1 and A2 acidic compounds were not examined due to their formation of sodium adducts, which complicates the ESI process model. 16:0 LPC, which was identified in the previous chapter as one of the major sources of bioanalysis matrix effects, was used to characterize the effects of GPCho lipid on analyte ionization. These works shed a new light on understanding the problem of ion suppression effects in biological sample analysis.

According to the equilibration model, the major factor determined the analyte MS response was analyte surface concentration, which depended on the analyte charge

balance process and its partitioning process between the droplet surface and interior phases (eq. II-2). However, the process by which counter ions $(X^-)_i$ balance the analyte charge in the droplet interior should be distinguished from the partitioning of the analyte ions between the two phases. The preference of a given ion distributing between these two phases primarily depends on its surface affinity. The chemical properties of an analyte ion, such as: solvation energy, hydrophobicity, and charge density as well as the nature of the solvent determine the surface affinity. The partition equilibrium process is analogous to liquid-liquid extraction, where partitioning depends on the molecule's intrinsic chemical potential, which includes entropy and solvent interactions. In addition, because the partition equilibrium constant represents the degree to which a given ion prefers for the two phases, it is reasonable to express the equilibrium coefficient as the concentration ratio of surface ions to interior ions. The total ion concentration in the two phases equals the initial analyte concentration. The excess charges are carried by ions at the droplet surface. Based on these considerations, an improved equation for analyte surface concentration is proposed.

For a single analyte (A) solution with electrolyte (E),

$$(A^+)_i \leftrightharpoons (A^+)_s \qquad\qquad (E^+)_i \leftrightharpoons (E^+)_s \qquad\qquad \text{(III-1)}$$

$$C_A = [A^+]_s + [A^+]_i \qquad\qquad C_E = [E^+]_s + [E^+]_i \qquad\qquad \text{(III-2)}$$

$$[Q] = [A^+]_s + [E^+]_s \qquad\qquad\qquad\qquad\qquad\qquad \text{(III-3)}$$

$$K_A = \frac{[A^+]_s}{[A^+]_i} = \frac{[A^+]_s}{C_A - [A^+]_s} \quad K_E = \frac{[E^+]_s}{[E^+]_i} = \frac{[E^+]_s}{C_E - [E^+]_s} \qquad \text{(III-4)}$$

$$\frac{K_A}{K_E} = \frac{[A^+]_s (C_E - [E^+]_s)}{[E^+]_s (C_A - [A^+]_s)}$$

$$[A^+]_s = \frac{C_A \cdot K_A / K_E}{K_A / K_E - 1 + C_E / [E^+]_s} \qquad \text{(III-5)}$$

For a solution containing two equally concentrated analytes, A and B,

$$\frac{[A^+]_s}{[B^+]_s} = \frac{C_A \cdot K_A / K_E (K_B / K_E - 1 + C_E / [E^+]_s)}{C_B \cdot K_B / K_E (K_A / K_E - 1 + C_E / [E^+]_s)} = \frac{K_A (C_E - [E^+]_S) + (K_A K_B / K_E)[E^+]_s}{K_B (C_E - [E^+]_S) + (K_A K_B / K_E)[E^+]_s}$$

$$\frac{[A^+]_s}{[B^+]_s} = \frac{K_A}{K_B} \cdot \frac{C_E + (K_B / K_E - 1)[E^+]_s}{C_E + (K_A / K_E - 1)[E^+]_s} \qquad \text{(III-6)}$$

In the improved equations (III-5 and III-6), element $[E^+]_s$ is used in order to obtain a linear equation. The surface analyte ion concentration is calculated using C_A, C_E, K_A/K_E, and $[E^+]_s$. Because ion concentration on droplet surface is calculated using the ratio of coefficients (K_A/K_E), the equations derived from the equilibrium model are not affected by the involving of charge balance process (eq. II-6 is same as III-5).

The MS response (R) of an analyte can be expressed as ion intensity, which is the rate of ions arriving at the detector (counts per second) and is directly proportional to the ion species surface concentration.

$$R_A = [A^+]_s F \nu p f \qquad \text{(III-7)}$$

Where F is Faraday's constant (C/mol); ν is flow rate (L/s); and f and p have the same definitions as in equation I-2: efficiency of converting ions carrying excess charge from droplet surface to the gas phase, and efficiency of the mass spectrometer to measure these gas phase ions.

5.1.4 Simulated Analyte MS Response by using Improved Model

To verify the effectiveness of improved equations, simulated analyte MS response curves calculated by using equations III-5 and III-6 are shown in Figures 5-2 and 5-3, respectively. Simulation is based on the following assumptions: the amount of excess

charge remains relatively constant; ions on the surface are responsible for the excess charge; and the ion partition coefficient determines their probability of residing on the droplet surface. In practice, ion current increases very slowly with increasing analyte concentration ($I = H\kappa^n v_f^{\ v} E_c^{\ \sigma}$, $\kappa = \sum_i \lambda_m^{\ 0} C_i$). It has been reported that a 50-fold increase in concentration results in about 2-fold enhancement in ion current [44,69]. Because increased analyte concentration leads to only a slight [Q] enrichment, it can be assumed that [Q] is relatively constant for MS response predictions.

For a single analyte solution (Fig. 5-2), the concentration of background electrolytes (C_E), which was due to solvent impurities, was set at 10^{-5} M based on reference data [44]. When analyte concentration C_A is lower than electrolyte concentration, 10^{-10} - 10^{-6} M, the [Q] should be comprised mainly of surface electrolyte ions $[E^+]_s$. The $[E^+]_s$ was assumed to be 10% of the solution phase concentration. Because [Q] remains constant, the ratio of C_E / $[E^+]_s$ is relatively invariable. The analyte surface concentration, $[A^+]_s$, is proportional to C_A regardless of the value of K_A/K_E. When C_A is similar to C_E at 10^{-6} - 10^{-4} M, analyte ions compete with electrolyte ions as excess charge carriers. Due to the consistency of excess charge, $[E^+]_s$ decreases with increasing C_A. The more surface affinity an ion possesses, the more powerful that ion is in competing for the excess charge. Therefore, as the coefficients ratio (K_A/K_E) becomes larger, $[E^+]_s$ is expected to decrease rapidly when C_A increases. As a result of the increasing ratio C_E /$[E^+]_s$, $[A^+]_s$ deviates from being linearly proportional to C_A. Depending on the ratio of K_A/K_E, the deviation will occur to differing degrees: the larger the K_A/K_E value, the larger the deviation. Ultimately, when analyte ions carry almost all of the excess charges, $[Q] \approx [A^+]_s$, saturation will occur.

Figure 5-2. Simulated relationship between $[A^+]_s$ and C_A for single analyte with different partition coefficients relative to background electrolytes
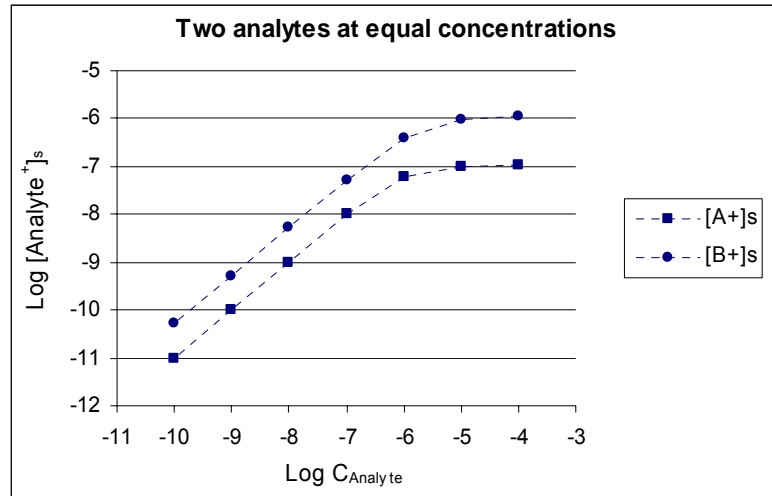
$$Log[A^+]_s = LogC_A + Log\frac{K_A/K_E}{K_A/K_E - 1 + C_E/[E^+]_s}$$
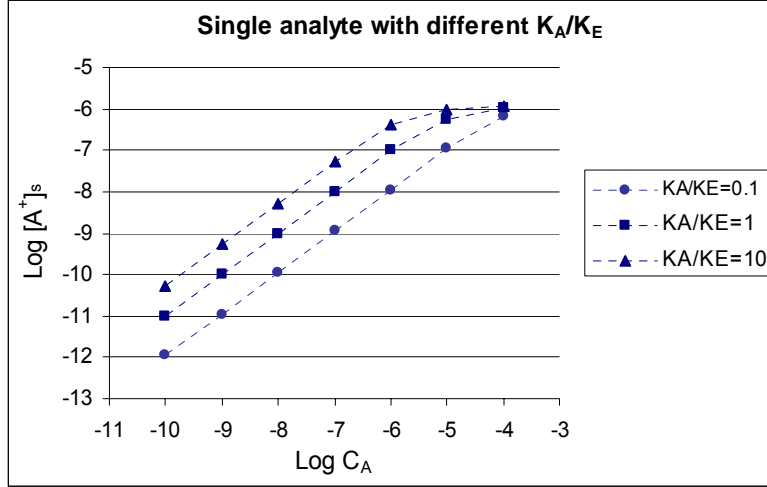
C_A	Log C_A	C_E	K_A/K_E	$[E^+]_S$	$[A^+]_S$	[Q]	Log $[A^+]_S$
1.0E-04	-4	1.0E-05	0.1	6.0E-07	6.3E-07	1.2E-06	-6.20
1.0E-05	-5	1.0E-05	0.1	1.0E-06	1.1E-07	1.1E-06	-6.96
1.0E-06	-6	1.0E-05	0.1	1.0E-06	1.1E-08	1.0E-06	-7.96
1.0E-07	-7	1.0E-05	0.1	1.0E-06	1.1E-09	1.0E-06	-8.96
1.0E-08	-8	1.0E-05	0.1	1.0E-06	1.1E-10	1.0E-06	-9.96
1.0E-09	-9	1.0E-05	0.1	1.0E-06	1.1E-11	1.0E-06	-10.96
1.0E-10	-10	1.0E-05	0.1	1.0E-06	1.1E-12	1.0E-06	-11.96
1.0E-04	-4	1.0E-05	1	1.1E-07	1.1E-06	1.2E-06	-5.96
1.0E-05	-5	1.0E-05	1	5.5E-07	5.5E-07	1.1E-06	-6.26
1.0E-06	-6	1.0E-05	1	1.0E-06	1.0E-07	1.1E-06	-7.00
1.0E-07	-7	1.0E-05	1	1.0E-06	1.0E-08	1.0E-06	-8.00
1.0E-08	-8	1.0E-05	1	1.0E-06	1.0E-09	1.0E-06	-9.00
1.0E-09	-9	1.0E-05	1	1.0E-06	1.0E-10	1.0E-06	-10.00
1.0E-10	-10	1.0E-05	1	1.0E-06	1.0E-11	1.0E-06	-11.00
1.0E-04	-4	1.0E-05	10	1.2E-08	1.2E-06	1.2E-06	-5.93
1.0E-05	-5	1.0E-05	10	1.1E-07	1.0E-06	1.1E-06	-6.00
1.0E-06	-6	1.0E-05	10	6.5E-07	4.1E-07	1.1E-06	-6.39
1.0E-07	-7	1.0E-05	10	1.0E-06	5.3E-08	1.1E-06	-7.28
1.0E-08	-8	1.0E-05	10	1.0E-06	5.3E-09	1.0E-06	-8.28
1.0E-09	-9	1.0E-05	10	1.0E-06	5.3E-10	1.0E-06	-9.28
1.0E-10	-10	1.0E-05	10	1.0E-06	5.3E-11	1.0E-06	-10.28

Figure 5-3. Simulated analyte surface concentration as a function of solution concentration for two analytes (A and B) at equal concentrations

$$Log[A^+]_s - Log[B^+]_s = Log\frac{K_A}{K_B} + Log[C_E + (K_B/K_E - 1)[E^+]_s] - Log[C_E + (K_A/K_E - 1)[E^+]_s]$$

$K_A/K_E = 1$; $K_B/K_E = 10$								
$C = C_A = C_B$	Log C	C_E	$[E^+]_S$	$[A^+]_S$	$[B^+]_S$	[Q]	Log $[A^+]_S$	Log $[B^+]_S$
1.0E-04	-4	1.0E-05	1.1E-08	1.1E-07	1.1E-06	1.21E-06	-6.96	-5.96
1.0E-05	-5	1.0E-05	1.0E-07	1.0E-07	9.2E-07	1.12E-06	-7.00	-6.04
1.0E-06	-6	1.0E-05	6.0E-07	6.0E-08	3.9E-07	1.05E-06	-7.22	-6.41
1.0E-07	-7	1.0E-05	1.0E-06	1.0E-08	5.3E-08	1.06E-06	-8.00	-7.28
1.0E-08	-8	1.0E-05	1.0E-06	1.0E-09	5.3E-09	1.01E-06	-9.00	-8.28
1.0E-09	-9	1.0E-05	1.0E-06	1.0E-10	5.3E-10	1.00E-06	-10.00	-9.28
1.0E-10	-10	1.0E-05	1.0E-06	1.0E-11	5.3E-11	1.00E-06	-11.00	-10.28

For a solution containing two equal concentration analytes (Fig. 5-3), when analyte concentrations are low, $C_A = C_B < 10^{-6}$ M, C_E and $[E^+]_s$ are relatively constant, as in the single analyte system. The analyte MS responses depend on their partition coefficients. Since K_A, K_B and K_E are constant, the $[A^+]_s / [B^+]_s$ ratio is constant at low concentrations. When analyte concentration is similar or greater than that of the electrolyte, $[E^+]_s$ decreases due to competition for excess charge from the analytes. Both $[A^+]_s$ and $[B^+]_s$ are no longer proportional to their solution phase concentrations due to the rising $C_E / [E^+]_s$ ratio. When analyte concentration increases to a certain level, at which the surface excess charge is nearly completely carried by $[A^+]_s$ and $[B^+]_s$, $[E^+]_s$ becomes very small. Consequently, the ($C_E + (K_A/K_E - 1)[E^+]_s$) and ($C_E + (K_B/K_E - 1)[E^+]_s$) terms are approximately equal to C_E, and the response ratio for the analytes $[A^+]_s / [B^+]_s$ approaches the ratio of their coefficients (K_A/K_B).

The simulated MS response curves calculated by using linear equations III-5 and III-6 over a wide analyte concentration range are comparable with those generated by using the quadratic and cubic equations from the equilibration model. However, with the simple linear equations, the analyte MS response can be predicted without complicated mathematical calculations. When a solution contains more than one analyte, the advantages of using the simplified equations will be more obvious. Because the improved equations are easier to use and prove to be reliable for simulation results, they were utilized to model measured experimental data.

5.2 Discussion

5.2.1 MS Response for a Single Analyte in HPLC Compatible Solvent

The effects of partition coefficient on analyte MS response were examined by using a single analyte solution. The MS responses for analytes B1, B2, B3 and 16:0 LPC dissolved in 50:50 ACN:H_2O were separately measured (Fig. 5-4). The concentration range was from 1.0×10^{-9} to 1.0×10^{-5} M for B1, B2 and B3 and from 5.0×10^{-9} to 1.0×10^{-5} M for 16:0 LPC. A higher concentration range was not examined because the lower concentration range is used for quantitative analysis by mass spectrometry. A concentration below 1.0×10^{-9} M cannot be employed because the analyte signal intensity was not substantial higher than the background noise. The MS response signal was measured as the ion intensity with units of counts per second (cps). The results indicated that all examined analytes exhibited a linear relationship between MS response intensity and solution concentration (C_A) when $C_A < 10^{-6}$ M. These results are in agreement with the prediction of equation III-5 at low analyte concentration. It was also demonstrated that analyte B2 yielded a relatively larger MS response than those for the B1 and B3 and the ion intensities for B1 and B3 analytes were comparable. These three analytes yielded considerably more intense MS responses compared to that for 16:0 LPC. Because ions on the droplet surface come from ions in solution, the amount of surface electrolyte $[E^+]_s$ should be less than C_E and the $C_E / [E^+]_s$ ratio should be greater than one. Thus, according to equation III-5, an analyte with higher K_A and subsequently higher K_A/K_E will have a greater $[A^+]_s$, which was observed as a larger MS response. Because the ion intensity in the linear response region illustrated the effect of relative partition coefficient K_A/K_E, the MS response results of Figure 5-4 indicated that the relative coefficient for the four analytes was: $K_{B2}/K_E > K_{B1}/K_E \approx K_{B3}/K_E \gg K_{PC}/K_E$.

Figure 5-4. ESI response of single analyte B1, B2, B3 and 16:0 LPC in 50:50 ACN: H_2O as a function of analyte concentration at three different ion spray voltages
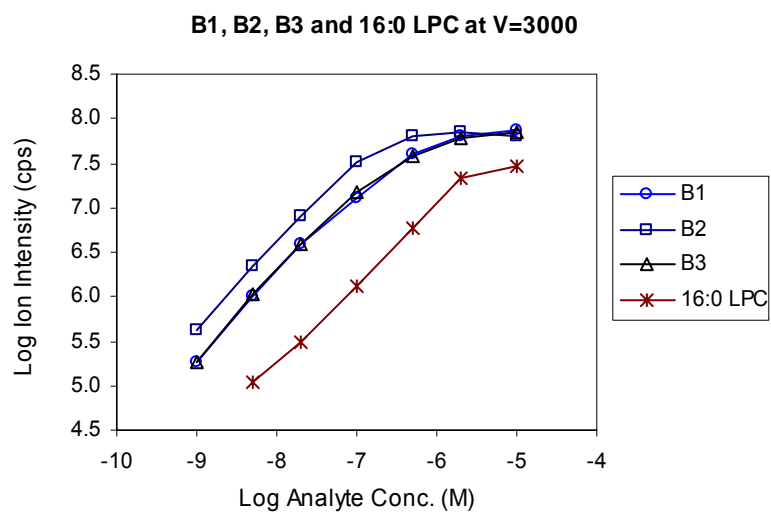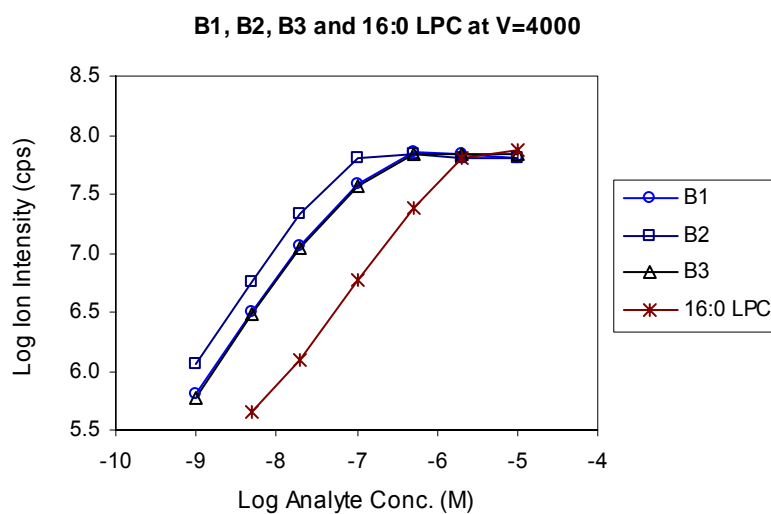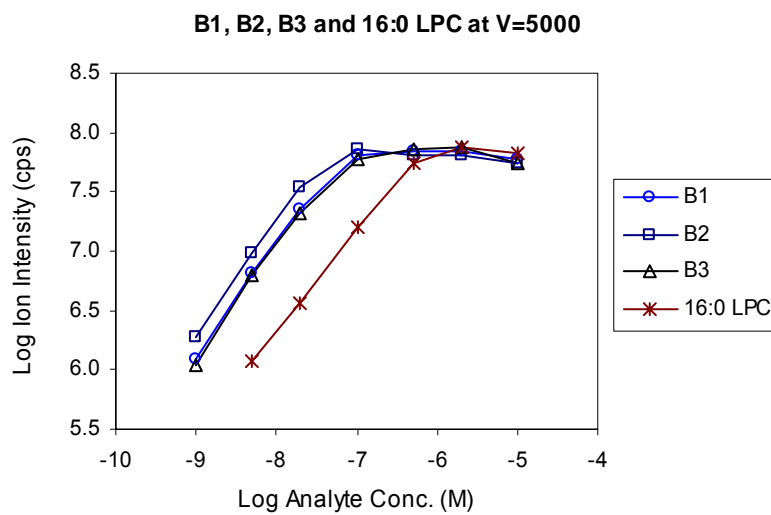
When analyte concentration exceeds 10^{-6} M, the analyte response curves begin to deviate from the linearity. This analyte MS response deviation from concentration is called saturation. However, the saturation exhibited in Figure 5-4 was different from that shown in Figure 5-2. The deviation in Figure 5-2 was caused by the limited increase in [Q]. Because of this limitation, the fraction of analyte contributing to the excess surface charge was not proportional to the concentration increase. Under such circumstances, the magnitude of the response curve deviation depended on the ratio of K_A/K_E and the leveling off effect was expected to occur at analyte concentrations greater than the electrolyte concentration, $C_A > 10^{-5}$ M. However, the non-linear MS response shown in Figure 5-4 occurred at relatively low concentration ($C_A < 10^{-5}$ M) and was independent of the K_A/K_E ratio. It was suspected that this deviation was the result of saturation caused by the mass spectrometer detector. As indicated by equation III-7, the MS response was proportional to the efficiency of the instrument measuring these gas phase ions (f). When the amount of a given ion is beyond the measuring capability of the detector, the detected amount for that ion reaches a constant value even though the gas phase ion concentration increased.

The effects of ion spray voltage on analyte MS response was evaluated at three voltages: 5000, 4000, and 3000 V. The ion intensities of all the analytes increased with increasing ion spray voltage, and the slopes of the response curves appeared to be unrelated to voltage. These results are consistent with the quantitative prediction for $[A^+]_s$. Because [Q] is proportional to ion spray voltage, a larger [Q] increases the fraction of charged analyte. Moreover, as ion spray voltage decreases, the detector saturation occurs at a higher concentration due to decreased ion intensity.

Because of the mass spectrometer detector saturation, the approach for determining analyte coefficient ratio by measuring response curves for two analytes with equal concentration was not successful. The MS response curves for simultaneously determined analytes B2 and B3 exhibited saturation when $C_{B2} = C_{B3} > 10^{-5}$ M. The expected result that the ion intensity ratio of B2 to B3 reaches a constant (K_{B2}/K_{B3}) at high concentration cannot be verified due to detector saturation. The representative coefficient ratios for the four analytes were therefore not been obtained.

5.2.2 Effects of Mass Spectrometer Compatible Buffers on Analyte Ionization

The MS responses for B1, B2, B3 and 16:0 LPC analytes dissolved in 50:50 ACN:H_2O containing mass spectrometer compatible buffers are shown in Figures 5-5 to 5-8, respectively. With analyte concentration fixed at 10^{-7} M, three buffers: ammonium acetate (AA), formic acid (FA), and ammonium hydroxide (AH) were separately employed with concentrations varied from 0 M, 10^{-7} M to 10^{-2} M. Before discussing the results, it is useful to introduce several measured partition coefficients (Table 1 in Ref. 44). Assuming the value of coefficient $Cs^+ = 1$, coefficients for several analytes were deduced by using equation I-3 ($I_{A+}/I_{Cs+} = k_A/k_{Cs}$). Although the meaning of k is different from that defined for the partition equilibrium model (eq. III-4), a k value determined from the MS response ratio for two equally concentrated analytes is still valid. The determined k values for Na^+, K^+ and NH_4^+ were 1.6, 1.0 and 1.3, respectively. Codeine, heroin and cocaine had relatively higher k values than those of the inorganic ions with values of 3.8, 5.5 and 8.3, respectively. These reported coefficients suggest that the partition coefficients for buffer ions might be smaller than the coefficients for measured analytes and probably even smaller than for background electrolytes.

Figure 5-5. Effects of ammonium acetate concentration on ESI response of single analyte B1, B2 and B3 at three different ion spray voltages
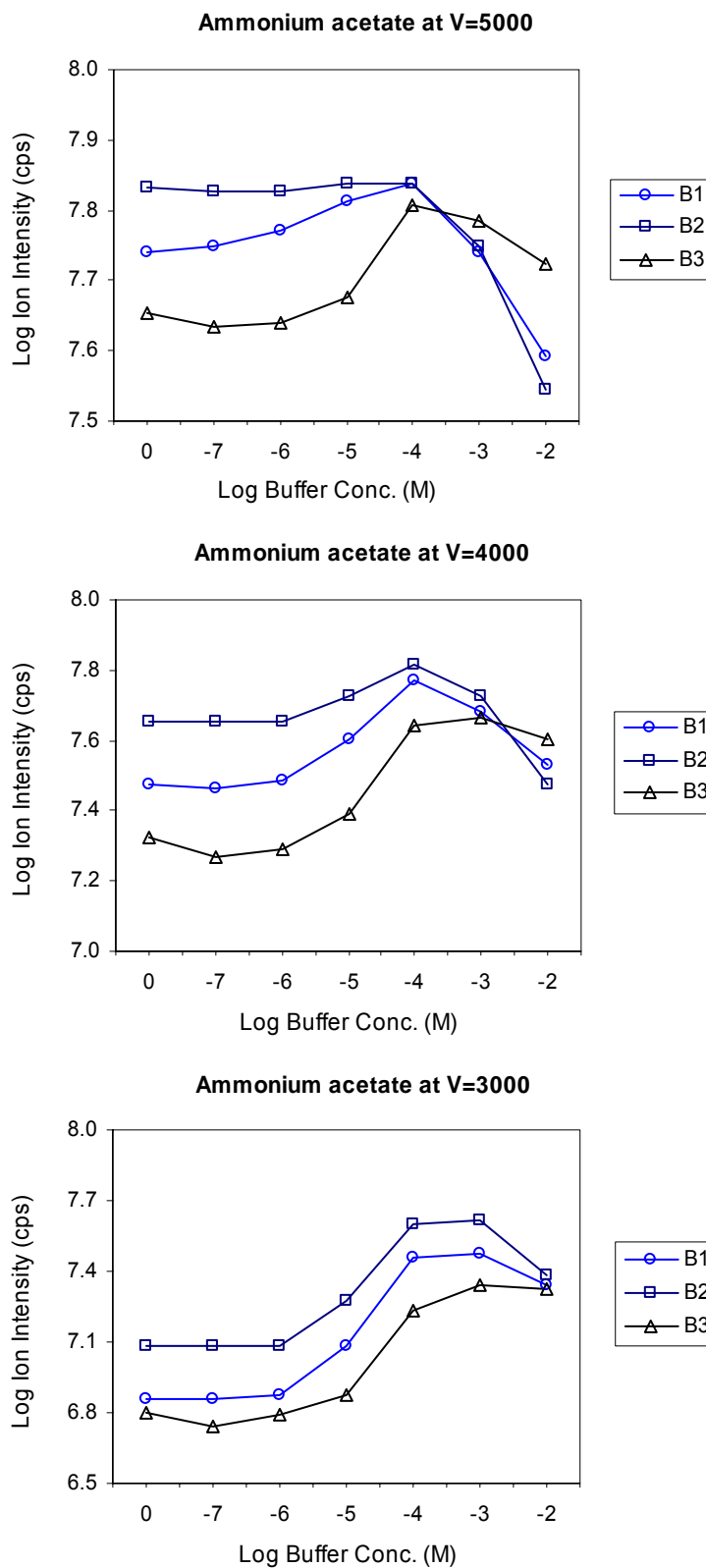
Figure 5-6. Effects of formic acid concentration on ESI response of single analyte B1, B2 and B3 at three different ion spray voltages
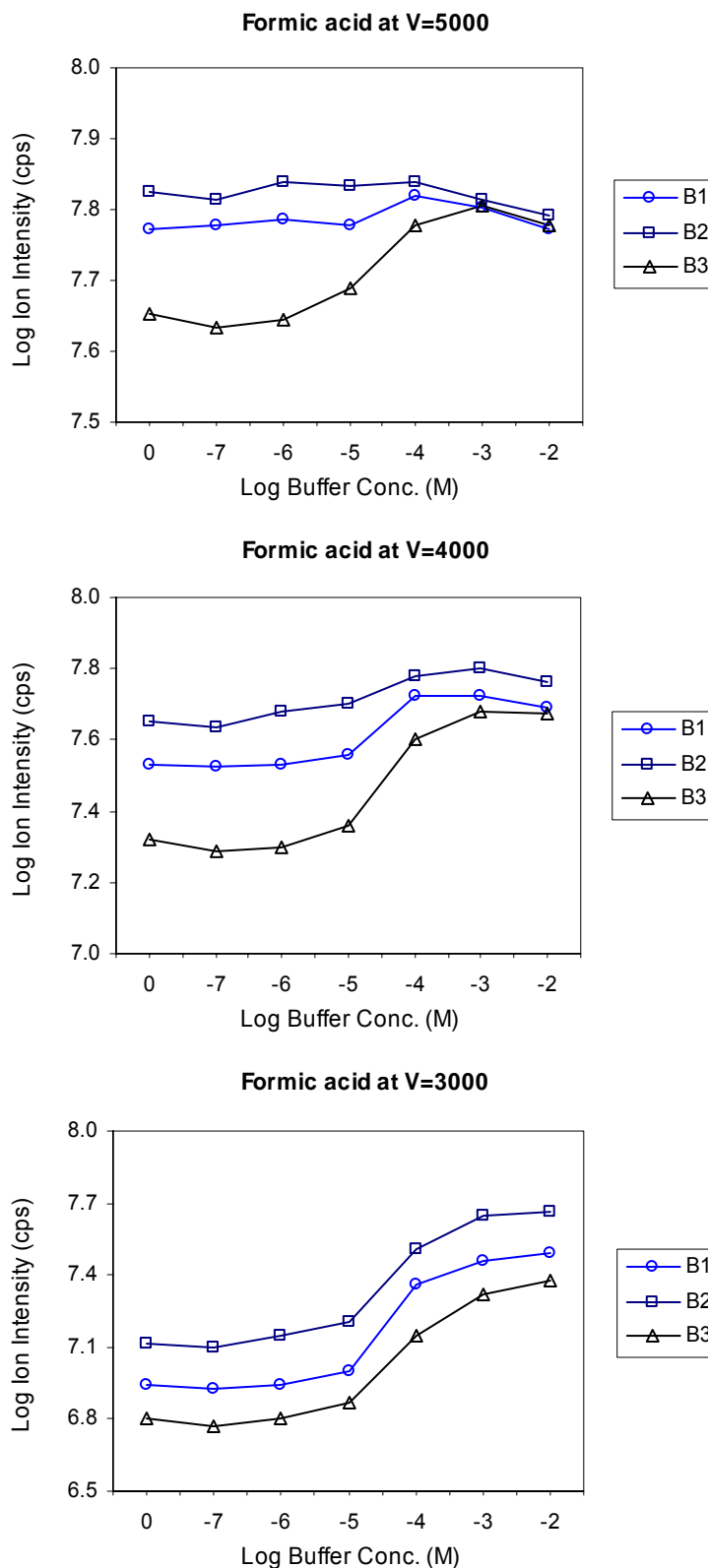

Formic acid at V=5000

Formic acid at V=4000

Formic acid at V=3000

Figure 5-7. Effects of ammonium hydroxide concentration on ESI response of single analyte B1, B2 and B3 at three different ion spray voltages
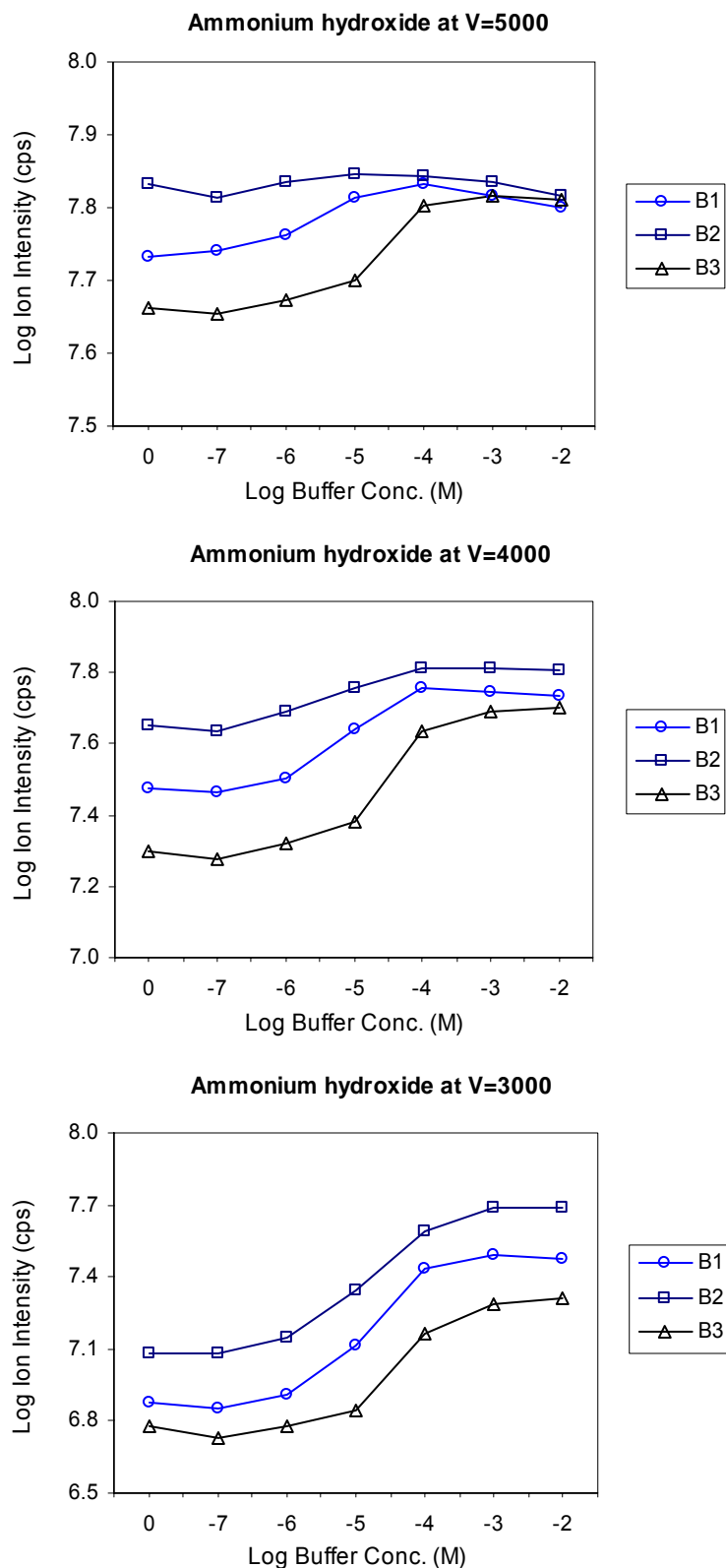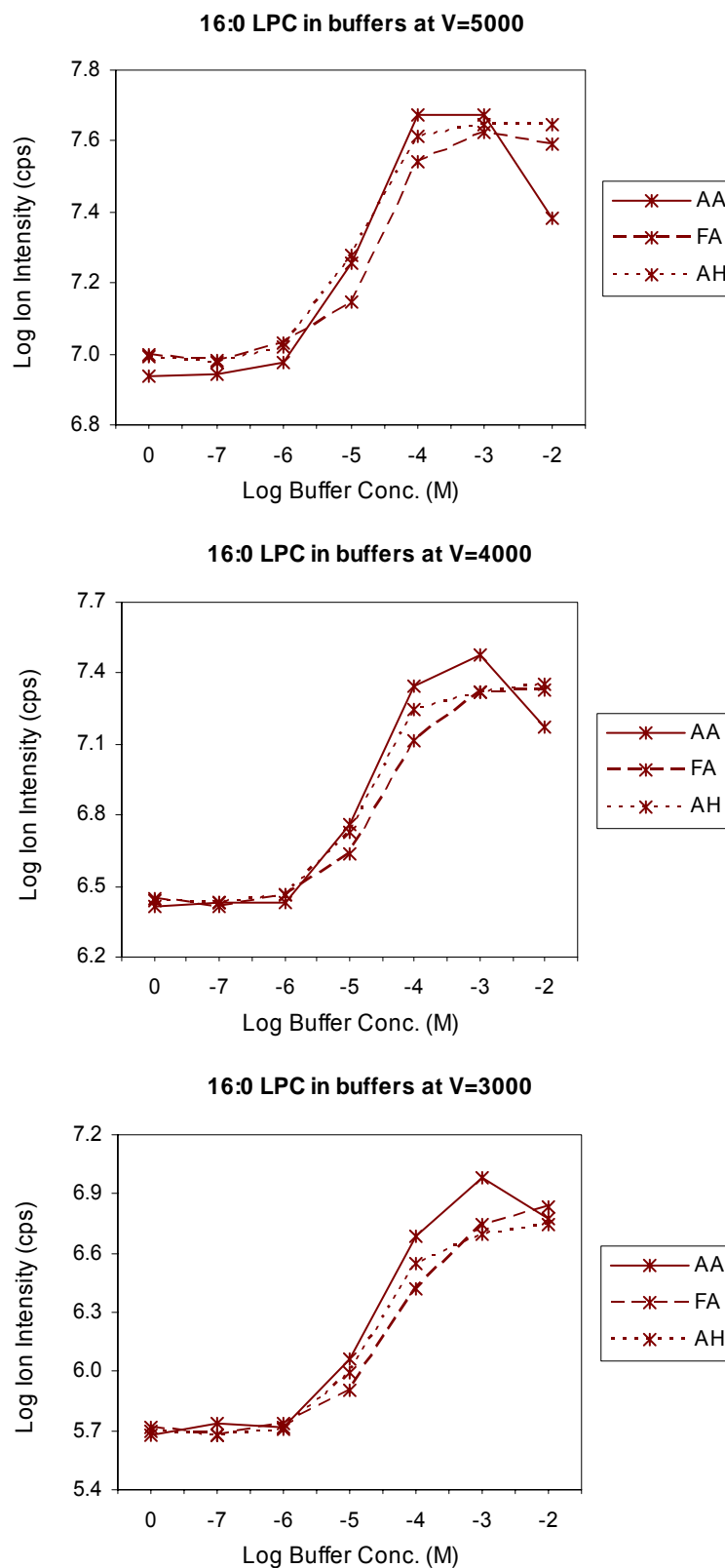

Ammonium hydroxide at V=5000

Ammonium hydroxide at V=4000

Ammonium hydroxide at V=3000

Figure 5-8. Effects of buffer concentration on ESI response of analyte 16:0 LPC at three different ion spray voltages

16:0 LPC in buffers at V=5000

16:0 LPC in buffers at V=4000

16:0 LPC in buffers at V=3000

The effects of buffer concentration, pH value and buffer type on analyte MS response were discussed by using the results obtained with a 4000 V ion spray voltage. When the buffers were added to the analyte solutions, MS responses of all analytes remained relatively constant for buffer concentrations $C_{Buf} \leq 10^{-6}$ M. There was no significant difference among tested buffers. These observations indicated that these mass spectrometer compatible buffers should have comparable small partition coefficients. For a low buffer concentration, the main factor determining the analyte MS response should be the partition coefficient of buffer. If the buffer possesses a K_{Buf} close to or less than the background electrolyte K_E value, the competitive impact of the buffer on $[A^+]_s$ should not be substantial because the concentration of buffer is lower than that of background electrolyte and $[E]_s$ is the primary carriers for excess charge. The surface concentration of the analyte can still be expressed as: $[A^+]_s = \dfrac{C_A \cdot K_A / K_E}{K_A / K_E - 1 + C_E / [E^+]_s}$. When the analyte concentration (C_A) remains constant, the MS response is relatively invariable.

It is shown in the plots that further increases in C_{Buf} led to an analyte MS signal increase, followed by a signal decrease at $C_{Buf} > 10^{-3}$ M. When buffer concentration is comparable to background electrolyte concentration ($10^{-6} < C_{Buf} < 10^{-4}$ M), buffer ions compete with analyte and electrolyte for excess charge on the droplet surface. If the buffer was treated as a portion of the background electrolytes, the corresponding partition coefficient, called K_M, would be a mixed function of K_E and K_{Buf} ($K_M = \dfrac{[E^+]_s + [Buf^+]_s}{[E^+]_i + [Buf^+]_i} = \dfrac{[M^+]_s}{[M^+]_i}$). Analyte surface concentration in this region was thus expressed as: $[A^+]_s = \dfrac{C_A \cdot K_A / K_M}{K_A / K_M - 1 + C_M / [M^+]_s}$. Because K_{Buf} was most likely to be

172

smaller than K_E, K_M should also be smaller than K_E. As C_{Buf} increased, the contribution of K_{Buf} to K_M was greater, and consequently K_M became smaller. The order of coefficient ratios for a solution containing 10^{-4}, 10^{-6} and 0 M buffer were: $K_A/K_{M(-4)} > K_A/K_{M(-6)} > K_A/K_E$. Therefore, $[A^+]_s$ increased with increasing buffer concentration when $C_{Buf} \approx C_E$. The partition process under these conditions might also be described as: buffer ions competed for excess droplet surface charge with background electrolytes when their concentrations were comparable. Because K_{Buf} was smaller than K_E, buffer ions were weaker than background electrolyte ions for keeping excess charges. Therefore, analyte ions were able to replace surface buffer ions relatively easily when partition equilibrium was established. Because the addition of buffer reduced the capability of the electrolyte to carry the excess charge, the MS response for analytes increased with increasing buffer concentration.

When the buffer concentration was much greater than the background electrolyte concentration ($C_{Buf} > 10^{-4}$ M), the [Q] was mainly carried by surface buffer ions $[Buf^+]_s$. K_M was determined primarily by K_{Buf} and the effects of K_E was not important. The analyte surface concentration was changed to: $[A^+]_s = \dfrac{C_A \bullet K_A/K_{Buf}}{K_A/K_{Buf} - 1 + C_{Buf}/[Buf^+]_s}$.

Because available excess charge was limited, the $[Buf^+]_s$ could not increase proportionally with the increasing C_{Buf}. The deviation from $C_{Buf}/[Buf^+]_s$ became more and more significant and turned out to be a principal factor that dominated the analyte MS response. As a result of buffer saturation, analyte surface concentration decreased with increasing buffer concentration. With the improved linear equation, the effects of adding buffer on analyte MS responses, which could not be explained by the partition

equilibrium model, were clarified by using constant partition coefficients over a wide concentration range.

In addition, a non-linear fitting was conducted for FA buffer effects on 16:0 LPC MS responses. Because $C_E = [E^+]_s + [E^+]_i$ $\qquad$ $K_E = [E^+]_s / [E^+]_i$

thus, $\quad [E^+]_s = \dfrac{C_E}{1 + 1/K_E}$ $\qquad\qquad$ $[E^+]_i = \dfrac{C_E}{1 + K_E}$

and $\quad C_{Buf} = [Buf^+]_s + [Buf^+]_i$ $\qquad$ $K_{Buf} = [Buf^+]_s / [Buf^+]_i$

$$[Buf^+]_s = \frac{C_{Buf}}{1 + 1/K_{Buf}} \qquad\qquad [Buf^+]_i = \frac{C_{Buf}}{1 + K_{Buf}}$$

Therefore, $K_M = \dfrac{[E^+]_s + [Buf^+]_s}{[E^+]_i + [Buf^+]_i} = \dfrac{\dfrac{C_E}{1 + 1/K_E} + \dfrac{C_{Buf}}{1 + 1/K_{Buf}}}{\dfrac{C_E}{1 + K_E} + \dfrac{C_{Buf}}{1 + K_{Buf}}}$

Since $[M^+]_s = [E^+]_s + [Buf^+]_s$, $C_M = C_E + C_{Buf}$ and $R_A = [A^+]_s F v p f$

Thus, the equation for surface analyte concentration $[A^+]_s = \dfrac{C_A \cdot K_A / K_M}{K_A / K_M - 1 + C_M / [M^+]_s}$ is

converted to: $\dfrac{R_A}{Fvpf} = \dfrac{\dfrac{C_A K_A \left(\dfrac{C_E}{1 + K_E} + \dfrac{C_{Buf}}{1 + K_{Buf}} \right)}{\dfrac{C_E}{1 + 1/K_E} + \dfrac{C_{Buf}}{1 + 1/K_{Buf}}}}{\dfrac{K_A \left(\dfrac{C_E}{1 + K_E} + \dfrac{C_{Buf}}{1 + K_{Buf}} \right)}{\dfrac{C_E}{1 + 1/K_E} + \dfrac{C_{Buf}}{1 + 1/K_{Buf}}} - 1 + \dfrac{C_E + C_{Buf}}{\dfrac{C_E}{1 + 1/K_E} + \dfrac{C_{Buf}}{1 + 1/K_{Buf}}}}$

$$\frac{R_A}{Fvpf} = \frac{C_A K_A \left(\dfrac{C_E}{1 + K_E} + \dfrac{C_{Buf}}{1 + K_{Buf}} \right)}{K_A \left(\dfrac{C_E}{1 + K_E} + \dfrac{C_{Buf}}{1 + K_{Buf}} \right) - \dfrac{C_E}{1 + 1/K_E} - \dfrac{C_{Buf}}{1 + 1/K_{Buf}} + C_E + C_{Buf}}$$

174

Because C_{Buf} is the only variable in the above equation and all the other parameters including C_A, C_E, K_A, K_E, K_{Buf}, F, v, p, f and R_A are constants, the measured data were simulated by using this equation with a non-linear fitting software KyPlot. The fitted curve and the measured data for FA buffer at 5000 V are shown in Figure 5-9. The simulated parameters were $C_A \bullet (F v p f) = 9900$, $C_E = 2.2 \times 10^{-5}$, $K_A = 0.56$, $K_E = 3.39$, and $K_{Buf} = 3.75$. For the five fitted parameters, $C_A \bullet (F v p f)$ are difficult to evaluate due to the lack of efficiency parameters p and f information. C_E, K_E and K_{Buf} are reasonably compatible with the reported data [44] and K_A is lower than the predicted coefficient. Considering the fact that seven measured points were simulated by five parameters, these results are logically acceptable.

Figure 5-9. Simulated effects of FA concentration on ESI response of analyte 16:0 LPC
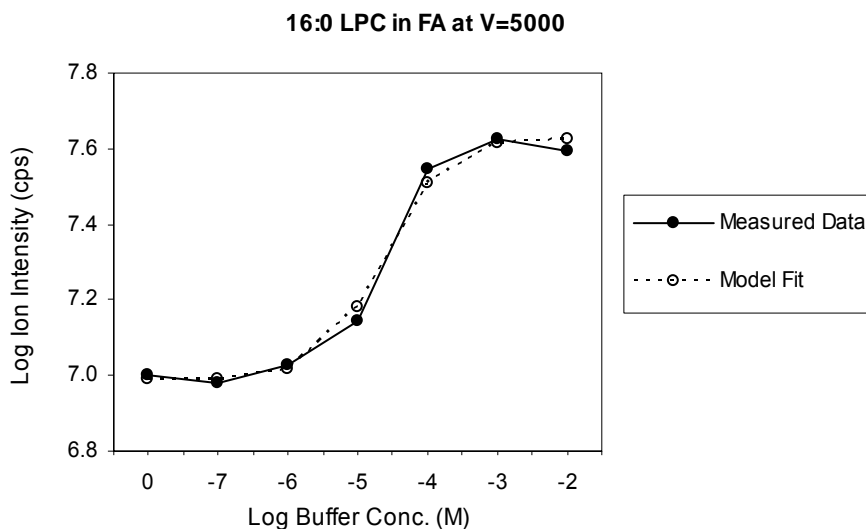
Comparing the signal intensity plots for formic acid and ammonium hydroxide (Fig. 5-6 and 5-7), differences due to buffer type could be distinguished. The pH difference for these two buffers was about 7 units. Such a pH variation can substantially change the acid-base equilibrium of analytes in solution, but the observed MS responses appeared to be independent on the degree of analyte protonation in solution. The production of equally intense protonated analytes ions in acidic and basic solutions indicated that it is the nature of the analyte and the ESI process, not the solution phase equilibrium, that are responsible for analyte MS intensity. These observations are analogous with the so-called "wrong-way-around" electrospray where intense protonated ions from strongly basic solutions and deprotonated ions from strongly acidic solutions are detected. The proposed mechanisms for the "wrong-way-around" observation imply that this type of phenomena can be attributed to a transition process during gas phase ions formation [28-30]. For example, a possible process for analyte in ammonia solution is that the gas phase adults from electrolyte ions ($[M+NH_4^+]$) are initially formed, and that these adult ions undergo evaporation and collision induced dissociation (CID) in the declustering interface to yield protonated ions. The explanations for "wrong-way-around" electrospray observations are consistent with the quantitative theory of partition equilibrium for ESI process. As indicated by equation III-5, the analyte surface concentration, which is determined by the relative partitioning capability of compounds, is independent of solution phase acid-base equilibra. Under the same concentration and instrumental conditions, analytes can exhibit comparable MS response in acidic or basic solutions provided that the solution phase background electrolytes posses similar partition coefficients.

The most distinct difference in the plots was that analytes B1 and B2 exhibit a steeper slope in AA than in FA and AH at high buffer concentration whereas analyte B3 gave comparable MS responses in the three buffers. The ion intensities for analytes B1 and B2 in 10^{-2} M AA were near or below their responses in pure solvent, whereas their MS responses in 10^{-2} M FA and AH were higher than those in pure solvent. The similar analyte MS responses for solutions with low buffer concentration indicate that the three buffers have comparable small K_{Buf} and plots from Figure 5-4 show that the analytes B1, B2 and B3 posses comparable K_A. These results are confirmed by the similar signal increases for mid-range buffer concentrations. Thus, according to the proposed equations for $[A^+]_s$ at high buffer concentrations, analytes should exhibit similar signal decreases in the three buffers. To rationalize the lack of correlation between observed and predicted MS responses, the ion evaporation process has to be considered. Based on the current knowledge of ESI processes, ions escaping from small droplets are not naked ions, but solvated ion clusters [53,54]. These cluster ions undergo subsequent evaporation and CID to form the mass analyzer detected ions, M^+. Employing the IEM model, the generally agreed mechanism for production of small ions, the rate of ion evaporation from the charged droplet, should certainly have an effect on the analyte signal intensity. The ion evaporation rate (k_I) depends on the free energy of activation ($\Delta G^{\neq}$), which is directly related with $\Delta G_{sol}[M^+(sol)_n]$, the free energy released when an ion (M^+) surround by n solvent molecules is moved from infinity into an uncharged droplet of the same solvent [1]. Ions with small desolvation energies, $-\Delta G_{sol}[M^+(sol)_n]$ will have high ion evaporation rates, which will increase the ion intensity in the mass spectrum. Due to difficulties in obtaining accurate data for the dissolvation energies, particularly for organic ions,

quantitative evaluation the role of dissolvation energy in ionization processes and comparisons of predicted results with experimental observations are not possible. It was speculated that as the concentration of buffer increases, the escaping cluster ions from shrinking droplets might be present in a form of: $[M^+(sol-buf)_n]$. If the dissolvation energy of $[M^+(sol-buf)_n]$ depends on the type of buffer, the ion evaporation rate for the same analyte in different buffer solutions would be different. Therefore, even if the analyte has the same surface concentration in different buffer solutions, differences in ion evaporation rates will lead to different MS responses. The ion intensity difference for analytes B1 and B2 in the AA modified solution compared to the FA and AH modified solutions might be explained by using this argument. If the dissolvation energies for analytes B1 and B2 in AA were larger than in FA and AH, the ion evaporation rates for B1 and B2 from droplets containing AA would be less than those from droplets containing FA and AH. Although the surface concentrations of $[B1]_s$ and $[B2]_s$ were comparable in the three buffers, their relative small ion evaporation rates in the AA modified solution caused them to produce fewer $B1^+$ and $B2^+$ ions detected by the mass spectrometer. The findings from an interesting amino acid protonation study are consistent with this speculation. The author concluded that the degree of ion clustering was affected by the type of solvent and solvent additives [45].

By comparing the MS responses of the four analytes at ion spray voltages of 5000 and 4000 V, it was found that the slope increase for the mid-range buffer concentrations at 5000 V was less than that at 4000 V, especially for analyte B2. Theoretically, the MS response profile for an analyte should not be dependent on the ion voltage except for the measuring sensitivity. The major factor influenced by the voltage was the excess charge

and [Q] normally had no effect on the fraction of the analyte at the droplet surface. Thus, the variations in MS response profiles were attributed to instrumental saturation effects. Analyte ion intensity at 5000 V was truncated to the maximum count limit for the mid-range buffer concentration solutions. The analyte MS responses at 3000 V exhibited a relatively small decrease for high buffer concentration solutions. This subtle difference may be due in part to a non-linear variation of capillary current with voltage as buffer concentration was increased.

5.2.3 Effects of Co-analytes on Analyte Ionization

Signal intensities for analyte ions from solutions containing a co-analyte, which was a compound with similar chemical properties or was a representative interference from biological samples, were measured. Ion intensity variations for analyte B1 with B2, B3 and 16:0 LPC co-analytes, analyte B2 with B1, B3 and 16:0 LPC co-analytes, and analyte B3 with B1, B2 and 16:0 LPC co-analytes are shown in Figures 5-10 to 5-12, respectively. The analyte concentration was maintained at 10^{-7} M whereas the co-analyte concentration was varied from 0 M, 10^{-9} to 10^{-4} M. The plots show a trend that when the concentration of the co-analyte exceeds 10^{-7} M, the analyte MS response decreases, regardless of the ion spray voltage setting. The mutual suppression effects between compounds B1, B2 and B3 were not substantially different. The extent of intensity decrease caused by 16:0 LPC was greater than that caused by these three compounds, especially at high concentration.

The principles of partition equilibrium applied to the buffer effects can also be utilized for this case. When co-analyte concentrations are low, background electrolyte ions are the predominant droplet excess charge carriers. Analyte and co-analyte

Figure 5-10. Effects of co-analyte concentration on ESI response of analyte B1 at three different ion spray voltages
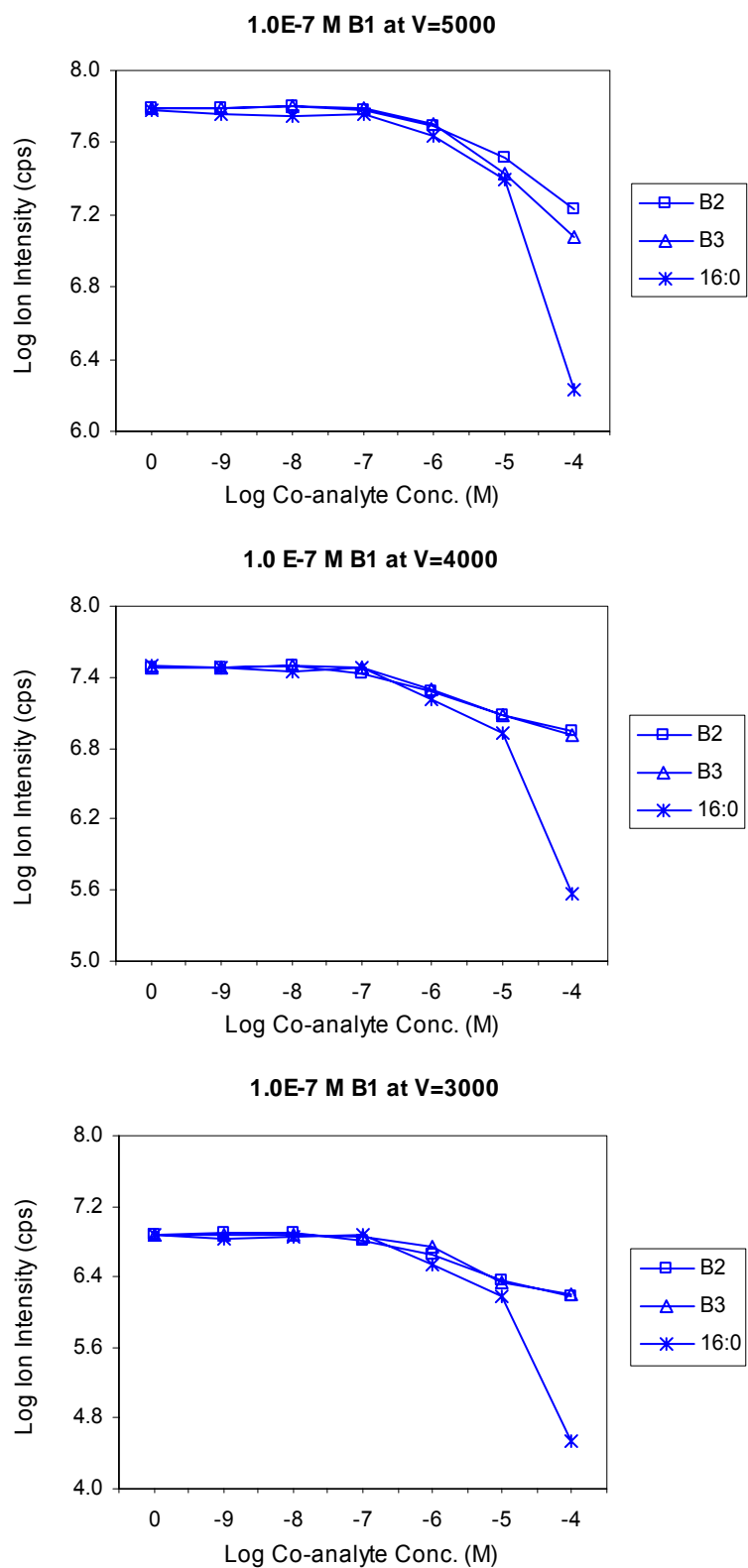
Figure 5-11. Effects of co-analyte concentration on ESI response of analyte B2 at three different ion spray voltages
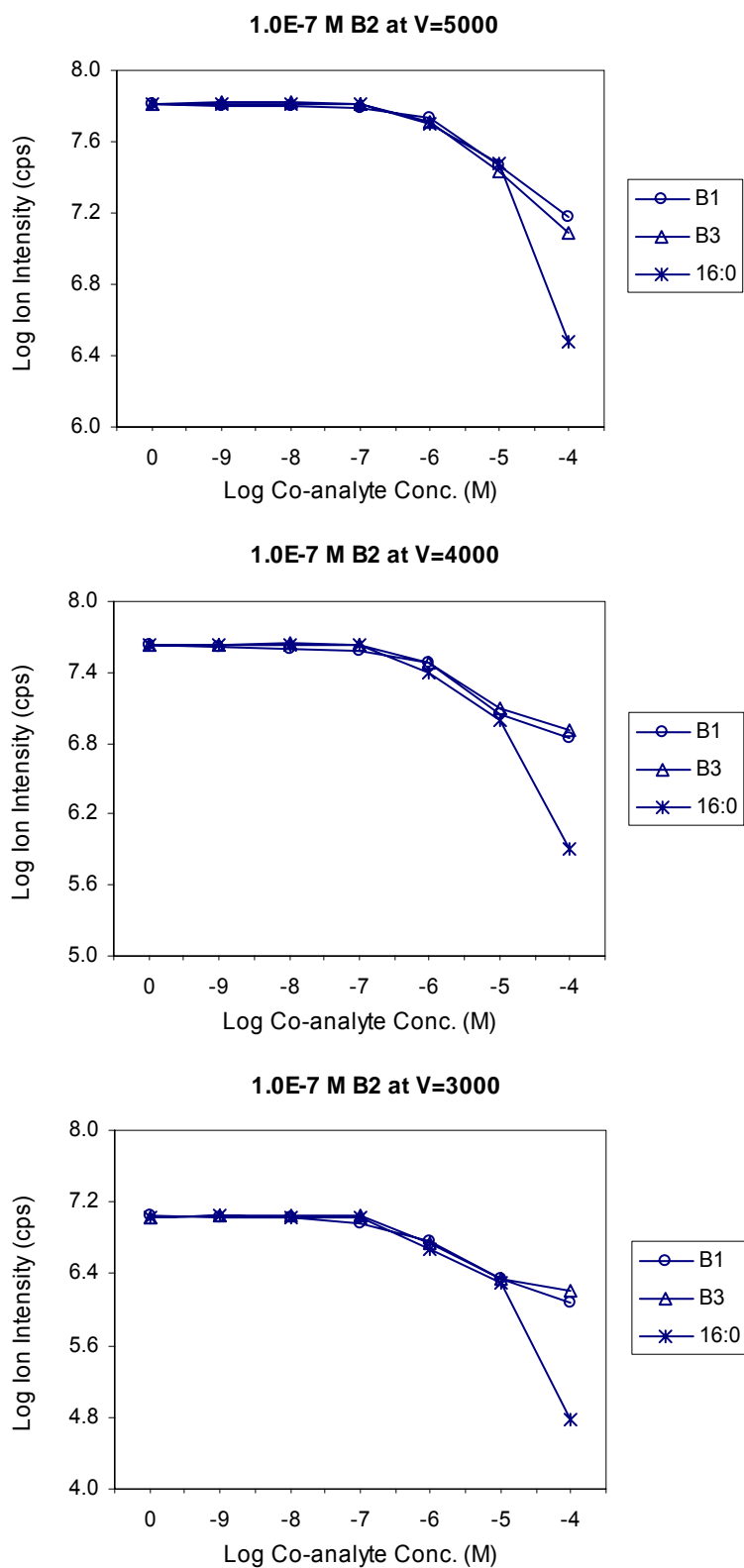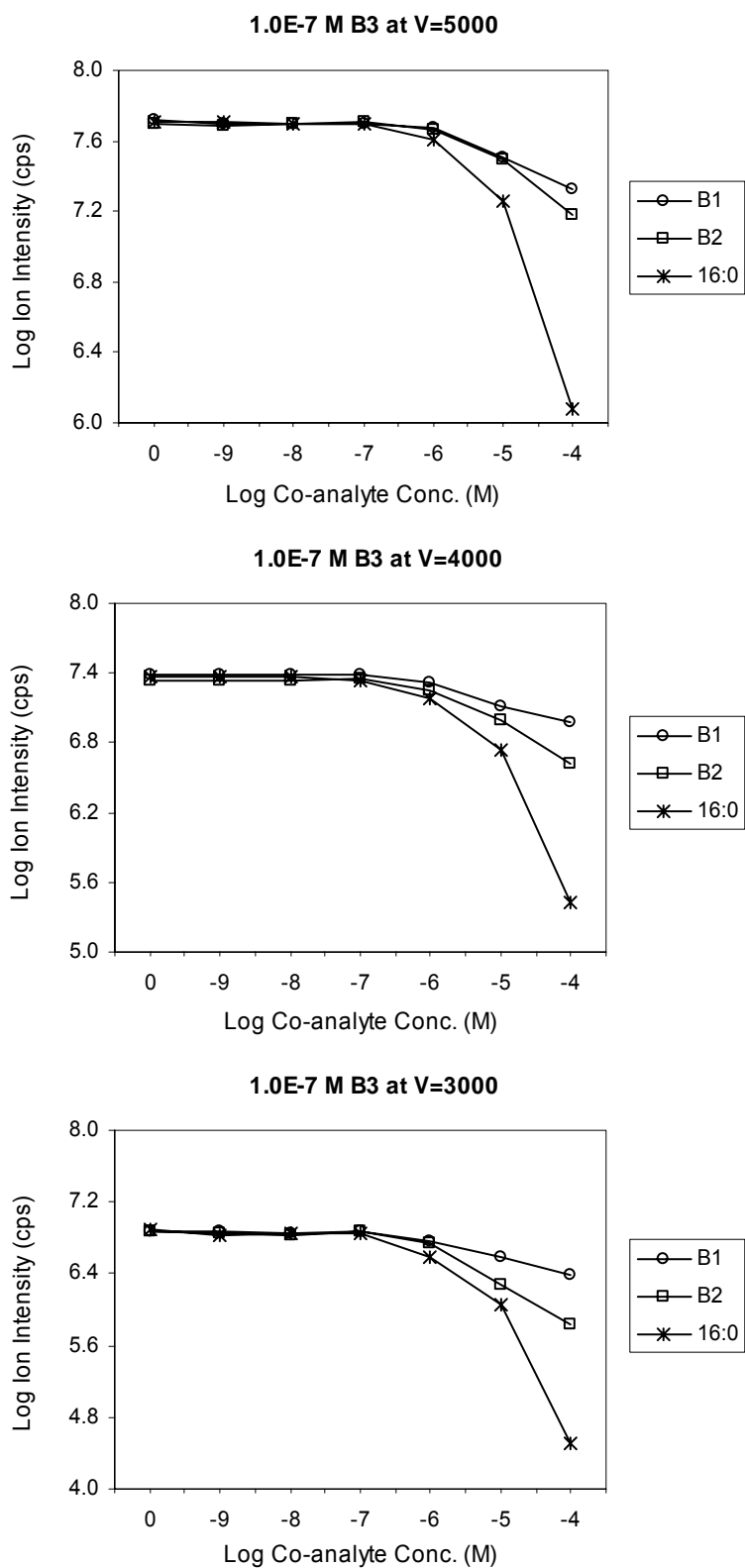
1.0E-7 M B2 at V=5000

1.0E-7 M B2 at V=4000

1.0E-7 M B2 at V=3000

Figure 5-12. Effects of co-analyte concentration on ESI response of analyte B3 at three different ion spray voltages

1.0E-7 M B3 at V=5000

1.0E-7 M B3 at V=4000

1.0E-7 M B3 at V=3000

independently complete with electrolytes for the excess charge, the existence of co-analyte will not affect the MS response of analyte. When co-analyte ions play a role in partitioning, either because of increased concentration or by having a greater coefficient, they will carry some of the excess charge previously carried by electrolytes. Under such circumstances, the partition environment for analyte ions will be changed and the presence of co-analyte affects the ability of the analyte to compete for the excess charge. It was expected that a co-analyte having a greater partition coefficient would affect the analyte surface concentration at relatively low concentrations. Therefore, Depending on the partition coefficient of the co-analyte, the concentration range, where the equation

$$[A^+]_s = \frac{C_A \cdot K_A/K_E}{K_A/K_E - 1 + C_E/[E^+]_s}$$ is valid, may vary. A required condition is that the

contribution of co-analyte ion to [Q] must be negligible. The results that compounds B1, B2 and B3 did not affect the MS response of each other until they reached comparable concentration, 10^{-7} M, indicate that these three analytes possess comparable coefficients. Although the results in Figure 5-4 show that K_{B2} is relatively larger than K_{B1} and K_{B3}, this difference appears not significantly affecting their contributions to [Q].

The decreased analyte MS responses at co-analyte concentrations greater than 10^{-7} M was consistent with the equation derived for mid-range buffer effects:

$$[A^+]_s = \frac{C_A \cdot K_A/K_M}{K_A/K_M - 1 + C_M/[M^+]_s}.$$ When co-analytes contribute considerably to [Q],

analyte ions must compete with co-analyte ions for excess charge, which is equivalent to a change in the value of K_E. As the co-analyte concentration increases, the contribution of $K_{co-analyte}$ to K_M increases, and consequently K_M increases because $K_{co-analyte}$ should be larger than K_E. Therefore, $[A^+]_s$ becomes smaller and a decrease in analyte MS response

is observed. An alternative explanation for the effects of co-analytes is to treat the co-analyte as analyte. Assuming that co-analyte (B) possesses a similar partition coefficient as analyte (A), increasing C_B is equivalent to increasing the total analyte concentration (C_{total}). When $C_A \approx C_{total}$, the effects of C_B are negligible. As C_{total} rises to a concentration level, where the surface analyte ions as a function of concentration is no longer linear due to [Q] limitation, analyte MS response will decrease. Because the fraction of C_A in C_{total} proportionally decreases, $[A^+]_s$ will decrease. A calculation based on above considerations is listed in the below table. It shows that the rough estimation by using the simulated data in Figure 5-2 provides a reasonable match with experimental results.

Table 5-1. Calculated co-analyte effects by using the [Q] values from Figure 5-2

|						
C_A	1.0E-07	1.0E-07	1.0E-07	1.0E-07	1.0E-07	1.0E-07
C_B	1.0E-09	1.0E-08	1.0E-07	1.0E-06	1.0E-05	1.0E-04
C_{total}	1.0E-07	1.1E-07	2.0E-07	1.1E-06	1.0E-05	1.0E-04
$\%C_A$	99.0	90.9	50.0	9.1	1.0	0.1
$[A^+]_s + [B^+]_s$ **	5.3E-08	5.3E-08	5.3E-08	4.1E-07	1.0E-06	1.2E-06
$[A^+]_s = \%C_A ([A^+]_s + [B^+]_s)$	5.2E-08	4.8E-08	2.6E-08	3.7E-08	9.9E-09	1.2E-09
$Log [A^+]_s$	-7.3	-7.3	-7.6	-7.4	-8.0	-8.9

** Copied from the simulated data in Fig. 5-2 for $K_A/K_E = 10$.

One thing that cannot be explained is why 16:0 LPC shows a greater suppression for analytes than when B1, B2 and B3 were used as co-analytes. According to the linear MS response graphs in Figure 5-4, the partition coefficient for 16:0 LPC should be considerably smaller than the coefficients for B1, B2 and B3. Therefore, the K_M modification extent for 16:0 LPC should be less than for the other compounds, and consequently a result of $K_{M(PC)} < K_{M(B)}$ would be obtained. According to the explanations for co-analytes B1, B2 and B3, 16:0 LPC would be expected to have the smallest

suppression effects.

Considering the factors inherent in the equilibrium partitioning process, the excess charge provides the principle driving force for the conversion of ions from solution to the gas phase, and the charges are distributed among gas phase ions according to the analytes partition coefficients. If the significant suppression effects of 16:0 LPC on analyte are not due to the partition coefficient, another possibility is that the amount of excess charge is decreased as the concentration of 16:0 LPC increases. Total ion current (TIC), which is the sum of MS responses for all ions in a certain scan range, should be a measure of [Q] because the detected ions were almost certainly excess charge carriers. The individual TIC values for the four analytes in various concentrations (10^{-9} to 10^{-4} M) were measured over a scan range of m/z 150 to 550. Ions with $m/z < 150$ are mainly from solvent impurities and should be fairly constant. Excluding the MS response for these ions should not affect relative TIC intensities. Figure 5-13 shows the TIC curves for analyte B3 and 16:0 LPC at three ion spray voltages. The TIC spectra for analytes B1 and B2 are very similar to that for B3. The TIC spectra for B3 shows that when $C_{B3} < 10^{-6}$ M, the variation of TIC with the changing C_{B3} was not significant; when $C_{B3} > 10^{-6}$ M, the TIC at 5000 V decreased whereas the TIC at 4000 and 3000 V increased. The amount of increase at 3000 V was greater than at 4000 V. These results are similar to the reported observations for capillary current I [44,69]. When the concentration of C_{B3} was less than that of the electrolytes, [Q] is mainly contributed by $[E^+]_s$ and I was relatively constant. A fixed TIC signal was detected. When C_{B3} becomes higher than C_E, the increase in C_{B3} will lead to an increase of κ and a subsequent increase of I. Therefore, more charged ions will be formed and the sum of all charged ion intensities reflected in TIC measurements

Figure 5-13. Total ion counts of single analyte B3 and 16:0 LPC in 50:50 acetonitrile:H$_2$O as a function of analyte concentration at three ion spray voltages
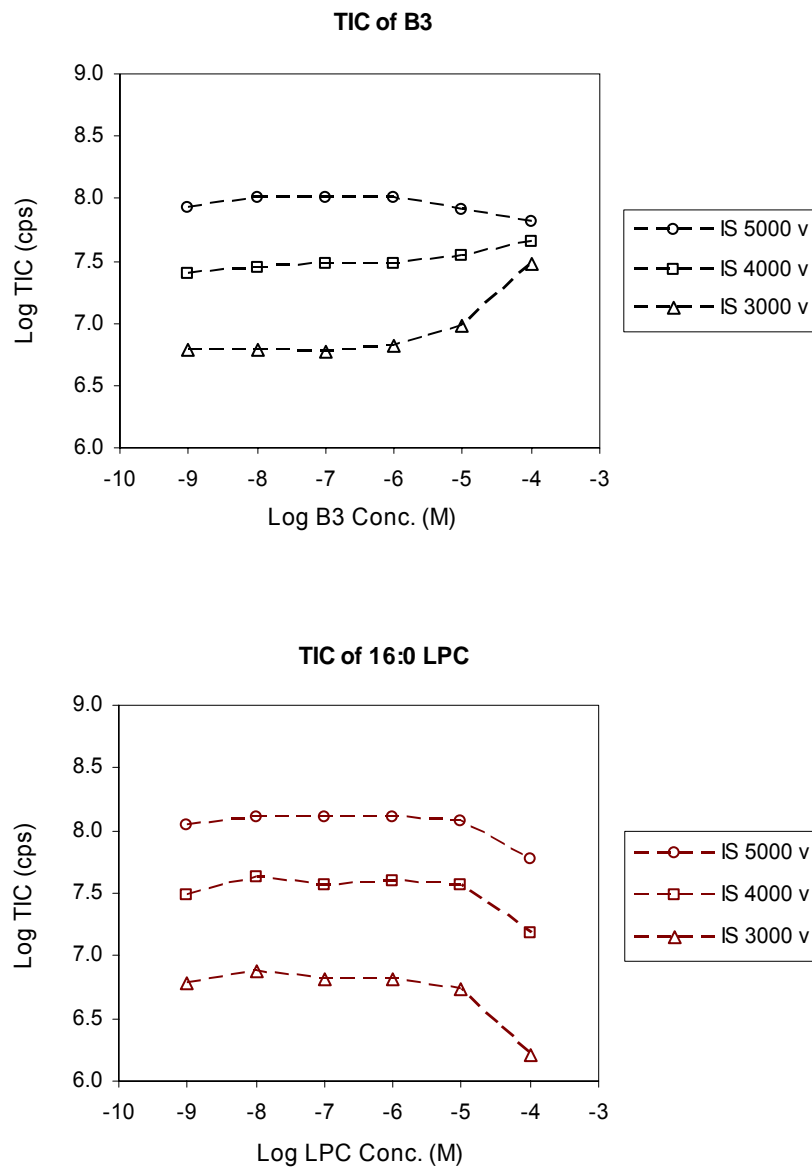
will increase. The observed TIC decrease for analyte B3 at 5000 V was caused by the detector saturation. After the saturation limit was reached, with the increasing C_{B3}, a constant ion intensity was measured for $[B3^+]_s$ ions, whereas the MS responses for other ions decreased due to the fraction of [Q] occupied by $[B3^+]_s$ ions increased.

In contrast, the TIC values for 16:0 LPC exhibit a constant decreasing trend when $C_{PC} > 10^{-6}$ M regardless of the voltage. The TIC signals at $C_{PC} < 10^{-6}$ M are relatively constant and comparable with the TIC responses for B3 in the same concentration range. It is clear that other factors besides conductivity dominate the production of capillary current for solutions with high concentrations of 16:0 LPC. It is known that addition of phospholipids will decrease solution surface tension as a result of the hydrophilic head and hydrophobic tail adsorbing to the air-solution interface of the droplet. The equation $I \approx f(\gamma \kappa v_f \frac{\varepsilon}{\varepsilon_0})^{1/2}$ derived from experimental data [14] indicates that surface tension (γ) and conductivity (κ) are joint factors that affect capillary current. Since the TIC signal decreased with the increasing C_{PC}, it appeared that a decrease in surface tension played a more important role than the conductivity increase for capillary currents generated with 16:0 LPC solutions. Due to the decrease of current, there was less excess charge available for analyte ions, and hence the amount of gas phase ions formed was reduced. Therefore, when 16:0 LPC is a co-analyte, besides competing with the analyte ion for excess charge, it has an additional effect of causing analyte signal suppression: decreasing the amount of excess charge by reducing the solution surface tension.

5.2.4 Effects of Buffered GPCho Lipid Solutions on Analyte Ionization

To elucidate the analyte ion suppression effects observed in Chapter 4, the effects of 16:0 LPC on analyte MS response were studied under two conditions: 16:0 LPC

solutions containing 1 mM buffer and no buffer (Fig. 5-14 to 5-16). With C_{PC} varying from 10^{-6} to 10^{-4} M, the MS response for analytes B1, B2 and B3 at 10^{-7} M was separately measured in LPC solution containing AA, FA, or AH. The analyte ionization was studied under such conditions because analytes experience severe suppression effects from 16:0 LPC in the 10^{-6} to 10^{-4} M range and HPLC analysis normally requires millimolar level buffers for chromatographic reasons.

The three analytes demonstrated comparable responses under the measured conditions. The signal intensity in a buffered solution was greater than in non-buffered solutions, and buffers AA, FA and AH exhibited similar effects on the signal. The deduced equations for buffer effects and co-analyte effects can also be applied to explain these observations. All of the compounds in solution except the analyte were treated as background electrolytes. For the non-buffered solution, background electrolytes (C_E) included 16:0 LPC and impurities from solvent whereas the C_E in 1 mM buffered solutions was mainly composed of the buffer itself due to $C_{Buf} > C_{PC}$ and $C_{impurity}$. Accordingly, the K_E for the single analyte solution was modified to be K_M and K_{Buf}, and the analyte surface concentration was calculated as: $[A^+]_s = \dfrac{C_A \cdot K_A / K_M}{K_A / K_M - 1 + C_M / [M^+]_s}$

and $[A^+]_s = \dfrac{C_A \cdot K_A / K_{Buf}}{K_A / K_{Buf} - 1 + C_{Buf} / [Buf^+]_s}$ for non-buffered and buffered solutions,

respectively. Here, K_M was expressed as: $K_M = \dfrac{[E^+]_s + [PC^+]_s}{[E^+]_i + [PC^+]_i}$. A K_M value modified

by 16:0 LPC surface concentration ($[PC^+]_s$) was expected to be larger than the background electrolyte coefficient (K_E) due to the fact that K_{PC} should be larger than K_E. An approximate order for the partition coefficients is $K_A > K_{PC} > K_M > K_E > K_{Buf}$.

Figure 5-14. Effects of adding buffer on ESI response of analyte B1 mixed with different concentration of 16:0 LPC at three ion spray voltages
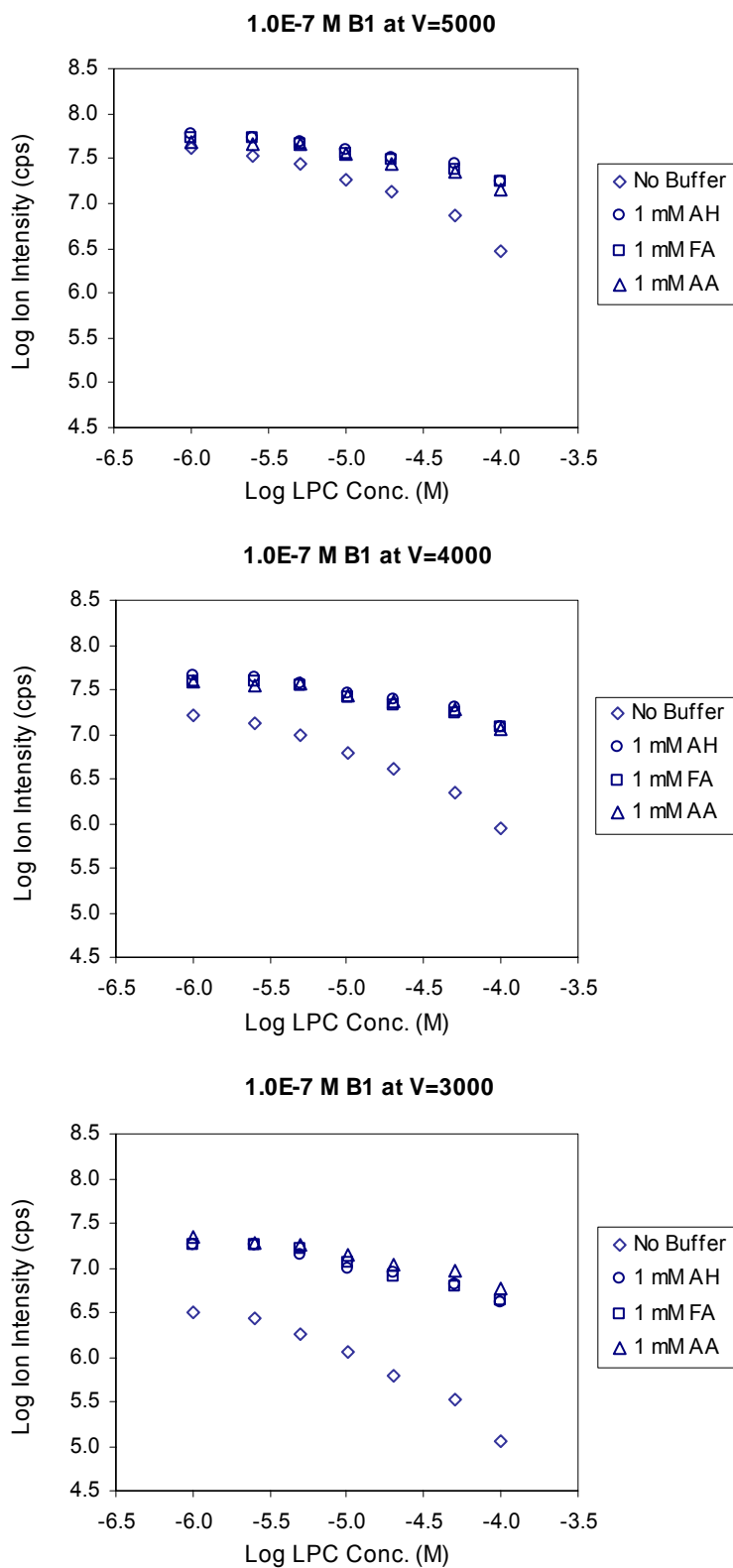

1.0E-7 M B1 at V=5000

1.0E-7 M B1 at V=4000

1.0E-7 M B1 at V=3000

Figure 5-15. Effects of adding buffer on ESI response of analyte B2 mixed with different concentration of 16:0 LPC at three ion spray voltages

1.0E-7 M B2 at V=5000

Legend:
◇ No Buffer
○ 1 mM AH
□ 1 mM FA
△ 1 mM AA

1.0E-7 M B2 at V=4000

Legend:
◇ No Buffer
○ 1 mM AH
□ 1 mM FA
△ 1 mM AA

1.0E-7 M B2 at V=3000
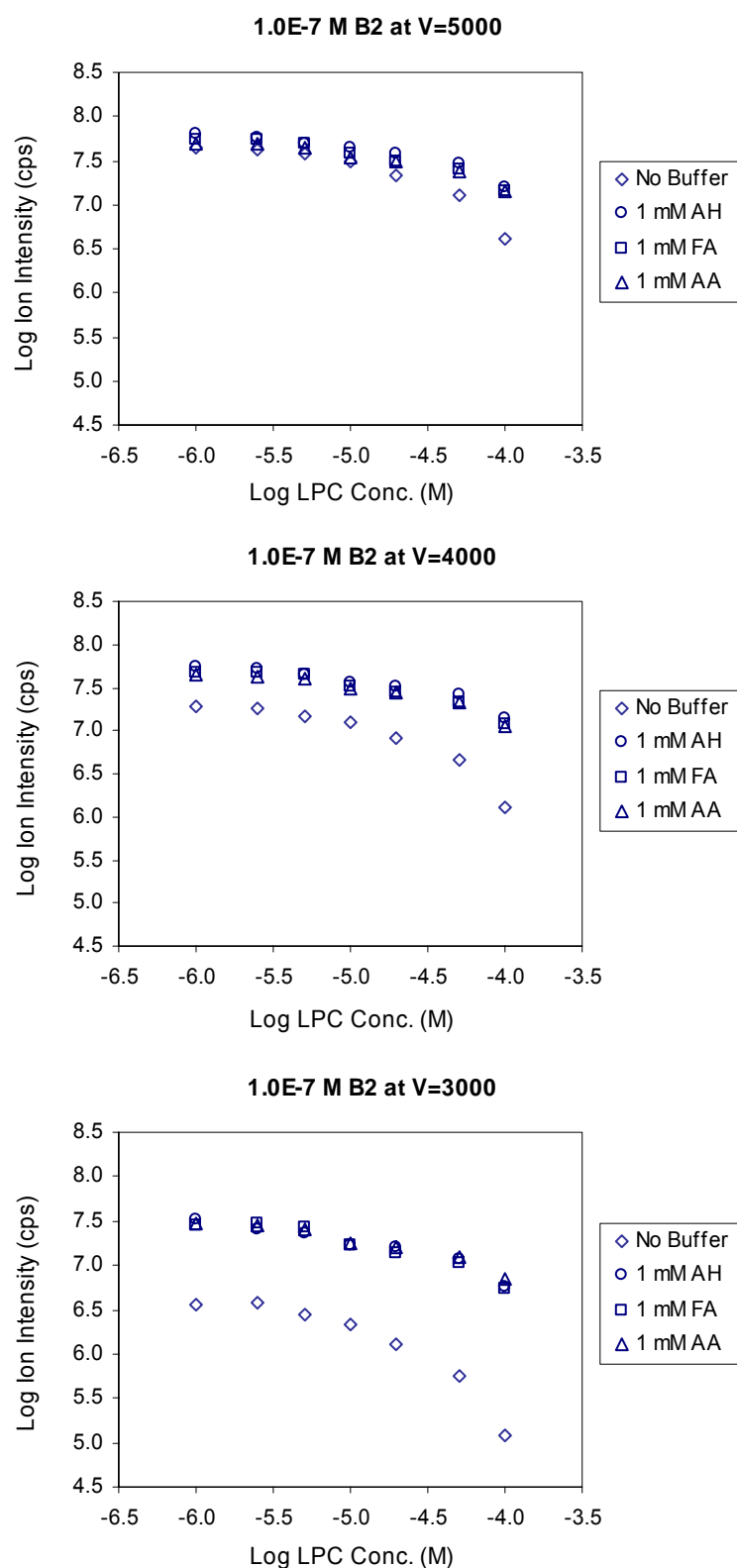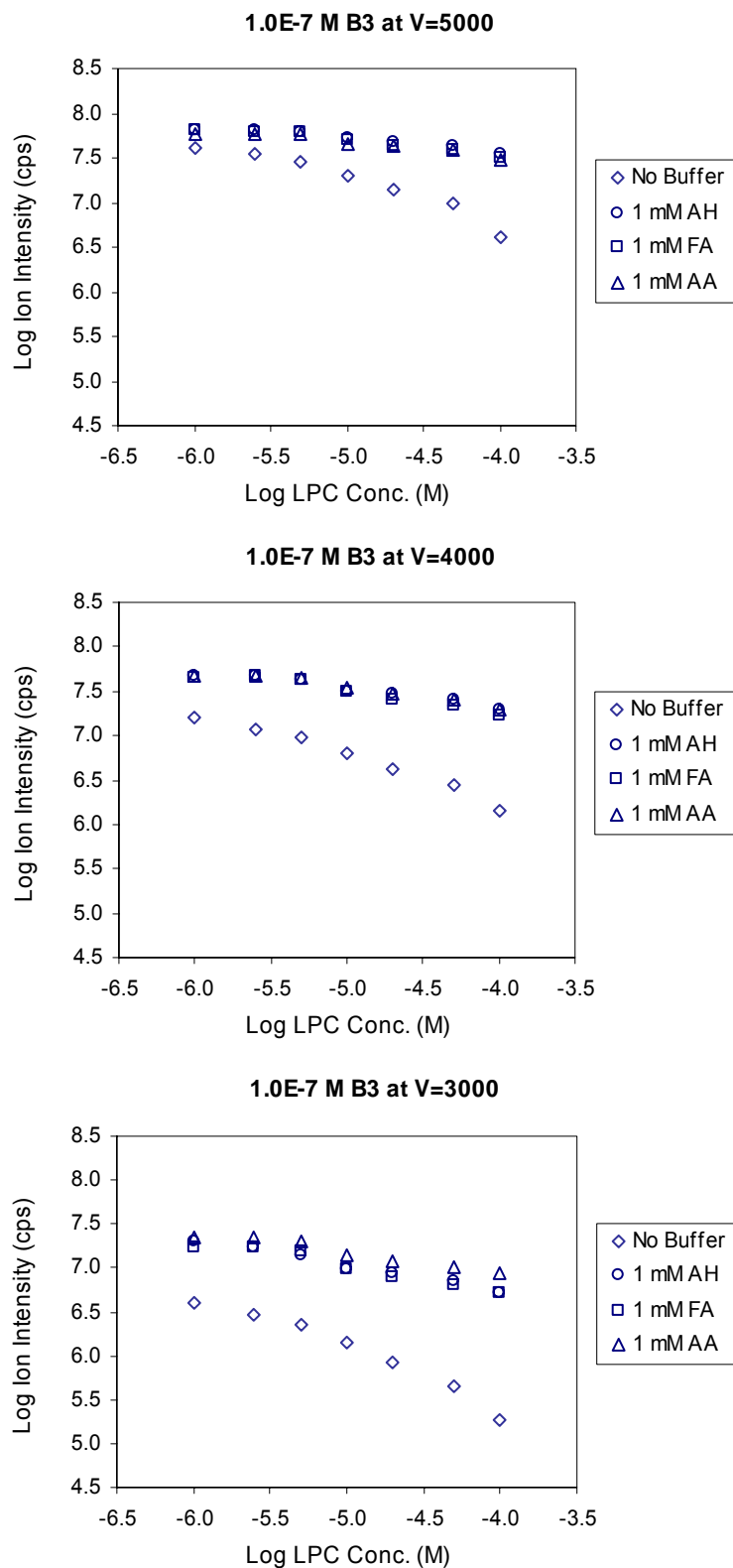
Legend:
◇ No Buffer
○ 1 mM AH
□ 1 mM FA
△ 1 mM AA

190

Figure 5-16. Effects of adding buffer on ESI response of analyte B3 mixed with different concentration of 16:0 LPC at three ion spray voltages

1.0E-7 M B3 at V=5000



1.0E-7 M B3 at V=4000

1.0E-7 M B3 at V=3000

Therefore, $[A^+]_s$ in a non-buffered solution was smaller than in a buffered solution. Since the analytes B1, B2 and B3 had similar partition coefficients and so did the three buffers, the measured responses demonstrated comparable results. Because the concentration of background electrolytes was not very high (10^{-3} M for buffered solutions and 10^{-4} M for non-buffered solutions), it was reasonable to consider the analyte competition for excess charge occurred in an unsaturated condition where the amount of excess charge was sufficient for gas phase ions. Under such circumstances, $[A^+]_s$ is more affected by the K_A/K_E coefficient ratio rather than the $C_E/[E^+]_s$ ratio.

In addition, with increasing C_{PC}, analyte MS response was reduced in non-buffered solutions more than in buffered solutions. The two factors: the coefficient ratio and amount of excess charge were examined again to elucidate these observations. For the non-buffered solution, when C_{PC} was gradually increased to 10^{-6}, 10^{-5} and 10^{-4} M, the contribution of K_{PC} to K_M increased and the corresponding coefficient order should be: $K_{M(-6)} < K_{M(-5)} < K_{M(-4)}$. In contrast, the coefficient for buffered solutions was relatively constant when C_{PC} was varied because C_{Buf} was much greater than C_{PC}, and $K_{Buf(-6)} \approx K_{Buf(-5)} \approx K_{Buf(-4)}$. Therefore, the coefficient ratio for analyte to background electrolyte decreased more rapidly in the non-buffered solution than in the buffered solution.

The amount of excess charge was evaluated by measuring the TIC over a scan range of *m/z* 150 to 550 for solutions containing only background electrolytes (Figure 5-17). When C_{PC} increased from 10^{-6} to 10^{-4} M, TIC measurements for 16:0 LPC in non-buffered solutions decreased by 80 - 90% whereas the decrease for buffered solutions was 20 - 30%. Buffers FA and AH had similar TIC results to that of AA. Since capillary current is determined by the combined effects of conductivity and surface tension, the

Figure 5-17. Total ion counts of 16:0 LPC in solution (50:50 acetonitrile:water) and solution with 1 mM ammonium acetate at three different ion spray voltages

TIC of 16:0 LPC in a solution with 1.0E-3 M AA

TIC of 16:0 LPC in non-buffer solution
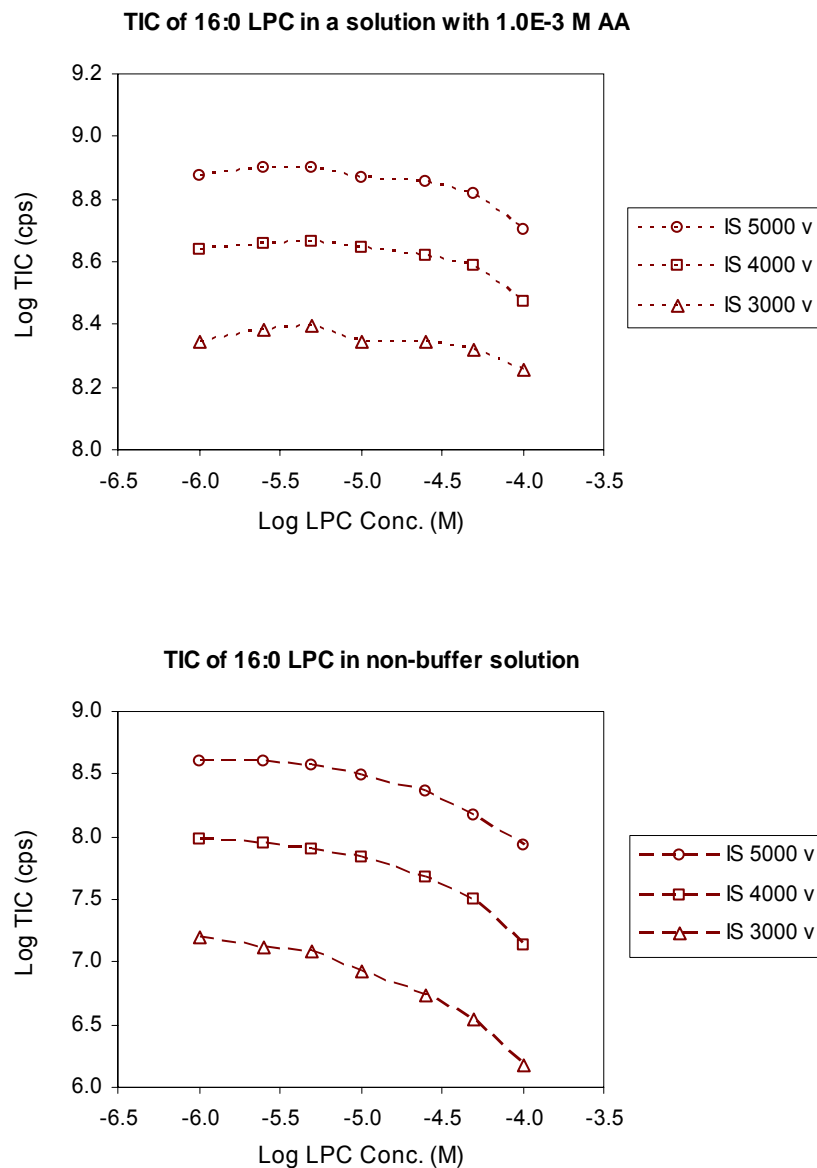
effect of surface tension on current for low conductivity solutions should be more substantial than for high conductivity solutions. This was demonstrated by a greater TIC decrease in non-buffered solutions (low conductivity) than in buffered solutions (high conductivity). Because both the amount of excess charge and the relative coefficient of analyte to electrolyte had a greater decrease in non-buffered than buffered solutions, $[A^+]_s$ was more suppressed in non-buffered solutions. The similar MS responses for the three analytes under the three buffer conditions suggests that adding a suitable amount of buffer reduces the suppression effects of 16:0 LPC on analyte ionization.

5.2.5 Conclusions:

The improved equations driven form the partition equilibrium mode was able to explain the analyte MS responses for all studied conditions: single analyte solutions, buffered solutions, co-analyte solutions and buffered GPCho lipid solutions. The buffer concentration effects, which could not be explained by the partition equilibrium mode, were clarified by using the improved equations. The significant ion suppression effects of GPCho lipids were proved to be a combined result. Lipids not only competed with analyte for excess charge but also decreased the excess charge amount through reducing droplet surface tension. This suppression effect can be reduced by adding buffer to a concentration higher than that of lipids. Because the improved equation is linear and simple, and demonstrated to be valid, it can be applied for predicting analyte MS response in biological sample.

LC-ESI-MS is by far the predominant technique used for determining drug concentrations in biological samples. The inherent selectivity derived from mass spectrometry detection reduces the need for completely separating analytes from

interfering materials, which simplifies assay methodologies. However, the research described here indicates that endogenous lipid interferences, which are not directly detected during assays involving MS detection, can significantly affect the reliability of plasma sample analyses. GPCho lipids exhibited greater analyte MS response suppression than other compounds present in sample matrices because they not only competed with target analytes for excess charge during ion formation processes, but also reduced the amount of charge available. High GPCho lipid plasma concentrations and large inter-batch concentration variations result in poor analyte MS signal reproducibility. Unfortunately, LLE and HTLC online extraction methods proved ineffective for removal of GPCho lipid interferences.

For hydrophobic analyte assays, the key step in the analytical procedure is column separation, and 16:0 LPC can be used as a diagnostic probe of separation efficiency. If analytes elute prior to 16:0 LPC, they mostly likely will not be affected by endogenous lipid interferences. If analytes co-elute or elute after 16:0 LPC, sample preparation procedures must be employed to eliminate or greatly reduce these interferences. For either hydrophobic or hydrophilic analytes, gradient elution minimizes the possibility of interfering species co-elution. A strong solvent at the end of the gradient should be used to wash lipids with long retention times out of the column. If this is not done, these lipids may elute during subsequent injections.

When sample preparation methods are employed to compensate for ineffective chromatographic lipid separation, HTLC online extraction or SPE are good choices, whereas conventional LLE would not be preferred unless the analyte can be extracted with hexane. For a particular assay, transfer conditions for HTLC online extraction and

elution conditions for SPE can be determined from results of analyte recovery and lipid removal studies. In order to effectively eliminate matrix interferences, analyte recovery may have to be sacrificed. UPLC analysis requires high pressure LC and may not always be available, but columns with relatively small particles (~2.2 µm columns have recently been introduced for use with conventional HPLC systems) are effective for separating extracted analytes from interferences.

Mobile phase buffer concentrations (1 – 10 mM) should be properly optimized for the best assay performance. In addition to improving analyte peak shapes and assay reproducibility, the buffer dilutes the suppression effects of GPCho lipids and reduces inter-batch variations. Although high buffer concentrations help to reduce matrix variations, analyte sensitivity is sacrificed. Mechanistic studies have demonstrated that an effective ISTD must co-elute with the target analyte. If the analyte and ISTD are subjected to different ionization conditions, a quantitative calculation based on the peak area ratio of the analyte to ISTD MS signals would likely be inaccurate.

Identification of GPCho lipids as one of the major sources of ESI interferences in biological samples was a significant finding. It was determined that matrix interference effects can be directly related to the lipid concentration in analyzed samples. These adverse matrix interference effects can be minimized by either adjusting LC conditions or improving extraction procedures. The ionization suppression mechanism investigations described here help to elucidate the relationship between analyte MS response and solution phase matrix constituents, which include mobile phase composition, buffers and interfering compounds. An understanding of these correlations provides fundamental guidance for designing reproducible and accurate assay methods.

5.3 References

[1] Kebarle, P.; Ho Y. *Electrospray Ionization Mass Spectrometry,* Cole R.D. (ed.) Wiley, Now York, 1997

[2] Spiros, A. P.; Kevin A. F.; Walter G.; Jane E. T. *Anal. Chem.***1997**, 69, 4931

[3] Jon, C. R.; Kent, J. V. *Rapid Commun. Mass Spectrom.* **2005**, 19, 2757

[4] Suzuki, S.; Kakehi, K.; Honda, S. *Anal. Chem.* **1996**, 68, 2073

[5] Wyatt, M. F.; Stein, B. K.; Brenton, A. G. *Anal. Chem.* **2006**, 78, 199

[6] David, C. M.; Arkady, I. G.; David, M. H. *Mass Spectrom. Rev.* **1995**, 14, 383

[7] Andrea, R.; Paola, C.; Cristina, F.; Luciano, M.; Roberta, S.; Pietro, T. *J. Mass Spectrom.* **2006**, 41, 1232

[8] Yamashita, M.; Fenn, J. B. *J. Phys. Chem.* **1984**, 88, 4451 and 4671

[9] Taylor, G. I. *Proc. R. Soc. London A* **1964**, A280, 383

[10] Pfeifer, R. J.; Hendricks, C. D. *AIAA J.* **1968**, 6, 496

[11] Smith, D. P. H. *IEEE Trans. Ind. Appl.* **1986**, IA-22, 527

[12] Cloupeau, M.; Prunet-Foch, R. J. *Aerosol Sci.* **1994**, 25, 1021

[13] Horming, D. W.; Hendricks, C. D. *J. Appl. Phys.* **1979**, 50, 2614

[14] Fernandez de la Mora, J.; Locertales, I. G. *J. Fluid Mech.* **1994**, 243, 561

[15] Ikonomou, M. G.; Blades, A. T.; Kebarle, P. *Anal. Chem.* **1991**, 63, 1989

[16] Kebarle, P.; Tang, L. *Anal. Chem.* **1993**, 65, 972A

[17] Ji, Z.; Li, J.; Zhou, J.; Hui, L.; Yuan, G.; Cai, S. *J. Phys. Chem. B.* **2005**, 109, 17162

[18] Fernandez de la Mora, J.; Van Berkel, G. J.; Enke, C. G.; Cole, R. B.; Martinez-Sanchez, M.; Fenn, J. B. *J. Mass Spectrom.* **2000**, 35, 939

[19] Blades, A. T.; Ikonomou, M. G.; Kebarel, P. *Anal. Chem.* **1991**, 63, 2109

[20] Van Berkel, G. J. *J. Mass Spectrom.* **2000**, 35, 773

[21] Van Berkel, G. J.; Asano, K. G.; Kertesz, V. *Anal. Chem.* **2002**, 74, 5047

[22] Quirke, J. M. E.; Van Berkel, G. J. *J. Mass Spectrom.* **2001**, 36, 1294

[23] Van Berkel, G. J.; Zhou, F. *Anal. Chem.* **1995**, 67, 2916

[24] Van Berkel, G. J.; Zhou, F. *Anal. Chem.* **1995**, 67, 3643

[25] Van Berkel, G. J.; Asano, K. G.; Granger, M. C. *Anal. Chem.* **2004**, 76, 1493

[26] Kertesz, V.; Van Berkel, G. J. *J. Mass Spectrom.* **2001**, 36, 204

[27] Iavarone, A. T.; Williams, E. R. *J. Am. Chem. Soc.* **2003**, 125, 2319

[28] Mansoori, B. A.; Volmer, D. A.; Boyd, R. K. *Rapid Commun. Mass Spectrom.* **1997**, 11, 1120

[29] Wu, Z.; Gao, W.; Phelps, M. A.; Wu, D.; Miller, D. D.; Dalton, J. T. *Anal. Chem.* **2004**, 76, 839

[30] Zhou, S.; Cook, K. D. *J. Am. Soc. Mass Spectrom.* **2000**, 11, 961

[31] Taflin, D. C.; Ward, T. L.; Davis, E. J. *Langmuir* **1989**, 5, 376

[32] Davis, E. J. *ISA Trans.* **1987**, 26, 1

[33] Gomez, A.; Tang, K. *Phys. Fluids* **1994**, 6, 404

[34] Rayleigh, Lord *Philos. Mag.* **1882**, 14, 184

[35] De Juan, L.; Fernandez de la More, J. *J. Colloid Interface Sci.* **1997**, 186, 280

[36] Fernandez de la More, J. *J. Colloid Interface Sci.* **1996**, 178, 209

[37] Dole, M.; Mack, L. L.; Hines, R. L.; Mobley, R. C.; Ferguson, L. D.; Alice, M. B. *J. Chem. Phys.* **1968**, 49, 2240

[38] Mack, L. L.; Kralik, P.; Rheude, A.; Dole, M. *J. Chem. Phys.* **1970**, 52, 4977

[39] RÖllgen, F. W.; Bramer-Wegner, E.; Buttering, L. *J. Phys. Colloq.* **1984**, 45, C9

[40] Schmelzeisen-Redeker, G.; Buttering, L.; RÖllgen, F. W. *Int. J. Mass Spectrom. Ion Processes* **1989**, 90, 139

[41] Iribarne, J. V.; Thomson, B. A. *J. Chem. Phys.* **1976**, 64, 2287

[42] Thomson, B. A.; Iribarne, J. V. *J. Chem. Phys.* **1979**, 71, 4451

[43] Fenn, J. B.; Mann, M.; Meng, C.K.; Wong, S. F.; Whitehouse, C. M. *Science,* **1989**, 246, 64

[44] Tang, L.; Kebarle, P. *Anal. Chem.* **1993**, 65, 3654

[45] Kebarle, P. *J. Mass Spectrum.* **2000**, 35, 804

[46] Cole, R. B. *J. Mass Spectrum.* **2000**, 35, 763

[47] Fenn, J. B. *J. Am. Soc. Mass Spectrom.* **1993**, 4, 524

[48] Nohmi, T.; Fenn, J. B. *J. Am. Soc. Mass Spectrom.* **1991**, 114, 3241

[49] Locertales, I. G.; Fernandez de la More, J. *J. Chem. Phys.* **1995**, 103, 5041

[50] Fernandez de la More, J. *Anal. Chim. Acta* **2000**, 406, 93

[51] Lavarone, A. T.; Williams, E. R. *J. Am. Chem. Soc.* **2003**, 125, 2319

[52] Ku, B. K.; Fernandez de la More, J. *J. Phys. Chem. B.* **2005**, 109, 11173

[53] Kebarle, P.; Peschke, M. *Anal. Chim. Acta* **2000**, 406, 11

[54] Schlosser, G., Takáts, Z.; VéKey, K. *J. Mass Spectrum.* **2003**, 38, 1245

[55] Gamero-Castaño, M.; Fernandez de la More, J. *Anal. Chim. Acta* **2000**, 406, 67

[56] Takáts, Z.; Drahos, L.; Schlosser, G.; VéKey, K. *Anal. Chem.* **2002**, 74, 6427

[57] Ku, B. K.; Fernandez de la More, J. *J. Phys. Chem. B.* **2004**, 108, 14915

[58] Blades, A. T.; Peschke, M.; Verkerk, U. H.; Kebarle, P. *J. Am. Chem. Soc.* **2004**, 126, 11995

[59] Amad, M. H.; Cech, N. B.; Jackson, G. S.; Enke, C. G. *J. Mass Spectrum.* **2000**, 35, 784

[60] Ma, S.; Wang, F.; Cooks, R. G. *J. Mass Spectrum.* **1998**, 33, 943

[61] Patrick, J. S.; Yang, S. S.; Cooks, R. G. *J. Am. Chem. Soc.* **1996**, 118, 231

[62] Strittmatter, E. F.; Wong, R. L.; Williams, E. R. *J. Phys. Chem. A* **2000**, 104, 10271

[63] Enke, C.G. Anal. Chem. **1997**, 69, 4885

[64] Constantopoulos, T. L.; Jackson, G. S.; Enke, C. G. *J. Am. Soc. Mass Spectrom.* **1999**, 10, 625

[65] Cech, N. B.; Enke, C. G. *Anal. Chem.* **2001**, 73, 4632

[66] Bökman, C. F.; Bylund, D.; Sjöberg, P. J. R.; Markides, K. E. *J. Am. Soc. Mass Spectrom.* **2006**, 17, 318

[67] Sjöberg, P. J. R.; Bökman, C. F.; Bylund, D.; Markides, K. E. *Anal. Chem.* **2001**, 73, 23

[68] Zhou, S.; Cook, K. D. *J. Am. Soc. Mass Spectrom.* **2001**, 12, 206

[69] Tang, L.; Kebarle, P. *Anal. Chem.* **1991**, 63, 2709